Ghent University

Faculty of Pharmaceutical Sciences

# DESIGN OF PROTEIN-REACTIVE POLYMERS AND CORE-CROSSLINKED NANOPARTICLES IN VIEW OF VACCINE DELIVERY

**Nane Vanparijs**

Master of Science in Drug Development

Thesis submitted to obtain the degree of Doctor in Pharmaceutical Sciences.

2016

Promoter:

**Prof. Dr. Ir. Bruno G. De Geest**

Laboratory of Pharmaceutical Technology

The author and the promoters give the authorization to consult and to copy part of this thesis for personal use only. Any other use is limited by the Laws of Copyright, especially concerning the obligation to refer to the source whenever results are cited from this thesis.

Ghent, July 1st, 2016

**The promotor**

Prof. Dr. Ir. Bruno G. De Geest

**The author**

Nane Vanparijs

# Acknowledgements

**Laboratory of Pharmaceutical Technology, Ghent University**

My promotor Prof. Bruno G. De Geest

Prof. Jean Paul Remon, Prof. Chris Vervaet and Prof. Thomas De Beer

Secretary & technical staff Katharine Wullaert, Ilse Dupon and Christine Geldof

Thesis students Frederik B., Frederick D., Ellen and Aurélie

Moral supporters Fien De Leersnyder and Valérie Vanhoorne

Lunch buddies Benoit, Ruben, Simon and Lutz

All other colleagues wandering the third floor including Laurens, Lien, Tinne, Liesbeth, Kaat, Davinia, Sabah and many others

All former colleagues that already managed to obtain their PhD

**University of California, Los Angeles (UCLA)**

Prof. Heather D. Maynard

Adoptive scientists including Emma, Sam, Nathalie and JK

**Department of Pharmaceutics, Utrecht University**

Prof. Wim E. Hennink

Helping hands Luis, Orn(chuma) and Yang Shi

**Department of Organic Chemistry, Ghent University**

Prof. Richard Hoogenboom, Dr. Qilu Zhang and Dr. Samarendra Maji

Prof. Johan Winne and Dr. Duchan Laplace

**Vlaams Instituut voor Biotechnologie (VIB)**

DC experts Dr. Stefaan De Koker, Ans De Beuckelaer and Vimal Kumar

**Friends and Family**

A long but indisputably important list in alphabetical order:

Daddy Cool, Eline, Feeny, Fiefie, Fiene, Florka, Gertjan, Gugu, Ine, Ineke, Kaarie, Kasey, Laaiza, Landy, Leni, Lore, Maaike, Marty, Midget, Mrizzie, Najwa, Rita, Sebie, Suzie, Sylvster, Tsaarie, Valerke

Thank you!
Nane ☺

# Table of contents


| | | |
|---|---|---|
| **List of abbreviations and symbols** | | 1 |
| **Outline and aim of this thesis** | | 7 |
| **PART I** | **General introduction & background** | |
| **Chapter 1** | The immune system and vaccine development | 13 |
| **Chapter 2** | Transiently thermoresponsive polymers and their application in biomedicine | 27 |
| **PART II** | **Design of protein-reactive polymeric nanoparticles** | |
| **Chapter 3** | Synthesis of protein-reactive polymers via RAFT polymerization | 103 |
| **Chapter 4** | Polymer-protein conjugation via a 'grafting-to' approach | 129 |
| **Chapter 5** | Polymer-protein conjugates via a 'grafting-from' approach for the delivery of immune-modulators | 149 |
| **Chapter 6** | Hydrogel nanocapsules for lymph node targeted vaccine delivery | 171 |
| **Chapter 7** | Covalently crosslinked nanogels for immune activation and antigen conjugation | 185 |
| **PART III** | **Future perspectives & general conclusions** | |
| **Chapter 8** | Broader international context, relevance and future perspectives | 221 |
| **Chapter 9** | Summary and general conclusions | 233 |
| **Curriculum Vitae** | | 241 |

# List of abbreviations and symbols

| | |
|---|---|
| ADMO | N-acryloyl-2,2-dimethyl-1,3-oxazolidine |
| AEE | amino acid esters |
| AIBN | azobisisobutyronitrile |
| Al | alanine |
| AMPEG | α-amino-ω-methoxy-poly(ethylene glycol) |
| APCs | antigen-presenting cells |
| ATRP | atom transfer radical copolymerization |
| BADS | bis(2-acryloyloxyethyl) disulfide |
| BB | backbone functionalization |
| BCN | bicyclononyne |
| BCR | B cell receptor |
| BM-DCs | bone marrow-derived dendritic cells |
| BMDO | 5,6-benzo-2-methylene-1,3-dioxepane |
| BSA | bovine serum albumin |
| c/tNEM | cis/trans N-(2-ethoxy-1,3-dioxan-5-yl)methacrylamide |
| c/tNMM | cis/trans N-(2-methoxy-1,3-dioxan-5-yl) methacrylamide |
| CDTPA | 4-cyano-4-[(dodecylsulfanylthiocarbonyl)sulfanyl]pentanoic acid |
| CE | chain end functionalization |
| CETPA | 4-cyano-4-[(ethylsulfanylthiocarbonyl)sulfanyl]pentanoic acid |
| cgt | critical gelation temperature |
| cmc | critical micellar concentration |
| cmt | critical micellization temperature |
| CROP | cationic ring-opening polymerization |
| CTAs | chain transfer agents |
| CTB-AF488 | cholera toxin subunit B - Alexa Fluor® 488 conjugate |
| CTL | cytotoxic T cells |

| | |
|---|---|
| CTLA-4 | cytotoxic T-lymphocyte antigen 4 |
| CU | carbonate unit |
| CuAAC | copper(I)-catalyzed cyclo-addition |
| Cy | cyanine |
| Đ | dispersity |
| DAD | diode array detector |
| DBA | dimethyl-ɣ-butyrolactone acrylate |
| DCM | dichloromethane |
| DCs | dendritic cells |
| DEA | 2-(1,3-dioxan-2-yloxy)ethyl acrylate |
| DIC | N,N'-diisopropylcarbodiimide |
| DLN | draining lymph node |
| DLS | dynamic light scattering |
| DMA | dimethylacetamide |
| DMAP | 4-dimethylaminopyridine |
| DMDEA | 2-(5,5-dimethyl-1,3-dioxan-2-yloxy)ethyl acrylate |
| DMDMA | (2,2-dimethyl-1,3-dioxolane-4-yl)methyl acrylate |
| DMDOMAm | (N-(2,2-dimethyl-1,3-dioxolane)-methyl) acrylamide |
| DMF | dimethylformamide |
| DMNA | 5-(2'-(dimethylamino)ethoxy)-2-nitrobenzyl acrylate |
| DMSO | dimethylsulfoxide |
| DNA | deoxyribonucleic acid |
| DOX | doxorubicin |
| DP | degree of polymerization |
| DTT | 1,4-dithiothreitol |
| EDC | 1-(3-dimethylaminopropyl)-3-ethylcarbodiimide |
| EDTA | ethylenediaminetetraacetic acid |
| EEP | 2-ethoxy-2-oxo-1,3,2-dioxaphospholane |
| ELPs | elastin-like poly(peptide)s |
| EMEP | 2-ethoxy-4-methyl-2-oxo-1,3,2-dioxaphospholane |
| EtOx | 2-ethyl-2-oxazoline |

| | |
|---|---|
| FACS | fluorescence-activated cell sorting (flow cytometry) |
| Fp | furan-protected |
| FRET | fluorescence resonance energy transfer |
| GC | gas chromatography |
| HCV | hepatitis C virus |
| HEA | 2-hydroxyethyl acrylate |
| HEMA-$Lac_n$ | 2-hydroxyethyl methacrylate oligolactate |
| HEMAm-$Lac_n$ | N-(2-hydroxyethyl)methacrylamide oligolactate |
| HEPDS | hydroxyethyl pyridyl disulfide |
| HEPES | 4-(2-hydroxyethyl)-1-piperazineethanesulfonic acid |
| hGH | human Growth Hormone |
| HIV | human immunodeficiency virus |
| HPMAm-$Lac_n$ | 2-hydroxypropyl methacrylamide oligolactate |
| IFN-β | interferon-β |
| IleOEt | L-isoleucine ethyl |
| IMDQ | 1-(4-(aminomethyl)benzyl)-2-butyl-1H-imidazo[4,5-c]quinolin-4-amine |
| IPP | 2-isopropoxy-2-oxo-1,3,2-dioxaphospholane |
| MAL | maleimide |
| MDO | 2-methylene-1,3-dioxepane |
| MEM | minimum essential medium |
| $MEO_2MA$ | 2-(2-methoxyethoxy)ethyl methacrylate |
| MEP | 2-methoxy-2-oxo-1,3,2-dioxaphospholane |
| MFI | mean fluorescence intensity |
| MHC | major histocompatibility complex |
| $M_n$ / MW | (number average) molecular weight |
| MRI | magnetic resonance imaging |
| MS | mesoporous silica |
| mTEG(M)A | methoxy tri(ethylene glycol) (meth)acrylate |
| MWCO | molecular weight cutoff |
| N-Asn | N-substituted α/β-asparagines |
| NBA | 2-nitrobenzylacrylate |

| | |
|---|---|
| NCAs | N-carboxyanhydrides |
| NDM(M)Am | N-(2,2-dimethyl-1,3-dioxan-5-yl) (meth)acrylamide |
| NEAA | non-essential amino acids |
| NHS | N-hydroxysuccinimide |
| NIPAAm | N-isopropylacrylamide |
| NMR | nuclear magnetic resonance |
| NO | nitric oxide |
| NP | nanoparticle |
| NTAs | N-thiocarboxyanhydrides |
| NVBA | N-vinylbutyramide |
| NVF | N-vinylformamide |
| NVIBA | N-vinylisobutyramide |
| OEA | orthoester amide |
| OEG | oligo(ethylene glycol) |
| OEG(M)A | oligo(ethylene glycol) methyl ether (meth)acrylate |
| OVA | ovalbumin |
| PAMPs | pathogen-associated molecular patterns |
| PBS | phosphate buffered saline |
| PCEs | poly(carbonate-ether)s |
| PCL | poly(ε-caprolactone) |
| PD-(L)1 | programmed death-(ligand) 1 |
| PDI | polydispersity index |
| PDS | pyridyl disulfide |
| PEG | poly(ethylene glycol) |
| PEGD(M)A | poly(ethylene glycol) di(meth)acrylates |
| $PEG^{MAL}$ | maleimide-functionalized poly(ethylene glycol) |
| $PEG^{SH}$ | thiol-functionalized poly(ethylene glycol) |
| PEI | poly(ethyleneimine) |
| PEO | poly(ethylene oxide) |
| PFP | pentafluorophenyl |
| PFPMA | pentafluorophenyl methacrylate |

| | |
|---|---|
| PGL | propargyl glycolide |
| Phe | phenyl alanine |
| PISA | polymerization-induced self-assembly |
| PKA | protein kinase A |
| PLA | poly(lactic acid) |
| PLGA | poly(D,L-lactide-*co*-glycolide) |
| $PMA^{PDA}$ | pyridine dithioethylamine-modified poly(methacrylic acid) |
| $PMA^{SH}$ | cysteamine-modified poly(methacrylic acid) |
| PMMA | poly(methylmethacrylate) |
| PPE | poly(phosphoesters) |
| PPO | poly(propylene oxide)- |
| PRRs | pattern recognition receptors |
| PS | propylene sulfide |
| pTHAM | 5-acrylamido-5-hydroxymethyl-2,2-dimethyl-1,3-dioxane |
| PTMC | poly(trimethylene carbonate)s |
| PTX | paclitaxel |
| RAFT | reversible addition-fragmentation chain transfer |
| RNA | ribonucleic acid |
| ROP | ring-opening polymerization |
| ROS | reactive oxygen species |
| RP | radical polymerization |
| RPMI | roswell park memorial institute medium |
| SA | succinic anhydride |
| SATP | N-succinimidyl-S-acetylthiopropionate |
| SDS-PAGE | sodium dodecyl sulfate-polyacrylamide gel electrophoresis |
| SEC | size exclusion chromatography |
| SET-LRP | single-electron transfer living radical copolymerization |
| SI | succinimide |
| siRNA | short interfering RNA |
| SPAAC | strain-promoted azide–alkyne cycloadditions |
| STED | stimulated emission depletion microscopy |

| | |
|---|---|
| STORM | stochastic optical reconstruction microscopy |
| TAAg | tumor-associated antigens |
| TCEP | tris(2-carboxyethyl)phosphine |
| $T_{cp}$ | cloud point temperature |
| TCR | T cell receptor |
| TEGEA | ethoxy tri(ethylene glycol) acrylate |
| TEM | transmission electron microscopy |
| Th cells | T-helper cells |
| THAM | tris(hydroxymethyl) acrylamidomethane |
| THF | tetrahydrofuran |
| THP | tetrahydropyran |
| TIRF | total internal reflection fluorescence |
| TLRs | toll-like receptors |
| TMR | tetramethylrhodamine |
| TMS | tetramethylsilane |
| tNEA | trans-N-(2-ethoxy-1,3-dioxan-5-yl)acrylamide |
| UV-Vis | Ultraviolet–visible spectroscopy |
| VA-044 | 2,2’-azobis[2-(2-imidazolin-2-yl)propane] dihydrochloride |
| VAm | vinylamine |
| VS | vinyl sulfone |

# Outline and aim of this thesis

Delivering tumour-associated antigens (TAAg) to dendritic cells (DCs), the most potent class of antigen presenting cells (APCs) of our immune system, has emerged as a promising anti-cancer therapy by harnessing patients' own immune system at recognizing and eliminating metastatic growth. Currently, several clinical trials obtain promising results with adoptive transfer of DCs and T cells that were conditioned ex vivo with TAAg. An even more viable approach, with broader clinical feasibility, is direct in vivo delivery of peptide- or protein-based TAAg to DCs in combination with specific immune-activating stimuli. The major bottleneck of this approach is the lack of efficiency, upon administration, of TAAg to reach and activate DCs. Indeed, due to their small size and low immunogenicity, peptides rapidly diffuse in the body, bind to randomly encountered MHCI molecules and are incapable of providing DCs with the correct stimuli to steer the immune response towards the induction of cytotoxic T cells (CTLs) that can recognize and kill cancer cells. Thus, there is a clear need to investigate how TAAg and immune-activating stimuli can be delivered more efficiently to DCs. This need will become even more urgent with the emergence of personalized medicine, which involves mutanome analysis of individual patients to identify neoantigens that are uniquely expressed by tumours of specific patients. As these can vary in composition and physicochemical properties, it is of great interest to develop a generic vaccine design platform that can cope with these heterogeneities.

With respect to the improvement of CTL responses, molecular adjuvants have been developed that bind to pathogen recognition receptors (PRR) – such as Toll-like receptors (TLRs) – which are expressed on the cell surface or endosomal membrane of DCs. Among the different TLR agonists that are under investigation, agonists for TLR7/8 are highly promising as their receptors are found on a broad spectrum of APC subsets, both in mice and in humans. In addition, whereas TLR7/8 receptors from the evolutionary point of view recognize single stranded RNA from infecting viruses, synthetic small molecule TLR7/8 agonists – such as imidazoquinolines – have been developed that strongly activate DCs to promote Th1-type immune responses. However, a major hurdle that hampers successful clinical translation of these components is the systemic inflammation caused when they

enter systemic circulation. Especially in immune-compromised and weakened patients, such systemic inflammation should be avoided at all costs.

The aim of this thesis is the exploration of a materials chemistry approach to engineer the immune system by developing well-defined polymeric materials that can accommodate vaccine antigens and immune-modulatory components, and delivery these to DCs. From the materials chemistry side, efforts will focus on elucidating optimal conjugation strategies to link polymers to proteins, assemble proteins and polymers into nanoparticles, and formulate molecular adjuvants in polymeric nanoparticles. From the immunological side, efforts will focus on elucidating the *in vitro* and *in vivo* behaviour of the developed systems.

In **Chapter 1**, a brief introduction is given on the workings of the immune system, alongside the opportunities for nanotechnology to engineer the immune system. Delivering antigens formulated as nano- or microparticles can dramatically enhance priming of naïve T and B lymphocytes. This can be attributed to their high tissue mobility and efficient passive transport to the draining lymph nodes, and the promotion of cross-presentation. Moreover, the evoked adaptive immune responses can be further improved by co-delivery of potent immune-modulators.

In **Chapter 2**, an extensive overview is given on transiently thermoresponsive polymers. In the following chapters, this class of polymers will be used to generate polymer-protein conjugates with temperature-triggered self-assembly and acid-triggered disassembly behaviour.

**Chapters 3-5** deal with different strategies for the design of such polymer-protein conjugates. Polymer-protein conjugation has received increasing interest owing to the ability to engineer proteins with a wide variety of properties, by simply coupling protein-reactive polymers to certain amino acid residues. Controlled radical polymerization such as reversible addition-fragmentation chain transfer (RAFT) polymerization offers an excellent tool to synthesize polymers with well-defined composition, chain length, narrow dispersity and functional end groups that can be used for protein conjugation.

In **Chapter 3**, four different protein-reactive RAFT chain transfer agents (CTAs) are prepared containing either a N-hydroxysuccinimide (NHS) or pentafluorophenyl (PFP) ester moiety that can conjugate to lysine residues, and alternatively a maleimide or pyridyl disulfide (PDS) moiety for conjugation to cysteine residues. In **Chapter 4**, a head-tot-head comparison of these different conjugation strategies is performed in their bioconjugation

efficiency to albumin via a 'grafting-to' approach. To this end, both hydrophilic model polymers as well as transiently thermoresponsive polymers are used. In addition, the applicability of strain-promoted azide–alkyne cycloadditions (SPAAC) for the conjugation of azide-functionalized protein to cyclooctyne-containing polymers is explored.

In **Chapter 5**, we elaborate on a 'grafting-from' approach as an alternative strategy for the synthesis of polymer-protein conjugates. The major advantage of this method is that the obtained polymer-protein conjugates do not have to be purified from unreacted polymer, which is often tedious and requires preparative gel filtration chromatography. Here, the polymer chain is grown directly from a protein that is modified with a CTA. By polymerizing a transiently thermoresponsive polymer from the protein surface, conjugates are obtained with temperature-triggered self-assembly and acid-triggered disassembly behavior. Moreover hydrophobic compounds including immune-modulating compounds can be encapsulated into the core of these self-assembled globules.

As it remains unclear whether non-covalently assembled nanoparticles remain intact *in vivo*, it is of interest to develop covalently linked nanostructures with increased stability. In **Chapter 6**, we therefore investigate the effect of surface chemistry on the *in vitro* and *in vivo* immune-biological behavior of covalently bound hydrogel nanoparticles. In addition, we explore the applicability of super resolution microscopy for imaging the intracellular fate of such nanoparticles.

In **Chapter 7**, we introduce a versatile nanogel system based on a RAFT-based block copolymer containing a solvophylic poly(ethylene glycol)-like block and a solvophobic activated ester block. The latter allows for core-crosslinking and various functionalizations with amine-containing compounds. This was demonstrated by dialing in a TLR agonist, that yielded nanogels with alluring properties in view of vaccine applications. Moreover, the nanogels were rendered protein-reactive by introducing vinyl sulfone moieties at the chain ends of the RAFT polymers upon post-polymerization aminolysis of the thiocarbonyl group.

A discussion of the results obtained in this thesis in view of the broader international context is given in **Chapter 8**. In addition, we highlight some future developments that are expected in this field of research. Finally, a general conclusion and brief summary can be found in **Chapter 9**.

# PART I

## General introduction & background

# Chapter 1

# The immune system and vaccine development

## The immune system

Our immune system plays a critical role in providing protection against microbial attack and possibly against the development of tumors. Upon their invasion of epithelial cells, pathogens can bind receptors on innate immune cells (e.g. neutrophils and macrophages) that recognize conserved molecular motifs characteristic of bacteria, viruses and fungi. This enables innate immune cells to quickly phagocytose (i.e. internalize) pathogens and secrete reactive oxygen species or cytokines, providing an immediate but relatively non-specific antimicrobial and inflammatory defense. In addition to this conserved innate immune system, the adaptive immune system provides a more specific and long-term defense mechanism. It is comprised of B cells and T cells that express a large diversity of clonal antigen receptors, allowing recognition of specific antigens expressed by foreign pathogens or cancer cells. Moreover, these cells can differentiate into long-lived memory cells, that elicit a rapid immune response upon re-exposure to previously encountered antigens.

Upon antigen recognition via their B cell receptor, B cells produce antibodies that bind and neutralize the ability of pathogens to invade host cells and/or promote their phagocytosis (i.e. humoral immunity). T cells by contrast, recognize antigen-derived peptides presented by antigen-presenting cells (APCs) via their T cell receptor (TCR) and differentiate into effector T cells when the appropriate signals are present. CD4 T cells differentiate into T-helper (Th) cells, that secrete cytokines to direct the immune functions of other white blood cells. CD8 T cells by contrast, differentiate into cytotoxic T cells (CTLs), which have the capacity to recognize and kill infected or transformed cells (i.e. cellular immunity). To prime a naïve T cell to become an effector T cell (Th or CTL) three signals are needed (**Figure 1**).

First, the antigen needs to be processed by antigen presenting cells (APCs) and displayed as a peptide on their surface receptors, i.e. major histocompatibility complex (MHC) molecules, to enable presentation to T cells. In this respect, two different pathways can be distinguished. In most cell types, MHCI molecules are loaded with cytosolic proteins in the endoplasmatic reticulum after cleavage by the proteasome, to allow presentation to CD8 T cells. In this way, the internal proteome of the cell is made accessible for surveillance by CTLs. The MHCII processing pathway by contrast, is restricted to professional APCs (e.g. B cells, macrophages, dendritic cells) and enables the presentation of endocytosed proteins on MHCII to CD4 T cells after degradation in endo-lysosomal compartments.[1]

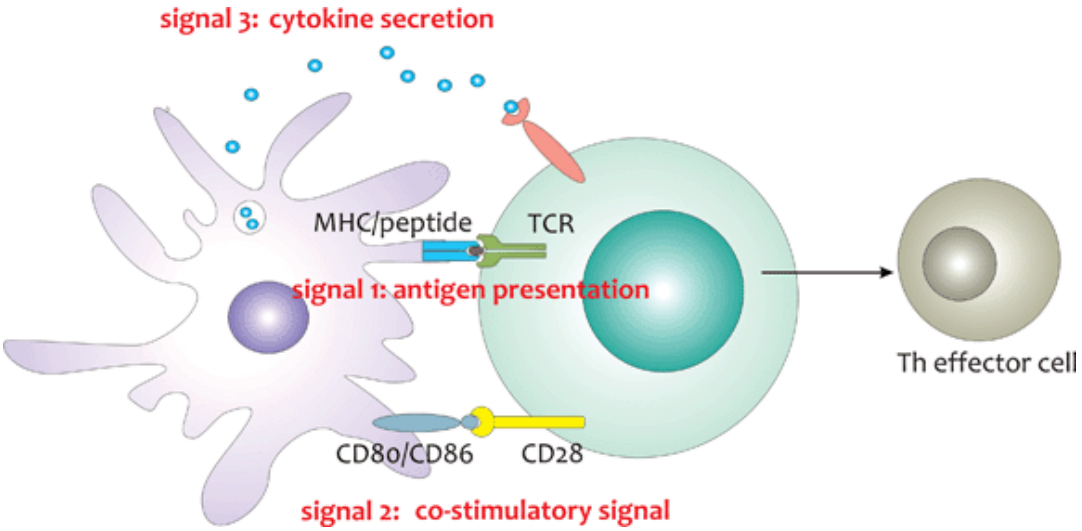


**Figure 1.** Initiation of effector T cell responses requires three signals. Stimulation of the TCR by MHC/peptide complexes delivers signal 1, interactions between co-stimulatory ligands on the APC and CD28 on the T cell provide signal 2 and the secretion of inflammatory cytokines that polarize T cell responses delivers signal 3. *Reprinted from reference 2.*

Dendritic cells (DCs) are the most potent class of APC in our immune system, with multiple subtypes displaying different functional properties.[3-5] Resident lymphoid DCs directly migrate to lymphoid tissue after their emigration from the blood and can be divided into CD8α- and CD8α+ subsets. The CD8α+ subset has been reported to be more efficient in a process called cross-presentation, in which endocytosed antigens are loaded onto MHCI molecules instead of MHCII.[6,7] This pathway is essential for the induction of CTL responses against viruses and intracellular bacteria that do not infect DCs, and against tumor growth. By contrast, CD8α- DCs are more potent in MHCII-mediated antigen presentation, and thus in the priming of CD4 T cells.[8] In addition to these resident lymphoid DCs, lymph nodes also contain DCs that have migrated from peripheral tissues, where they continuously sample antigens. Before migration to the lymph nodes however, these immature DCs have poor antigen presenting properties as they show a show a low expression of co-stimulatory ligands that are necessary for priming of naïve T cells.

Indeed, priming of naïve T cells requires a second co-stimulatory signal being delivered by the APC, in addition to antigen presentation on MHC molecules (**Figure 1**). This is mediated by interactions between the co-stimulatory ligands CD80 and CD86 on the DC and the receptor CD28 on the T cell. In case of infection, triggering of pattern recognition receptors (PRRs) on the DC surface results in upregulation of these co-stimulatory ligands and secretion of inflammatory cytokines by the activated DCs.[9] In addition, inflammatory monocytes are recruited to the site of inflammation, which subsequently differentiate into DCs that are also capable of priming CD4 and CD8 T cell responses.[9,10] Interestingly, even in absence of inflammation or infection, peripheral tissue DCs appear to mature and migrate to the lymph nodes where they present sampled antigen to naive T cells with appropriate co-stimulatory ligands. However, this process leads to tolerance rather than immunity and is an important mechanism for the maintenance of tolerance to self-antigens.[11]

Depending on the set of PRRs triggered, DCs secrete different cytokine profiles which is the third signal required for priming naïve T cells (**Figure 1**) and largely determines the nature of the induced immune response.[12,13] This pathogen-based distinction is of crucial importance to mount effective immune defenses against a variety of pathogens. PRRs typically recognize pathogen-associated molecular patterns (PAMPs) that are essential for pathogen survival and thus evolutionary conserved.[14-17] The most studied PPRs are Toll-like receptors (TLRs), that can be localized at the plasma membrane or the endosomal

membrane. The cytokine microenvironment that is generated by DCs upon PPR triggering will steer the differentiation of naïve CD4 T cell into a specific subset, following recognition of a MHCII/peptide complex. These CD4 T helper subsets include Th1 cells that activate cellular immunity responses against intracellular pathogens, and Th2 cells that promote humoral immunity.[18] More recently, Th17 cells have been identified as a new subset of T-helper cells that mediate protection against extracellular bacteria and potentially fungi.[19-21] **Figure 2** gives a simplified schematic overview to illustrate the various aspect of our immune systems described above.

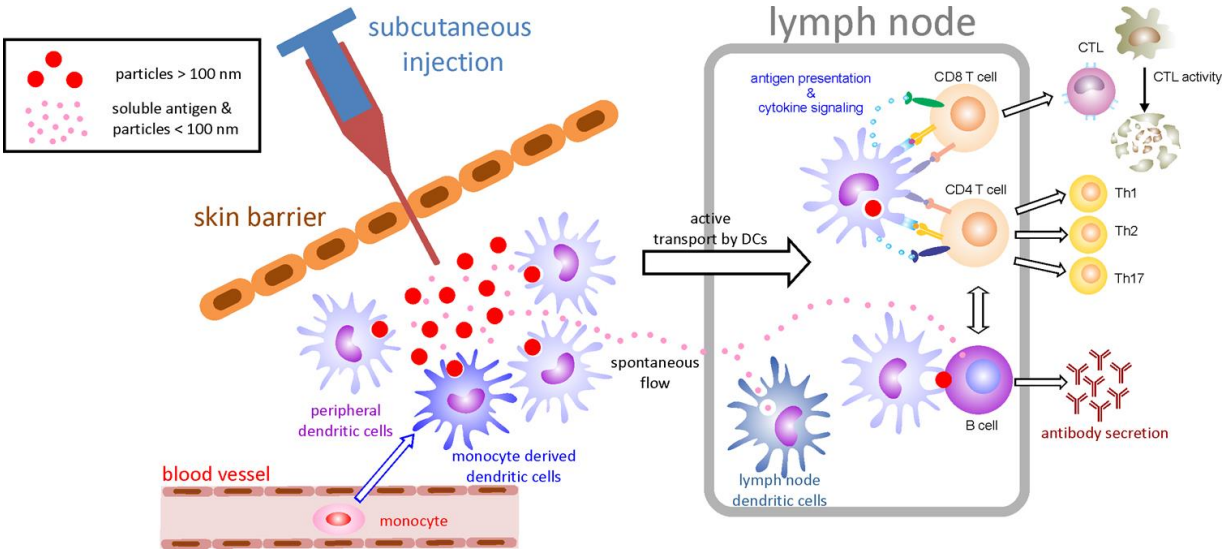


**Figure 2.** Schematic overview of the adaptive immune system.

## Nanoparticles in vaccine development[2,22]

A fundamental property of the adaptive immune system is the capacity of B-cells and T-cells to differentiate into long-lived memory cells, that will react faster and more vigorously when the same pathogen is encountered in the future. This immunological memory underlies the success of vaccination. By pre-exposing the immune system to either weakened/killed pathogens or immunogenic components of the pathogen, a fast and strong immune response can be evoked upon re-exposure to the native pathogen, ideally preventing illness. Since the pioneering work of Jenner and Pasteur over 200 years ago, vaccines have dramatically improved human health by preventing numerous infectious

diseases including smallpox, poliomyelitis and tetanus.[23,24] Nevertheless, many challenges remain.

For most prophylactic vaccines, effectiveness is measured by the ability to produce long-lasting neutralizing antibodies to block infection. However, to develop effective preventive vaccines against insidious pathogens such as human immunodeficiency virus (HIV), Plasmodium (the causative agent of malaria) and Mycobacterium tuberculosis; CD8+ T cell responses are required to act synergistically with humoral immunity to eliminate infected cells. Given the high virulence of these pathogens, vaccines composed of live attenuated strains (that typically elicit strong CD8+ T cell priming) impose serious safety issues. In this respect, entirely synthetic vaccines composed of recombinant antigens are much safer, but require the addition of molecular adjuvants due to their poor immunogenicity.

The design of vaccines that induce strong cytotoxic T cell responses is also applicable for the development of immunotherapeutic treatments of cancer and chronic viral infections such as HIV and hepatitis C virus (HCV).[25] In this regard, the use of so-called checkpoint inhibitors that block inhibitory receptors on T cells are likely to provide additional opportunities to enhance vaccine efficacy in cancer patients.[26] These include antibodies against cytotoxic T-lymphocyte antigen 4 (CTLA-4) and antibodies against programmed death-1 (PD-1) and programmed death-ligand 1 (PD-L1).

***Size-based lymph node targeting and cross-presentation***

Targeting of lymph node resident DCs is an attractive approach in view of vaccine development, as lymph nodes are the sites of lymphocyte priming by APCs and subsequent adaptive immune responses. Antigen targeting towards DCs can be obtained by coupling the antigens to antibodies or ligands specific for DC surface receptors,[27] or alternatively by delivering antigens associated with particles in the 0.1–10 μm range.[28,29] Particulates in this size range indeed mimic the dimensions of bacteria and viruses, to which DCs have evolved to react. To directly target the lymphoid DC population however, ultra-small nanoparticles (20 – 100 nm) are more effective as they rapidly reach the lymph nodes through passive drainage via the lymphatics. In contrast to these ultra-small nanoparticles, particles in the lower micron range are more tightly retained in the interstitial space and require active transport by migratory DCs to reach the lymph nodes; whilst even smaller materials will

predominately clear to the blood (**Figure 2**).[30,31] Moreover, it was found that small nanoparticles were primarily taken up by CD8α+ DCs, which are reported to be specialized in cross-presentation.[7]

The most appealing part of using particulate carriers for antigen delivery is indeed their capacity to promote cross-presentation of endocytosed exogenous antigens via the MHCI route, rather than the usual MHCII antigen processing pathway. For soluble antigens, this process appears to be dependent on their routing to stable early endosomes specialized for cross-presentation.[32,33] Targeting of antigens to these specialized compartments is mediated by binding to specific endocytotic receptors such as DEC205[27], the mannose receptor[32] and langerin[34]; which are mainly expressed on CD8α+ DCs. Nevertheless, although receptor-mediated endocytosis of soluble antigens can result in cross-presentation, the efficiency of this process is rather inefficient. Antigens delivered to DCs in a particulate form by contrast, such as viruses and bacteria, are internalized via macropinocytosis or phagocytosis and are far more efficiently cross-presented to CD8 T cells. Multiple studies have indeed demonstrated a strong increase in cross-presentation and the induction of CTL responses after antigen encapsulation in carriers that mimic the particulate nature of viruses and bacteria.[35-40]

Multiple mechanisms have been proposed as to how particles promote cross-presentation. The phagosomal escape hypothesis suggests that antigen is exported from the macropinosome or phagosome and subsequently enters the classical MHCI processing route, similar to cytosolic proteins (**Figure 3A**).[35,41] Therefore, hydrazide- or acetal-based pH-responsive particles have been developed that degrade or disassemble upon phagosomal acidification. Subsequently, their single components exert osmotic pressure on the phagosomal membrane, leading to its rupture and the release of their payload directly into the cytosol.[39,42,43] Alternatively, amine-containing polymers can exhibit a so-called *proton sponge effect,* thereby buffering the phagosomal compartment and preventing the phagosomal acidification process. The subsequent influx of protons to force acidification, induces an osmotic pressure which is also able to rupture the phagosomal membrane.[44,45]

However, phagosomes and macropinosomes might be able to recruit all the necessary machinery for MHCI-mediated antigen presentation themselves, by fusing with ER membranes.[46-48] This proposed mechanisms suggests that antigens are exported from the phagosomal lumen, processed by recruited immunoproteasomes, and re-imported into the

same phagosome for loading onto MHCI molecules (**Figure 3B**).[49] Recent evidence indicates that antigen processing and loading onto MHCI and MHCII actually occur in the same phagosome but at distinct time intervals following particle internalization, mediated by variations in the phagosomal pH. In this respect, initial active alkalization of the phagosome appears to be crucial for MHCI loading by preventing activation of lysosomal proteases and consequently rescuing antigens from fast processing for MHCII loading.[50,51]

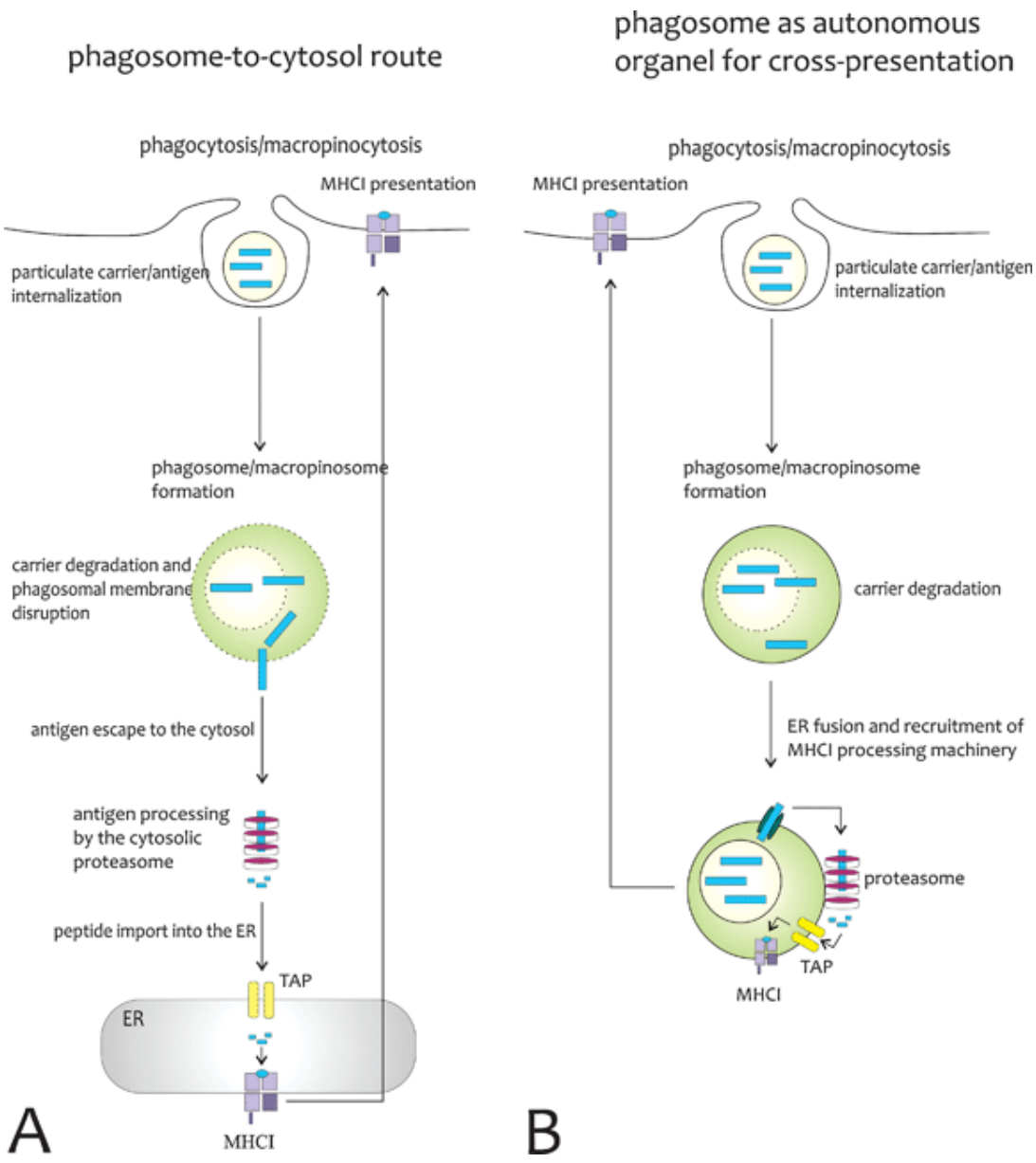


**Figure 3.** Proposed mechanisms for antigen cross-presentation, mediated by particulate carriers. **(A)** Phagosome-to-cytosol route for cross-presentation. **(B)** Phagosomes as fully competent organelles for cross-presentation. *Reprinted from reference 2.*

In literature, several conflicting observations have been reported regarding the optimal particle size to promote cross-presentation.[38,52-54] Although microparticles might be intrinsically superior in promoting antigen processing towards the MHCI route, upon subcutaneous injection they are primarily taken up by other phagocytic cells (e.g. macrophages) rather than by DCs. As a result, microparticles generally target fewer DCs *in vivo* compared to nanoparticles, that passively migrate to the draining lymph node via the lymphatics. Therefore, strategies that allow microparticle targeting to DCs might result in superior cross-presentation. In this respect, particulate carriers can be modified with antibodies or ligands specific for DC surface markers and endocytosis receptors, including anti-CD11c antibody derivatives[55,56], anti-DEC205 antibodies[56,57] and anti-CD40 antibodies[56,58].

***Nanoparticles as adjuvants***

As most recombinant antigens fail to activate DCs, they require the addition of adjuvants that can enhance the intrinsic immunogenicity of the antigen *in vivo*. Most adjuvants, including the widely used aluminum hydroxide[59], have been derived empirically based on their capacity to increase adaptive immune responses to co-delivered antigens, but their mode of action remained elusive for a long time.[60] Only recently, it was found that at least part of the adjuvant properties of aluminum hydroxide can be attributed to formation of the NALP3 inflammasome and the subsequent release of the potent pro-inflammatory cytokine IL-1β.[59,61-65] NALP3 belongs to a class of cytosolic PRRs that can be triggered by various endogenous and microbial danger signals and mediates inflammatory responses.[66] Interestingly, particulate adjuvants also appear to activate the NALP3 inflammasome, which seems crucial for the activation of cellular immune responses.[63,67] For humoral immune responses however, NALP3 activation was completely dispensable, suggesting that additional pathways must be involved in the adjuvant properties of particulates. Proposed mechanisms are interactions with dendritic cell membrane lipids that promote antigen uptake, and induction of cell death with subsequent release of host cell DNA. [68,69]

Although the particulate nature of delivery vehicles might be sufficient to be recognized by the immune system as intrinsically dangerous via inflammasome activation, most particulates are only poor activators of DCs. Moreover, classical adjuvants largely fail to activate the cellular arm of the immune response, making them ineffective against many

intracellular pathogens. Consequently, there is an urgent need to develop new adjuvants that also allow the induction of Th1, Th17 and CTL responses. In this regard, co-delivery of particulate antigen formulations with PRR agonists might work synergistic in evoking potent immune responses.[70-74] Moreover, particulate delivery of PPR agonists significantly reduces inflammatory toxicity that is generally associated with the use of immune potentiators, by limiting their systemic distribution.[75-77] Most of the PAMP mimics currently tested are TLR agonists that, in contrast to aluminum salts, have the capacity to steer DCs to activate Th1 and CTL responses.[78-81] Co-administration of antigen carriers and TLR agonists can be achieved by either mere co-injection, or by physical association of the TLR agonist and the carrier via surface adsorption and encapsulation. Recent data clearly indicate that the latter strategy is superior in inducing strong effector T cell responses.[82-87] Moreover, the selection of specific functional ligands might also allow to steer the immune response towards the desired direction, e.g. Th1 or Th17 skewed responses.

Although the benefits of co-encapsulating antigen and TLR agonist in microparticles have clearly been demonstrated, the encapsulation process itself remains a challenging task. Developing polymeric particles with strong intrinsic immune activating properties could alleviate these complex procedures. In this regard, a promising approach might be the use of biomaterials that activate the complement system. This ancient component of the immune system provides a direct biochemical defense mechanism to kill and opsonize microorganisms, but can also activate adaptive immune responses. Literature has shown that activation of the complement by nanoparticles is dependent on their surface chemistry. Biomaterials containing high levels of free hydroxyls and amine nucleophiles for example, strongly activate the complement cascade.[88] Alternatively, intrinsic adjuvant capacity of nanoparticles might be derived from their hydrophobicity, which might be an important conserved danger signal.[89,90] Unfolded proteins, microbes and dying cells indeed all possess hydrophobic properties.

## References


1 Jensen, P. E. Recent advances in antigen processing and presentation. *Nat Immunol* **8**, 1041-1048 (2007).

2 De Koker, S. *et al.* Designing polymeric particles for antigen delivery. *Chem. Soc. Rev.* **40**, 320-339 (2011).

3 Banchereau, J. *et al.* Immunobiology of dendritic cells. *Annu. Rev. Immunol.* **18**, 767-+ (2000).

4 Heath, W. R. *et al.* Cross-presentation, dendritic cell subsets, and the generation of immunity to cellular antigens. *Immunological Reviews* **199**, 9-26 (2004).

5 Banchereau, J. & Steinman, R. M. Dendritic cells and the control of immunity. *Nature* **392**, 245-252 (1998).

6 den Haan, J. M. M., Lehar, S. M. & Bevan, M. J. Cd8+ but Not Cd8− Dendritic Cells Cross-Prime Cytotoxic T Cells in Vivo. *The Journal of Experimental Medicine* **192**, 1685-1696 (2000).

7 Dudziak, D. *et al.* Differential Antigen Processing by Dendritic Cell Subsets in Vivo. *Science* **315**, 107-111 (2007).

8 Lin, M.-L. *et al.* The cell biology of cross-presentation and the role of dendritic cell subsets. *Immunol Cell Biol* **86**, 353-362 (2008).

9 Segura, E. & Villadangos, J. A. Antigen presentation by dendritic cells in vivo. *Current Opinion in Immunology* **21**, 105-110 (2009).

10 Leon, B. & Ardavin, C. Monocyte-derived dendritic cells in innate and adaptive immunity. *Immunol Cell Biol* **86**, 320-324 (2008).

11 Luckashenak, N. *et al.* Constitutive Crosspresentation of Tissue Antigens by Dendritic Cells Controls CD8+ T Cell Tolerance In Vivo. *Immunity* **28**, 521-532 (2008).

12 Pulendran, B. Modulating vaccine responses with dendritic cells and Toll-like receptors. *Immunological Reviews* **199**, 227-250 (2004).

13 Pulendran, B., Palucka, K. & Banchereau, J. Sensing Pathogens and Tuning Immune Responses. *Science* **293**, 253-256 (2001).

14 Kabelitz, D. & Medzhitov, R. Innate immunity — cross-talk with adaptive immunity through pattern recognition receptors and cytokines. *Current Opinion in Immunology* **19**, 1-3 (2007).

15 Medzhitov, R. Recognition of microorganisms and activation of the immune response. *Nature* **449**, 819-826 (2007).

16 Medzhitov, R. & Janeway, C., Jr. Innate immune recognition: mechanisms and pathways. *Immunological Reviews* **173**, 89-97 (2000).

17 Pasare, C. & Medzhitov, R. Toll-like receptors and acquired immunity. *Seminars in Immunology* **16**, 23-26 (2004).

18 Bottomly, K. A functional dichotomy in CD4+ T lymphocytes. *Immunology Today* **9**, 268-274 (1988).

19 Huang, W. *et al.* Requirement of Interleukin-17A for Systemic Anti-Candida albicans Host Defense in Mice. *Journal of Infectious Diseases* **190**, 624-631 (2004).

20 Harrington, L. E., Mangan, P. R. & Weaver, C. T. Expanding the effector CD4 T-cell repertoire: the Th17 lineage. *Current Opinion in Immunology* **18**, 349-356 (2006).

21 van de Veerdonk, F. L. *et al.* Th17 responses and host defense against microorganisms: an overview. *BMB reports* **42**, 776-787 (2009).

22 Irvine, D. J. *et al.* Synthetic Nanoparticles for Vaccines and Immunotherapy. *Chemical Reviews* **115**, 11109-11146 (2015).

23 Rappuoli, R., Miller, H. I. & Falkow, S. The Intangible Value of Vaccination. *Science* **297**, 937-939 (2002).

24 Irvine, D. J., Swartz, M. A. & Szeto, G. L. Engineering synthetic vaccines using cues from natural immunity. *Nat Mater* **12**, 978-990 (2013).

25 Rappuoli, R. Bridging the knowledge gaps in vaccine design. *Nat Biotech* **25**, 1361-1366 (2007).

26 Pardoll, D. M. The blockade of immune checkpoints in cancer immunotherapy. *Nat Rev Cancer* **12**, 252-264 (2012).

27 Bonifaz, L. *et al.* Efficient Targeting of Protein Antigen to the Dendritic Cell Receptor DEC-205 in the Steady State Leads to Antigen Presentation on Major Histocompatibility Complex Class I Products and Peripheral CD8+ T Cell Tolerance. *The Journal of Experimental Medicine* **196**, 1627-1638 (2002).

28 O'Hagan, D. T. & Singh, M. Microparticles as vaccine adjuvants and delivery systems. *Expert Review of Vaccines* **2**, 269-283 (2003).

29 O'Hagan, D. T., Singh, M. & Ulmer, J. B. Microparticle-based technologies for vaccines. *Methods* **40**, 10-19 (2006).

30 Reddy, S. T. *et al.* Exploiting lymphatic transport and complement activation in nanoparticle vaccines. *Nat. Biotechnol.* **25**, 1159-1164 (2007).

31 Kaminskas, L. M. & Porter, C. J. H. Targeting the lymphatics using dendritic polymers (dendrimers). *Adv. Drug Deliv. Rev.* **63**, 890-900 (2011).

32 Burgdorf, S. *et al.* Distinct Pathways of Antigen Uptake and Intracellular Routing in CD4 and CD8 T Cell Activation. *Science* **316**, 612-616 (2007).

33 Burgdorf, S. *et al.* Spatial and mechanistic separation of cross-presentation and endogenous antigen presentation. *Nat Immunol* **9**, 558-566 (2008).

34 Idoyaga, J. *et al.* Cutting Edge: Langerin/CD207 Receptor on Dendritic Cells Mediates Efficient Antigen Presentation on MHC I and II Products In Vivo. *The Journal of Immunology* **180**, 3647-3650 (2008).

35 Shen, H. *et al.* Enhanced and prolonged cross-presentation following endosomal escape of exogenous antigens encapsulated in biodegradable nanoparticles. *Immunology* **117**, 78-88 (2006).

36 Partidos, C. D. *et al.* Induction of cytotoxic T-cell responses following oral immunization with synthetic peptides encapsulated in PLG microparticles. *J. Control. Release* **62**, 325-332 (1999).

37 Ataman-Önal, Y. *et al.* Surfactant-free anionic PLA nanoparticles coated with HIV-1 p24 protein induced enhanced cellular and humoral immune responses in various animal models. *J. Control. Release* **112**, 175-185 (2006).

38 Tran, K. K. & Shen, H. The role of phagosomal pH on the size-dependent efficiency of cross-presentation by dendritic cells. *Biomaterials* **30**, 1356-1362 (2009).

39 Murthy, N. *et al.* A macromolecular delivery vehicle for protein-based vaccines: Acid-degradable protein-loaded microgels. *Proceedings of the National Academy of Sciences* **100**, 4995-5000 (2003).

40 De Koker, S. *et al.* Polyelectrolyte Microcapsules as Antigen Delivery Vehicles To Dendritic Cells: Uptake, Processing, and Cross-Presentation of Encapsulated Antigens. *Angewandte Chemie International Edition* **48**, 8485-8489 (2009).

41 PANYAM, J. *et al.* Rapid endo-lysosomal escape of poly(dl-lactide-co-glycolide) nanoparticles: implications for drug and gene delivery. *The FASEB Journal* **16**, 1217-1226 (2002).

42 Haining, W. N. *et al.* pH-Triggered Microparticles for Peptide Vaccination. *The Journal of Immunology* **173**, 2578-2585 (2004).

43 Murthy, N. *et al.* A Novel Strategy for Encapsulation and Release of Proteins: Hydrogels and Microgels with Acid-Labile Acetal Cross-Linkers. *J. Am. Chem. Soc.* **124**, 12398-12399 (2002).

44 Hu, Y. *et al.* Cytosolic Delivery of Membrane-Impermeable Molecules in Dendritic Cells Using pH-Responsive Core−Shell Nanoparticles. *Nano Letters* **7**, 3056-3064 (2007).

45 Hu, Y. *et al.* Cytosolic Delivery Mediated via Electrostatic Surface Binding of Protein, Virus, or siRNA Cargos to pH-Responsive Core−Shell Gel Particles. *Biomacromolecules* **10**, 756-765 (2009).

46 Ackerman, A. L. *et al.* Early phagosomes in dendritic cells form a cellular compartment sufficient for cross presentation of exogenous antigens. *Proceedings of the National Academy of Sciences* **100**, 12889-12894 (2003).

47 Guermonprez, P. *et al.* ER-phagosome fusion defines an MHC class I cross-presentation compartment in dendritic cells. *Nature* **425**, 397-402 (2003).

48 Houde, M. *et al.* Phagosomes are competent organelles for antigen cross-presentation. *Nature* **425**, 402-406 (2003).

49 Burgdorf, S. & Kurts, C. Endocytosis mechanisms and the cell biology of antigen presentation. *Current Opinion in Immunology* **20**, 89-95 (2008).

50 Savina, A. *et al.* NOX2 Controls Phagosomal pH to Regulate Antigen Processing during Crosspresentation by Dendritic Cells. *Cell* **126**, 205-218 (2006).

51 Jancic, C. *et al.* Rab27a regulates phagosomal pH and NADPH oxidase recruitment to dendritic cell phagosomes. *Nat Cell Biol* **9**, 367-378 (2007).

52 Fifis, T. *et al.* Size-Dependent Immunogenicity: Therapeutic and Protective Properties of Nano-Vaccines against Tumors. *The Journal of Immunology* **173**, 3148-3154 (2004).

53 Lee, I.-H. *et al.* Imageable Antigen-Presenting Gold Nanoparticle Vaccines for Effective Cancer Immunotherapy In Vivo. *Angewandte Chemie International Edition* **51**, 8800-8805 (2012).

54 Ahn, S. *et al.* Gold Nanoparticles Displaying Tumor-Associated Self-Antigens as a Potential Vaccine for Cancer Immunotherapy. *Adv. Healthc. Mater.* **3**, 1194-1199 (2014).

55 van Broekhoven, C. L. *et al.* Targeting Dendritic Cells with Antigen-Containing Liposomes: A Highly Effective Procedure for Induction of Antitumor Immunity and for Tumor Immunotherapy. *Cancer Research* **64**, 4357-4365 (2004).

56 Cruz, L. J. *et al.* Targeting nanoparticles to CD40, DEC-205 or CD11c molecules on dendritic cells for efficient CD8+ T cell response: A comparative study. *J. Control. Release* **192**, 209-218 (2014).

57 Kwon, Y. J. *et al.* In vivo targeting of dendritic cells for activation of cellular immunity using vaccine carriers based on pH-responsive microparticles. *Proc. Natl. Acad. Sci. U. S. A.* **102**, 18264-18268 (2005).

58 Rosalia, R. A. *et al.* CD40-targeted dendritic cell delivery of PLGA-nanoparticle vaccines induce potent anti-tumor responses. *Biomaterials* **40**, 88-97 (2015).

59 Lambrecht, B. N. *et al.* Mechanism of action of clinically approved adjuvants. *Current Opinion in Immunology* **21**, 23-29 (2009).

60 De Gregorio, E., Tritto, E. & Rappuoli, R. Alum adjuvanticity: Unraveling a century old mystery. *European Journal of Immunology* **38**, 2068-2071 (2008).

61 Kool, M. *et al.* Alum adjuvant boosts adaptive immunity by inducing uric acid and activating inflammatory dendritic cells. *The Journal of Experimental Medicine* **205**, 869-882 (2008).

62 Li, H., Nookala, S. & Re, F. Aluminum Hydroxide Adjuvants Activate Caspase-1 and Induce IL-1β and IL-18 Release. *The Journal of Immunology* **178**, 5271-5276 (2007).

63 Li, H. *et al.* Cutting Edge: Inflammasome Activation by Alum and Alum's Adjuvant Effect Are Mediated by NLRP3. *The Journal of Immunology* **181**, 17-21 (2008).

64 Eisenbarth, S. C. *et al.* Crucial role for the Nalp3 inflammasome in the immunostimulatory properties of aluminium adjuvants. *Nature* **453**, 1122-1126 (2008).

65 de Zoete, M. R. *et al.* Inflammasomes. *Cold Spring Harbor Perspectives in Biology* **6** (2014).

66 Kool, M. *et al.* Cutting Edge: Alum Adjuvant Stimulates Inflammatory Dendritic Cells through Activation of the NALP3 Inflammasome. *The Journal of Immunology* **181**, 3755-3759 (2008).

67 Sharp, F. A. *et al.* Uptake of particulate vaccine adjuvants by dendritic cells activates the NALP3 inflammasome. *Proceedings of the National Academy of Sciences* **106**, 870-875 (2009).

68 Flach, T. L. *et al.* Alum interaction with dendritic cell membrane lipids is essential for its adjuvanticity. *Nat Med* **17**, 479-487 (2011).

69 Marichal, T. *et al.* DNA released from dying host cells mediates aluminum adjuvant activity. *Nat Med* **17**, 996-1002 (2011).

70 Baldridge, J. R. *et al.* Taking a Toll on human disease: Toll-like receptor 4 agonists as vaccine adjuvants and monotherapeutic agents. *Expert Opinion on Biological Therapy* **4**, 1129-1138 (2004).

71 Celis, E. Toll-like Receptor Ligands Energize Peptide Vaccines through Multiple Paths. *Cancer Research* **67**, 7945-7947 (2007).

72 Persing, D. H. *et al.* Taking toll: lipid A mimetics as adjuvants and immunomodulators. *Trends in Microbiology* **10**, s32-s37 (2002).

73 Schijns, V. E. J. C. & Degen, W. G. J. Vaccine Immunopotentiators of the Future. *Clinical Pharmacology & Therapeutics* **82**, 750-755 (2007).

74 Thompson, B. S. *et al.* The low-toxicity versions of LPS, MPL® adjuvant and RC529, are efficient adjuvants for CD4+ T cells. *Journal of leukocyte biology* **78**, 1273-1280 (2005).

75 Lingnau, K. *et al.* Poly-l-arginine synergizes with oligodeoxynucleotides containing CpG-motifs (CpG-ODN) for enhanced and prolonged immune responses and prevents the CpG-ODN-induced systemic release of pro-inflammatory cytokines. *Vaccine* **20**, 3498-3508 (2002).

76 Smirnov, D. *et al.* Vaccine adjuvant activity of 3M-052: An imidazoquinoline designed for local activity without systemic cytokine induction. *Vaccine* **29**, 5434-5442 (2011).

77 Ilyinskii, P. O. *et al.* Adjuvant-carrying synthetic vaccine particles augment the immune response to encapsulated antigen and exhibit strong local immune activation without inducing systemic cytokine release. *Vaccine* **32**, 2882-2895 (2014).

78 Pashine, A., Valiante, N. M. & Ulmer, J. B. Targeting the innate immune response with improved vaccine adjuvants. *Nat Med* (2005).

79 Chu, R. S. *et al.* CpG Oligodeoxynucleotides Act as Adjuvants that Switch on T Helper 1 (Th1) Immunity. *The Journal of Experimental Medicine* **186**, 1623-1631 (1997).

80 Napolitani, G. *et al.* Selected Toll-like receptor agonist combinations synergistically trigger a T helper type 1-polarizing program in dendritic cells. *Nat Immunol* **6**, 769-776 (2005).

81 Heit, A. *et al.* Protective CD8 T Cell Immunity Triggered by CpG-Protein Conjugates Competes with the Efficacy of Live Vaccines. *The Journal of Immunology* **174**, 4373-4380 (2005).

82 Blander, J. M. Coupling Toll-like receptor signaling with phagocytosis: potentiation of antigen presentation. *Trends in Immunology* **28**, 19-25 (2007).

83 Blander, J. M. & Medzhitov, R. Toll-dependent selection of microbial antigens for presentation by dendritic cells. *Nature* **440**, 808-812 (2006).

84 Schlosser, E. *et al.* TLR ligands and antigen need to be coencapsulated into the same biodegradable microsphere for the generation of potent cytotoxic T lymphocyte responses. *Vaccine* **26**, 1626-1637 (2008).

85 Westwood, A. *et al.* Immunological responses after immunisation of mice with microparticles containing antigen and single stranded RNA (polyuridylic acid). *Vaccine* **24**, 1736-1743 (2006).

86 Kazzaz, J. *et al.* Encapsulation of the immune potentiators MPL and RC529 in PLG microparticles enhances their potency. *J. Control. Release* **110**, 566-573 (2006).

87 Heit, A. *et al.* Antigen co-encapsulated with adjuvants efficiently drive protective T cell immunity. *European Journal of Immunology* **37**, 2063-2074 (2007).

88 Reddy, S. T. *et al.* Exploiting lymphatic transport and complement activation in nanoparticle vaccines. *Nat Biotech* **25**, 1159-1164 (2007).

89 Seong, S.-Y. & Matzinger, P. Hydrophobicity: an ancient damage-associated molecular pattern that initiates innate immune responses. *Nat Rev Immunol* **4**, 469-478 (2004).

90 Moyano, D. F. *et al.* Nanoparticle Hydrophobicity Dictates Immune Response. *J. Am. Chem. Soc.* **134**, 3965-3967 (2012).

# Chapter 2

# Transiently thermoresponsive polymers and their applications in biomedicine

## Introduction

Stimuli-responsive polymers are capable to undergo significant physical or chemical changes in response to small variations in the external environmental conditions. These variations can be classified as either physical stimuli including temperature, electric/magnetic fields and mechanical pressure, or chemical stimuli such as pH, ionic factors or chemical agents. In some examples, two or more stimuli-responsive mechanisms can be combined into one polymer system. In this chapter we introduce the term *transiently thermoresponsive polymers* for polymers that gradually alter their temperature-responsive behavior upon contact with another external stimulus. Typically, these thermoresponsive polymers bear additional stimuli-responsive moieties (to e.g. water, pH, light, reduction/oxidation) located in the polymer backbone or in the side chain that, upon cleavage, induce a permanent shift in the cloud point temperature ($T_{cp}$; i.e. the temperature at which the polymers transition from soluble to globular occurs). This class of polymers possess attractive properties for advanced applications in biomedicine.

For instance, block copolymers with a thermoresponsive segment have the ability to self-assemble into nanoparticles when aqueous solutions of these polymers are heated above their $T_{cp}$ (**Figure 1**).[1,2] These systems yield micellar drug delivery vehicles through self-assembly in aqueous media, thereby avoiding the use of harmful organic solvents for solubilization and subsequent solvent displacement. By engineering these polymers to lose their thermoresponsive behavior at body temperature upon contact with another external trigger within a physiologically relevant window, they can become fully water soluble and can be excreted from the body by renal clearance. Moreover, this hydrophobic-to-hydrophilic transformation and subsequent micellar destabilization can be exploited to release a therapeutic payload that is encapsulated within the hydrophobic core of these nanoparticles.[3-5] Alternatively the $T_{cp}$ of double-hydrophilic block copolymers comprising a thermoresponsive segment can be fine-tuned just above body temperature, which has been used for site-specific drug release upon locally induced hyperthermia that causes collapse of the thermoresponsive block and subsequent structural distortion of the micellar nanocarriers.[2-4]

Often, these transiently thermoresponsive polymer systems are used as biodegradable *in situ* reverse thermogelling injectables. An aqueous solution of this type of polymer is a free-flowing sol at room temperature, allowing homogeneous mixing of a therapeutic payload. Upon injection, sol-to-gel transition generates a synthetic tissue matrix or drug depot at body temperature. Moreover, this method avoid invasive surgery for implantation and allows formulation of therapeutically fragile macromolecules (e.g. DNA, RNA and proteins) at low temperature.[6-8]

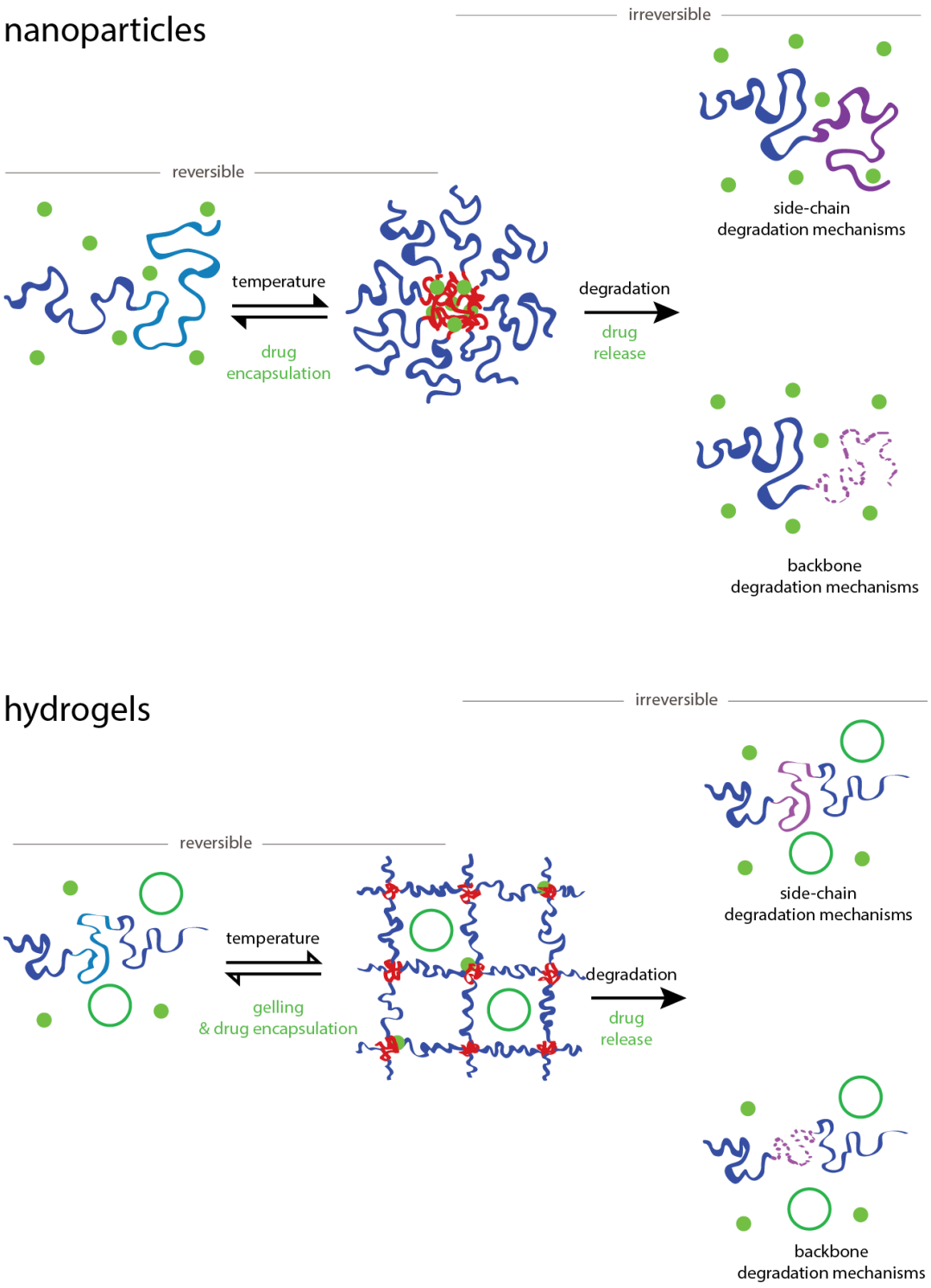


**Figure 1.** Schematic representation of transiently thermoresponsive polymer systems. Upon heating above the $T_{cp}$ of the thermoresponsive block, hydrophobic association between dehydrated polymer chains triggers reversible self-assembly into micellar nanoparticles or hydrogels, as exemplified for diblock and triblock copolymers respectively. The formation of hydrophobic pockets in the micelle core or within the hydrogel network, allows the encapsulation of hydrophobic drug molecules (plain green discs). Moreover, in case of the hydrogels, macromolecular therapeutic compounds (e.g. proteins, green circles) can be entrapped in the mesh of the polymer network. Upon contact with a second stimulus that triggers a degradation reaction in the polymer side chain or backbone, the polymers irreversibly transform into fully soluble unimers accompanied by an increase in the Tcp , and concomitant release of the encapsulated payload.

Thermoresponsive polymers that exhibit temperature-responsive behavior in aqueous solution are soluble at low temperature due to extensive hydrogen bonding with the surrounding water molecules and subsequent hindered polymer-polymer interactions. Heating above the $T_{cp}$ favors the disruption of these hydrogen bonds due to entropic reasons, which enables polymer-polymer interactions (i.e. hydrogen bonding or hydrophobic interactions) and limits the polymers' solubility in water.[9,10] Poly(N-isopropylacrylamide) or p(NIPAAm) is undoubtedly the most extensively studied thermoresponsive polymers having a $T_{cp}$ of about 32°C in aqueous solution (**Figure 2A**).[11-13] This value can easily be modulated by copolymerization with either hydrophobic or hydrophilic monomers, respectively leading to a decrease or increase of the copolymers´ $T_{cp}$.[14-16] Moreover NIPAAm can be copolymerized with degradable monomers affording transiently thermoresponsive behavior which, as introduced earlier, is an attractive feature for biomedical applications. More recently, alternative systems have emerged based on oligo(ethylene glycol) or OEG with a $T_{cp}$ tunable by both the OEG chain length and the introduction of comonomers (**Figure 2B**). This chapter will focus on the various chemistries that have been employed to allow a permanent upwards shift in $T_{cp}$ in response to base- or acid-catalyzed hydrolysis, light, enzymes or oxidation/reduction. The corresponding molecular structures are listed in **Table 1-5** for each type of chemistry used to endow polymers with transient properties. Throughout the text we will also highlight several applications of the polymers in drug delivery and tissue engineering.

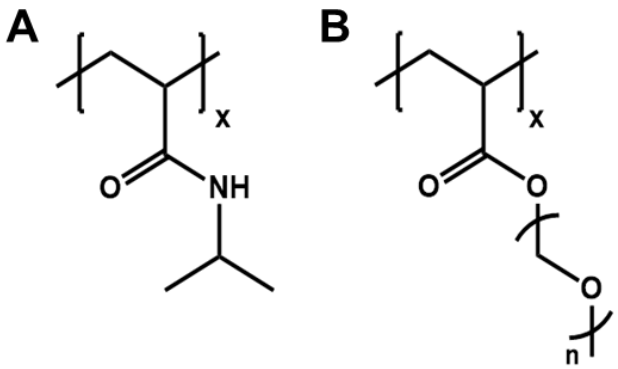


**Figure 2.** Molecular structure of **(A)** poly(N-isopropylacrylamide) or p(NIPAAm) and **(B)** poly[oligo(ethylene glycol) methyl ether methacrylate] or p(OEGMA) as the two most investigated thermoresponsive polymer systems.

## Transiently thermoresponsive polymers with base-sensitive groups

As water is abundantly present in the human body, the introduction of hydrolysable moieties is a popular feature to engineer biodegradable materials.[5] Several classes of hydrolytically degradable polymers have been reported, including poly(anhydride)s, poly(ester)s, poly(urethane)s, poly(carbonate)s, poly(phosphoester)s and poly(amide)s. In this section we will focus on thermoresponsive polymers that lose their temperature-responsive behavior upon base-catalyzed hydrolysis of pendant groups. This feature can be exploited for controlled drug delivery. The corresponding structures are shown in **Table 1**.

### *Esters*

*Ester moieties in polymer side chain*

The first reports on hydrolysis-dependent thermoresponsive behavior typically deal with copolymers of NIPAAm with comonomers that are more hydrophobic than NIPAAm, but contain hydrolytically labile ester moieties. Upon hydrolysis of the esters under neutral or basic conditions the comonomers become more hydrophilic, leading to a progressive increase of the copolymer´s $T_{cp}$ and finally result in fully water soluble polymers at body temperature. Pitt *et al.* were the first to synthesize transiently thermoresponsive p(NIPAAm) copolymers by introducing the hydrolytically labile N-acryloxy succinimide (i.e. an activated ester of acrylic acid) into the backbone **[1.1]**.[17]. Upon hydrolysis of the acryloxy succinimide groups into acrylic acid, an increase of the $T_{cp}$ takes place. Also monomers bearing hydrolytically labile lactate ester moieties such as 2-hydroxyethyl methacrylate oligolactate (HEMA-$Lac_n$)[18-22] and 2-hydroxypropyl methacrylamide oligolactate (HPMAm-$Lac_n$)[23,24] (where n is the number of lactic acid units per HEMA or HPMAm repeating unit) have been successfully copolymerized with NIPAAm **[1.2]**. In analogy to N-acryloxy succinimide, copolymers of HEAM-$Lac_n$ or HPMAm-$Lac_n$ with NIPAAm exhibit a hydrophobic-to-hydrophilic transformation upon hydrolysis of the lactic acid side chains with an increase of their $T_{cp}$. Note that in these cases, upon hydrolysis, (co)polymers are obtained with pending hydroxyl groups. This concept was exploited for the controlled instability of polymeric micelles composed of a hydrophilic poly(ethylene glycol) block and a thermoresponsive p(NIPAAm-co-HPMAm-$Lac_n$) block.[23] Additionally, this approach was extensively investigated to prepare degradable p(NIPAAm)-based injectable hydrogels with reverse thermogelling behavior. Typically NIPAAm is copolymerized with acrylic acid and HEMA-$Lac_n$ to manipulate

the $T_{cp}$ before (e.g. 23.5 – 34.9 °C) and after hydrolysis (e.g. 43.2 – 44.1 °C) respectively.[19,20] Additional comonomers can also be added to introduce various functionalities such as bioconjugation sites.[21,22]

Alternatively, p(NIPAAm)-based polymers have been grafted onto enzymatically degradable polysaccharide backbones such as chitosan[25,26], hyaluronic acid[27] and dextran[28-30] to design biodegradable nanoparticles or hydrogels. However, intact p(NIPAAm) chains remain after enzymatic degradation of the polysaccharide backbone and moreover, the specific enzymes required to decompose these biopolymers are not abundantly present in the human body. To cope with the latter issue, Lowe *et al*. copolymerized NIPAAm with a dextran-based macromer containing multiple hydrolytically degradable oligolactate-2-hydroxyethyl methacrylate units (Dex-lactate-HEMA) to generate thermoresponsive and hydrolytically degradable nanoparticles and hydrogels **[1.3]**.[31,32] However, here an increase of hydrophobicity was observed upon cleavage of the pendant oligolactate linker groups due to subsequent loss of the hydrophilic dextran moieties.

In 2004, Hennink and co-workers reported that also homopolymers of mono- and dilactate substituted HPMAm, thus without the need for copolymerization with NIPAAm, exhibited thermosensitive behavior with a lower $T_{cp}$ for the more hydrophobic p(HPMAm-$Lac_2$) compared to the monolactate variant **[1.4]**.[33] The $T_{cp}$ could be fine-tuned by copolymerization of HPMAm-$Lac_n$ with different values of n (typically combining mono- and dilactate). As described earlier, p(HPMAm-$Lac_n$) is transformed into the more hydrophilic and biocompatible p(HPMAm) upon hydrolysis of the labile lactate esters under neutral or basic conditions, thereby enabling a "hydrophobic-to-hydrophilic" conversion at body temperature. Hennink and co-workers exploited this chemistry to synthesize polymeric micelles that could be destabilized at body temperature with consequent release of their payload in a controlled way. Amphiphilic block copolymers were synthesized consisting of a hydrophilic poly(ethylene glycol) (PEG) block and a thermosensitive biodegradable p(HPMAm-$Lac_2$) block **[1.5]**.[34] These PEG-*b*-p(HPMAm-$Lac_2$) block copolymers formed micelles in water by heating an aqueous polymer solution from below to above the critical micellization temperature (cmt). The micelles were stable at pH 5, but gradually dissolved at pH 8.6 upon hydrolysis of the lactic acid side groups and the resulting irreversible hydrophobic-to-hydrophilic transition of the thermosensitive p(HPMAm-$Lac_2$) block. Pyrene loading studies (**Figure 3**) confirmed the applicability of these block copolymer micelles for

controlled delivery of hydrophobic drugs. In this regard, Hennink and co-workers employed these PEG-*b*-p(HPMAm-Lac$_2$) block copolymers for the preparation of a block copolymer micelle formulation of the anti-cancer drug paclitaxel (PTX).[35] Exploiting the copolymers´ thermoresponsive behavior, drug encapsulation was performed by simply mixing a small volume of a concentrated PTX solution in ethanol with an aqueous polymer solution followed by heating the solution above the cmt of the polymer. At pH 8.8 the PTX-loaded micelles destabilized within 10 hours due to the hydrolysis of the lactic acid side group of the pHPMAm-Lac$_2$, but remained stable over 200 hours at the physiological pH of 7.4. Nonetheless the simple preparation method, avoiding the use of harmful organic solvents, makes this kind of block copolymer micelles attractive as delivery vehicles for hydrophobic compounds as shown for photosensitizers[36], vitamin K[37] and MRI contrast agents[38].

As most long-circulating polymeric nanoparticles are cleared from systemic circulation in pre-clinical laboratory animal models within the first 8-10 h after intravenous administration, an ideal carrier should remain stable over this period of time and destabilizes upon arrival at its site of action with a concomitant release of its drug load.[39] Because the destabilization time of empty PEG-*b*-p(HPMAm-Lac$_2$) micelles was approximately 8 days at physiological conditions (37 °C, pH 7.4), the Hennink group aimed at the design of block copolymer micelles that could destabilize within 1 day under physiological conditions. From previous research it was known that the ester of the primary alcohol in (2-hydroxyethyl)methacrylate-dilactate (HEMA-Lac$_2$) showed faster hydrolysis than an ester of the secondary alcohol in the HPMAm. However, the corresponding p(HEMA) degradation product was insufficiently soluble at physiological temperature, thereby preventing the release of payload from the polymeric micelles at body temperature.[18] The authors anticipated that a methacrylamide with a primary alcohol function, such as N-(2-hydroxyethyl)methacrylamide (HEMAm), could be more suitable and therefore HEMAm-Lac$_n$ was used as a (co)monomer in various biodegradable (block co-) polymers.[40] Polymerization of HEMAm-Lac$_2$ yielded thermoresponsive polymers with a $T_{cp}$ of 22 °C that could be lowered by introducing HEMAm-Lac$_4$ as comonomer **[1.6]**. Moreover, PEG-*b*-p[(HEMAm-Lac$_2$)-*co*-(HEMAm-Lac$_4$)] block copolymers were found to self-assemble into compact spherical micelles **[1.7]**, that fully destabilized under physiological conditions within 8 h due to hydrolysis of the lactate side chains.

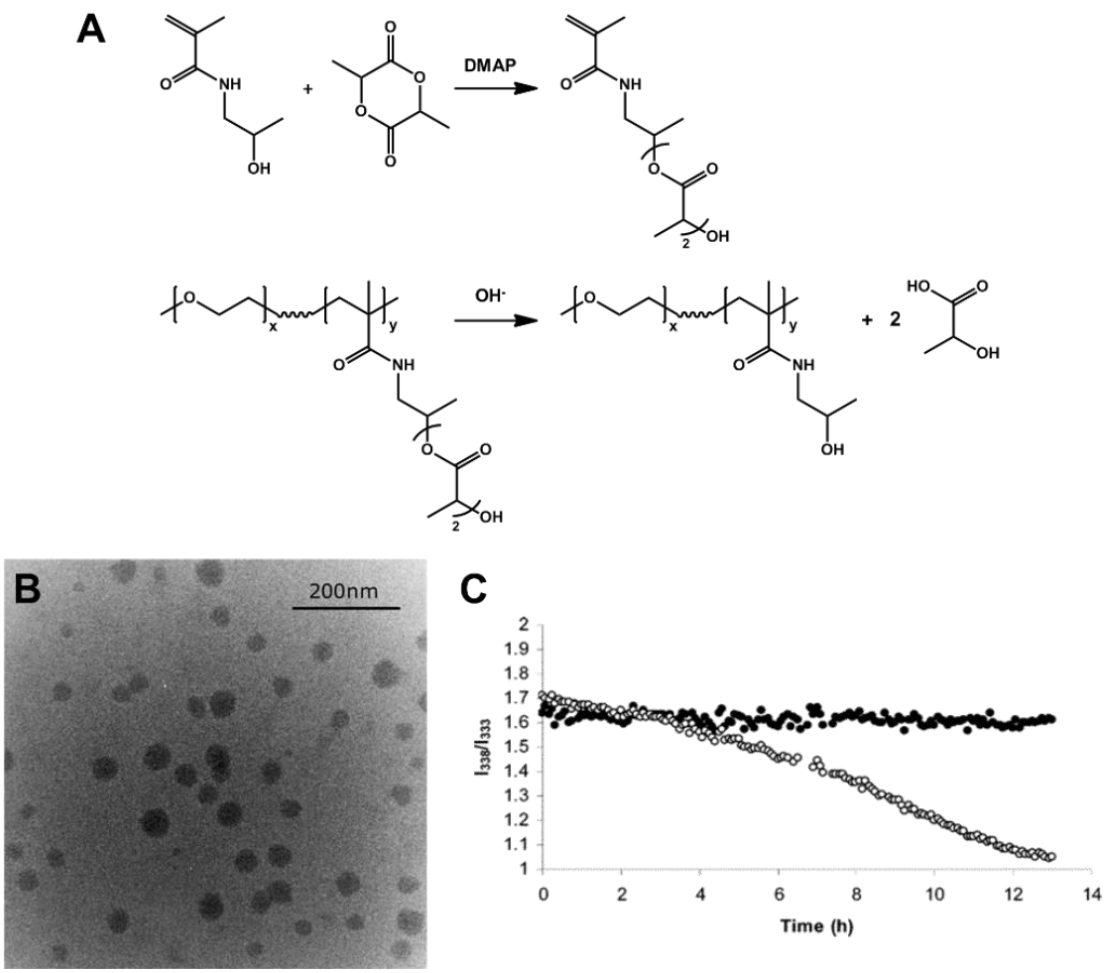


**Figure 3. (A)** Synthesis of HPMAm-$Lac_2$ and base-catalyzed hydrolysis of PEG-*b*-p(HPMAm-$Lac_2$) block copolymers. **(B)** Cryo-TEM of PEG-p(HPMAm-$Lac_2$) micelles. **(C)** Change in emission spectra ($I_{338}/I_{333}$ ratio) of pyrene solubilized in PEG-*b*-p(HPMAm-$Lac_2$) micelles at 37 °C and at pH 5.0 (closed circles) and pH 8.6 (open circles). *Reproduced from reference 34.*

Similar to modification with lactic acid moieties, also other hydrolytically labile ester groups were introduced into the side chain of the HEMA monomer in view of designing transiently thermoresponsive (co)polymers. An example is poly(ε-caprolactone)-2-hydroxylethyl methacrylate (HEMA-PCL) bearing hydrolytically labile caprolactone-derived ester moieties in the polymer side chains.[41,42] The HEMA-PCL monomer was further modified with the enzymatically degradable polysaccharide dextran and copolymerization of this Dex-PCL-HEMA monomer with NIPAAm yielded reverse thermogelling biomaterials for tissue engineering applications **[1.8]**. Implantation of the hydrogel into infarcted myocardium of rabbits prevented adverse cardiac remodelling and dysfunction. Rosellini *et al.* copolymerized 2-hydroxyethylmethacrylate-6-hydroxyhexanoate (HEMA-Hex) with NIPAAm,

which yielded copolymers with a $T_{cp}$ below body temperature **[1.9]**.[43] Hydrolysis was found to occur on the peripheral ester bond of the lateral chain, with the release of 6-hydroxyhexanoic acid and the subsequent increase of the $T_{cp}$ above body temperature.

Additionally, also other monomers bearing hydrolytically labile ester groups were copolymerized with NIPAAm. Vernon *et al.* reported on the synthesis of poly[(NIPAAm)-*co*-(dimethyl-ɣ-butyrolactone acrylate)] copolymers with a hydrolysis-dependent thermosensitivity.[44] The $T_{cp}$ could be tuned by varying the dimethyl-ɣ-butyrolactone acrylate (DBA) content, and increased above body temperature upon ring-opening hydrolysis of the DBA side group. The hydrolysis of the ester group in the ring structure was found to occur without cleavage of the ester near the backbone, thereby avoiding low molecular weight by-products and subsequent toxic effects. Nevertheless, the $T_{cp}$ of the initial polymers was below room temperature, which limited the applicability for *in situ* gelling injectable hydrogel purpose. Therefore, the authors added a third more hydrophilic comonomer, i.e. acrylic acid, to increase the initial $T_{cp}$. Moreover, it was suggested that the presence of acrylic acid facilitated the access of water to DBA ester groups, thereby accelerating the degradation rate **[1.10]**.[45,46]

A singular class of polymers are the poly(cyanoacrylate)s, that have been used as tissue adhesives.[47] It was found that the pendant esters in the side chain could be degraded by esterases (cfr. section enzyme-sensitive groups).[48] Moreover, thermogelling properties in aqueous solution were reported for poly(ethylene glycol)-*co*-poly(ethyl-2-cyanoacrylate) **[1.11]**.[49] Interestingly, their sol-to-gel transition temperature increased as the concentration increased.

In analogy with their earlier reports on p(HPMAm-$Lac_n$), Hennink *et al.* recently prepared a new series of polymers based on methyl, ethyl, and isopropyl esters of $N^{\alpha}$-(methacryloyl)-serine and –threonine; that exhibited thermosensitive behavior without the need for copolymerization with NIPAAm **[1.12]**.[50] The corresponding homo- and co-polymers exhibited thermoresponsive behavior with $T_{cp}$ values that were tailored by variation of the monomers hydrophobicity and ranged from 15 °C to above 100 °C. These monomers were used to synthesize amphiphilic block copolymers with PEG that formed nanoparticles above their $T_{cp}$. Upon incubation at physiological conditions, the $T_{cp}$ increased due to ester hydrolysis, resulting in nanoparticle destabilization.

*Ester moieties in polymer backbone*

In contrast to the presence of esters as pending side groups, ring-opening polymerization of lactide, ε-caprolactone (CL) or 2-methylene-1,3-dioxepane (MDO) introduces hydrolytically labile bonds into the polymer backbone (**Figure 4**). While lactide and CL are generally polymerized by cationic ring-opening polymerization (ROP), MDO can copolymerize with vinyl monomers by radical polymerization (RP), installing CL ester groups in the aliphatic polymer backbone.[51] In this regard, Liu *et al.* synthesized biodegradable p(NIPAAm-*co*-MDO) random copolymers where hydrolytically labile ester groups were present within the p(NIPAAm) backbone **[1.13]**.[52] These polymers were crosslinked using N,N'-methylenebisacrylamide to obtain biodegradable hydrogels. In general, block copolymers of p(NIPAAm) with hydrophobic blocks of both PCL **[1.14]** and poly(lactic acid) (PLA) **[1.15]** have been extensively employed by various groups to form micelles with a hydrated p(NIPAAm) corona below its $T_{cp}$.[53-64] When heated above the $T_{cp}$ the micelle shell becomes hydrophobic, leading to micelle destabilization and release of an encapsulated payload. To be suitable for *in vivo* applications, the $T_{cp}$ is fine-tuned above body temperature by mixing the p(NIPAAm) block with hydrophilic comonomers such as acrylamide[56-58], dimethylacrylamide[59-63] or methacrylic acid[64]. Upon degradation of the esters present in the backbone, it is suggested that the polymeric micelles dissociate into low molecular weight p(NIPAAm) segments that can be excreted by glomeral filtration.[53] However, the thermoresponsive properties of these p(NIPAAm) segments remain intact and thus globular precipitates are still expected to be formed at body temperature. Therefore we do not consider these systems as transiently thermoresponsive and will not further discuss them in this chapter. The same holds true for p(NIPAAm)-based block copolymers with poly(D,L-lactide-*co*-glycolide) (PLGA) that were developed to increase the drug loading capacity compared to PLA block copolymers;[65,66] and similar PLA/PCL block copolymer systems where pluronics or poly(N-vinylcaprolactam) are used as the thermoresponsive polymer blocks.[67-70] However, by replacing the poly(propylene oxide) block in ABA or BAB type triblock poly(ethylene oxide)-poly(propylene oxide)-poly(ethylene oxide) pluronics (PEO-PPO-PEO) with PLA, PLGA **[1.16]** or PCL, the resulting triblock copolymers lose their thermoresponsive behavior upon degradation of the labile ester moieties.[71-74] These are reverse thermogelling biodegradable block copolymers that have been explored as injectable *in situ* gelling systems

for drug delivery of tissue engineering. As these systems have already been thoroughly discussed by others, they will not be described in the current chapter. [6-8]

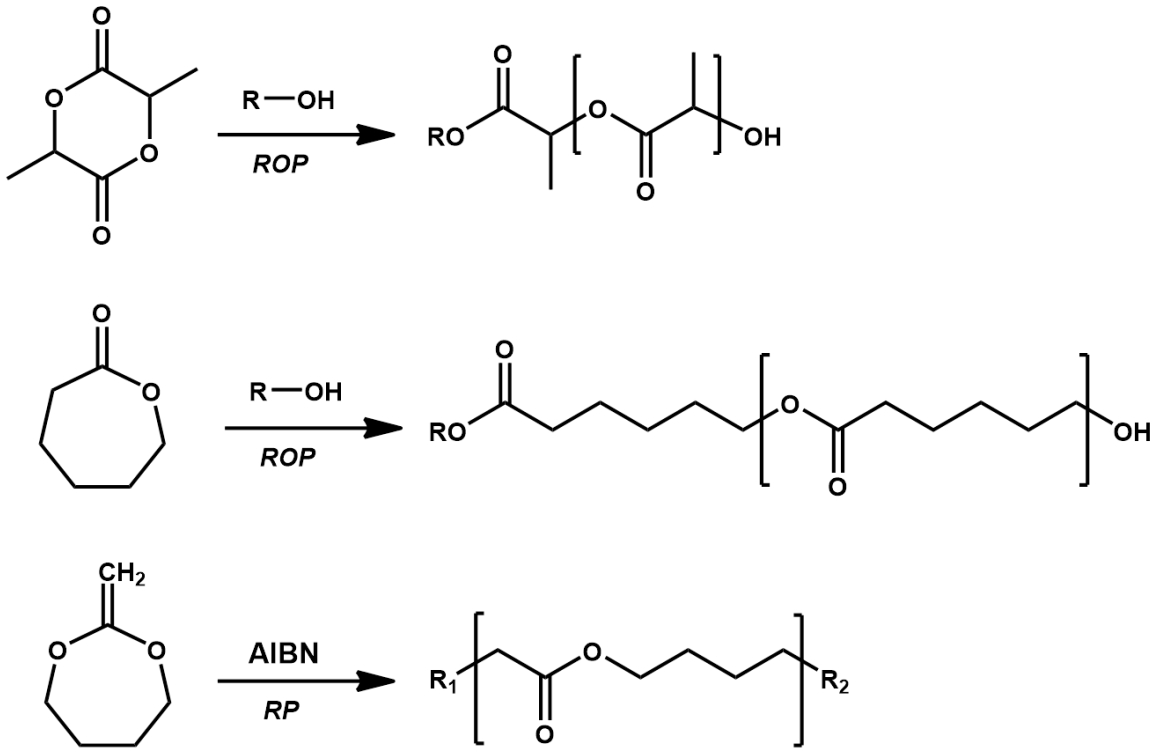


**Figure 4.** Polymerization of lactide (LA), ε-caprolactone (CL) or 2-methylene-1,3-dioxepane (MDO) *via* ring-opening polymerization (ROP) or radical polymerization (RP), generating a degradable poly(ester) backbone.

Poly(ethylene oxide) (PEO) or poly(ethylene glycol) (PEG) is a hydrophilic polymer that has been extensively used for the modification of therapeutic proteins (e.g. PEGylation) to prolong their body-residence time and to reduce the protein immunogenicity.[39,75-77] Although PEG is often used as a hydrophilic building block, it actually exhibits thermoresponsive behavior with a $T_{cp}$ around 85°C.[78] Various groups have introduced PEG side chains onto poly(ester) backbones to obtain biodegradable thermoresponsive polymers. Baker *et al.* synthesized a series of lactides that had one OEG monomethyl ether chain per lactic acid residue.[79] Their subsequent ring-opening polymerization yielded high molecular weight oligo(ethylene oxide)-grafted poly(lactide)s that exhibited thermoresponsive behavior dependent on the OEG chain length **[1.17]**. Polymers with 1 or 2 ethylene oxide repeat units were more hydrophilic than polylactide but still insoluble in water, whereas polymers having 3 or 4 ethylene oxide repeating units were water-soluble and exhibited a $T_{cp}$ of 19 and 37 °C respectively. The use of an acetylene-functionalized derivative of a lactide monomer, i.e. propargyl glycolide (PGL), allowed for further chemical modification via copper-mediated alkyne-azide "click" chemistry. Grafting mixtures of methoxy diethylene glycol (mDEG) and alkyl azides yielded water-soluble polymers with tunable $T_{cp}$ values in a range from 25 to 65 °C by adjusting the mDEG:alkyl ratio in the azide feed **[1.18]** (**Figure 5**).[80]

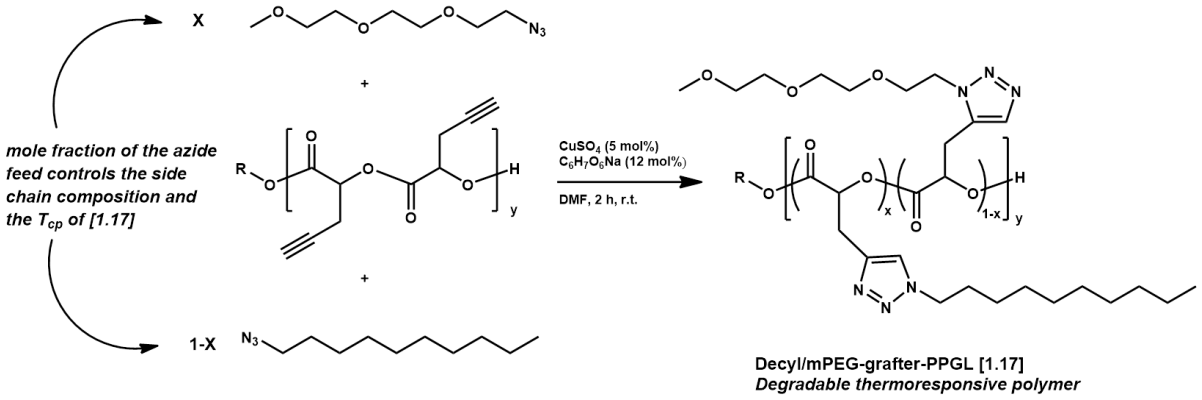


**Figure 5**. Design of poly(glycolide)-based thermoresponsive materials with tunable $T_{cp}$ via alkyne-azide 'click' chemistry. *Reproduced from reference 80.*

Li *et al.* also employed click chemistry to introduce PEG side chains on a poly(ester) backbone that was additionally modified with acid-labile ketal groups (cfr. section acetal/ketal) or redox-sensitive disulfide moieties (cfr. section reduction-sensitive groups) **[1.19]**.[81] It was found that increasing the length of the PEG side chain resulted in an increase of the $T_{cp}$ for the same polymer backbone. Degradation under either acidic or reductive conditions of the ketal-modified and disulfide-modified poly(ester)s respectively, induced a shift of the $T_{cp}$ values compared to precursor polymers. Reduction of the disulfide linkages resulted in a decreased $T_{cp}$ (ca. 5 °C), whereas an increase of $T_{cp}$ (ca. 3 °C) was observed after degradation of the ketal linkage. Hydrolysis of the unmodified poly(ester) backbone under basic conditions generated pH-sensitive thermoresponsive behavior. Stefan *et al.* prepared biodegradable thermoresponsive polymers with a $T_{cp}$ of 47.5°C by ring-opening polymerization of Ɣ-substituted 3-caprolactone derivatives containing a hydrophilic oligo(ethylene glycol) side chain.[82] The $T_{cp}$ could be lowered close to body temperature by adding a more hydrophobic polymer block based on a Ɣ-substituted 3-caprolactone monomer containing an octyloxy group **[1.20]**. Deng *et al.* reported on the alternating ring-opening copolymerization of succinic anhydride (SA) and a functionalized epoxide bearing OEG monomethyl ether pendant groups, which yielded thermoresponsive polymers with a degradable poly(ester) backbone **[1.21]**.[83,84] The $T_{cp}$ of the polymers could be tuned in a range from 18 to 50 °C by copolymerization of SA and a mixture of functionalized epoxides with varying OEG chain lengths.[85] Alternatively Shen *et al.* introduced hydrolytically labile β-thioether esters onto a PEG backbone by Michael addition reaction of dithiols and poly(ethylene glycol) diacrylates (PEGDA) or dimethacrylates (PEGDMA), with $T_{cp}$ values ranging from 10 to 50°C **[1.22]**.[86]

As an alternative to p(NIPAAm), Lutz *et al.* prepared well-defined thermoresponsive copolymers of 2-(2-methoxyethoxy)ethyl methacrylate ($MEO_2MA$) and oligo(ethylene glycol) methyl ether methacrylate (OEGMA).[87-89] The $T_{cp}$ of the p($MEO_2MA$-*co*-OEOMA) polymers in water could be varied from 25 to 90°C but their biomedical applications were limited and were not claimed to be degradable. To enhance the biocompatibility of these polymers, Lutz and coworkers introduced the MDO-like cyclic ketene 5,6-benzo-2-methylene-1,3-dioxepane (BMDO) monomer as third comonomer in atom transfer radical copolymerization (ATRP) of $MEO_2MA$ and OEGMA, which installed hydrolysable ester groups into the polymer backbone **[1.23]**.[90] The copolymers could be degraded both hydrolytically and enzymatically by

addition of KOH or *Candida antarctica* lipases respectively. In analogy to the work of Lutz and coworkers, Agarwal *et al.* found that ring-opening of BMDO during copolymerization with NIPAAm introduced degradable ester linkages into the p(NIPAAm) backbone **[1.24]**.[91] These p(NIPAAm-*co*-BMDO) copolymers were hydrolytically unstable under basic conditions and their thermoresponsive behavior could be tuned by controlling the amount of incorporated BMDO. Matyjaszewski *et al.* prepared similar p(NIPAAm-*co*-BMDO) polymers by ATRP and reversible addition-fragmentation chain transfer (RAFT)[92] and more recently the solid-state thermal degradation of these copolymers was investigated[93].

Via single-electron transfer living radical copolymerization (SET-LRP) of NIPAAm with an ester-containing comonomer, Kamigaito *et al.* obtained degradable and thermoresponsive polymers **[1.25]**.[94] Upon base-catalyzed hydrolysis of the ester-linked monomers in methanol, the degradation products exhibited higher $T_{cp}$ values than those of the original polymers due to the introduction of hydrophilic hydroxyl groups at the hydrolyzed chain end. Instead of radical polymerization, He *et al.* grafted both monomeric NIPAAm units and hydrophobic cholesteryl onto poly(amino ester)s containing secondary amines in their backbones, to obtain thermo- and pH-responsive degradable poly(amino ester)s with thermoresponsive properties similar to those of elastin-like poly(peptide)s **[1.26]** (ELPs, cfr. section enzyme-sensitive groups).[95] Inspired by these ELPs; Joy and coworkers synthesized polymers with a hydrolytically degradable poly(ester) backbone, bearing various amides in their sides chains **[1.27]**.[96] The polymers were thermoresponsive and their $T_{cp}$ could be tuned within a range of 7.2 to 53 °C through copolymerization of monomers containing different amide side chains. Above the $T_{cp}$ the (co)polymers formed coacervate droplets in which Nile Red could be encapsulated.

***Organophosphazenes***

Poly(phosphazenes) are inorganic polymers with a backbone consisting of alternating nitrogen and phosphor atoms linked by alternating single and double bonds. The phosphor atom can accommodate 2 organic side groups, which allows for tuning of the polymer properties.[97] Poly[(alkyl ether)phosphazenes] with oligo(ethylene glycol) segments for example have been reported to exhibit thermoresponsive behavior in aqueous solution[98,99] and were rendered biodegradable by Soo Sohn *et al.* via the introduction of amino acid esters (AAE) side groups in addition to methoxy PEG (MPEG) side groups[100] **[1.28]**. The $T_{cp}$

values of these polymers varied from 25 to 99 °C, depending on several factors such as composition of the substituents, chain length of MPEG, and the type of amino acid and ester side groups. Hydrolysis of the polymers was faster under acidic and basic conditions than at neutral pH.[101]

The hydrolytic degradation of poly(organophophazenes) substituted with AAE side groups has been proposed to occur via a carboxylic acid-catalyzed degradation pathway (**Figure 6**).[102-104] An initiating step is hydrolysis of the labile AAE which generates the corresponding free carboxylic acid groups that subsequently attacks the polymer backbone, resulting in backbone cleavage. The rate of ester hydrolysis in aqueous solution is known to decrease in the order of basic > acidic > neutral conditions. Therefore, the authors suggested that AAE may be rapidly hydrolyzed at basic pH but generates less free carboxylic acid moieties and more carboxylate anions than at acidic pH, resulting in no significant difference between the hydrolysis rates under both conditions. Polymer degradation led to fragmentation of the poly(phosphazene) backbone with mostly phosphates and ammonia as hydrolysis products. Whether this is to a more or lesser extent harmful towards protein- or DNA-based drugs and living tissue than acidic by-products from lactate ester hydrolysis still needs to be elucidated.

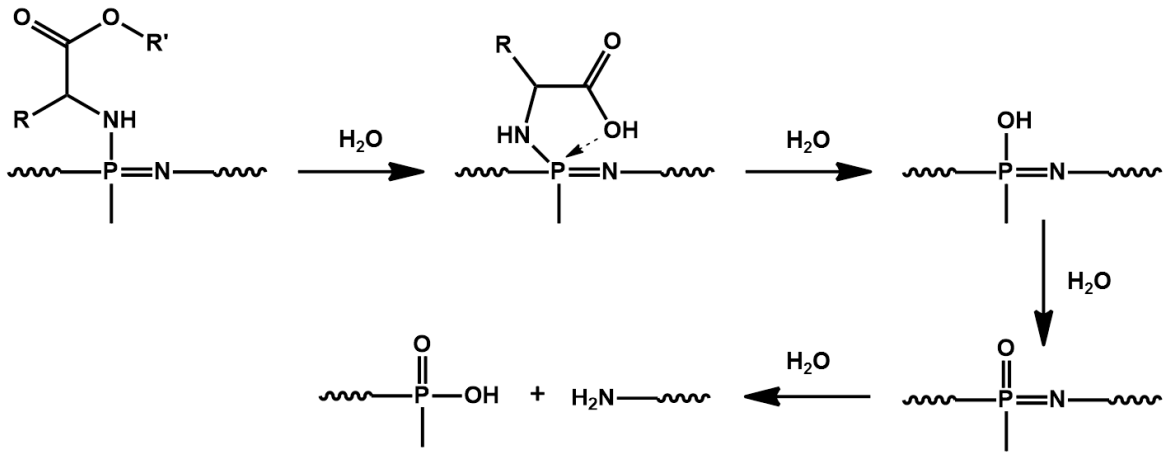


**Figure 6.** Proposed carboxylic acid-catalyzed hydrolytic pathway of poly(organophosphazene) with MPEG and amino acid esters as side groups. *Reproduced from reference 101.*

As an addition to these *O,N-systems*, the same group of authors examined the thermoresponsive and hydrolytic behavior of poly(organophosphazene)s bearing α-amino-ω-methoxy-poly(ethylene glycol) (AMPEG) and AAE in a *N,N-system* **[1.30]**.[105] These polymers exhibited higher $T_{cp}$ values and faster degradation rates than MPEG-based polymers, which is probably due to the higher hydrophilicity of AMPEG. When AMPEG was combined with hydrophobic L-isoleucine ethyl esters (IleOEt) as side groups, the polymers exhibited reversible sol-gel properties which are of interest for the development of injectable *in situ* gelling systems.[106] Therefore, the commonly used anticancer drugs PTX and doxorubicin (DOX) were conjugated to carboxylic acid-terminated poly(organophosphazene)s bearing AMPEG and IleOET side groups, to generate locally injectable and biodegradable thermosensitive hydrogels.[107,108].

Another application explored for these hydrogels was the localized and long-term delivery of short interfering RNA (siRNA) by conjugating low molecular weight poly(ethyleneimine) (PEI) to the poly(organophosphazene) backbone in a similar way as the PXT/DOX conjugates.[109] Being a polycation, PEI forms electrostatic complexes with siRNAs upon mixing, protecting complexed siRNA from nucleases, facilitating intracellular uptake and subsequent cytoplasmic localization. In a follow-up paper the same group of authors replaced PEI by protamine, a cell penetrating protein that forms electrostatic complexes with siRNA, which enhanced intracellular delivery and the subsequent gene silencing efficiency.[110] Similar protamine-poly(organophosphazene) conjugates could be used for the sustained release of the negatively charged human Growth Hormone (hGH).[111]

Thermogelling poly(organophosphazenes) have also been designed for long-term magnetic resonance imaging (MRI) by binding of ferrite ($CoFe_2O_4$) nanoparticles stabilized by hydrophobic surfactants. The latter allow interactions with the L-isoleucine ethyl esters side groups of the poly(organophosphazene).[112] In addition, PTX was loaded into these magnetic hydrogels by simple mixing to serve as an injectable MRI-monitored long-term therapeutic hydrogel system for solid tumors.[113,114]

In all these examples the hydrolytically labile AEE on the poly(phosphazene) backbone was the L-isoleucine ethyl esters (IleOEt). Soo Sohn *et al.* reported that attempts to employ other amino acids in combination with the PEG side groups were unsuccessful and suggested the amino acids were not able to form sufficiently strong physical junction zones to afford gel formation with OEG. However, by replacing the amino acid ester by more

hydrophobic oligopeptides, the gel strength of these thermogelling poly(organophosphazene)s could by increased.[115] Similarly, OEGs and various depsipeptide or dipeptide ethyl esters (DPEE) side groups were introduced onto the poly(organophosphazene) backbone to accelerate polymer degradation. Unfortunately, in none of these cases the $T_{cp}$ values were in a biologically relevant window.[116,117] By contrast, the use of short OEG fragments such as tri- or tetra(ethylene glycol) along with a dipeptide ethyl ester ($GlyGluEt_2$) afforded biocompatible and thermosensitive poly(organophosphazenes) with a $T_{cp}$ below body temperature **[1.29]**.[118] These amphiphilic polymers proved to be biocompatible in a local tolerance test using rabbits and were loaded with hGH as a model hydrophobic drug that could be released in a controlled fashion *in vitro*. Earlier, the authors introduced $GlyGluEt_2$ side chains to conjugate a platinum(II)-based anti-cancer drug to MPEG poly(organophosphazenes).[119] By replacing the AEE and PEG side groups with lactic acid esters and methoxyethoxyethoxy (MEE) groups respectively, Bi *et al.* also obtained thermosensitive and hydrolytic degradable poly(organophosphazenes) **[1.31]**.[120,121] Allcock *et al.* reported earlier on biodegradable poly(organophosphazenes) bearing lactic acid ester side group, but these polymers did not exhibit thermoresponsive behavior.[122] Alternatively Qiu *et al.* grafted amino terminated p(NIPAAm) onto poly(organophosphazenes) with AEE side groups, resulting in thermosensitivity and micellization behavior that could be exploited for drug delivery purposes **[1.32]**.[123-125]

Alternatively, Soo Sohn *et al.* synthesized hydrolytically degradable thermoresponsive oligomeric cyclophosphazenes bearing alkoxy PEG (APEG) and AEE side groups **[1.33]**.[126 127] By grafting hydrophobic oligopeptides as side groups on MPEG-bearing cyclotriphosphazenes, amphiphilic trimers were obtained that formed stable micelles by self-assembly in aqueous solution with a mean diameter ranging from 7.4 to 13.9 nm.[128,129] The drug entrapment efficiency and *in vitro* release profile of one of the trimers was studied using human growth hormone (hGH) as a model drug. The tripodal amphiphile containing MPEG with an average molecular weight of 750 as a hydrophilic group and a linear hexapeptide GlyPheLeuGlyPheLeuEt as a hydrophobic group was found to be most promising and further used for the encapsulation of various hydrophobic anti-cancer drugs including a platinum(II)-based compound[130] (**Figure 7**) and docetaxel (currently in preclinical studies as Phostaxel). [131,132] When the oligopeptide side chains were replaced by fatty acids as hydrophobic groups, the resulting amphiphiles were found to form more stable micelles

compared to the oligopeptide analogues and their highly hydrophobic core environment could be engineered to accommodate nonpolar drugs.[133] To ensure the presence of functional carboxylic acid groups allowing for phosphazene ring cleavage, the fatty acid was linked to the ring via a spacer group. Although all these cyclotriphosphazenes micelles are by definition transiently thermoresponsive polymeric systems with $T_{cp}$ values over a wide temperature range, it's their inherent amphiphilic character rather than their $T_{cp}$ that was exploited for biomedical applications and will therefore not be further discussed in this chapter.

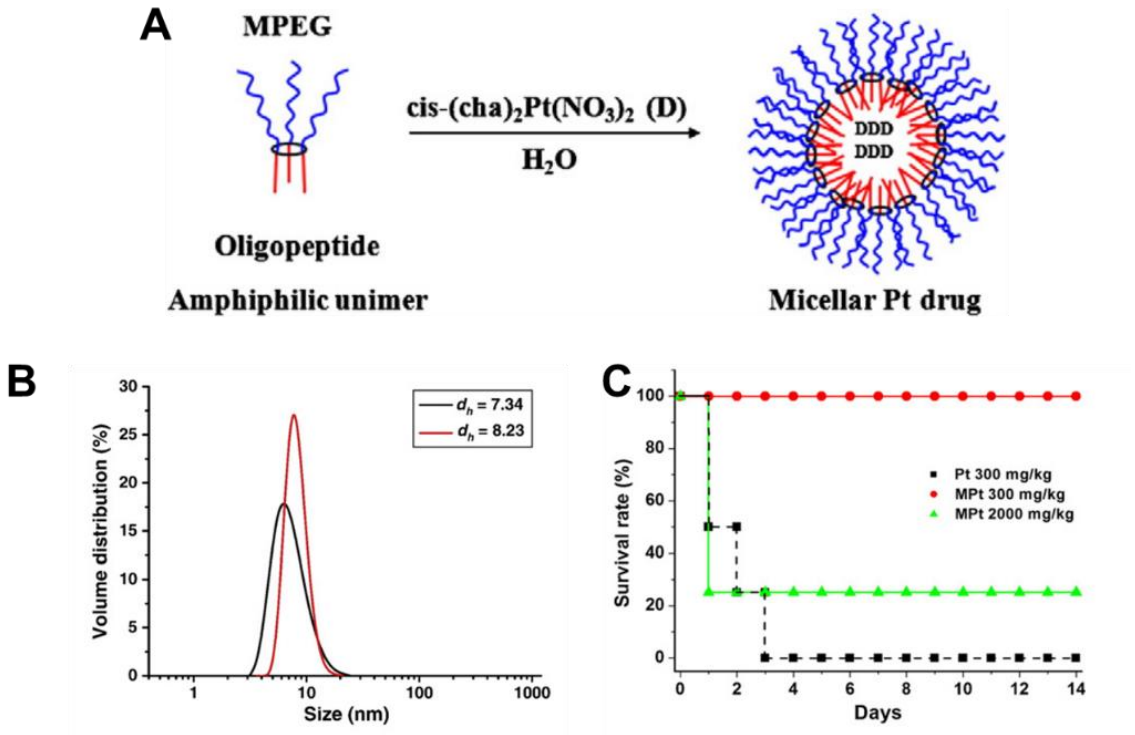


**Figure 7. (A)** Conceptual diagram for micelle encapsulation of a platinum(II)-based anti-cancer drug, i.e. cis-$(cha)_2Pt(NO_3)_2$, using a tripodal cyclotriphosphazene amphiphile $[NP(MPEG750)(GlyPheLeu)_2Et]_3$ in aqueous solution. **(B)** Size distributions of the micelles before (black) and after (red) drug loading. **(C)** Survival rate of the mice intravenously treated with different doses of free (Pt) or micellar (MPt) anti-cancer drug. *Reproduced from reference 130.*

***Phosphoesters***

Poly(phosphoester)s (PPEs) represent a wide range of biodegradable polymers with repeating phosphoester linkages in the backbone that allow various modifications through the pentavalent phosphor atom.[134] Much of the PPE chemistry and the biological relevance of these polymers was pioneered by Penczek and co-workers in the 1970s.[135-137] Due to the favorable degradation behavior via alkaline or enzyme-catalyzed hydrolysis of phosphoester linkages under physiological relevant conditions[134,138], PPEs have been explored for drug and gene delivery[139-142] and tissue engineering applications[143-145]. Iwasaki *et al.* were the first to report on thermoresponsive PPEs through copolymerization of 2-ethoxy-2-oxo-1,3,2-dioxaphospholane (EEP) and 2-isopropoxy-2-oxo-1,3,2-dioxaphospholane (IPP) **[1.34]**.[146] The $T_{cp}$ of p(EEP) was 38 °C and linearly decreased with an increase in the IPP content. Wurm and co-workers replaced IPP by the less hydrophobic 2-ethoxy-4-methyl-2-oxo-1,3,2-dioxaphospholane (EMEP), yielding p(EEP-co-EMEP) poly(phosphoester)s with thermoresponsive properties **[1.35]**.[147] Jun Wang *et al.* copolymerized EEP and IPP via ring-opening polymerization using monomethyl ether PEG as initiator and demonstrated the temperature-induced self-assembly of these block copolymers into nanoparticles **[1.36]**.[148] The polymers were found to be biocompatible and hydrolytically degradable under neutral conditions, with the generation of non-toxic degradation products. The same group of authors used hydrophobic PCL to initiate ring-opening polymerization of EEP in combination with IPP or 2-methoxy-2-oxo-1,3,2-dioxaphospholane (MEP) as co-monomers and investigated the influence of the block copolymer composition on their temperature-triggered phase transition behavior **[1.37]**.[149] Alternatively, Leong and coworkers found that aqueous solutions of poly(propylene phosphate) homopolymers displayed a sol-gel transition temperature in the presence of calcium ions **[1.38]**.[150]

***Formamides***

Akashi *et al.* reported on *N*-vinylalkylamide monomers that bear a vinyl group and various alkyl side chains connected via an amide linkage.[151-154] Interestingly, aqueous solutions of poly(*N*-vinylisobutyramide) or poly(NVIBA) exhibited a $T_{cp}$ of approximately 39°C.[153] Copolymerization with either hydrophilic or hydrophobic comonomers yielded copolymers with respectively a higher and lower $T_{cp}$.[154] In this regard, copolymerization of NVIBA with *N*-vinylformamide (NVF) yielded transiently thermoresponsive p(NVF-co-NVIBA)

copolymers with $T_{cp}$ values that could be tuned in the range of 45 to 70 °C, depending on the hydrophilic NVF content **[1.39]**.[155] As hydrolytic cleavage decreases with increasing hydrophobicity of the substituent, NVF units could be degraded into poly(vinylamine) or p(VAm) under both acidic and basic condition upon heating, whereas NVIBA units remained intact. Therefore p(NVF-co-NVIBA) could be selectively hydrolyzed to yield p(VAm-co-NVIBA) copolymers with an apparent loss of thermoresponsive behavior. However, in further work these authors found that only above the pKa of the side chain amino groups (pKa = 10) the thermoresponsive behavior of the p(VAm-co-NVIBA) copolymers emerged.[156] At a pH above these pKa values, the amino groups exist in their less hydrophilic free base form resulting in thermoresponsive behavior with successive increase in $T_{cp}$ values, depending on the p(VAm) content of the copolymer. More recently, the same group synthesized copolymers containing N-vinylbutyramide (NVBA) and VAm with more physiologically relevant $T_{cp}$ values ranging from 33 to 39.5°C **[1.40]**.[157] Note that poly(amino acids) bearing enzyme-degradable amide moieties will be discussed in the section discussing transiently thermoresponsive polymers with enzyme-sensitive groups.

***Carbonates***

Compared to typical aliphatic poly(ester)s, poly(trimethylene carbonate)s (PTMC) exhibit unique degradation behavior, such as resistance to non-enzymatic hydrolysis at physiological pH and the generation of non-acidic degradation products (i.e. 1,3-propanediol and carbon dioxide) in the presence of enzymes such as lipases (cfr. section enzyme-sensitive groups).[158] PTMC diblock copolymers of MPEG and PTMC were reported to undergo sol-to-gel transition as temperature increased but they indeed did not degrade in phosphate buffered saline at room temperature over 90 days **[1.41]**.[159,160] Lee and coworkers incorporated caprolactone moieties (cfr. section esters) into the PTMC block to generate MPEG poly(ester) diblock copolymers, but did not report on their hydrolysis rate **[1.42]**.[161] The Hedrick group synthesized thermoresponsive block copolymers by ring-opening polymerization of cyclic 2,2-bis(methylol) propionic acid derived carbonate monomers, functionalized with ester-linked hydrophilic PEG chains or hydrophobic alkyl groups **[1.43]**.[162] All the PTMC-based block copolymers were thermoresponsive but only one had a biorelevant $T_{cp}$ (36°C in PBS) and was used for the micellar encapsulation of PTX. Relative to a temperature below the $T_{cp}$, PTX release from the micelles at body temperature

was higher (**Figure 8**) and the subsequent anti-cancer activity more pronounced. Akashi and co-workers found that homopolymers of a cyclic trimethylol alkane derived carbonate bearing an ether-linked methoxy terminated tri(ethylene glycol) unit in the side chain had a $T_{cp}$ around body temperature **[1.44]**.[163] The $T_{cp}$ values ranged from 31 to 35 °C and were influenced by the molecular weight and polymer concentration. Similar homopolymers with more hydrophylic tetra(ethylene glycol) pendant moieties had a $T_{cp}$ of 72°C. Fosong Wang *et al.* synthesized biodegradable poly(carbonate-ether)s (PCEs) with $T_{cp}$ values in a broad window from 22 to 84 °C by copolymerization of $CO_2$ and ethylene oxide using a double metal cyanide catalyst **[1.45]**.[164] The $T_{cp}$ value was highly sensitive to the carbonate unit (CU) content and the molecular weight of PCEs, and it showed a linear relation with CU content for PCEs for a similar molecular weight. Recently, Xinling Wang *et al.* constructed a series of thermoresponsive poly(carbonate)s by polymerizing cyclic TMC monomers that bear OEG units via thioether or/and sulfone bonds **[1.46]**.[165] The $T_{cp}$ could be tuned from 0 to 46 °C by controlling the pendant OEG chain length and the thioether/sulfone bond. Oxidation of the more hydrophobic thioether to a sulfone moiety rendered the polymers more hydrophilic and hence increased the $T_{cp}$ of the poly(carbonate) polymers within a physiological relevant temperature window. It should be noted that none of the papers that describe these PTMC polymers, report on hydrolysis experiments to investigate the subsequent effect on their $T_{cp}$.

In analogy to the copolymerization of NIPAAm with monomers possessing a hydrolytic poly(ester) side chain with lactic acid or caprolactone moieties (cfr. section esters), Wagner *et al.* used a hydroxyethyl methacrylate-poly(trimethylene carbonate) (HEMA-PTMC) monomer to introduce biodegradability in p(NIPAAm)-based hydrogels.[166] By adding acrylic acid as a third co-monomer the $T_{cp}$ was adjusted below body temperature which allowed inverse thermogellation at body temperature upon injection **[1.47]**. Upon cleavage of the carbonate moieties in these polymers, the $T_{cp}$ rose above body temperature. Here the rather slow hydrolysis rate of the carbonate esters in PTMS was exploited to retain the gel structure over several weeks, which was necessary for the envisioned applications in cardiac tissue engineering. The De Geest group recently reported on HPMAm modified with an ethyl group (HPMAm-EC) via carbonate ester moiety.[167] Free radical polymerization of HPMAm-EC using a PEG-based macroinitiatior yielded degradable temperature-responsive block copolymers that assembled into micelles above their $T_{cp}$ of 17°C **[1.48] (Figure 8)**. These polymeric micelles could efficiently solubilize hydrophobic compounds such as dyes

and the anticancer drug PTX, thereby enhancing cellular uptake of these compounds *in vitro*. Under basic condition, these micelles disassembled into water-soluble unimers through hydrolytic degradation of the carbonate esters which connects the HPMAm backbone to the pending ethyl side chains. Similar as earlier reported for HPMAm modified with lactate esters, the micelles remained stable at physiological pH over prolonged periods of time.

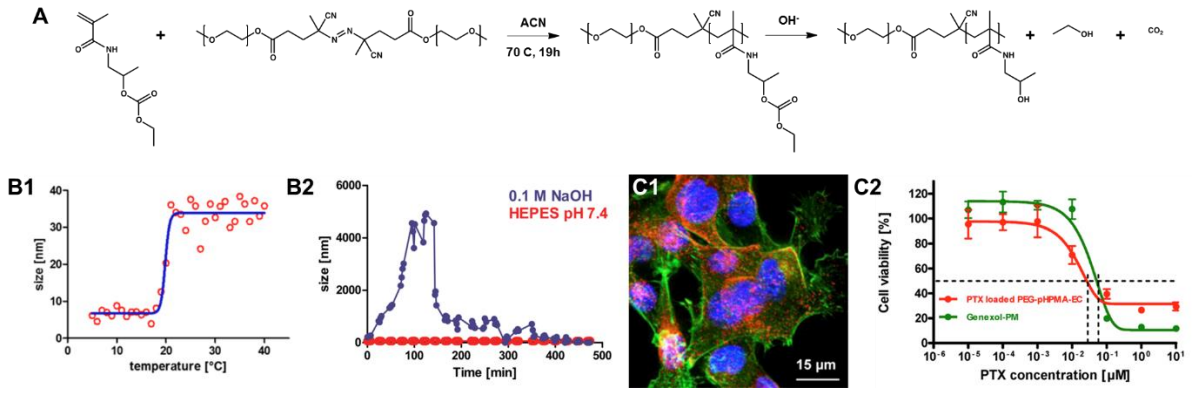


**Figure 8. (A)** Synthesis and degradation mechanism of PEG-*b*-p(HPMAm-EC) block copolymers. **(B)** Evolution of particle size distribution measured by DLS as a function of temperature (B1) and degradation time in aqueous medium of different pH (B2). **(C)** *In vitro* evaluation of PEG-*b*-p(HPMAm-EC) loaded with a hydrophobic compound. (C1) Confocal microscopy of B16.F10 melanoma cells pulsed with dye-loaded micelles and (C2) cell viability of SKOV-3 cells pulsed with PTX loaded micelles. Genexol-PM was used as control nanoformulation. *Reproduced from reference 167.*

**Table 1.** Transiently thermoresponsive polymers with base-sensitive groups

| **ESTERS** | | | | |
|---|---|---|---|---|
| 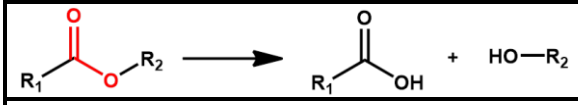 | | | | |
| **Label** | **Polymer** | **$T_{cp}$** | **T-responsive moiety** | **Ref.** |
| **1.1** | Poly[(N-isopropylacrylamide)-*co*-(*N*-acryloxy succinimide)] or p(NIPAAm-*co*-NAS) 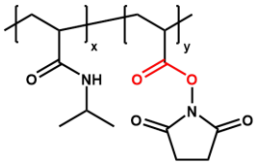 | 19 – 28°C | NIPAAm | 17 |
| **1.2** | Poly[(N-isopropylacrylamide)-*co*-(2-hydroxyethyl methacrylate oligolactate)] or p(NIPAAm-*co*-HEMA-$Lac_n$) | 12 – 30 °C | NIPAAm | 18-21 |
| | Poly[(N-isopropylacrylamide)-*co*-(2-hydroxypropyl methacrylamide lactate)] or p(NIPAAm-*co*-HPMAm-$Lac_n$) 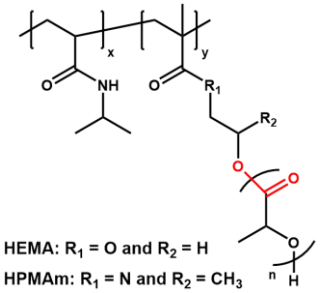 HEMA: $R_1$ = O and $R_2$ = H HPMAm: $R_1$ = N and $R_2$ = $CH_3$ | 10 – 30 °C | NIPAAm | 23,24 |
| **1.3** | Poly[(N-isopropylacrylamide)-*co*-(dextran oligolactate 2-hydroxyethyl methacrylate)] or p(NIPAAm-*co*-Dex-lactateHEMA) 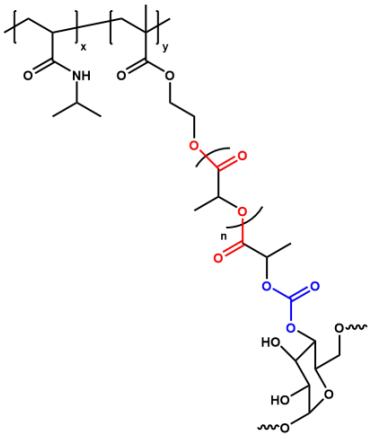 | 32°C *(cgt)* | NIPAAm | 31,32 |
| **1.4** | Poly(2-hydroxypropyl methacrylamide mono/dilactate) or p(HPMAm-$Lac_{1/2}$) 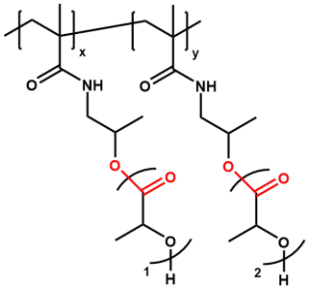 | 13 – 65 °C | inherent | 33 |

| | | | | |
|---|---|---|---|---|
| **1.5** | Poly(ethylene glycol)-*b*-poly(2-hydroxypropyl methacrylamide dilactate) or PEG-*b*-p(HPMAm-Lac$_2$)<br> 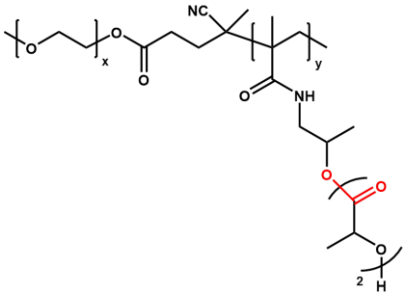 | 6 – 12.5 °C *(cmt)* | inherent | 34,35 |
| **1.6** | Poly(2-hydroxyethyl methacrylamide di/tetralactate) or p(HEMAm-Lac$_{2/4}$)<br> 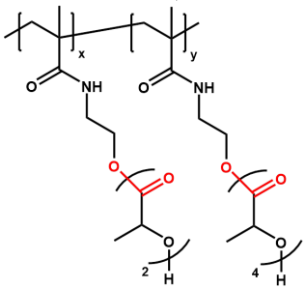 | 5 – 22 °C | inherent | 40 |
| **1.6** | Poly(ethylene glycol)-*b*-poly(2-hydroxyethyl methacrylamide lactate) or PEG-*b*-p(HEMAm-Lac$_{2/4}$)<br> 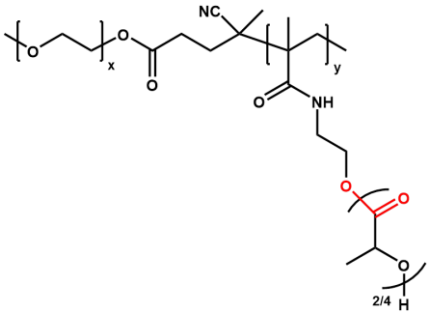 | 6 – 22 °C *(cmt)* | inherent | 40 |
| **1.8** | Poly[(N-isopropylacrylamide)-*co*-(dextran poly(ε-caprolactone) 2-hydroxyethyl methacrylate)] or p(NIPAAm-*co*-Dex-PCL-HEMA)<br> 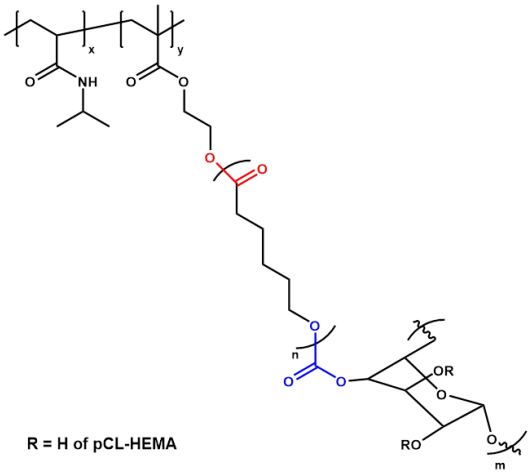 <br>R = H of pCL-HEMA | 33.2 °C *(cgt)* | NIPAAm | 41,42 |

| | | | | |
|---|---|---|---|---|
| **1.9** | Poly[(N-isopropylacrylamide)-*co*-(2-hydroxyethyl methacrylate-6-hydroxyhexanoate)]<br>or p(NIPAAm-*co*-HEMA-Hex)<br> 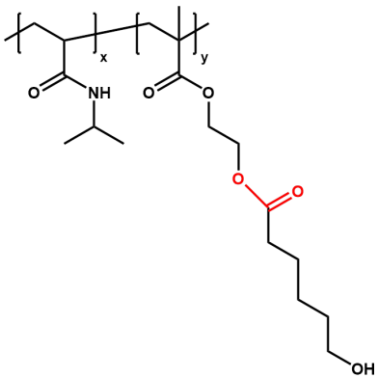 | 23 °C | NIPAAm | 43 |
| **1.10** | Poly[(N-isopropylacrylamide)-*co*-(dimethyl-ɣ-butyrolactone acrylate)-*co*-(acrylic acid)] or p(NIPAAm-*co*-DBA-*co*-AA)<br> 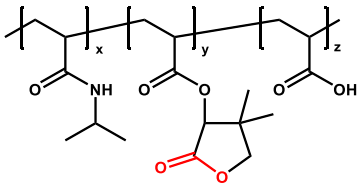 | 16.3 – 35.2 °C | NIPAAm | 44-46 |
| **1.11** | Poly(ethylene glycol)-*co*-poly(ethyl-2-cyanoacrylate)<br> 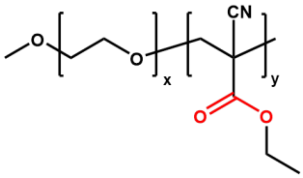 | 15 – 30 °C<br>*(cmt/cgt)* | OEG | 49 |
| **1.12** | (Co-)polymers of methyl (Me), ethyl (Et) and isopropyl (iPr) esters of $N^{\alpha}$-(methacryloyl)-serine and –threonine<br> 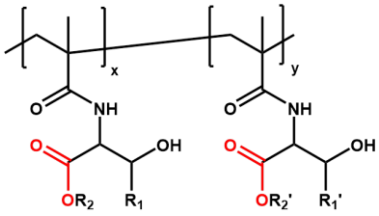 <br>**$R_1$ = H (serine) or $CH_3$ (threonine)**<br>**$R_2$ = Me, Et or iPr** | 1.5 – >100 °C | inherent | 50 |
| **1.13** | Poly[(N-isopropylacrylamide)-*co*-(2-methylene-1,3-dioxepane)] or p(NIPAAm-*co*-MDO)<br> 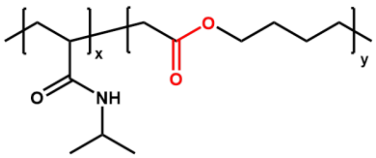 | 28 °C<br>*(cgt)* | NIPAAm | 52 |
| **1.14** | Poly(N-isopropylacrylamide)-*b*-poly(ε-caprolactone) or p(NIPAAm)-*b*-PCL)<br> 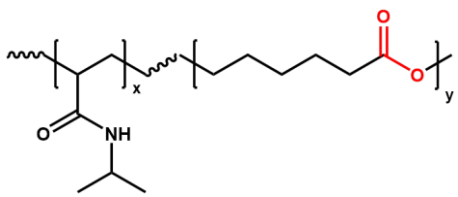 | *Variable b/c comonomers* | NIPAAm | 56,59,62 |

| | | | | |
|---|---|---|---|---|
| **1.15** | Poly(N-isopropylacrylamide)-*b*-poly(lactic acid) or p(NIPAAm)-*b*-PLA<br> 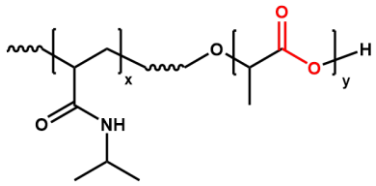 | *Variable b/c comonomers* | NIPAAm | 53-55,57,58, 60-64 |
| **1.16** | Poly(ethylene oxide)-*b*-poly(lactic acid / lactic acid-*co*-glycolic acid)-*b*-poly(ethylene oxide) or PEO-*b*-PLA/PLGA-*b*-PEO<br> 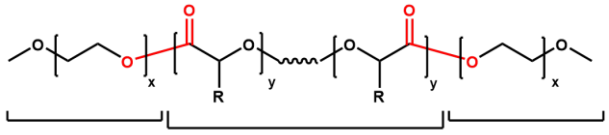 <br>**Lactic acid: R = $CH_3$**<br>**Glycolic acid: R = H** | *20 – 80°C (cgt)* | OEG | 71,72,74 |
| **1.17** | Poly(ethylene oxide)-grafted poly(lactide)s<br> 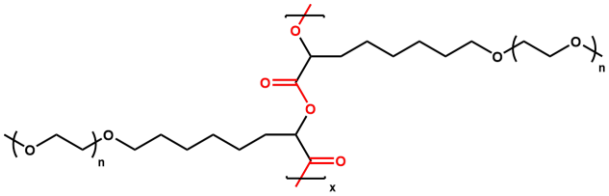 | 19 -37 °C | OEG | 79 |
| **1.18** | 1-decyl azide and methoxy diethylene glycol azide grafted on poly(propargyl glycolide); decyl/mDEG–grafted-PPGL<br> 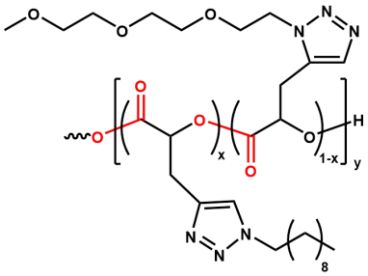 | 25 – 65 °C | OEG/alkyl ratio | 80 |
| **1.19** | Methoxy oligo(ethylene glycol) grafted on a (disulfide/ketal-modified) polyester backbone<br> 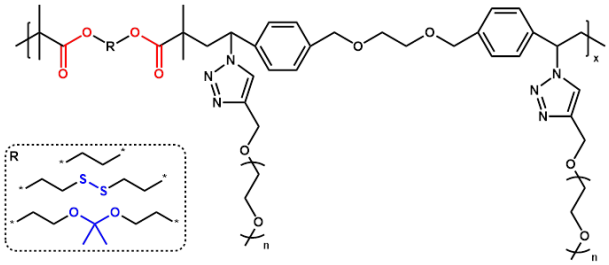 | 31.2 – 58.5 °C | OEG | 81 |
| **1.20** | Poly(ɣ-octyloxy-3-caprolactone)-*b*-poly[ɣ-2-(2-(2-methoxyethoxy) ethoxy) ethoxy-3-caprolactone]<br> 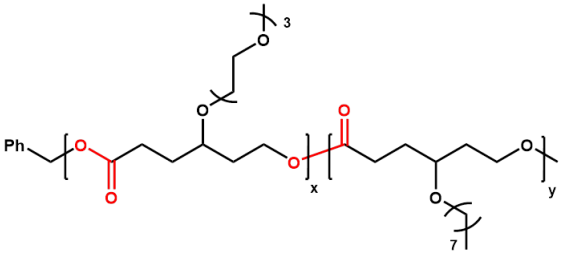 | 37.5 °C | OEG/alkyl ratio | 82 |

| | | | | |
|---|---|---|---|---|
| **1.21** | Poly[(2-(2-(2-methoxy)oligo(ethoxy))methyl)oxirane)-*alt*-(succinic anhydride)] or p($ME_nMO$-*alt*-SA)<br> 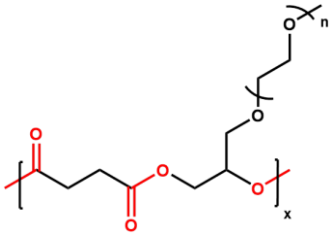 | 18 – 50 °C | OEG | 83-85 |
| **1.22** | Polycondensation of poly(ethylene glycol) diacrylates (PEGDA) or dimethacrylates (PEGDMA) with dithiols<br> 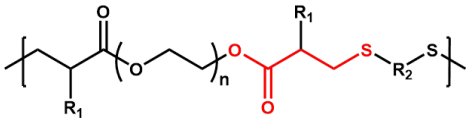 <br> 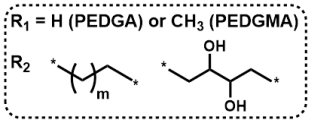 | 10 – 50°C | OEG/alkyl ratio | 86 |
| **1.23** | Poly[(2-(2-methoxyethoxy)ethyl methacrylate)-*co*-(oligo(ethylene glycol) methacrylate)-*co*-(5,6-benzo-2-methylene-1,3-dioxepane)]<br>or p($MEO_2MO$-*co*-OEGMA-*co*-BMDO)<br> 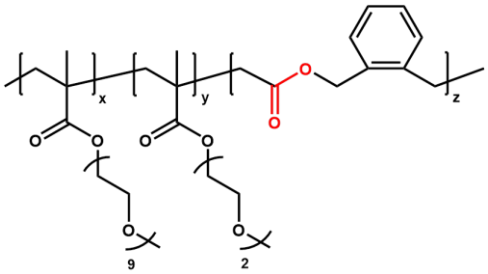 | 31 -67 °C | OEG | 90 |
| **1.24** | Poly[(N-isopropylacrylamide)-*co*-(5,6-benzo-2-methylene-1,3-dioxepane)] or p(NIPAAm-*co*-BMDO)<br> 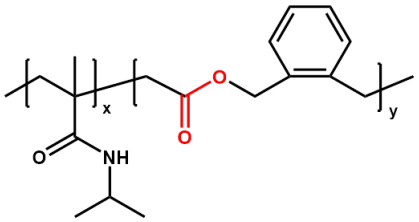 | 13 - 31.5 °C | NIPAAm | 91,92 |
| **1.25** | Poly[(N-isopropylacrylamide)-*co*-(3-butenyl 2-chloropropionate)]<br> 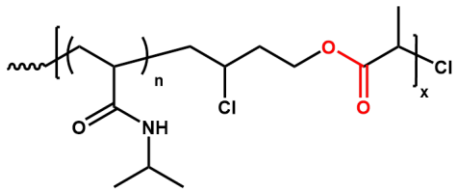 | 24.5 – 33.2 °C | NIPAAm | 94 |

| | | | | |
|---|---|---|---|---|
| **1.26** | Poly[(1,4-butanediol diacrylate)/(poly(ethylene glycol) diacrylate)-(1-(2-aminoethyl) piperazine)]-*g*-(cholesteryl)-*g*-(N-isopropylacrylamide)<br>or p(BDA/PEGDA-AEPZ)-*g*-CE-*g*-NIPAAm<br> 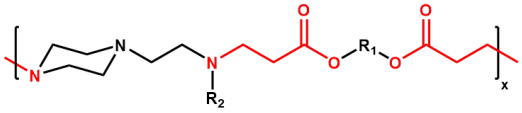 <br> 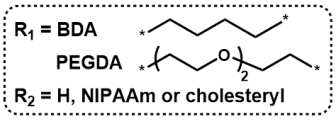 | 30.5 – 36.5 °C | NIPAAm/ OEG | 95 |
| **1.27** | Hydroxyethyl succinamide (HESA) based polymers<br> 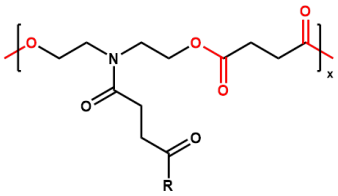 <br> 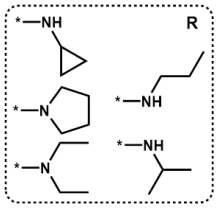 | 7.2 – 53 °C | ELP-like | 96 |

## ORGANOPHOSPHAZENES

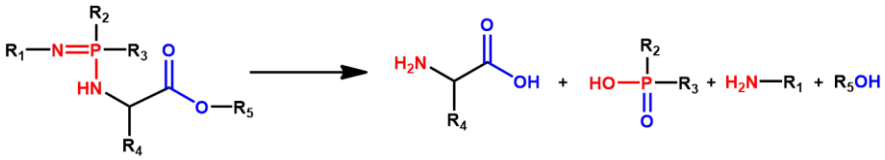

| Label | Polymer | $T_{cp}$ | T-responsive moiety | Ref. |
|---|---|---|---|---|
| **1.28**<br>**1.29** | Poly(organophosphazene)s with methoxy-poly(ethylene glycol) (MPEG) and amino acid ester side groups via *O,N-system*<br> 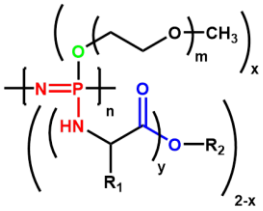 <br>**[1.28] (y = 1)**<br>**m = 7 or 16**<br>**$R_1$ = H ( Gly), $CH_3$ (Ala), COOR' (Mal), $CH_2COOR'$ (Asp) or $CH_2CH_2COOR'$ (Glu)**<br>**$R_2$ = $CH_3$ (Me), $C_2H_5$ (Et) or $CH_2C_6H_5$ (Bz)**<br>**[1.29] (y = 2)**<br>**m = 3 or 4**<br>**$R_1$ = H (Gly)**<br>**$R_1$' = $CH_2CH_2COOR'$ (Glu)**<br>**$R_2$ = $C_2H_5$ (Et)** | 25.2 – 98.5 °C<br>**[1.28]**<br>25 – 81 °C<br>**[1.29]** | OEG | 100,118 |
| **1.30** | Poly(organophosphazene)s with α-amino-ω-methoxy-poly(ethylene glycol) (AMPEG) and amino acid ester side groups via *N,N-system*<br> 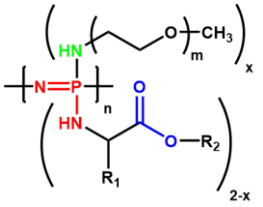 <br>**m = 7, 11 or 16**<br>**$R_1$ = H ( Gly), $CH_3$ (Ala), COOR' (Mal), $CH_2COOR'$ (Asp) or $CH(CH_3)CH_2CH_3$ (Ile)**<br>**$R_2$ = $C_2H_5$ (Et)** | 32 - >100 °C | OEG | 105,106 |

| | | | | |
|---|---|---|---|---|
| **1.31** | Poly(organophosphazene)s with methoxyethoxyethoxy (MEE) and lactic acid ester side groups via *O,O-system*<br> 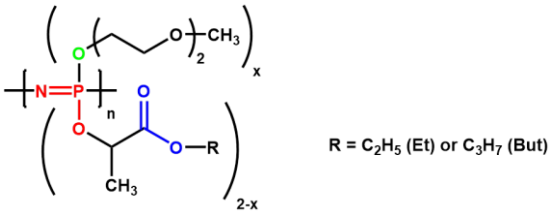 <br> | 33 – 52 °C | OEG | 120,121 |
| **1.32** | Poly(organophosphazene)s with poly(N-isopropylacrylamide) and glycine ethyl ester side groups via *N,N-system*<br> 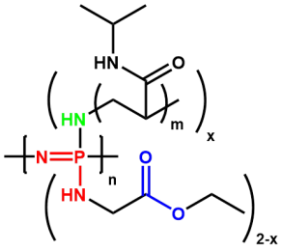 | 30 °C | NIPAAm | 123-125 |
| **1.33** | Cyclotriphosphazenes with methoxy poly(ethylene glycol) and amino acid ester (AAE) side groups<br> 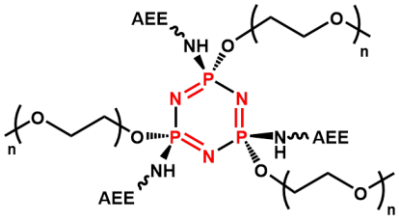 | 10.5 - >100 °C | OEG | 126-129 |
| **PHOSPHOESTERS** | | | | |
| | 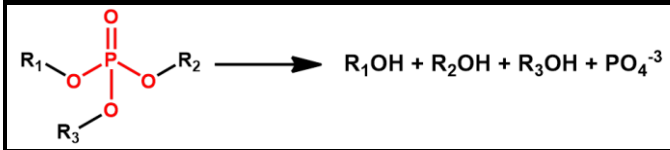 <br> | | | |
| **Label** | **Polymer** | **$T_{cp}$** | **T-responsive moiety** | **Ref.** |
| **1.34** | Poly[(2-ethoxy-2-oxo-1,3,2-dioxaphospholane)-*co*-(isopropoxy-2-oxo-1,3,2-dioxaphospholane)]<br>or p(EEP-*co*-IPP)<br> 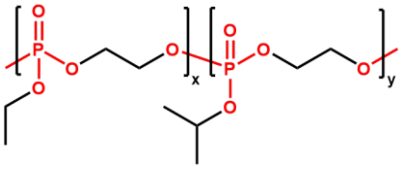 | 18 -38 °C | inherent | 146 |
| **1.35** | Poly[(2-ethoxy-2-oxo-1,3,2-dioxaphospholane)-*co*-(2-ethoxy-4-methyl-2-oxo-1,3,2-dioxaphospholane)]<br>or p(EEP-*co*-EMEP)<br> 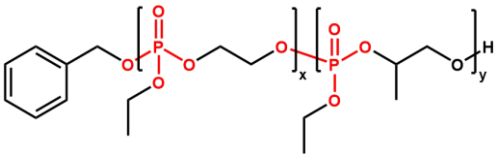 | 40 – 45 °C | inherent | 147 |

| | | | | |
|---|---|---|---|---|
| **1.36** | Monomethylether poly(ethylene glycol)-*b*-poly[(2-ethoxy-2-oxo-1,3,2-dioxaphospholane)-*co*-(isopropoxy-2-oxo-1,3,2-dioxaphospholane)] or mPEG-*b*-p(EEP-*co*-IPP)<br> 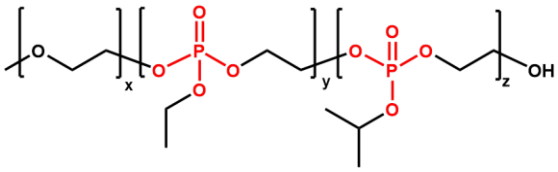 | 27 – 50 °C *(cmt)* | inherent | 148 |
| **1.37** | Poly(ε-caprolactone)-*b*-poly[(2-ethoxy-2-oxo-1,3,2-dioxaphospholane)-*co*-(isopropoxy-2-oxo-1,3,2-dioxaphospholane)/(2-methoxy-2-oxo-1,3,2-dioxaphospholane)] or PCL-*b*-p(EEP-*co*-IPP/MEP)<br> 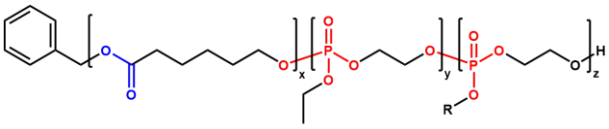 <br>R = $CH_3$ (MEP) or $CH(CH_3)_2$ (IPP) | 14 – 54 °C *(cmt)* | inherent | 149 |
| **1.38** | Poly(propylene phosphate)<br> 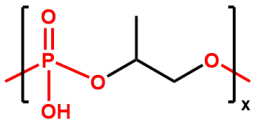 | 35 – 65 °C *(cgt with $Ca^{2+}$ present)* | inherent | 150 |
| **FORMAMIDES** | | | | |
| | 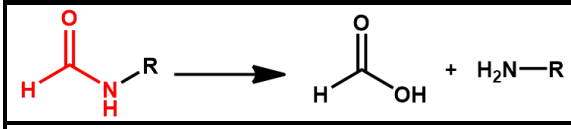 | | | |
| **Label** | **Polymer** | **$T_{cp}$** | **T-responsive moiety** | **Ref.** |
| **1.39** | Poly[(N-vinylformamide)-*co*-(N-vinylisobutyramide)] or poly(NVF-*co*-NVIBA) | 45 -70 °C [1.39] | inherent | 155,157 |
| **1.40** | Poly[(N-vinylformamide)-*co*-( N-vinylbutyramide)] or poly(NVF-*co*-NVBA)<br> 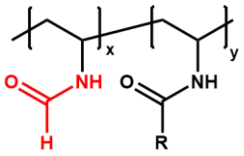 <br>[1.39] R = $CH_2(CH_3)_2$ (NVIBA)<br>[1.40] R = $CH_2CH_2CH_3$ (NVBA) | 33 – 39.5 °C [1.40] | | |
| **CARBONATES** | | | | |
| | 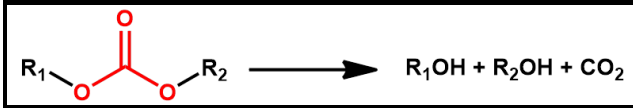 | | | |
| **Label** | **Polymer** | **$T_{cp}$** | **T-responsive moiety** | **Ref.** |
| **1.41** | Methoxy poly(ethylene glycol)-*b*-poly(trimethylene carbonate) or MPEG-*b*-PTMC<br> 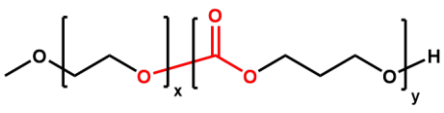 | 20 – 75°C *(cgt)* | OEG | 159,160 |

| | | | | |
|---|---|---|---|---|
| **1.42** | Methoxy poly(ethylene glycol)-*b*-poly[(ε-caprolactone)-*co*-(trimethylene carbonate)] or MPEG-*b*-(PCL-*co*-PTMC)<br> 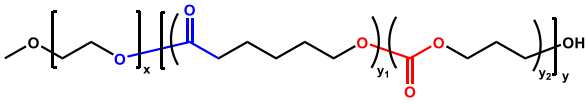 | 37 – 47 °C | OEG | 161 |
| **1.43** | Poly(ethyl methyl trimethylene carbonate)-*b*-poly[(PEG methyl trimethylene carbonate)-*co*-(dodecyl methyl trimethylene carbonate)] or p[MTC-$C_2$-*b*-(MTC-PEG-*co*-MTC-$C_{12}$)]<br> 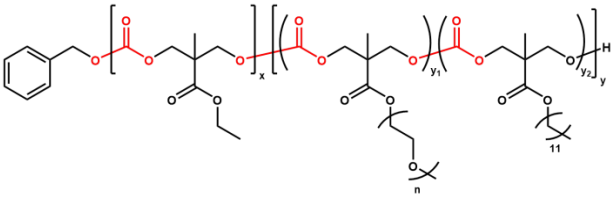 | 40 – 60 °C | OEG/alkyl ratio | 162 |
| **1.44** | Poly[5-(2-methoxy oligo(ethyoxy) methyl)-5-methyl-1,3-dioxa-2-one] or p(MTC-$MOE_nOM$).<br> 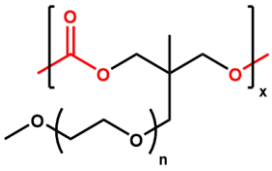 | 31 – 72 °C | OEG | 163 |
| **1.45** | Poly(carbonate-ether)s or PCE<br> 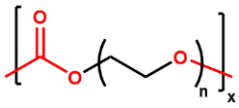 | 21.5 – 84.1 °C | OEG | 164 |
| **1.46** | Poly(PEG thioether/sulphone methyl trimethylene carbonate) or p(MTC-S/SO-$EG_n$)<br> 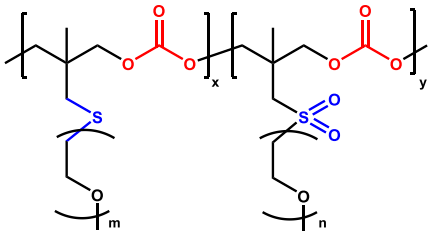 | 0 – 46° C | OEG | 165 |
| **1.47** | Poly[(N-isopropylacrylamide)-*co*-(acrylic acid)-*co*-(hydroxyethyl methacrylate-poly(trimethylene carbonate))] or p(NIPAAm-*co*-AAc-*co*-HEMAPTMC).<br> 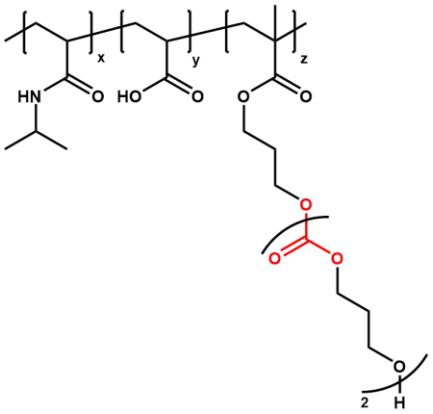 | 29.1 – 44.5 °C *(cgt)* | NIPAAm | 166 |

| | | | | |
|---|---|---|---|---|
| **1.48** | Poly(ethylene glycol)-*b*-poly[N-(2-hydroxypropyl) methacrylamide ethyl carbonate] or PEG-*b*-p(HPMAm-EC) 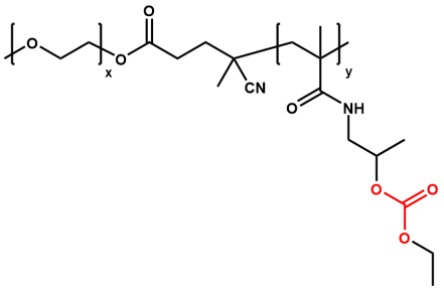 | 17 °C (*cmt*) | inherent | 167 |

cmt = critical micellization temperature, cgt = critical gelation temperature

## Transiently thermoresponsive polymers with acid-sensitive groups

In most examples described before, the cleavable moieties are preferentially hydrolyzed at neutral or basic pH, but are relatively stable under acidic conditions. In the following paragraphs various acid-degradable thermoresponsive polymers will be discussed, including their advantage over ester-based systems in view of biomedical applications Thermoresponsive polymers that have the ability to self-assemble into nanoparticles above their $T_{cp}$, but lose this feature upon acid-catalyzed cleavage of a usually hydrophobic moiety are of interest for the selective delivery of drugs to diseased tissues or upon internalization in intracellular acidic vesicles such as endosomes, lysosomes and phagosomes. Indeed, due to the fact that cancer cells have an abnormal acidic extracellular environment,[168,169] acid-sensitivity of a polymeric nanocarrier is an attractive trigger for drug release. Several pH-responsive nanoparticle systems have been reported to increase the efficacy of anticancer drugs in cancer therapy.[170-173] Moreover, drug delivery vehicles with pH-responsive shedding have been exploited for the cytoplasmic delivery of therapeutically fragile macromolecules (e.g. DNA, RNA and proteins) upon acidification of the late endosome and lysosome.[174,175]

According to the difference in response mechanism, pH-sensitive polymers can be classified into two categories. The first category of pH-sensitive polymers contains reversible ionizable segments such as poly(acid)s and poly(base)s[176-178], whose properties change reversibly by protonation or deprotonation as the pH of the surrounding environment changes. However, it should be noted that ionization can also cause permanent morphological changes of polymer particles, yielding out-of-equilibrium "frozen" structures.[179,180] The second category encompasses polymers with acid-labile linkages or moieties such as acetals[181-188], orthoesters[189-193], hydrazones[194-197], anhydrides[198] and

others[199,200] into the polymer main or side chain. As thermoresponsive polymers with reversibly ionizable segments are not transiently responsive to temperature and are already reviewed by others,[2,201-203] they will not be further discussed here. In the following section we will focus on polymers that are temperature-responsive, but lose their $T_{cp}$ upon acidic catalyzed hydrolysis (**Table 2**).

***Ortho-esters***

Li *et al.* prepared acid-labile, thermoresponsive poly(methacrylamide)s with pendant cyclic orthoester groups by free radical copolymerization of N-(2-methoxy-1,3-dioxan-5-yl) methacrylamide (NMM) and N-(2-ethoxy-1,3-dioxan-5-yl)methacrylamide (NEM) **[2.1]**.[204] The $T_{cp}$ of these copolymers could be tuned by changing the feed ratio of the two monomers and increased by gradual hydrolysis of the acid-labile orthoester groups. Upon complete hydrolysis, the polymers became fully water-soluble in aqueous medium. In a following study the trans and cis isomers of NEM were separated and used for radical polymerization, yielding p(tNEM) and p(cNEM) respectively.[205] They found that the stereochemical structures of the pendant cyclic orthoester groups in these poly(methacrylamide)s strongly affected their aqueous solution properties as well as their hydrolysis kinetics. P(cNEM) had a higher $T_{cp}$ with a smaller transition enthalpy compared to p(tNEM). Around their respective $T_{cp}$ values, p(cNEM) exhibited a liquid-liquid phase separation whereas p(tNEM) displayed a liquid-solid phase transition. Moreover, the products that were formed upon acid-triggered hydrolysis were affected by the configuration of the pendant cyclic groups.

In parallel, the same group of authors also prepared poly(acrylamides) with pendant cyclic orthoester groups by ATRP of trans-N-(2-ethoxy-1,3-dioxan-5-yl)acrylamide (tNEA) using a PEG macroinitiator **[2.2]**.[206] These block copolymers exhibited thermoresponsive behavior, with decreasing $T_{cp}$ for increasing p(tNEA) block length. The hydrophobic dye Nile Red could be loaded into the corresponding micelles that were stable at neutral pH, but were destabilized by acid-triggered hydrolysis of the orthoester moieties with subsequent release of Nile Red. To enable simultaneous loading of hydrophilic compounds through the formation of polymersomes (i.e. vesicles composed of amphiphilic block copolymers), a series of diblock copolymers containing a short PEG segment and p(tNEA) blocks with different lengths were synthesized.[207] These were water-soluble at low temperature, but upon heating above the $T_{cp}$ they self-assembled into different morphologies, depending on

the chain length of p(tNEA) and the polymer concentration. Micellar nanoparticles dissociated faster than polymersomes, but both showed accelerated hydrolysis under acidic conditions. Polymersomes could co-encapsulate both a water-soluble biomacromolecule (i.e. FITC-labeled lysozyme) and a hydrophobic drug (i.e. DOX) without the use of organic solvent, and exhibited pH-dependent drug release.

In a following study, a series of poly[(meth)acrylamide] derivatives with pendant orthoester groups were synthesized, varying in the type of alkyl substitutes, the stereochemical structures (trans versus cis) and the main chain structures, i.e. poly(methacrylamide) versus poly(acrylamide) **[2.3]**.[208] Aqueous solution properties and pH-dependent hydrolysis behavior of these polymers were studied. In general, poly(methacrylamide)s displayed higher $T_{cp}$ values than poly(acrylamide)s. Polymers with larger alkyl substitutes and trans configuration had a lower $T_{cp}$ and exhibited liquid-solid phase transitions, while those with smaller alkyl substitutes and cis configuration displayed liquid-liquid phase separation. The acid-triggered hydrolysis rate of the pendant orthoesters increased as the alkyl substitutes changed from methyl to isopropyl, and the configuration changed from cis to trans.

Also poly(acrylate) derivatives with six-member cyclic orthoester groups, i.e. 2-(1,3-dioxan-2-yloxy)ethyl acrylate (DEA) and 2-(5,5-dimethyl-1,3-dioxan-2-yloxy) ethyl acrylate(DMDEA) have been synthesized.[209] These two monomers were copolymerized with oligo(ethylene glycol) acrylate (OEGA) by ATRP yielding two series of thermoresponsive copolymers, i.e. p(DEA-co-OEGA) and p(DMDEA-co-OEGA), with $T_{cp}$ values ranging from 13 to 36 °C **[2.4]**. Compared to analogous poly(acrylamides) (*vide infra*), these acid-labile poly(acrylate)s are supposed to be less cytotoxic since they yield 2-hydroxyethyl acrylate instead of 2-hydroxyethyl acrylamide upon acid-catalyzed hydrolysis in the body. Therefore this chemistry was used to synthesize a series of multi-responsive nanogels by mini-emulsion copolymerization of OEGA and DMDEA, using bis(2-acryloyloxyethyl) disulfide (BADS) as a crosslinker.[210] These thermoresponsive nanogels were capable of encapsulating hydrophobic compounds such as Nile Red, PTX and DOX, with accelerated drug release by a cooperative effect of both acid-triggered hydrolysis and 1,4-dithiothreitol (DTT) induced reductive degradation (**Figure 9**).

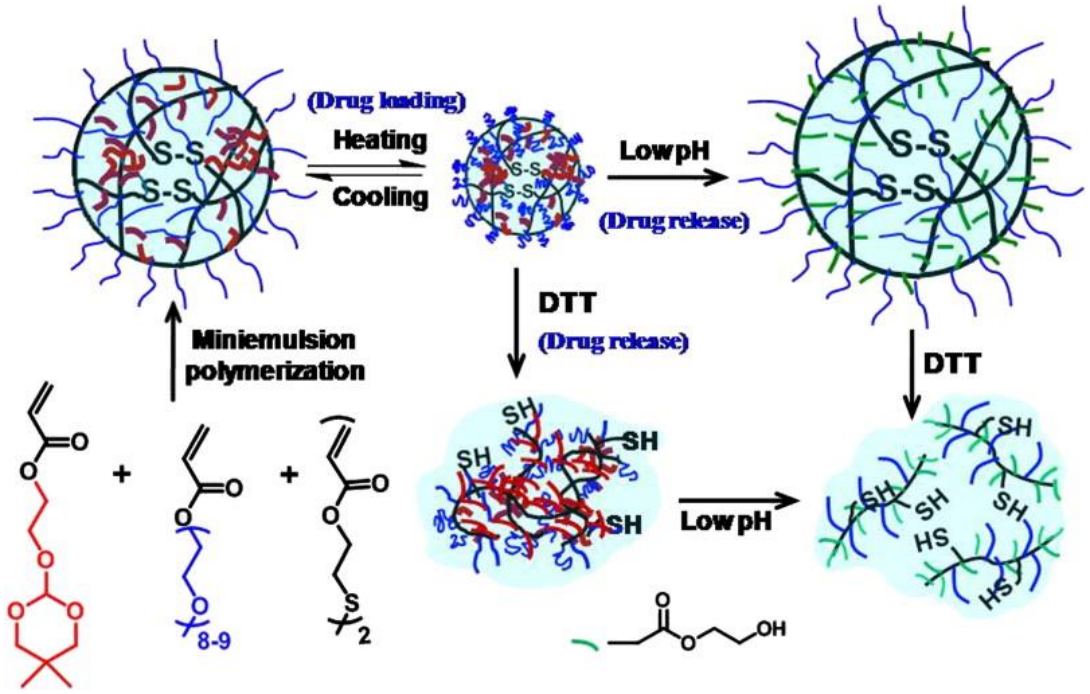


**Figure 9.** Synthesis and stimuli-responsive properties of p(OEGA-co-DMDEA-co-BADS) nanogels. *Reprinted from reference 210.*

Alternatively, Heller *et al.* prepared reverse thermogelling PEG-grafted poly(orthoester)s bearing acid-labile moieties in the polymer backbone.[211] Initially, reverse thermogelling PEG-grafted poly(acetals) (cfr. section acetals/ketals) were developed, but their degradation was too slow at physiological pH. This issue was addressed by grafting PEG onto a poly(orthoester) or poly(acetal-*co*-orthoester) backbone **[2.5] Similarly,** Wang and co-workers synthesized acid-labile poly(orthoester amide) or p(OEA) copolymers by polycondensation of a monomeric diamine containing a stabilized orthoester group with diacid esters of different chain lengths **[2.6]**.[212] The resulting p(OEA) copolymers exhibited a temperature-triggered reversible sol-gel phase transition in water which was exploited for the encapsulation of fluorescently labeled dextran as a model macromolecular drug. The p(OEA) hydrogels were capable of releasing the model drug through surface-erosion in response to mildly acidic pH. Later the same acid labile orthoester motif was incorporated in the side chain of a methacrylate monomer that was polymerized via ATRP from a PEG macro-initiator.[213] The resulting amphiphilic diblock copolymers self-assembled into micelles and were loaded with DOX that was released at a much higher rate in response to a decrease in pH. However, the authors did not report on any thermoresponsive behavior of these polymers.

***Acetals/ketals***

The Fréchet group was the first to report on acid-labile acetal moieties in a polymer side chain to allow for a hydrophobic-to-hydrophylic conversion upon hydrolysis.[214] By attaching a cyclic benzylidene acetal side group, monomers were equipped with hydrophobic groups via an acid-sensitive linkage and could be used as core constituent of block copolymer micelles (**Figure 10**). Upon acid-triggered hydrolysis of the cyclic acetal groups, the generation of more hydrophilic diol moieties caused destabilization of the micelles with subsequent release of an encapsulated payload. However, the authors did not mention any temperature-responsive behavior of these systems. A similar approach was used by Endo *et al.* to synthesize statistical amphiphilic copolymers containing 2,3-dihydroxypropyl methacrylate with a lilial-derived acetal moiety as a hydrophobic side chain and PEG as a hydrophilic side chain **[2.7]**.[215] Although these polymers also did not exhibit typical thermoresponsive behavior, the aggregation-dissociation behavior of one of the polymers in aqueous media was dependent on temperature in the presence of NaCl. In aqueous solution without NaCl the polymers self-assembled into micelles independent of the solution temperature, but upon addition of NaCl the micelles assembled into larger aggregates upon heating above the $T_{cp}$. Based on this temperature-responsive behavior, hydrolysis of the acid-labile acetal side chain could be inhibited upon heating-induced aggregation. Alternatively Alexander *et al.* used a similar acetal-bearing hydrophobic monomer for copolymerization with NIPAAm, aiming at loss of thermoresponsive self-assembly behavior upon acid-catalyzed hydrolysis of the dioxolane moieties with subsequent increase of $T_{cp}$ **[2.8]**.[216] These polymers were used to graft to branched PEI as a model polycation used in nucleic acid delivery systems.

Thayumanavan *et al.* reported on triple stimuli-responsive block copolymers with an acid-sensitive tetrahydropyran-protected poly(2-hydroxyethyl methacrylate) or p(THP-HEMA) as the hydrophobic part and temperature-responsive p(NIPAAm) as the hydrophilic part, linked via a redox-sensitive disulfide bond **[2.9]**.[217] Deprotection of the THP moieties under mild acidic conditions converts the hydrophobic block to a hydrophilic p(HEMA) and resulted in a loss of the block copolymers' thermoresponsive behavior. However, upon reduction of the disulfide bond connecting both blocks, the polymers disintegrate into their constituent homopolymers, thereby yielding thermoresponsive p(NIPAAm) segments (**Figure 11**). Analogously Yue Zhao *et al.* prepared diblock copolymers composed of hydrophilic PEG

and hydrophobic poly(2-tetrahydropyranyl methacrylate) or p(THPMA) blocks.[218] The PEG-b-p(THPMA) block copolymers formed micelles in aqueous solution that could be destabilized by hydrolytic cleavage of the THP groups, but did not exhibit temperature-responsive behavior.

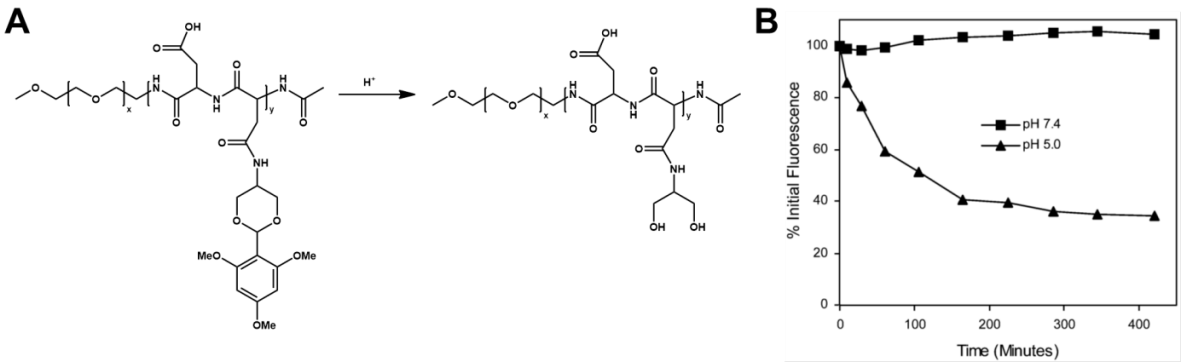


**Figure 10**. **(A)** Acid-catalyzed hydrolysis of a poly(ethylene glycol)-*b*-poly(cyclic benzylidene acetal-functionalized aspartic acid) block copolymer or PEG-*b*-p(CBA-Asp) and **(B)** subsequent release of their fluorescent payload. *Reproduced from reference 214.*

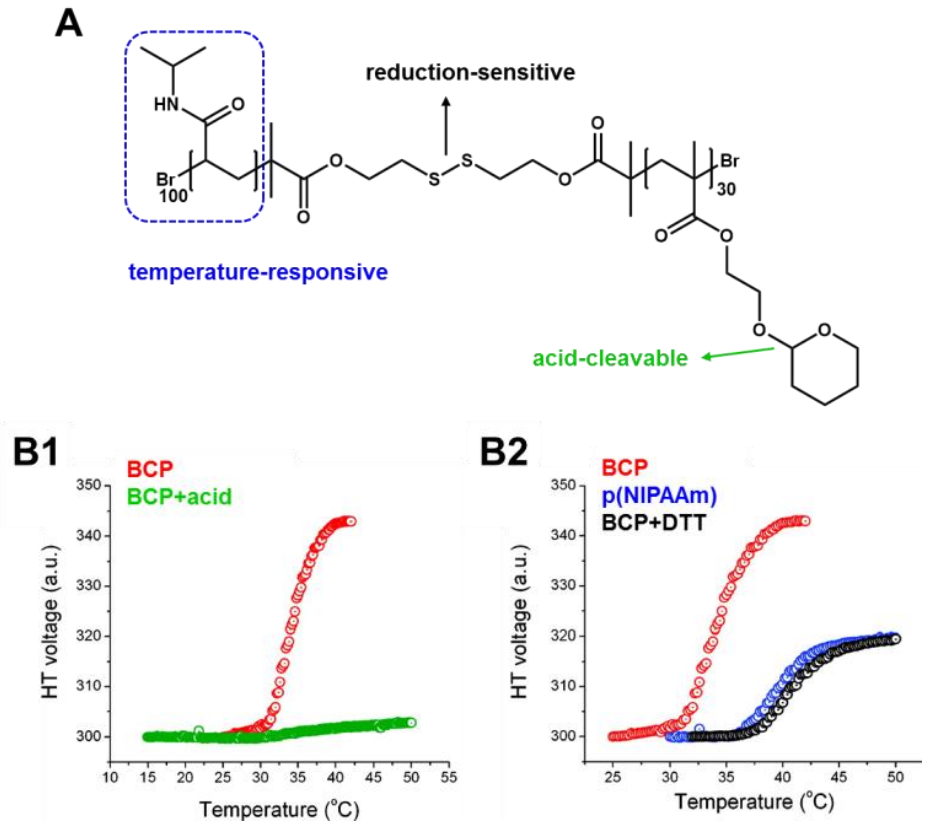


**Figure 11. (A)** Molecular structure of p(NIPAAm)-SS-p(THP-HEMA) block copolymers (BCP) with temperature-, reduction- and acid-sensitive moieties. **(B)** Thermoresponsive behavior of the BCP upon treatment with acid (B1) or the reductive agent DTT (B2). *Reproduced from reference 217.*

In analogy to their previous work (*vide infra*), Li and co-workers synthesized another type of acid-labile thermoresponsive polymers with pendant six-membered acetal groups by radical homopolymerization of N-(2,2-dimethyl-1,3-dioxan-5-yl) methacrylamide (NDMMAm) and N-(2,2-dimethyl-1,3-dioxan-5-yl) acrylamide (NDMAm) **[2.10]**.[219] Both polymers were pH-sensitive and upon acid-catalyzed hydrolysis of the acetal groups, the $T_{cp}$ of p(NDMMAm) gradually increased. However, the hydrolysis rate of these six-membered cyclic acetals was about 10 times slower compared to their previously reported orthoester-based polymers, which is in accordance with other findings in literature.[220] However, because the degradation products of acetal hydrolysis are neutral, the authors suggested they may avoid the inflammatory problems associated with the acidic degradation products of commonly used poly(ester)s or poly(orthoester)s. Robin *et al.* prepared a structural analogue of NDMA, i.e. 5-acrylamido-5-hydroxymethyl-2,2-dimethyl-1,3-dioxane (pTHAM), which was copolymerized with the corresponding acetal-free tris(hydroxymethyl) acrylamidomethane (THAM) monomer **[2.11]**.[221] Statistical p(pTHAM-co-THAM) copolymers exhibited thermoresponsive behavior, but transformed into the fully water-soluble p(THAM) upon acid-catalyzed hydrolysis.

Kizhakkedathu *et al.* reported on a thermoresponsive poly(N-alkylacrylamide)s with pendant five-membered acetal groups, i.e. poly[(N-(2,2-dimethyl-1,3-dioxolane)-methyl) acrylamide] or p(DMDOMAm) **[2.12]**.[222] Aqueous solutions of p(DMDOMAm) homopolymers exhibited a $T_{cp}$ around 23 °C that increased upon acid-catalyzed cleavage of the pendant dioxolane groups into hydrophilic diol repeating units (**Figure 12 A-B**). This approach afforded the synthesis of a series thermoresponsive polymers with different $T_{cp}$ values from a single batch of polymer with constant degree of polymerization. The diol moiety generated during hydrolysis was further oxidized to create reactive aldehyde functionalities along the polymer backbone, which could be exploited for the conjugation of various biomolecules. The same monomer was used by the De Geest group for the RAFT polymerization using a protein-based macro chain transfer agent (CTA).[223] Upon growth of the DMDOMAm polymer chain from the protein surface, the polymer-protein conjugates self-assembled into nanoparticles with a hydrophobic cavity that served for intracellular co-delivery of proteins and hydrophobic molecules. Acid-triggered hydrolysis of the dioxolane units into diol moieties rendered the conjugates fully water soluble irrespective of temperature (**Figure 12 C**). The applicability of these self-assembled nanoparticles for vaccine delivery was

demonstrated by the encapsulation of a hydrophobic immune-stimulatory Toll-like receptor agonist.

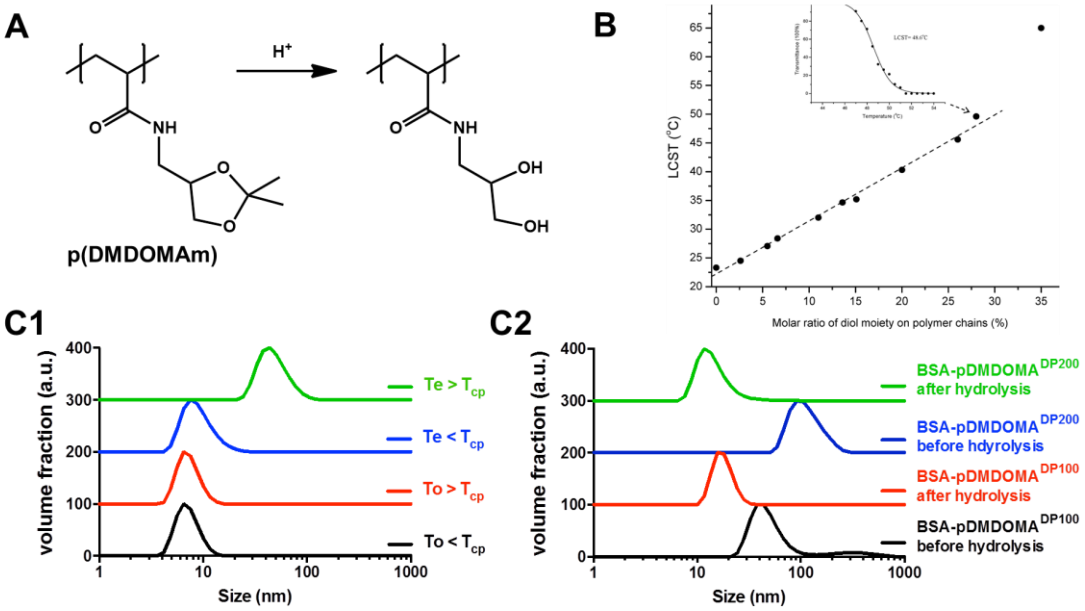


**Figure 12. (A)** Acid-catalyzed hydrolysis of p(DMDOMAm) with transformation of the pendant dioxolane groups into hydrophilic diol repeating units. **(B)** Relationship between $T_{cp}$ (LCST) and molar ratio of the diol moiety on p(DMDOMAm). **(C)** *Reproduced from references 222,223.*

The acrylate analogue of the DMDOMAm was used by Nie *et al.* to synthesize amphiphilic Y-shaped polymers by ATRP, containing MPEG as a hydrophilic block and two poly[(2,2-dimethyl-1,3-dioxolane-4-yl)methyl acrylate] or p(DMDMA) branches as hydrophobic blocks **[2.13]**.[224] These amphiphilic block copolymers self-assembled in aqueous solution into micellar aggregates and exhibited $T_{cp}$ values in a range from 30 to 60°C. Upon heating the authors observed a decrease in particle size, which they exploited for the accelerated release of encapsulated Nile Red. De Geest and Hoogenboom copolymerized DMDMA with either methoxy tri(ethylene glycol) acrylate (mTEGA) or 2-hydroxyethyl acrylate (HEA), yielding copolymers with $T_{cp}$ values that could be tailored by varying the DMDMA feed ratio **[2.14]**.[225,226] Both copolymers degraded into fully soluble unimers under acidic conditions, but the degradation rate was significantly higher when using HEA as a comonomer. This was ascribed to the better hydration of the hydroxy-containing collapsed p(HEA-co-DMDMA) globules in conjunction with autocatalytic acceleration of the hydrolysis reactions by the hydroxyl groups. To assess the bio-applicability of these block copolymers,

PTX was loaded in block copolymers containing p(HEA) as hydrophilic block and a p(HEA-co-DMDMA) copolymer as thermoresponsive block, thereby increasing PTX solubility and allowing pH-triggered drug release (**Figure 13**).[227]

Shinde *et al.* used the same acetal motif that is present in DMDOMAm and DMDMA to protect a glucose- and galactose-derived glycomonomers that each were copolymerized with NIPAAm **[2.15]**.[228,229] The $T_{cp}$ values decreased linearly with an increasing protected glycomonomer content in the copolymers. Upon acidic hydrolysis of acetonide-protected polymers the $T_{cp}$ of the copolymers increased to around or above body temperature.

More recently, Koberstein and coworkers reported on thermoresponsive polymers bearing acetal moieties in their backbone, allowing for acid-catalyzed hydrolysis into aldehyde and neutral diol degradation products **[2.16]**.[230] The polymers were synthesized by step growth polymerization of divinyl ether with diol monomers, that each comprised a hydrophobic part containing methylene units and a hydrophilic part with ethylene oxide units. The hydrophilic/hydrophobic balance could be tuned by altering the ratio of methylene to ethylene oxide moieties in either of the two monomers, yielding $T_{cp}$ values in a temperature range of about 6 – 80 °C.

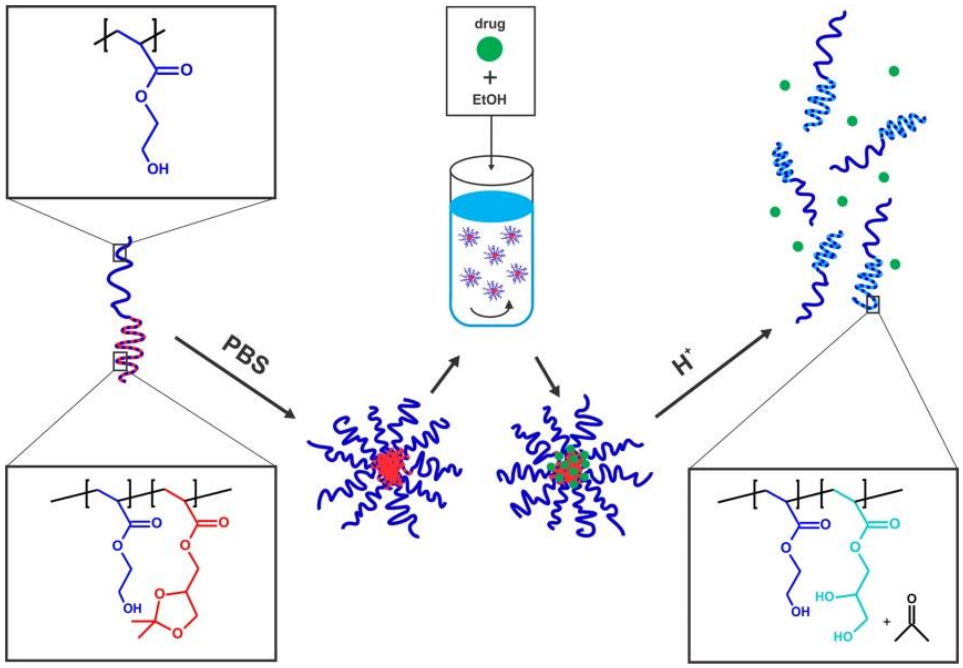


**Figure 13**. Self-assembly behavior, loading strategy (solvent displacement) and acid-triggered degradation of responsive p(HEA)-*b*-p(HEA-*co*-DMDMA) block copolymer drug nanocarriers. *Reprinted from reference 227.*

***Oxazolidines***

In addition to cyclic acetals and orthoester, oxazolidines are another class of pH-sensitive moieties that undergo facile and complete hydrolysis over a wide pH range, producing the corresponding carbonyl and b-amino alcohol compounds as degradation products.[231] Oxazolidines can be regarded as cyclic acetal analogs with one oxygen atom replaced by nitrogen that can bear additional functional groups that can influence the hydrolysis behavior.[232] Erjian Wang *et al.* reported on the RAFT polymerization of a oxazolidine based acid-labile monomer N-acryloyl-2,2-dimethyl-1,3-oxazolidine (ADMO) using a PEG-based chain transfer agent **[2.17]**.[233] The resulting PEG-*b*-p(ADMO) block copolymers formed micelles in water that could be disrupted with release of their payload upon acidic hydrolysis due to transformation of hydrophobic p(ADMO) into hydrophilic poly(2-hydroxyethyl acrylamide). The $T_{cp}$ of these polymers could be modulated from 40° to 72°C by varying the p(ADMO) block length or by partial acidic hydrolysis of the p(ADMO) segments.[234]

***Hydrazones/oximes***

Hruby *et al.* reported on biodegradable thermoresponsive copolymers of N-isopropylmethacrylamide and a methacrylamide monomer containing hydrophobic n-alkyl groups attached via a hydrolytically labile hydrazone bond **[2.18]**.[235] The cloud point of these copolymers could be adjusted by varying the copolymer composition and upon acid-catalyzed cleavage of the hydrazone bonds, the polymers became fully water soluble at body temperature. These thermoresponsive polymers were proposed to serve as carriers in radiotherapeutic applications by entrapping the model therapeutic radionuclide $^{64}Cu$ in its hydrophobic chelate form until complete dissolution by hydrolytic degradation. Fulton *et al.* engineered thermoresponsive copolymer scaffolds containing reactive aldehyde moieties that allowed for conjugation of alkoxyamine and hydrazide residues through oxime **[2.19]** or hydrazone **[2.20]** ligation respectively.[236] One could envision that conjugation of hydrophobic molecules could lower the $T_{cp}$ of a polymer scaffold to below body temperature, but exhibit a hydrophobic-to-hydrophilic conversion at 37°C upon hydrolysis of the acid-labile oximes and hydrazones. However, the authors found that conjugation of hydrophobic residues yields copolymers whose $T_{cp}$ values are in most cases unexpectedly higher than those of the parent copolymer scaffold.

**Table 2.** Transiently thermoresponsive polymers with acid-sensitive groups

**ORTHOESTER**

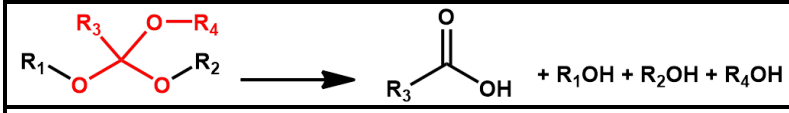


| Label | Polymer | $T_{cp}$ | T-responsive moiety | Ref. |
|---|---|---|---|---|
| **2.1** | Poly[(N-(2-methoxy-1,3-dioxan-5-yl)methacrylamide)-*co*-(N-(2-ethoxy-1,3-dioxan-5-yl)methacrylamide)] or p(NMM-*co*-NEM) 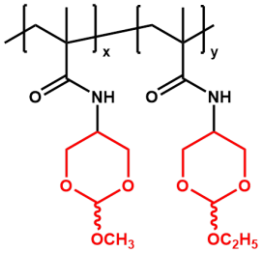  | 22.5 – 52.1 °C | inherent | 204 |
| **2.2** | Poly(ethylene glycol)-*b*-poly[trans-N-(2-ethoxy-1,3-dioxan-5-yl)acrylamide] or PEG-*b*-p(tNEA) 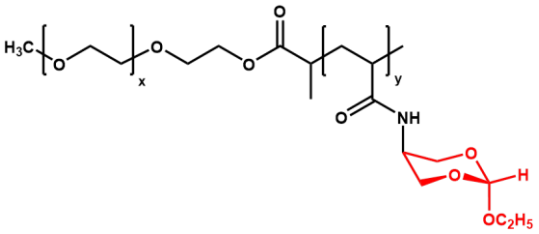  | 13.7 – 17.5 °C (*cmt*) | inherent | 206 |
| **2.3** | Poly[N-(2-alkyloxy-1,3-dioxan-5-yl)acrylamide] (A)<br>Poly[N-(2-alkyloxy-1,3-dioxan-5-yl)methacrylamide] (M) 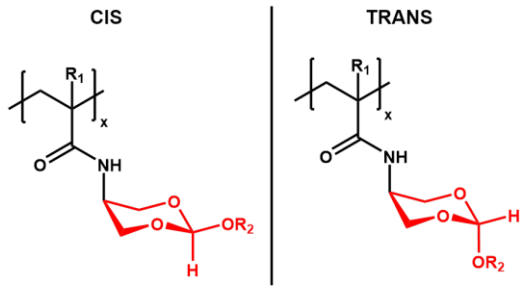  $R_1$ = H (A) or $CH_3$ (M)<br>$R_2$ = $CH_3$ (M), $C_2H_5$ (E), $C_3H_7$ (P) or $CH(CH_3)_2$ (iP) | 12 – 36.6 °C<br>11.5 – 40 °C | inherent | 208 |
| **2.4** | Poly[(oligo(ethyleneglycol) acrylate)-*co*-(2-(1,3-dioxan-2-yloxy) ethyl acrylate)] or p(OEGA-*co*-DEA)<br>Poly[(oligo(ethyleneglycol) acrylate)-*co*-(2-(5,5-dimethyl-1,3-dioxan-2-yloxy) ethyl acrylate)] or p(OEGA-*co*-DMDEA) 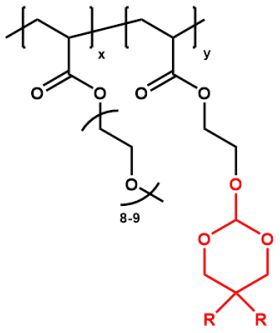  R = H (DEA) or $CH_3$ (DMDEA) | 12.9 – 30.8 °C<br>22.1 – 35.8 °C | OEG | 209 |

| | | | | |
|---|---|---|---|---|
| **2.5** | Poly(acetal-*co*-orthoester)-*g*-poly(ethylene glycol)<br> 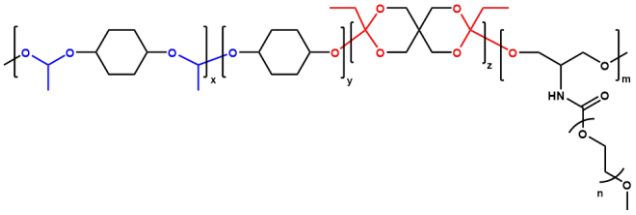 | 26 – 34 °C<br>*(cgt)* | OEG | 211 |
| **2.6** | Polycondensation of 4-Aminomethyl-2-aminopentyloxy-2-methyl-(1,3)-dioxolan with disuccinimidyl suberate, sebacate, or dodecanoate<br> 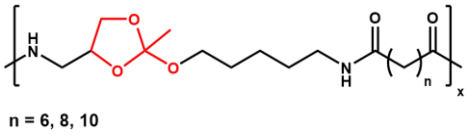 <br>n = 6, 8, 10 | 40 – 80 °C | inherent | 212 |
| **ACETALS/KETALS** | | | | |
| 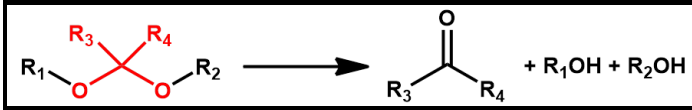 | | | | |
| **Label** | **Polymer** | **$T_{cp}$** | **T-responsive moiety** | **Ref.** |
| **2.7** | Poly(ethylene glycol)-*co*-poly(cyclic acetal-functionalized 2,3-dihydroxypropyl methacrylate)<br> 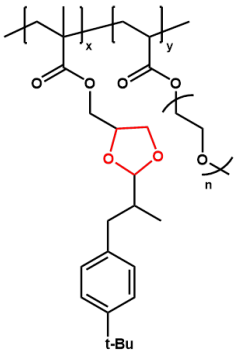 | 59 °C<br>(*cmt in salt*) | OEG/alkyl ratio | 215 |
| **2.8** | Poly[(N-isopropylacrylamide)-*co*-(N-(2-(2,4,6-trimethoxy phenyl)-1,3-dioxan-5-yl)acrylamide] or p(NIPAAm-*co*-TMPDA)<br> 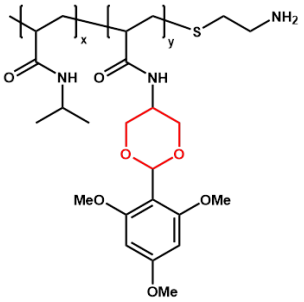 | 16 – 33 °C | NIPAAm | 216 |
| **2.9** | Poly[(N-isopropylacrylamide)-*b*-(tetrahydropyran-protected 2-hydroxyethyl methacrylate)] or p(NIPAAm-*b*-THP-HEMA)<br> 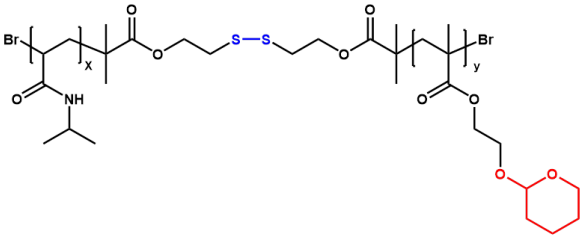 | 35 °C | NIPAAm | 217 |

| | | | | |
|---|---|---|---|---|
| **2.10** | Poly[N-(2,2-dimethyl-1,3-dioxan-5-yl)acrylamide] or p(NDMAm)<br>Poly[N-(2,2-dimethyl-1,3-dioxan-5-yl)methacrylamide] or p(NDMMAm)<br> 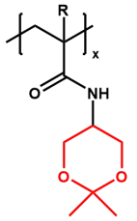 <br>**R = H (NDMAm) or $CH_3$ (NDMMAm)** | 17.8 °C<br><br>15.3 °C | inherent | 219 |
| **2.11** | Poly[(5-acrylamido-5-hydroxymethyl-2,2-dimethyl-1,3-dioxane)-*co*-(tris(hydroxymethyl)acrylamidemethane)] or p(pTHAM-*co*-THAM)<br> 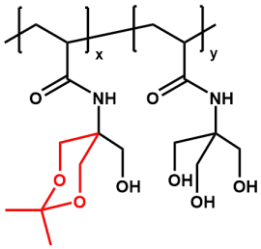 | 12.5 –58 °C | inherent | 221 |
| **2.12** | Poly[(N-(2,2-dimethyl-1,3-dioxolane)methyl)acrylamide] or p(DMDOMAm)<br> 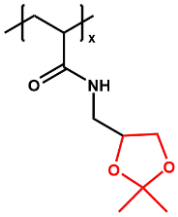 | 23 °C | inherent | 222,223 |
| **2.13** | Monomethoxy poly(ethylene glycol)-*b*-poly[(2,2-dimethyl-1,3-dioxolane-4-yl)methyl acrylate]$_2$ or MPEG-*b*-p(DMDMA)$_2$<br> 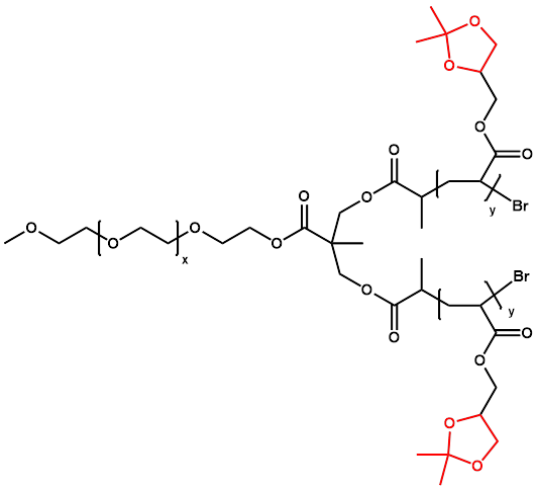 | 30 – 60 °C | OEG | 224 |

| | | | | |
|---|---|---|---|---|
| **2.14** | Poly[(2,2-dimethyl-1,3-dioxolane-4-yl)methyl acrylate]-*co*-poly[methoxy tri(ethylene glycol)acrylate] or p(DMDMA)-*co*-p(mTEGA)<br>Poly[(2,2-dimethyl-1,3-dioxolane-4-yl)methyl acrylate]-*co*-poly(2-hydroxyethyl acrylate) or p(DMDMA)-*co*-p(HEA)<br> 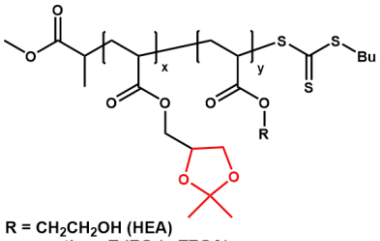 <br>R = $CH_2CH_2OH$ (HEA)<br>or methoxyTriEG (mTEGA) | 13.6 – 67.8 °C<br>9 – 70 °C | inherent | 225,226 |
| **2.15** | Copolymer of N-isopropylacrylamide with 3-Acrylamido-3-deoxy-1,2:5,6-di-O-isopropylidene-α-D-glucofuranose or an 6-azido-6-deoxy-1,2:3,4-di-O-isopropylidene-α-D galactopyranose based acrylate<br>Glucofuranose Galactopyranose<br> 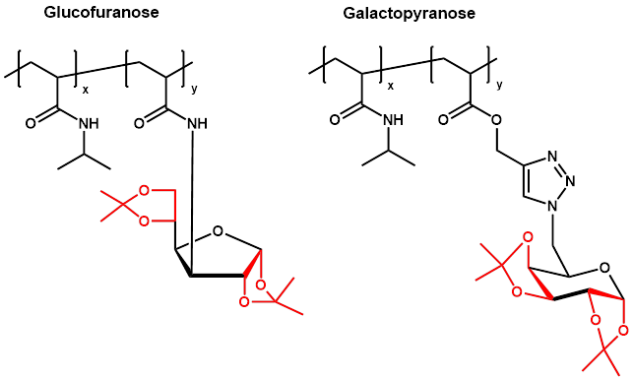 | 13.1 – 28.6 °C<br>20 – 28 °C | NIPAAm | 228<br>229 |
| **2.16** | Poly(acetals) via step growth polymerization of divinyl ethers with diols<br> 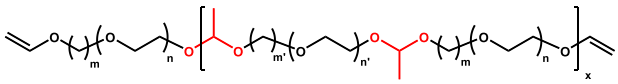 | 6 – 80 °C | OEG/alkyl | 230 |
| **OXAZOLIDINES** | | | | |
| | 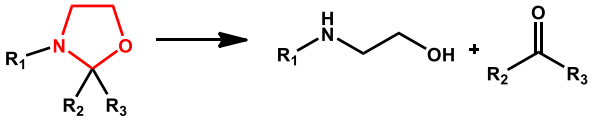 | | | |
| **Label** | **Polymer** | **$T_{cp}$** | **T-responsive moiety** | **Ref.** |
| **2.17** | Poly(ethylene glycol)-*b*-poly(N-acryloyl-2,2-dimethyl-1,3-oxazolidine) or PEG-*b*-p(ADMO)<br> 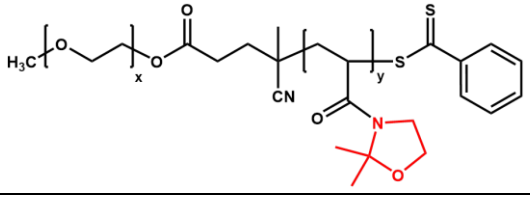 | 40 – 72 °C *(cmt)* | OEG | 233,234 |

## HYDRAZONES/OXIMES

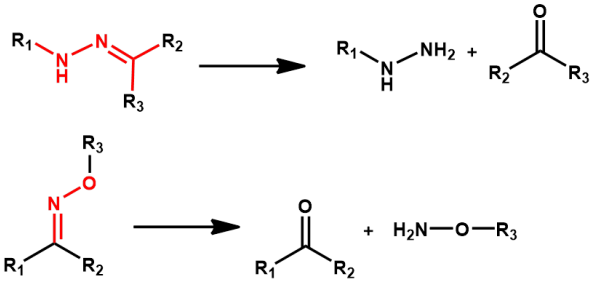

| Label | Polymer | $T_{cp}$ | T-responsive moiety | Ref. |
|---|---|---|---|---|
| **2.18** | Poly(N-isopropylmethacrylamide)-*co*-poly[N-(5-((propen/hexan/dodecan-2-ylidenehydrazino) carbonyl)pentyl)methacrylamide] 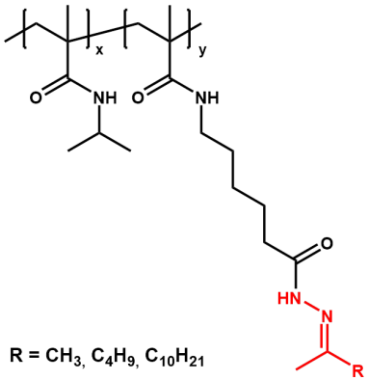 R = $CH_3$, $C_4H_9$, $C_{10}H_{21}$ | 13 – 44 °C | NIPMAm | 235 |
| **2.19** | Poly[oligo(ethylene glycol) monomethyl ether methacrylate]-*co*-poly[acylhydrazide-reacted (methacryloxyethoxy) benzaldehyde] of p(OEGMA)-*co*-p(AH-MAEBA) 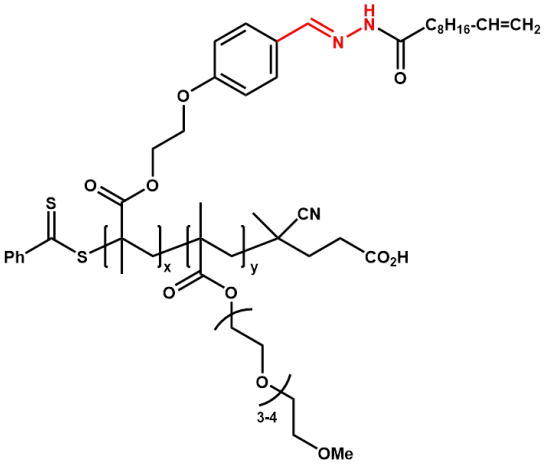 | 38 °C | OEG/alkyl | 236 |

| | | | | |
|---|---|---|---|---|
| **2.20** | Poly[oligo(ethylene glycol) monomethyl ether methacrylate]-*co*-poly[alkoxyamine-reacted (methacryloxyethoxy) benzaldehyde] of p(OEGMA)-*co*-p(AA-MAEBA) 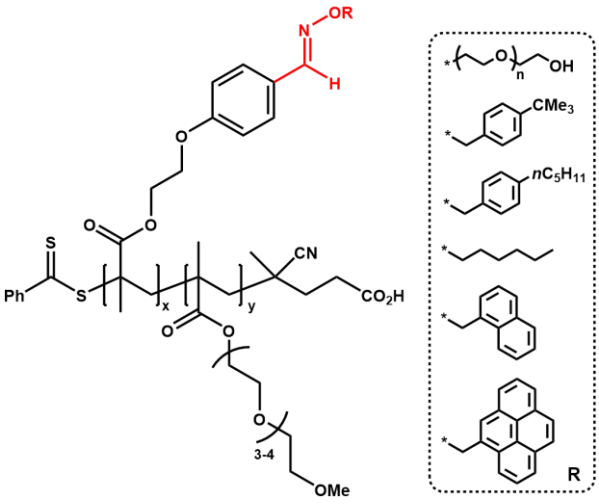 | 42 -48.5 °C | OEG/alkyl | 236 |

cmt = critical micellization temperature, cgt = critical gelation temperature

## Transiently thermoresponsive polymers with photo-sensitive groups

Various groups have explored photo-induced switching of the $T_{cp}$ of thermoresponsive polymers. Typically photochromic side-groups such as azobenzenes[237-241], 1,2-dithienylethene derivatives[242] or spirobenzopyran[243] are incorporated into a thermoresponsive polymer backbone (**Figure 14 A**). Upon UV radiation, these groups undergo photo-isomerization (cis/trans), resulting in a shift of the $T_{cp}$. Another example of a photo-responsive compound is the dye malachite green that changes from a nonionic structure to a cationic form upon UV irradiation, which has been reported to cause an upwards shift in $T_{cp}$ of a random copolymer with NIPAAm compared to the $T_{cp}$ in the dark.[244] However, these are multicycle photoswitches that are reversible and hence do not result in transiently thermoresponsive polymers. Single-cycle photoswitches can be obtained by the removal of photo-cleavable protective groups upon photo-irradiation and have been used for various biomedical applications (**Figure 14 B**).[245,246] The Zhao group for example, synthesized various amphiphilic block copolymers where the hydrophobic block was functionalized with light-cleavable moieties such as ester derivatives of pyrenylmethyl,[247] 2-nitrobenzyl,[248] and 7-(diethylamino)coumarin.[249] Upon irradiation and subsequent cleavage of the photo-labile moieties the hydrophobic polymer blocks became hydrophilic, resulting in disruption of micellar nanoparticles derived from these polymers and subsequent release of their payload.

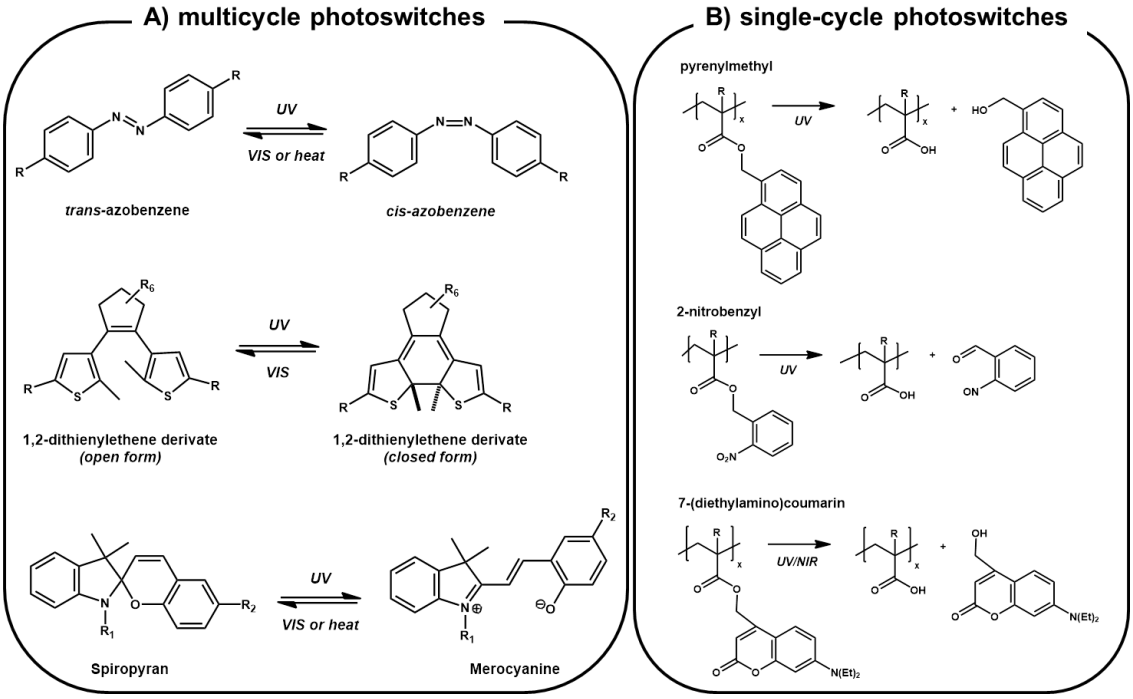


**Figure 14**. Overview of multicycle **(A)** and single-cycle **(B)** photoswitches that can be exploited to induce hydrophobic-to-hydrophylic conversions in polymer chains.

The 2-nitrobenzyl motif in particular has been used by various groups to engineer photo-sensitive transiently thermoresponsive polymers **(Table 3)**. Diez *et al.* exploited this chemistry to devise a photolithographic approach based on thermoresponsive poly(N-isopropylacrylamide-co-2-nitrobenzylacrylate) random copolymers, i.e. p(NIPAAm-co-NBA) **[3.1]**.[250] Incorporating hydrophobic 2-nitrobenzyl photocleavable groups into the p(NIPAAm) chains resulted in a decrease in $T_{cp}$ compared to a p(NIPAAm) homopolymer. However, upon UV irradiation the $T_{cp}$ of the copolymers gradually increased to above 50°C due to the formation of poly(N-isopropylacrylamide-co-acrylic acid). Illuminated parts of a thin casted p(NIPAAm-co-NBA) film will therefore dissolve at higher temperatures than the surrounding areas, leading to pattern development (**Figure 15**). Similarly, Zhao and coworkers prepared thermo- and light-sensitive diblock copolymers by copolymerizing a mixture of ethoxytri(ethylene glycol) acrylate (TEGEA) and 2-nitrobenzyl acrylate (NBA) from a PEG macroinitiator **[3.2]**.[251] The resulting PEG-b-p(TEGEA-co-NBA) copolymers were water soluble at low temperature but self-assembled into micelles when the solution was heated above the $T_{cp}$ of the p(TEGEA-co-NBA) polymer block. Upon UV irradiation, the 2-nitrobenzyl group was cleaved and the $T_{cp}$ of the thermosensitive block increased, causing the

dissociation of micelles and release of encapsulated Nile Red. By further increasing the temperature above the $T_{cp}$ of the newly formed thermosensitive block, micellization reoccurred and the released Nile Red could be re-encapsulated into the micelle core. Liu *et al.* synthesized diblock copolymers comprising a PEG block and a dual thermo- and light-responsive block based on p(NIPAAm) and the light-cleavable poly[5-(2'-(dimethylamino)ethoxy)-2-nitrobenzyl acrylate] or p(DMNA) **[3.3]**.[252] For their application, either a fluorescence resonance energy transfer (FRET) donor or acceptor moiety was also included in the multiresponsive blocks. After mixing these two different block copolymers, they self-assembled into micelles when heating above the $T_{cp}$. This induced a closer spatial proximity between the FRET pair within the micellar core and led to substantially enhanced FRET efficiency. Upon UV irradiation, the DMNA moieties underwent light-induced cleavage, yielding negatively charged carboxylate groups which caused an increase in $T_{cp}$ from 31 to 46°C, thereby leading to micellar disruption accompanied by a decrease in FRET efficiency.

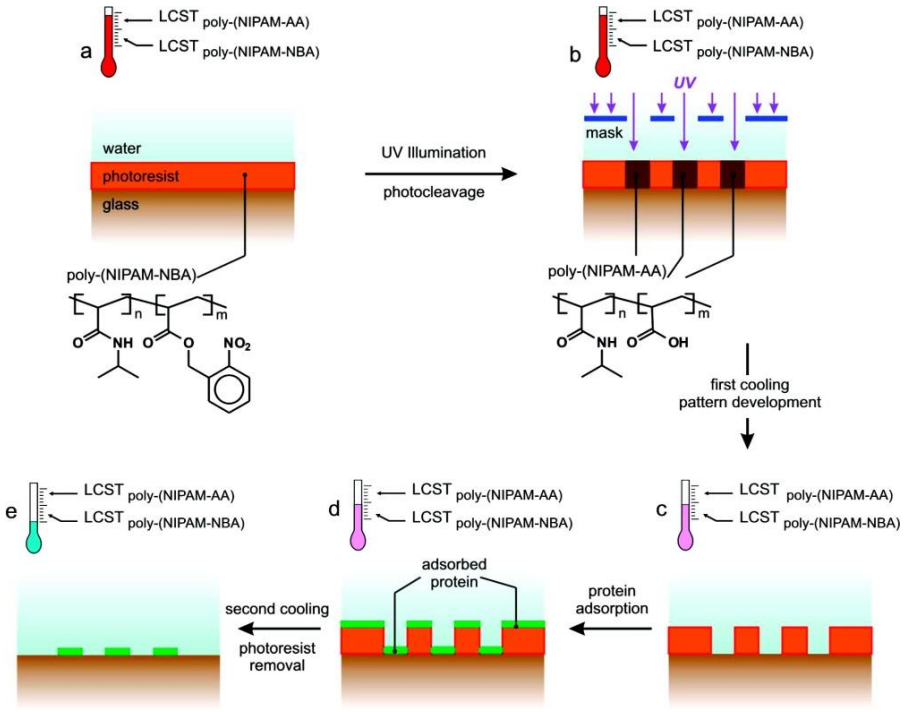


**Figure 15.** Scheme of photopatterning using p(NIPAAm)-based photoresists with temperature-triggered development. Thermoresponsive poly(2-nitrobenzylacrylate-co-N-isopropylacrylamide) is deposited as photoresist onto a substrate **(a)**. Illumination of the photoresist **(b)** results in photocleavage of nitrobenzyl acrylate groups, increasing the $T_{cp}$ (LCST). After the photoresist pattern is developed at slightly lower temperature **(c)**, proteins are adsorbed **(d)**. The photoresist (together with the proteins on top) can be completely removed in aqueous environment at low temperatures **(e)**. *Reprinted from reference 250.*

**Table 3.** Transiently thermoresponsive polymers with photo-sensitive groups

**NITROBENZYL DERIVATIVES**

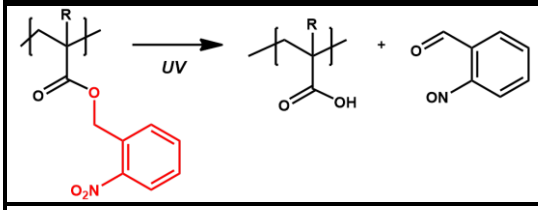


| Label | Polymer | $T_{cp}$ | T-responsive moiety | Ref. |
|---|---|---|---|---|
| **3.1** | Poly[(N-isopropylacrylamide)-*co*-(2-nitrobenzylacrylate) or p(NIPAAm-*co*-NBA) 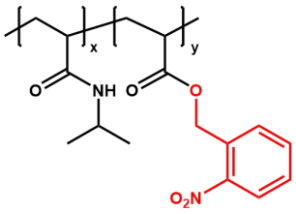 | 5 – 24 °C | NIPAAm | 250 |
| **3.2** | Poly[(ethoxytri(ethylene glycol) acrylate)-*co*-(2-nitrobenzyl acrylate)] or p(TEGEA-*co*-NBA)<br>Poly(ethylene glycol)-*b*-poly[(ethoxytri(ethylene glycol) acrylate)-*co*-(2-nitrobenzyl acrylate)] or PEG-*b*-p(TEGEA-co-NBA) 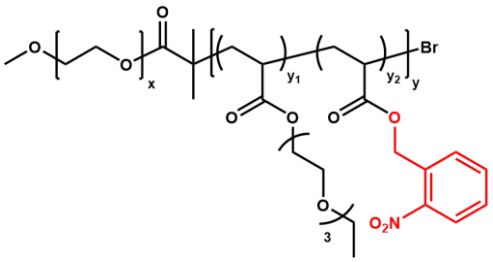 | 18 °C<br>21 – 25 °C *(cmt)* | OEG | 251 |
| **3.3** | Poly(ethylene glycol)-*b*-poly[(N-isopropylacrylamide)-*co*-(5-(2'-(Dimethylamino)ethoxy)-2-nitrobenzyl acrylate)-*co*-(FRET-active acrylate)] 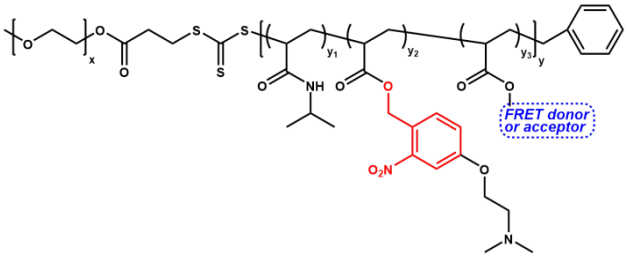 | 30 – 32 °C | NIPAAm | 252 |

cmt = critical micellization temperature

## Transiently thermoresponsive polymers with enzyme-sensitive groups

Poly(peptide)s have been proposed as promising biomaterials for drug delivery and tissue engineering due to their structural similarity to natural proteins and their enzymatic degradability.[253-259] Most aqueous poly(peptide) solutions form a gel phase at low temperatures due to strong hydrogen bonding or ionic interactions and undergo a gel-to-sol transition as temperature increases. A typical example are triblock copoly(peptides) with relatively short *leucine zipper* end blocks that flank a water-soluble poly(electrolyte) domain.[256] Natural poly(peptides) such as β-lactoglobulin[260,261] and elastin-like poly(peptide)s (ELP)[262-264] however, have reported to exhibit reverse thermal gelation properties. ELPs are oligomeric repeats of the penta(peptide) Val-Pro-Gly-Xaa-Gly where the *guest residue* Xaa can be any amino acid with the exception of proline. Similar to synthetic thermoresponsive polymers, they are highly soluble in water below their $T_{cp}$, but precipitate and aggregate when temperature is raised above this $T_{cp}$. This point is dependent on the guest residues and the number of repeats in the primary sequence, and may be tailored to the desired application.[265] This unique property has been exploited for the purification of recombinant ELP(-tagged) proteins by simple centrifugation cycles at elevated temperature and was termed *inverse transition cycling* by the Chilkoti group.[266-269] By combining a thermosensitive ELP segment, bearing valine as the Xaa *guest residue,* with silk-like Gly-Ala-Gly-Ala-Gly-Ser fragments[270,271] or collagen-derived Pro-Hyp-Gly sequences[272], polymers with reversed thermogelling properties were obtained. Furthermore, elastin-like poly(peptides) have been explored as biodegradable thermoresponsive materials for drug delivery such as hyperthermic cancer treatment. These systems have already been discussed by others[2,8,271,273-276] and are beyond the scope of the current chapter.

In addition to ELP-based polymers, various other biodegradable thermoresponsive poly(amino acids) have been described **(Table 4)**. Poly(aspartic acid) or p(Asp) in particular has drawn attention as water-soluble biomaterial owing to its facile synthesis from aspartic acid via poly(succinimide) or p(SI) and versatile modification by nucleophilic substitution reactions.[277,278] Jeong *et al.* introduced hydrophobic phenyl alanine ethyl esters and α-amino-*o*-methoxy PEGs onto a p(SI) backbone, resulting in poly(N-substituted α/β-asparagine)s or p(N-Asn) with $T_{cp}$ values ranging from 30 to 40°C depending on the number of grafted PEG-chains **[4.1]**.[279] When p(N-Asn) with a $T_{cp}$ of 30°C was dissolved in phosphate buffer, the $T_{cp}$ of the polymer increased to about 40 °C over two weeks due to the hydrolysis

of the ethyl esters into the corresponding carboxylic acids. By grafting amino poly(propylene glycol) (PPG) onto the p(SI) backbone, the resulting p(Asp)-g-PPG polymers exhibited thermogelling behavior with a pH-dependent $T_{cp}$ due to the ionization of aspartic acid moieties **[4.2]**.[280] Similarly, Kobayashi *et al.* prepared biodegradable thermoresponsive p(N-Asn) through the reaction of p(SI) with amino alcohols.[281] By covalent crosslinking of these polymers with diisocyanates, hydrogels were obtained that allowed for temperature-triggered release of a model drug.[282] Later, the same group of authors found that p(N-Asn) with thermogelation properties could be obtained by grafting more hydrophobic amino alkyl groups onto a p(SI) backbone, in addition to amino alcohols **[4.3]**.[283]

In analogy to poly(N-substituted α/β-asparagine)s, Kobayashi and coworkers reacted poly(ɣ-glutamic acid) with amino alcohols to obtain stimuli-responsive poly(α-N-substituted ɣ-glutamine) with $T_{cp}$ values that were sensitive to pH changes **[4.4]**.[284] Akashi *et al.* also prepared thermosensitive poly(ɣ-glutamic acid) by introducing hydrophobic n-propyl groups onto the polymeric chain **[4.5]**[285], while Li and coworkers prepared PEGylated poly-L-glutamates with thermoresponsive properties **[4.6]**[286]. Although all these polymers are presumed to be biodegradable, no degradation studies were performed in the corresponding papers of all three groups (e.g. Kobayashi, Akashi and Li). Jeong *et al.* reported on PEG-*b*-poly(alanine) or PEG-p(Al) block copolymers **[4.7],**poly(alanine) end-capped poloxamers **[4.8]** and PEG-*b*-poly(alanine-*co*-phenyl alanine) or PEG-*b*-p(Al-Phe) **[4.9]** as reverse thermogelling poly(peptides).[287-289] The p(Al)-PLX-p(Al) and PEG-*b*-p(Al-Phe) gels were stable in phosphate buffer saline but degraded in the subcutaneous layer of rats and in presence of the enzyme elastase.

Zhang and coworkers reported on random copolymers based on N-substituted N-carboxyanhydrides (NCA) monomers, i.e. Et-NCA and Bu-NCA **[4.10]**.[290] The resulting poly[(N-ethyl glycine)-*r*-(N-butyl glycine)] poly(peptoid) polymers were thermoresponsive and their $T_{cp}$ could be tuned in the temperature range of 20 °C to 60 °C. Because NCAs are sensitive to moisture and heat however, synthesis must be conducted in an anhydrous and anaerobic environment. Therefore Ling *et al.* copolymerized two N-substituted glycine N-thiocarboxyanhydrides (NTAs) monomers, i.e. sarcosine NTA (Sar-NTA) and N-butylglycine NTA (NBG-NTA), which are more stable than NCA analogues **[4.11]**.[291] The resulting p(Sar-*r*-NBG)s polymers were thermoresponsive and their $T_{cp}$ values could be tuned between 27 and 71 °C by adjusting the sarcosine molar fraction in the copolymers. Both groups stated that

these N-substituted poly(glycine) backbones are known to be biodegradable, but did not include degradation studies in their respective papers.

Well-established thermoresponsive polymers such as p(NIPAAm) have also been grafted onto poly(amino acid)s.[292,293] As mentioned before, these systems are not transiently thermoresponsive as the p(NIPAAm) chains stay intact upon enzymatic degradation of the poly(amino acid)s. The same holds true for p(NIPAAm)-based hydrogels with peptide crosslinkers as described by the Healy group.[294] Alternatively Katayama *et al.* introduced a peptide bearing monomer onto a p(NIPAAm) backbone that could be enzymatically degraded.[295] They synthesized a thermosensitive copolymer of NIPAAm with N-methacryloyl-GLRRASLG which contains a peptide substrate for protein kinase A (PKA) **[4.12]**, a key kinase in intracellular signal transduction. In response to phosphorylation by activated PKA, the $T_{cp}$ of the copolymer increased from below to above body temperature due to the hydrophobic-to-hydrophylic transition of the peptide side chains (**Figure 16**). When introducing N-methacryloyl-PEG as a third comonomer, the resulting copolymers formed micellar nanoparticles above their $T_{cp}$ that could disintegrate into soluble unimers in response to the PKA signal with subsequent release of an encapsulated payload. The authors suggested that this strategy could be applied to target kinases that are exclusively activated in disordered cells by changing the substrate peptide sequence, which would allow site-specific drug release into these specific cells if intracellular uptake and subsequent cytosolic translocation occurred.

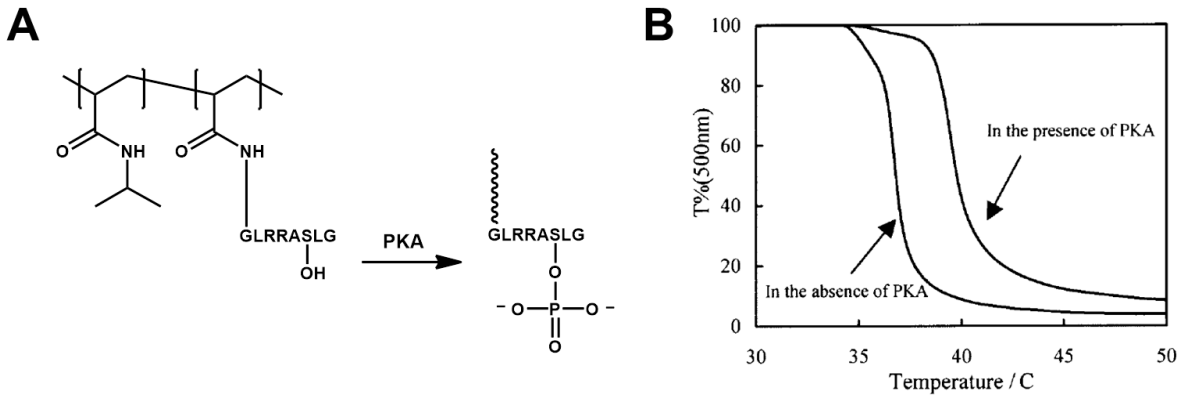


**Figure 16**. **(A)** Molecular structure of p(NIPAAm-*co*-N-methacryloyl-GLRRASLG) and phosphorylation by protein kinase A (PKA). **(B)** Temperature dependence of the light transmittance of a p(NIPAAm-*co*-N-methacryloyl-GLRRASLG) solution before and after phosphorylation with activated PKA. *Reproduced from reference 295.*

**Table 4.** Transiently thermoresponsive polymers with enzyme-sensitive groups

**POLY(AMINO ACIDS)**

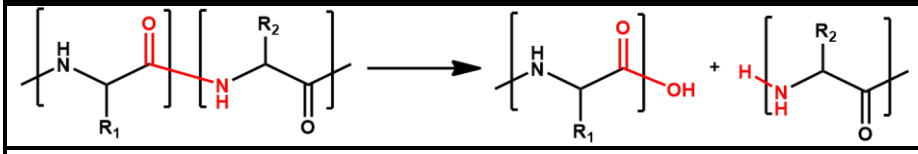

| Label | Polymer | $T_{cp}$ | T-responsive moiety | Ref. |
|---|---|---|---|---|
| **4.1** | Poly[(aspartic acid)-*g*-(α-amino-*o*-methoxy poly(ethylene glycol))]-*co*-poly[(aspartic acid)-*g*-(phenyl alanine ethyl ester)] 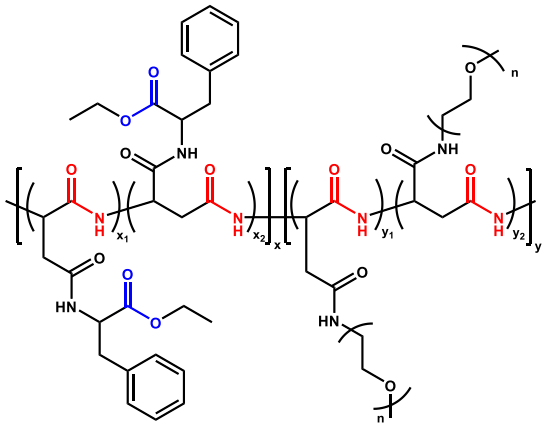 | 30 – 40 °C | OEG/alkyl ratio | 279 |
| **4.2** | Poly[(aspartic acid)-*g*-(amino-poly(propylene glycol))] 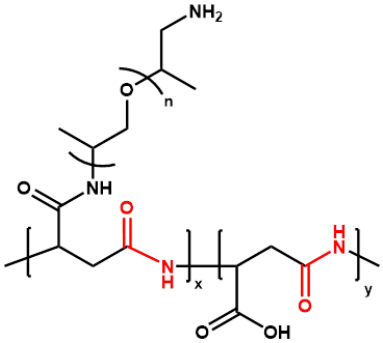 | 21 – 28 °C *(at pH 3)* | OEG | 280 |
| **4.3** | Poly[(aspartic acid)-*g*-(amino alcohols/amino alkyls)] 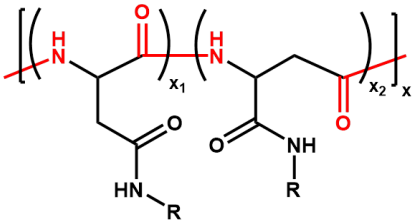 **R = $(CH_2)_{5\text{-}6}OH$ or $C_{12}H_{25}$** | 23 – 44 °C | inherent | 281,283 |
| **4.4** | Poly[(ɣ-glutamic acid)-*g*-(amino alcohols)] 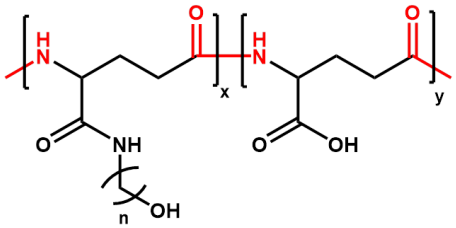 | 21 – 50 °C | inherent | 284 |

| | | | | |
|---|---|---|---|---|
| **4.5** | Poly[(Ɣ-glutamic acid)-*g*-(n-propyl)]<br> 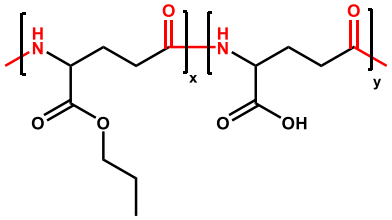 | 25 – 83 °C<br>*(in salt)* | inherent | 285 |
| **4.6** | Poly[(Ɣ-(2-Methoxy-oligo(ethoxy))esteryl-L-Glutamate] or p($EG_n$Glu)<br> 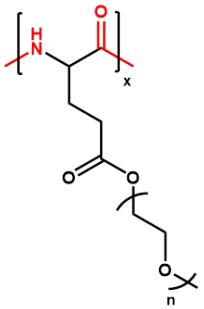 | 32 – 57 °C | OEG | 286 |
| **4.7** | Poly(ethylene glycol)-*b*-poly(alanine) or PEG-*b*-p(Al)<br> 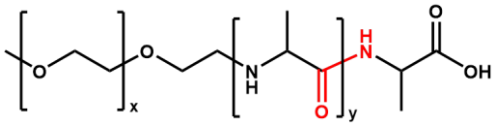 | 10 – 80 °C | OEG | 288 |
| **4.8** | Poly(alanine) end-capped poly(propylene glycol)-poly(ethylene glycol)-poly(propylene glycol) or p(Al)-PLX-p(Al)<br> 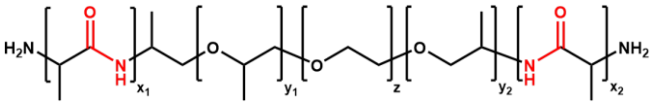 | 13 – 39 °C<br>*(cgt)* | poloxamer | 287 |
| **4.9** | Poly(ethylene glycol)-*b*-poly(alanine-*co*-phenyl alanine) or PEG-*b*-p(Al-*co*-Phe)<br> 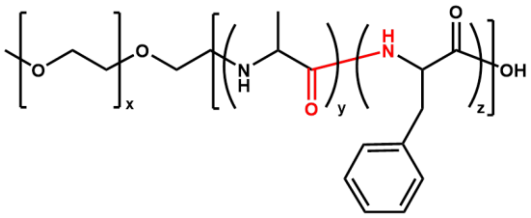 | 10 -22 °C<br>*(cgt)* | OEG | 289 |
| **4.10** | Poly[(N-ethyl glycine)-*r*-(N-butyl glycine)]<br> 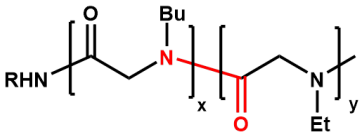 <br>**R = Bu or Bn** | 20 – 60°C | inherent | 290 |
| **4.11** | Poly[(sarcosine NTA)-*r*-(N-butylglycine NTA)] or p(Sar-*r*-NBG)<br> 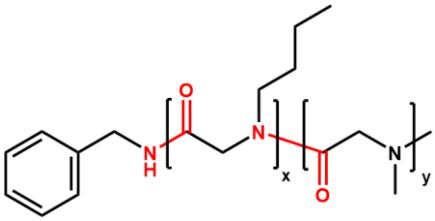 | 27 – 71 °C | inherent | 291 |

**KINASE SUBSTRATES**

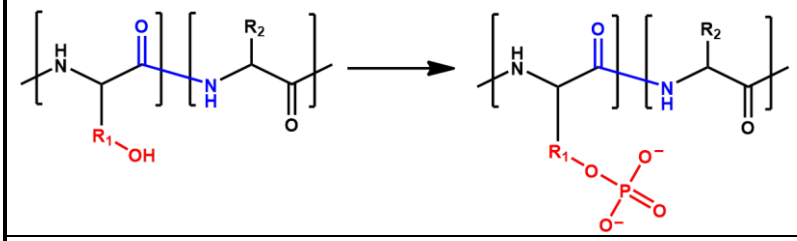

| Label | Polymer | $T_{cp}$ | T-responsive moiety | Ref. |
|---|---|---|---|---|
| **4.12** | Poly[(N-isopropylacrylamide)-*co*-(N-methacryloyl-GLRRASLG)-*co*-(N-methacryloyl-poly(ethylene glycol))] 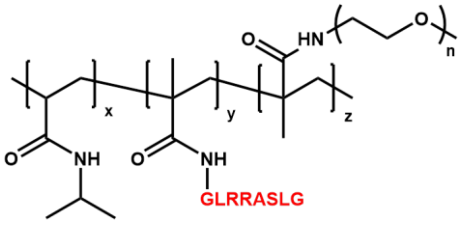 | 36.7 °C | NIPAAm | 295 |

cgt = critical gelation temperature

## Transiently thermoresponsive polymers with redox-sensitive groups

### *Reduction-sensitive groups*

Several groups have introduced reduction-sensitive disulfide moieties into thermoresponsive polymers to allow for glutathione-triggered disassembly **(Table 5)**. Glutathione is the main reducing agent (antioxidant) that is present in the human body. Moreover, intracellular glutathione concentrations are significantly higher than in systemic circulation (millimolar vs micromolar levels) which can be exploited to trigger degradation following cellular internalization.[296-299] In this regard, it is crucial to note that elevated glutathione levels are only found in the cytoplasm and not in endosomal vesicles where nanoparticles are typically stored upon endocytosis. Thus to be useful for cell uptake triggered drug release, additional cues to promote endosomal release should be used or one should speculated on disulfide exchange with cysteine moieties of cellular proteins.[300] Gibson *et al.* introduced disulfide linkages into p(NIPAAm) by polycondensation of a RAFT-derived telechelic macromonomer, yielding polymers with redox-sensitive thermoresponsive behavior **[5.1]**.[301] For this purpose, NIPAAm was polymerized using a RAFT agent with a pyridyl disulfide moiety at the α-terminus, which allowed a polycondensation-type, step-growth polymerization following aminolysis of the ω-terminal dithioester. Upon reduction

and subsequent cleavage of the polymer chain, the $T_{cp}$ increased from 46 to 62 °C (**Figure 17**). Later the shift in $T_{cp}$ was engineered to occur in a more physiologically relevant window.[302]

A similar approach was employed by Kwon Oh and coworkers to tune the thermoresponsive properties of p(OEGMA) units that were first described by *Lutz et al.* (cfr. section esters).[303] They used a bifunctional phenylthiocarbonylthio-based RAFT agent containing an internal disulfide bond. Aminolysis of the phenylthiocarbonylthiol groups yielded thermoresponsive polymers with both middle disulfide and terminal thiol groups, which allowed thiol-disulfide exchange reactions to form p(OEGMA)-multisegmented poly(disulfide)s **[5.2]**. Upon reduction, the authors also observed a significant upward shift in $T_{cp}$ compared to the non-cleaved polymer chains. Alternatively, they introduced a hydrophobic poly(methacrylate) functionalized with pendant disulfide linkages into the copolymers, resulting in lower $T_{cp}$ values **[5.3]**.[304] Upon cleavage of the pendant disulfide linkages into the corresponding thiols in response to external reducing agents, the copolymers became more hydrophilic, resulting in a shift in $T_{cp}$ from 29 to 38 °C. Upon conversion of the free pendant thiols to sulfides linkages by thiol–ene reactions Michael addition with acrylates, the $T_{cp}$ decreased again. This strategy could allow for the incorporation of additional reactive moieties or the conjugation of therapeutic molecules. Later on, these redox-sensitive thermoresponsive copolymers where used as a second block in combination with a PEG block to generate double hydrophilic diblock copolymers that can be converted into disulfide-crosslinked nanogels at temperatures above the $T_{cp}$.[305]

Alternatively Jeong *et al.* prepared thermoresponsive PEG disulfide multiblock co-polymers by oxidative coupling of α,ω-dithio-PEG chains of 400 Da and 600 Da respectively, which introduced redox-sensitive linkages along the PEG backbone **[5.4]**.[306] Depending on the ratio of the $PEG_{400}$ disulfide to $PEG_{600}$ disulfide, the $T_{cp}$ of the polymers could be controlled between 27 and 35 °C. The PEG disulfide multiblock co-polymer could be degraded in the presence of glutathione in a thiol-concentration-dependent manner.

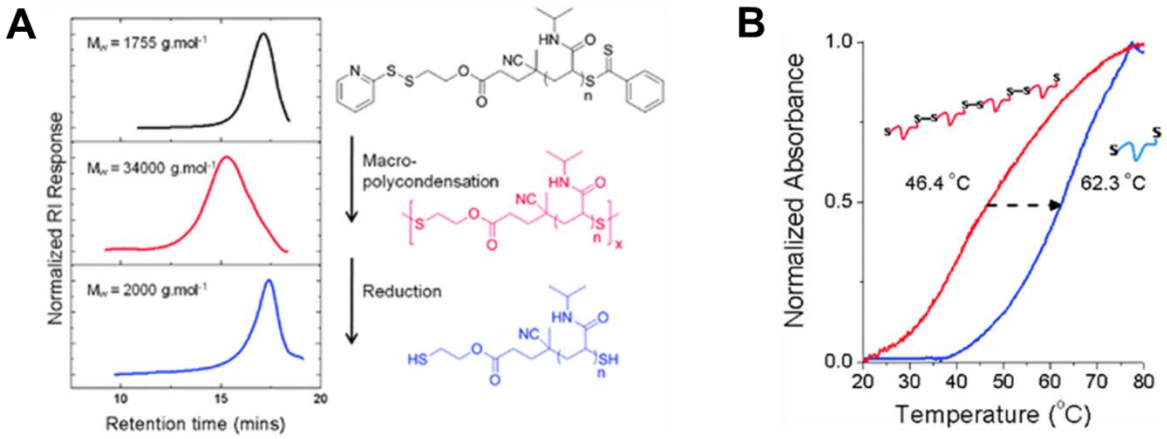


**Figure 17**. **(A)** SEC analysis demonstrating the successful polymer "condensation" procedure using a telechelic p(NIPAAm) macromonomer and subsequent reduction of the introduced backbone disulfides. **(B)** Turbidimetry curves showing an upwards shift in $T_{cp}$ of p(NIPAAm) following reduction of backbone disulfide bonds. *Reproduced from reference 301.*

***Oxidation-sensitive groups***

As mentioned in the section discussing carbonate-bearing polymers, Wang *et al.* constructed a series of thermoresponsive poly(carbonate)s by polymerizing cyclic TMC monomers that bear OEG units via thioether or/and sulfone bonds **[1.44] (Table 1)**.[165] Oxidation of the more hydrophobic thioether to a sulfone moiety rendered the polymers more hydrophilic and hence increased the $T_{cp}$ of the poly(carbonate) polymers.

Duval and coworkers prepared an ABC triblock polymer poly[(propylenesulfide)-*b*-(N,N-dimethylacrylamide)-*b*-(N-isopropylacrylamide)] or p(PS-*b*-DMA-*b*-NIPAAm) that can degrade upon contact with reactive oxygen species (ROS) **[5.5]**.[307] Due to the hydrophobicity of the p(PS) block, these polymers self-assemble into micelles at room temperature containing a hydrophobic p(PS) core that can accommodate hydrophobic drugs, and a p(NIPAAm) outer corona. Upon heating p(PS-*b*-DMA-*b*-NIPAAm) solutions above the $T_{cp}$ of p(NIPAAm), stable hydrated gels were formed. When exposed to ROS, the p(PS) block slowly transforms into the more hydrophilic poly(propylene sulfoxide) and ultimately poly(propylene sulfone), resulting in hydrogel degradation and drug release. Using ROS as a trigger for degradation and drug release has potential for biomedical applications as upregulation of oxidative stress is associated with various pathologies, including arthritis, atherosclerosis and cancer.

Davis *et al.* prepared thermoresponsive diblock copolymers of PEG and p(NIPAAm) that were sensitive to the biological messenger molecule nitric oxide (NO).[308] Using a functionalized PEG-based macroinitiator for ATRP polymerization of NIPAAm, both blocks were linked by an *o*-nitroaniline motif that could be reduced to an amide-functionalized o-phenylenediamine moiety **[5.6]**. In the presence of NO, the o-phenylenediamine groups were transformed into hydrolytically labile benzotriazoles, resulting in spontaneous hydrolysis and scission of the original diblock copolymers with subsequent decrease in $T_{cp}$ of the remaining p(NIPAAm) chains. Although this synthetic approach could allow for NO-triggered release of an encapsulated payload, it yields polymers that are the opposite of transiently thermoresponsive systems covered in this chapter.

**Table 5.** Transiently thermoresponsive polymers with redox-sensitive groups

| **REDUCTION-SENSITIVE DISULFIDES** | | | | |
|---|---|---|---|---|
| 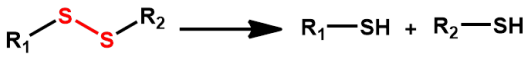 | | | | |
| **Label** | **Polymer** | **$T_{cp}$** | **T-responsive moiety** | **Ref.** |
| **5.1** | Polycondensation of thiol-terminated telechelic poly(N-isopropylacrylamide) 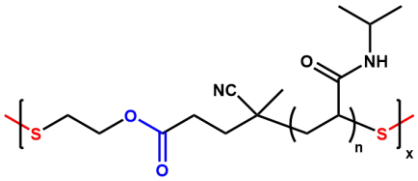 | 46.4 °C | NIPAAm | 301 |
| **5.2** | Polycondensation of thiol-terminated telechelic poly[oligo(ethylene glycol) monomethyl ether methacrylate] 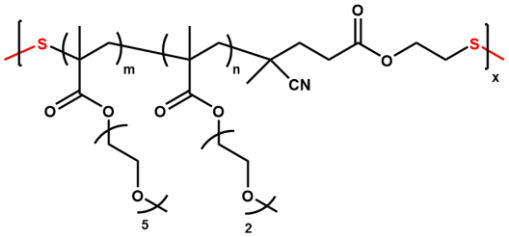 | 36 °C | OEG | 303 |
| **5.3** | Poly[oligo(ethylene glycol)monomethyl ether methacrylate]-*co*-poly(HMssEt methacrylate)] 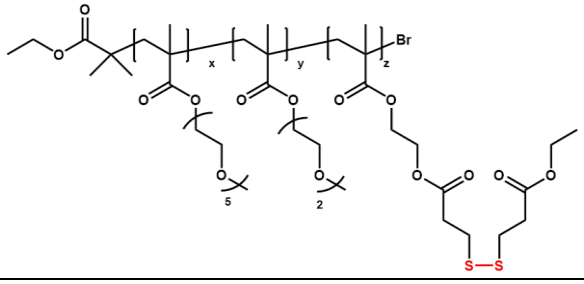 | 29.2 °C | OEG | 304 |

| | | | | |
|---|---|---|---|---|
| **5.4** | Polycondensation of α,ω-dithio-$PEG_{400}$ and α,ω-dithio-$PEG_{600}$ 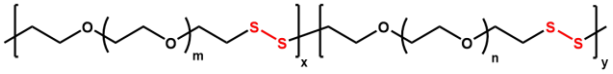 | 27 – 35 °C | OEG | 306 |
| **OXIDATION-SENSITIVE SULFIDES** | | | | |
| 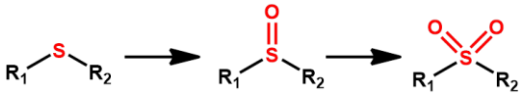 | | | | |
| **Label** | **Polymer** | **$T_{cp}$** | **T-responsive moiety** | **Ref.** |
| ***1.44*** *(Table 1)* | Poly(PEG thioether/sulphone methyl trimethylene carbonate) or p(MTC-S/SO-$EG_n$) 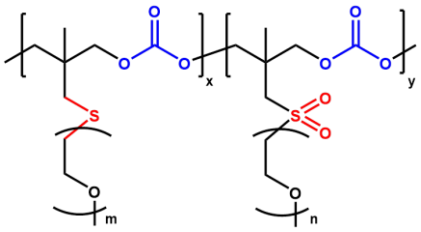 | 0 – 46° C | OEG | 165 |
| **5.5** | Poly[(propylenesulfide)-*b*-(N,N-dimethylacrylamide)-b-(N-isopropylacrylamide)] or p(PS-*b*-DMA-*b*-NIPAAm) 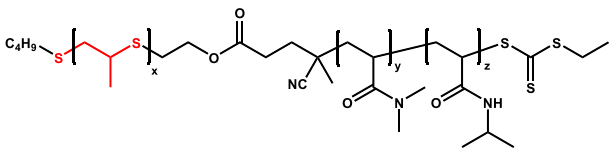 | 32 °C *(cgt)* | NIPAAm | 307 |
| **NO-MEDIATED OXIDATION** | | | | |
| 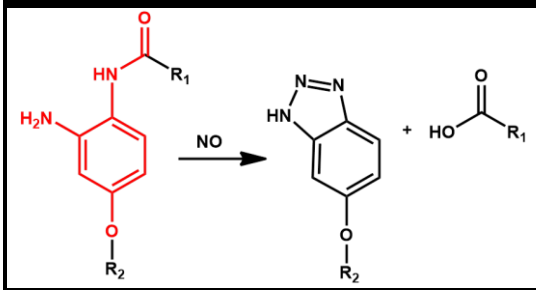 | | | | |
| **Label** | **Polymer** | **$T_{cp}$** | **T-responsive moiety** | **Ref.** |
| **5.6** | Poly(ethylene glycol)-*b*-(*o*-phenylenediamine)-poly(N-isopropylacrylamide) or PEG-*b*-($NH_2$)-p(NIPAAm) 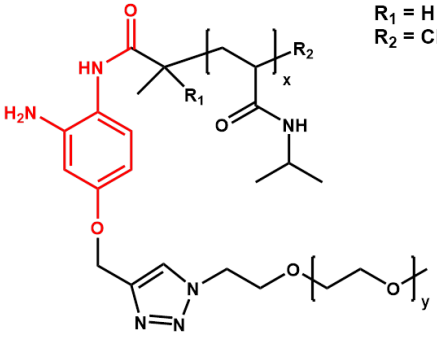  | 43.2 – 48.6 °C | NIPAAm / OEG | 308 |

cgt = critical gelation temperature

## Conclusion

Summarizing, we have covered in this chapter the state of the art in the field of transiently thermoresponsive polymers and highlighted some of their applications in drug delivery and tissue engineering. Due to the formation of hydrophobic domains, such polymers are very well suited to self-assemble into supramolecular structures such as micelles and hydrogels. Several types of chemistry have been explored to alleviate the thermoresponsive properties of this class of polymers, leading to gradual or triggered disassembly and/or drug release. Ester chemistry has so far been the most popular route to confer polymers with transiently thermoresponsive properties and micellar anti-cancer drug formulation based on this approach are currently in clinical trial, as is the case for *in situ* gelling hydrogels. The ongoing revolution in highly controlled macromolecular chemistry could open new avenues for the design of transiently thermoresponsive materials with precisely tailored properties. Furthermore, as is often the case in advanced drug delivery, a rational choice will need to be made between functionality, simplicity, robustness, reproducibility and regulatory approval.

## References


1 Stuart, M. A. C. *et al.* Emerging applications of stimuli-responsive polymer materials. *Nat. Mater.* **9**, 101-113 (2010).

2 Gil, E. S. & Hudson, S. M. Stimuli-reponsive polymers and their bioconjugates. *Prog. Polym. Sci.* **29**, 1173-1222 (2004).

3 Talelli, M. & Hennink, W. E. Thermosensitive polymeric micelles for targeted drug delivery. *Nanomedicine* **6**, 1245-1255 (2011).

4 Rijcken, C. J. F. *et al.* Triggered destabilisation of polymeric micelles and vesicles by changing polymers polarity: An attractive tool for drug delivery. *J. Control. Release* **120**, 131-148 (2007).

5 Deshayes, S. & Kasko, A. M. Polymeric biomaterials with engineered degradation. *J. Polym. Sci. Pol. Chem.* **51**, 3531-3566 (2013).

6 Park, M. H. *et al.* Biodegradable Thermogels. *Accounts Chem. Res.* **45**, 424-433 (2012).

7 Liow, S. S. *et al.* Thermogels: In Situ Gelling Biomaterial. *ACS Biomater.-Sci. Eng.* **2**, 295-316 (2016).

8 Joo, M. K. *et al.* Reverse thermogelling biodegradable polymer aqueous solutions. *J. Mater. Chem.* **19**, 5891-5905 (2009).

9 Fujishige, S., Kubota, K. & Ando, I. Phase transition of aqueous solutions of poly(N-isopropylacrylamide) and poly(N-isopropylmethacrylamide). *The Journal of Physical Chemistry* **93**, 3311-3313 (1989).

10 Roy, D., Brooks, W. L. A. & Sumerlin, B. S. New directions in thermoresponsive polymers. *Chem. Soc. Rev.* **42**, 7214-7243 (2013).

11 Scarpa, J. S., Mueller, D. D. & Klotz, I. M. Slow hydrogen-deuterium exchange in a non-alpha-helical polyamide. *J. Am. Chem. Soc.* **89**, 6024-& (1967).

12 Schild, H. G. Poly (n-isopropylacrylamide) - experiment, theory and application. *Prog. Polym. Sci.* **17**, 163-249 (1992).

13 Heskins, M. & Guillet, J. E. Solution Properties of Poly(N-isopropylacrylamide). *Journal of Macromolecular Science: Part A - Chemistry* **2**, 1441-1455 (1968).

14 Feil, H. *et al.* Effect of comonomer hydrophilicity and ionization on the lower critical solution temperature of N-isopropylacrylamide copolymers. *Macromolecules* **26**, 2496-2500 (1993).

15 Shibayama, M. & Tanaka, T. Volume phase-transition and related phenomena of polymer gels. *Adv. Polym. Sci.* **109**, 1-62 (1993).

16 Chen, G. H. & Hoffman, A. S. Graft-copolymers that exhibit temperature-induced phase-transitions over a wide-range of pH. *Nature* **373**, 49-52 (1995).

17 Shah, S. S. *et al.* Polymer-drug conjugates: manipulating drug delivery kinetics using model LCST systems. *J. Control. Release* **45**, 95-101 (1997).

18 Neradovic, D. *et al.* Poly(N-isopropylacrylamide) with hydrolyzable lactic acid ester side groups: a new type of thermosensitive polymer. *Macromol. Rapid Commun.* **20**, 577-581 (1999).

19 Lee, B. H. & Vernon, B. Copolymers of N-isopropylacrylamide, HEMA-lactate and acrylic acid with time-dependent lower critical solution temperature as a bioresorbable carrier. *Polymer International* **54**, 418-422 (2005).

20 Lee, B. H. & Vernon, B. In Situ-Gelling, Erodible N-Isopropylacrylamide Copolymers. *Macromol. Biosci.* **5**, 629-635 (2005).

21 Taylor, D. K. *et al.* Temperature-Responsive Biocompatible Copolymers Incorporating Hyperbranched Polyglycerols for Adjustable Functionality. *Journal of Functional Biomaterials* **2**, 173 (2011).

22 Guan, J. *et al.* Protein-Reactive, Thermoresponsive Copolymers with High Flexibility and Biodegradability. *Biomacromolecules* **9**, 1283-1292 (2008).

23 Neradovic, D., van Nostrum, C. F. & Hennink, W. E. Thermoresponsive Polymeric Micelles with Controlled Instability Based on Hydrolytically Sensitive N-Isopropylacrylamide Copolymers. *Macromolecules* **34**, 7589-7591 (2001).

24 Neradovic, D. *et al.* Degradation Mechanism and Kinetics of Thermosensitive Polyacrylamides Containing Lactic Acid Side Chains. *Macromolecules* **36**, 7491-7498 (2003).

25 Yuan, Q. *et al.* A stimulus-responsive magnetic nanoparticle drug carrier: Magnetite encapsulated by chitosan-grafted-copolymer. *Acta Biomaterialia* **4**, 1024-1037 (2008).

26 Jung, H. *et al.* Synthesis and characterization of thermosensitive nanoparticles based on PNIPAAm core and chitosan shell structure. *Macromol. Res.* **17**, 265-270 (2009).

27 Ohya, S., Nakayama, Y. & Matsuda, T. Thermoresponsive Artificial Extracellular Matrix for Tissue Engineering: Hyaluronic Acid Bioconjugated with Poly(N-isopropylacrylamide) Grafts. *Biomacromolecules* **2**, 856-863 (2001).

28 Kurisawa, M. & Yui, N. Modulated degradation of dextran hydrogels grafted with poly(N-isopropylacrylamide-co-N,N-dimethylacrylamide) in response to temperature. *Macromolecular Chemistry and Physics* **199**, 2613-2618 (1998).

29 Kumashiro, Y. *et al.* Modulatory factors on temperature-synchronized degradation of dextran grafted with thermoresponsive polymers and their hydrogels. *Biomacromolecules* **2**, 874-879 (2001).

30 Zhang, J. L., Srivastava, R. S. & Misra, R. D. K. Core−Shell Magnetite Nanoparticles Surface Encapsulated with Smart Stimuli-Responsive Polymer: Synthesis, Characterization, and LCST of Viable Drug-Targeting Delivery System. *Langmuir* **23**, 6342-6351 (2007).

31 Huang, X. & Lowe, T. L. Biodegradable thermoresponsive hydrogels for aqueous encapsulation and controlled release of hydrophilic model drugs. *Biomacromolecules* **6**, 2131-2139 (2005).

32 Huang, X. *et al.* Novel Nanogels with Both Thermoresponsive and Hydrolytically Degradable Properties. *Macromolecules* **41**, 8339-8345 (2008).

33 Soga, O., van Nostrum, C. F. & Hennink, W. E. Poly(N-(2-hydroxypropyl) Methacrylamide Mono/Di Lactate): A New Class of Biodegradable Polymers with Tuneable Thermosensitivity. *Biomacromolecules* **5**, 818-821 (2004).

34 Soga, O. *et al.* Physicochemical Characterization of Degradable Thermosensitive Polymeric Micelles. *Langmuir* **20**, 9388-9395 (2004).

35 Soga, O. *et al.* Thermosensitive and biodegradable polymeric micelles for paclitaxel delivery. *J. Control. Release* **103**, 341-353 (2005).

36 Rijcken, C. J. F. *et al.* Photo sensitiser-loaded biodegradable polymeric micelles: Preparation, characterisation and in vitro PDT efficacy. *J. Control. Release* **124**, 144-153 (2007).

37 van Hasselt, P. M. *et al.* The influence of bile acids on the oral bioavailability of vitamin K encapsulated in polymeric micelles. *J. Control. Release* **133**, 161-168 (2009).

38 Talelli, M. *et al.* Superparamagnetic Iron Oxide Nanoparticles Encapsulated in Biodegradable Thermosensitive Polymeric Micelles: Toward a Targeted Nanomedicine Suitable for Image-Guided Drug Delivery. *Langmuir* **25**, 2060-2067 (2009).

39 Moghimi, S. M., Hunter, A. C. & Murray, J. C. Long-circulating and target-specific nanoparticles: Theory to practice. *Pharmacol. Rev.* **53**, 283-318 (2001).

40 Rijcken, C. J. F. *et al.* Novel Fast Degradable Thermosensitive Polymeric Micelles Based on PEG-block-poly(N-(2-hydroxyethyl)methacrylamide-oligolactates). *Biomacromolecules* **6**, 2343-2351 (2005).

41 Wu, D.-Q. *et al.* Toward the Development of Partially Biodegradable and Injectable Thermoresponsive Hydrogels for Potential Biomedical Applications. *ACS Applied Materials & Interfaces* **1**, 319-327 (2009).

42 Wang, T. *et al.* Novel thermosensitive hydrogel injection inhibits post-infarct ventricle remodelling. *European Journal of Heart Failure* **11**, 14-19 (2009).

43 Rosellini, E. *et al.* Synthesis and characterization of a novel PNIPAAm-based copolymer with hydrolysis-dependent thermosensitivity. *Biomed. Mater.* **5** (2010).

44 Cui, Z., Lee, B. H. & Vernon, B. L. New Hydrolysis-Dependent Thermosensitive Polymer for an Injectable Degradable System. *Biomacromolecules* **8**, 1280-1286 (2007).

45 Zhanwu, C. *et al.* Manipulating degradation time in a n-isopropylacrylamide-based co-polymer with hydrolysis-dependent LCST. *J. Biomater. Sci. Polym. Ed.* **21**, 913-926 (2010).

46 Henderson, E. *et al.* In vivo evaluation of injectable thermosensitive polymer with time-dependent LCST. *J. Biomed. Mater. Res. Part A* **90A**, 1186-1197 (2009).

47 Vauthier, C. *et al.* Poly(alkylcyanoacrylates) as biodegradable materials for biomedical applications. *Adv. Drug Deliv. Rev.* **55**, 519-548 (2003).

48 Muller, R. H. *et al.* Invitro model for the degradation of alkylcyanoacrylate nanoparticles. *Biomaterials* **11**, 590-595 (1990).

49 Choi, B. G., Sohn, Y. S. & Jeong, B. Closed-loop sol-gel transition of PEG-PEC aqueous solution. *J. Phys. Chem. B* **111**, 7715-7718 (2007).

50 van Dijk, M. *et al.* Synthesis and characterization of tailorable biodegradable thermoresponsive methacryloylamide polymers based on l-serine and l-threonine alkyl esters. *Polymer* **51**, 2479-2485 (2010).

51 Jin, S. & Gonsalves, K. E. A Study of the Mechanism of the Free-Radical Ring-Opening Polymerization of 2-Methylene-1,3-dioxepane. *Macromolecules* **30**, 3104-3106 (1997).

52 Sun, L. F., Zhuo, R. X. & Liu, Z. L. Studies on the synthesis and properties of temperature responsive and biodegradable hydrogels. *Macromol. Biosci.* **3**, 725-728 (2003).

53 Kohori, F. *et al.* Preparation and characterization of thermally responsive block copolymer micelles comprising poly(N-isopropylacrylamide-b-DL-lactide). *J. Control. Release* **55**, 87-98 (1998).

54 Hales, M. *et al.* Shell-cross-linked vesicles synthesized from block copolymers of poly(D,L-lactide) and poly (N-isopropyl acrylamide) as thermoresponsive nanocontainers. *Langmuir* **20**, 10809-10817 (2004).

55 Kim, I. S. *et al.* Core-shell type polymeric nanoparticles composed of poly(L-lactic acid) and poly(N-isopropylacrylamide). *Int. J. Pharm.* **211**, 1-8 (2000).

56 Tabatabaei Rezaei, S. J. *et al.* Multifunctional and thermoresponsive unimolecular micelles for tumor-targeted delivery and site-specifically release of anticancer drugs. *Polymer* **53**, 3485-3497 (2012).

57 Liu, B. R. *et al.* The antitumor effect of novel docetaxel-loaded thermosensitive micelles. *Eur. J. Pharm. Biopharm.* **69**, 527-534 (2008).

58 Yang, M. *et al.* Novel thermosensitive polymeric micelles for docetaxel delivery. *J. Biomed. Mater. Res. Part A* **81A**, 847-857 (2007).

59 Bian, Q., Xiao, Y. & Lang, M. Thermoresponsive biotinylated star amphiphilic block copolymer: Synthesis, self-assembly, and specific target recognition. *Polymer* **53**, 1684-1693 (2012).

60 Kohori, F. *et al.* Process design for efficient and controlled drug incorporation into polymeric micelle carrier systems. *J. Control. Release* **78**, 155-163 (2002).

61 Kohori, F. *et al.* Control of adriamycin cytotoxic activity using thermally responsive polymeric micelles composed of poly(N-isopropylacrylamide-co-N,N-dimethylacrylamide)-b-poly(d,l-lactide). *Colloids and Surfaces B: Biointerfaces* **16**, 195-205 (1999).

62 Nakayama, M. *et al.* Molecular design of biodegradable polymeric micelles for temperature-responsive drug release. *J. Control. Release* **115**, 46-56 (2006).

63 Akimoto, J. *et al.* Temperature-Induced Intracellular Uptake of Thermoresponsive Polymeric Micelles. *Biomacromolecules* **10**, 1331-1336 (2009).

64 Lo, C. L., Lin, K. M. & Hsiue, G. H. Preparation and characterization of intelligent core-shell nanoparticles based on poly(D,L-lactide)-g-poly(N-isopropyl-acrylamide-co-methacrylic acid). *J. Control. Release* **104**, 477-488 (2005).

65 Liu, S. Q., Tong, Y. W. & Yang, Y. Y. Incorporation and in vitro release of doxorubicin in thermally sensitive micelles made from poly(N-isopropylacrylamide-co-N,N-dimethylacrylamide)-b-poly(D,L-lactide -co-glycolide) with varying compositions. *Biomaterials* **26**, 5064-5074 (2005).

66 Liu, S. Q., Tong, Y. W. & Yang, Y. Y. Thermally sensitive micelles self-assembled from poly(N-isopropylacrylamide-co-N,N-dimethylacrylamide)-b-poly(D,L-lactide -co-glycolide) for controlled delivers of paclitaxel. *Mol. Biosyst.* **1**, 158-165 (2005).

67 Cohn, D. *et al.* PEO–PPO–PEO-based poly(ether ester urethane)s as degradable reverse thermo-responsive multiblock copolymers. *Biomaterials* **27**, 1718-1727 (2006).

68 Yaozong, Y. *et al.* Well-defined poly(DL-lactide)- b-poly( N-vinylcaprolactam) copolymers: synthesis, solution properties and in vitro degradation. *J. Polym. Res.* **21**, 549 (549 pp.)-549 (549 pp.) (2014).

69 Wu, Q. H. *et al.* Synthesis and self-assembly of a new amphiphilic thermosensitive poly(N-vinylcaprolactam)/poly(epsilon-caprolactone) block copolymer. *Polym. Bull.* **71**, 1-18 (2014).

70 Yu, Y. C., Kang, H. U. & Youk, J. H. Synthesis and micellar characterization of thermosensitive amphiphilic poly(epsilon-caprolactone)-b-poly(N-vinylcaprolactam) block copolymers. *Colloid Polym. Sci.* **290**, 1107-1113 (2012).

71 Jeong, B. *et al.* Biodegradable block copolymers as injectable drug-delivery systems. *Nature* **388**, 860-862 (1997).

72 Jeong, B., Bae, Y. H. & Kim, S. W. Thermoreversible Gelation of PEG−PLGA−PEG Triblock Copolymer Aqueous Solutions. *Macromolecules* **32**, 7064-7069 (1999).

73 Bae, S. J. *et al.* Gelation Behavior of Poly(ethylene glycol) and Polycaprolactone Triblock and Multiblock Copolymer Aqueous Solutions. *Macromolecules* **39**, 4873-4879 (2006).

74 Na, K. *et al.* Biodegradable thermo-sensitive nanoparticles from poly(l-lactic acid)/poly(ethylene glycol) alternating multi-block copolymer for potential anti-cancer drug carrier. *European Journal of Pharmaceutical Sciences* **27**, 115-122 (2006).

75 Roberts, M. J., Bentley, M. D. & Harris, J. M. Chemistry for peptide and protein PEGylation. *Adv. Drug Deliv. Rev.* **54**, 459-476 (2002).

76 Duncan, R. The dawning era of polymer therapeutics. *Nat Rev Drug Discov* **2**, 347-360 (2003).

77 Harris, J. M. & Chess, R. B. Effect of pegylation on pharmaceuticals. *Nat. Rev. Drug Discov.* **2**, 214-221 (2003).

78 Alarcon, C. D. H., Pennadam, S. & Alexander, C. Stimuli responsive polymers for biomedical applications. *Chem. Soc. Rev.* **34**, 276-285 (2005).

79 Jiang, X., Smith, M. R. & Baker, G. L. Water-Soluble Thermoresponsive Polylactides. *Macromolecules* **41**, 318-324 (2008).

80 Jiang, X. *et al.* "Clickable" Polyglycolides: Tunable Synthons for Thermoresponsive, Degradable Polymers. *Macromolecules* **41**, 1937-1944 (2008).

81 Zhang, L.-J. *et al.* Degradable Thermoresponsive Polyesters by Atom Transfer Radical Polyaddition and Click Chemistry. *Macromolecules* **45**, 8580-8587 (2012).

82 Hao, J. *et al.* Temperature-sensitive aliphatic polyesters: synthesis and characterization of [gamma]-substituted caprolactone monomers and polymers. *J. Mater. Chem.* **21**, 10623-10628 (2011).

83 Feng, L. *et al.* A novel biodegradable and thermosensitive polymer with PEG-analogue macromolecular structure. *Chem. Commun.*, 4411-4413 (2009).

84 Feng, L. *et al.* Synthesis and Properties of Novel Thermoresponsive Polyesters with Oligo(ethylene glycol) Pendent Chains. *Macromolecular Chemistry and Physics* **212**, 2626-2632 (2011).

85 Feng, L. *et al.* Alternating copolymers with degradability and quantitatively controlled thermosensitivity. *Journal of Polymer Science Part A: Polymer Chemistry* **50**, 1812-1818 (2012).

86 Wang, N. *et al.* Thermoresponsive degradable poly(ethylene glycol) analogues. *J. Biomed. Mater. Res. Part A* **84A**, 148-157 (2008).

87 Lutz, J.-F. *et al.* About the Phase Transitions in Aqueous Solutions of Thermoresponsive Copolymers and Hydrogels Based on 2-(2-methoxyethoxy)ethyl Methacrylate and Oligo(ethylene glycol) Methacrylate. *Macromolecules* **40**, 2503-2508 (2007).

88 Lutz, J.-F. & Hoth, A. Preparation of Ideal PEG Analogues with a Tunable Thermosensitivity by Controlled Radical Copolymerization of 2-(2-Methoxyethoxy)ethyl Methacrylate and Oligo(ethylene glycol) Methacrylate. *Macromolecules* **39**, 893-896 (2006).

89 Lutz, J. F., Akdemir, O. & Hoth, A. Point by point comparison of two thermosensitive polymers exhibiting a similar LCST: Is the age of poly(NIPAM) over? *J. Am. Chem. Soc.* **128**, 13046-13047 (2006).

90 Lutz, J.-F. *et al.* Biocompatible, Thermoresponsive, and Biodegradable: Simple Preparation of "All-in-One" Biorelevant Polymers. *Macromolecules* **40**, 8540-8543 (2007).

91 Ren, L. & Agarwal, S. Synthesis, Characterization, and Properties Evaluation of Poly[(N-isopropylacrylamide)-co-ester]s. *Macromolecular Chemistry and Physics* **208**, 245-253 (2007).

92 Siegwart, D. J. *et al.* Synthesis, characterization, and in vitro cell culture viability of degradable poly(N-isopropylacrylamide-co-5,6-benzo-2-methylene-1,3-dioxepane)-based polymers and crosslinked gels. *J. Biomed. Mater. Res. Part A* **87A**, 345-358 (2008).

93 Stanescu, P. O. *et al.* Kinetic Study upon the Thermal Degradation of Poly(N-isopropylacrylamide-co-5,6-benzo-2-methylene-1,3-dioxepane) Statistical Copolymers. *Mater. Plast.* **52**, 193-197 (2015).

94 Mizuntani, M., Satoh, K. & Kamigaito, M. Degradable Poly(N-isopropylacrylamide) with Tunable Thermosensitivity by Simultaneous Chain- and Step-Growth Radical Polymerization. *Macromolecules* **44**, 2382-2386 (2011).

95 Wu, D. C., Liu, Y. & He, C. B. Thermal- and pH-responsive degradable polymers. *Macromolecules* **41**, 18-20 (2008).

96 Swanson, J. P. *et al.* A Library of Thermoresponsive, Coacervate-Forming Biodegradable Polyesters. *Macromolecules* **48**, 3834-3842 (2015).

97 Allcock, H. R. Generation of structural diversity in polyphosphazenes. *Appl. Organomet. Chem.* **27**, 620-629 (2013).

98 Allcock, H. R. *et al.* Poly(organophosphazenes) with poly(alkyl ether) side groups: a study of their water solubility and the swelling characteristics of their hydrogels. *Macromolecules* **25**, 5573-5577 (1992).

99 Allcock, H. R. & Dudley, G. K. Lower Critical Solubility Temperature Study of Alkyl Ether Based Polyphosphazenes. *Macromolecules* **29**, 1313-1319 (1996).

100 Song, S.-C. *et al.* A New Class of Biodegradable Thermosensitive Polymers. I. Synthesis and Characterization of Poly(organophosphazenes) with Methoxy-Poly(ethylene glycol) and Amino Acid Esters as Side Groups. *Macromolecules* **32**, 2188-2193 (1999).

101 Lee, S. B. *et al.* A New Class of Biodegradable Thermosensitive Polymers. 2. Hydrolytic Properties and Salt Effect on the Lower Critical Solution Temperature of Poly(organophosphazenes) with Methoxypoly(ethylene glycol) and Amino Acid Esters as Side Groups. *Macromolecules* **32**, 7820-7827 (1999).

102 Allcock, H. R., Pucher, S. R. & Scopelianos, A. G. Poly[(amino acid ester)phosphazenes]: Synthesis, Crystallinity, and Hydrolytic Sensitivity in Solution and the Solid State. *Macromolecules* **27**, 1071-1075 (1994).

103 Crommen, J. H. L., Schacht, E. H. & Mense, E. H. G. Biodegradable polymers. *Biomaterials* **13**, 601-611 (1992).

104 Vandorpe, J. & Schacht, E. Synthesis and evaluation of polyphosphazene derivatives with ω-methylpoly(ethylene oxide) side-groups. *Polymer* **37**, 3141-3145 (1996).

105 Lee, S. B. & Song, S.-C. Hydrolysis-improved thermosensitive polyorganophosphazenes with α-amino-ω-methoxy-poly(ethylene glycol) and amino acid esters as side groups. *Polymer International* **54**, 1225-1232 (2005).

106 Lee, B. H. *et al.* A thermosensitive poly(organophosphazene) gel. *Macromolecules* **35**, 3876-3879 (2002).

107 Chun, C. *et al.* Thermosensitive poly(organophosphazene)–paclitaxel conjugate gels for antitumor applications. *Biomaterials* **30**, 2349-2360 (2009).

108 Chun, C. *et al.* Doxorubicin–polyphosphazene conjugate hydrogels for locally controlled delivery of cancer therapeutics. *Biomaterials* **30**, 4752-4762 (2009).

109 Kim, Y.-M., Park, M.-R. & Song, S.-C. Injectable Polyplex Hydrogel for Localized and Long-Term Delivery of siRNA. *ACS Nano* **6**, 5757-5766 (2012).

110 Kim, Y.-M., Park, M.-R. & Song, S.-C. An injectable cell penetrable nano-polyplex hydrogel for localized siRNA delivery. *Biomaterials* **34**, 4493-4500 (2013).

111 Park, M.-R. *et al.* Cationic and thermosensitive protamine conjugated gels for enhancing sustained human growth hormone delivery. *Biomaterials* **31**, 1349-1359 (2010).

112 Kim, J. I. *et al.* Thermosensitive/magnetic poly(organophosphazene) hydrogel as a long-term magnetic resonance contrast platform. *Biomaterials* **33**, 218-224 (2012).

113 Kim, J. I. *et al.* Long-term theranostic hydrogel system for solid tumors. *Biomaterials* **33**, 2251-2259 (2012).

114 Kim, J. I. *et al.* MRI-monitored long-term therapeutic hydrogel system for brain tumors without surgical resection. *Biomaterials* **33**, 4836-4842 (2012).

115 Seong, J.-Y. *et al.* New thermogelling poly(organophosphazenes) with methoxypoly(ethylene glycol) and oligopeptide as side groups. *Polymer* **46**, 5075-5081 (2005).

116 Kim, J. I. *et al.* Synthesis and characterization of nanosized poly(organophosphazenes) with methoxy-poly(ethylene glycol) and dipeptide ethyl esters as side groups. *Polymer* **45**, 7083-7089 (2004).

117 Lee, B. H. *et al.* Thermosensitive and hydrolysis-sensitive poly(organophosphazenes). *Polymer International* **51**, 658-660 (2002).

118 Seong, J. Y. *et al.* Synthesis and characterization of biocompatible poly(organophosphazenes) aiming for local delivery of protein drugs. *Int. J. Pharm.* **314**, 90-96 (2006).

119 Song, R. *et al.* Synthesis, characterization, and tumor selectivity of a polyphosphazene–platinum(II) conjugate. *J. Control. Release* **105**, 142-150 (2005).

120 Bi, Y. M. *et al.* Synthesis and characterization of new biodegradable thermosensitive polyphosphazenes with lactic acid ester and methoxyethoxyethoxy side groups. *Chin. Chem. Lett.* **21**, 237-241 (2010).

121 Bi, Y. *et al.* Polyphosphazenes containing lactic acid ester and methoxyethoxyethoxy side groups — Thermosensitive properties and, in vitro degradation, and biocompatibility. *Canadian Journal of Chemistry* **89**, 1249-1256 (2011).

122 Allcock, H. R., Pucher, S. R. & Scopelianos, A. G. Synthesis of poly(orgnaophosphazenes) with glycolic acid ester and lactic acid ester side groups: prototypes for new bioerodible polymers. *Macromolecules* **27**, 1-4 (1994).

123 Zhang, J. X. *et al.* Thermosensitive micelles self-assembled by novel N-isopropylacrylamide oligomer grafted polyphosphazene. *Macromol. Rapid Commun.* **25**, 1563-1567 (2004).

124 Zhang, J. X. *et al.* Thermally responsive polymeric micelles self-assembled by amphiphilic polyphosphazene with poly(N-isopropylacrylamide) and ethyl glycinate as side groups: Polymer synthesis, characterization, and in vitro drug release study. *J. Biomed. Mater. Res. Part A* **76A**, 773-780 (2006).

125 Qiu, L. Y., Wu, X. L. & Jin, Y. Doxorubicin-Loaded Polymeric Micelles Based on Amphiphilic Polyphosphazenes with Poly(N-isopropylacrylamide-co-N,N-dimethylacrylamide) and Ethyl Glycinate as Side Groups: Synthesis, Preparation and In Vitro Evaluation. *Pharm. Res.* **26**, 946-957 (2009).

126 Lee, S. B. *et al.* Thermosensitive Cyclotriphosphazenes. *J. Am. Chem. Soc.* **122**, 8315-8316 (2000).

127 Lee, S. B. *et al.* Structural and Thermosensitive Properties of Cyclotriphosphazenes with Poly(ethylene glycol) and Amino Acid Esters as Side Groups. *Macromolecules* **34**, 7565-7569 (2001).

128 Jun, Y. J. *et al.* Thermoresponsive micelles from oligopeptide-grafted cyclotriphosphazenes. *Angew. Chem.-Int. Edit.* **45**, 6173-6176 (2006).

129 Toti, U. S. *et al.* Thermosensitive and biocompatible cyclotriphosphazene micelles. *J. Control. Release* **119**, 34-40 (2007).

130 Jadhav, V. B. *et al.* A novel micelle-encapsulated platinum(II) anticancer agent. *J. Control. Release* **147**, 144-150 (2010).

131 Jun, Y. J. *et al.* Stable and efficient delivery of docetaxel by micelle-encapsulation using a tripodal cyclotriphosphazene amphiphile. *Int. J. Pharm.* **422**, 374-380 (2012).

132 Chae, S. W. *et al.* Preclinical evaluation of efficacy and stability of docetaxel micelle-encapsulated by a tripodal cyclotriphosphazene amphiphile. *Biomedicine & Pharmacotherapy* **68**, 649-655 (2014).

133 Avaji, P. G. *et al.* Synthesis and physicochemical properties of new tripodal amphiphiles bearing fatty acids as a hydrophobic group. *Bioorganic & Medicinal Chemistry Letters* **23**, 1763-1767 (2013).

134 Wang, Y.-C. *et al.* Recent Progress in Polyphosphoesters: From Controlled Synthesis to Biomedical Applications. *Macromol. Biosci.* **9**, 1154-1164 (2009).

135 Penczek, S. *et al.* Thermodynamics and kinetics of ring-opening polymerization of cyclic alkylene phosphates. *Makromolekulare Chemie. Macromolecular Symposia* **73**, 91-101 (1993).

136 Baran, J., Klosinski, P. & Penczek, S. Poly(alkylene phosphate)s by polycondensation of phosphonic diamides with diols. *Die Makromolekulare Chemie* **190**, 1903-1917 (1989).

137 Pretula, J. & Penczek, S. High-molecular-weight poly(alkylene phosphonate)s by condensation of dialkylphosphonates with diols. *Die Makromolekulare Chemie* **191**, 671-680 (1990).

138 Renier, M. L. & Kohn, D. H. Development and characterization of a biodegradable polyphosphate. *J. Biomed. Mater. Res.* **34**, 95-104 (1997).

139 Lu, Z.-Z. *et al.* Biodegradable polycation and plasmid DNA multilayer film for prolonged gene delivery to mouse osteoblasts. *Biomaterials* **29**, 733-741 (2008).

140 Wang, Y.-C. *et al.* Self-Assembled Micelles of Biodegradable Triblock Copolymers Based on Poly(ethyl ethylene phosphate) and Poly(ϵ-caprolactone) as Drug Carriers. *Biomacromolecules* **9**, 388-395 (2008).

141 Wang, J. *et al.* New polyphosphoramidate with a spermidine side chain as a gene carrier. *J. Control. Release* **83**, 157-168 (2002).

142 Huang, S. W. *et al.* Water-soluble and nonionic polyphosphoester: Synthesis, degradation, biocompatibility and enhancement of gene expression in mouse muscle. *Biomacromolecules* **5**, 306-311 (2004).

143 Li, Q. *et al.* Biodegradable and photocrosslinkable polyphosphoester hydrogel. *Biomaterials* **27**, 1027-1034 (2006).

144 Wan, A. C. A. *et al.* Fabrication of poly(phosphoester) nerve guides by immersion precipitation and the control of porosity. *Biomaterials* **22**, 1147-1156 (2001).

145 Wang, D. A. *et al.* Bioresponsive phosphoester hydrogels for bone tissue engineering. *Tissue Eng.* **11**, 201-213 (2005).

146 Iwasaki, Y., Wachiralarpphaithoon, C. & Akiyoshi, K. Novel Thermoresponsive Polymers Having Biodegradable Phosphoester Backbones. *Macromolecules* **40**, 8136-8138 (2007).

147 Steinbach, T. *et al.* Microstructure analysis of biocompatible phosphoester copolymers. *Polym. Chem.* **4**, 4469-4479 (2013).

148 Wang, Y.-C. *et al.* Thermoresponsive Block Copolymers of Poly(ethylene glycol) and Polyphosphoester: Thermo-Induced Self-Assembly, Biocompatibility, and Hydrolytic Degradation. *Biomacromolecules* **10**, 66-73 (2009).

149 Wang, Y.-C. *et al.* Tunable Thermosensitivity of Biodegradable Polymer Micelles of Poly(ε-caprolactone) and Polyphosphoester Block Copolymers. *Macromolecules* **42**, 3026-3032 (2009).

150 Wang, J. *et al.* Stimuli-Responsive Hydrogel Based on Poly(propylene phosphate). *Macromolecules* **37**, 670-672 (2004).

151 Akashi, M. *et al.* A novel synthetic procedure of vinylacetamide and its free radical polymerization. *Journal of Polymer Science Part A: Polymer Chemistry* **28**, 3487-3497 (1990).

152 Akashi, M., Nakano, S. & Kishida, A. Synthesis of poly(N-vinylisobutyramide) from poly(N-vinylacetamide) and its thermosensitive property. *Journal of Polymer Science Part A: Polymer Chemistry* **34**, 301-303 (1996).

153 Suwa, K. *et al.* Synthesis and functionalities of poly(N-vinylalkylamide). IV. Synthesis and free radical polymerization of N-vinylisobutyramide and thermosensitive properties of the polymer. *Journal of Polymer Science Part A: Polymer Chemistry* **35**, 1763-1768 (1997).

154 Suwa, K. *et al.* Synthesis and functionalities of poly(N-vinylalkylamide). V. Control of a lower critical solution temperature of poly(N-vinylalkylamide). *Journal of Polymer Science Part A: Polymer Chemistry* **35**, 3087-3094 (1997).

155 Yamamoto, K. *et al.* Synthesis and functionalities of poly(N-vinylalkylamide). XII. Synthesis and thermosensitive property of poly(vinylamine) copolymer prepared from poly(N-vinylformamide-co-N-vinylisobutyramide). *Journal of Polymer Science Part A: Polymer Chemistry* **38**, 3674-3681 (2000).

156 Yamamoto, K. *et al.* Synthesis and Functionalities of Poly(N-vinylalkylamide). 13. Synthesis and Properties of Thermal and pH Stimuli-Responsive Poly(vinylamine) Copolymers. *Macromolecules* **34**, 8014-8020 (2001).

157 Tachaboonyakiat, W., Ajiro, H. & Akashi, M. Synthesis of a thermosensitive polycation by random copolymerization of N-vinylformamide and N-vinylbutyramide. *Polym J* **45**, 971-978 (2013).

158 Fukushima, K. Poly(trimethylene carbonate)-based polymers engineered for biodegradable functional biomaterials. *Biomaterials Science* **4**, 9-24 (2016).

159 Kim, S. Y. *et al.* Reverse Thermal Gelling PEG−PTMC Diblock Copolymer Aqueous Solution. *Macromolecules* **40**, 5519-5525 (2007).

160 Kim, S. Y. *et al.* Vesicle-to-Spherical Micelle-to-Tubular Nanostructure Transition of Monomethoxy-poly(ethylene glycol)−poly(trimethylene carbonate) Diblock Copolymer. *The Journal of Physical Chemistry B* **112**, 7420-7423 (2008).

161 Kim, M. S. *et al.* Preparation of Thermosensitive Diblock Copolymers Consisting of MPEG and Polyesters. *Macromolecules* **39**, 3099-3102 (2006).

162 Kim, S. H. *et al.* Thermoresponsive nanostructured polycarbonate block copolymers as biodegradable therapeutic delivery carriers. *Biomaterials* **32**, 5505-5514 (2011).

163 Ajiro, H., Takahashi, Y. & Akashi, M. Thermosensitive Biodegradable Homopolymer of Trimethylene Carbonate Derivative at Body Temperature. *Macromolecules* **45**, 2668-2674 (2012).

164 Lin, G. *et al.* Biodegradable poly(carbonate-ether)s with thermoresponsive feature at body temperature. *J. Polym. Sci., A, Polym. Chem.* **51**, 282-289 (2013).

165 Yu, L. *et al.* Synthesis and properties of tunable thermoresponsive aliphatic polycarbonate copolymers with oligo ethylene glycol containing thioether and/or sulphone groups. *RSC Advances* **5**, 64832-64840 (2015).

166 Fujimoto, K. L. *et al.* Synthesis, characterization and therapeutic efficacy of a biodegradable, thermoresponsive hydrogel designed for application in chronic infarcted myocardium. *Biomaterials* **30**, 4357-4368 (2009).

167 Kasmi, S. *et al.* Transiently Responsive Block Copolymer Micelles Based on N-(2-Hydroxypropyl)methacrylamide Engineered with Hydrolyzable Ethylcarbonate Side Chains. *Biomacromolecules* **17**, 119-127 (2016).

168 Sounni, N. E. & Noel, A. Targeting the Tumor Microenvironment for Cancer Therapy. *Clin. Chem.* **59**, 85-93 (2013).

169 Tannock, I. F. & Rotin, D. Acid pH in Tumors and Its Potential for Therapeutic Exploitation. *Cancer Research* **49**, 4373-4384 (1989).

170 Ge, Z. S. & Liu, S. Y. Functional block copolymer assemblies responsive to tumor and intracellular microenvironments for site-specific drug delivery and enhanced imaging performance. *Chem. Soc. Rev.* **42**, 7289-7325 (2013).

171 Oh, K. T. *et al.* Polymeric nanovehicles for anticancer drugs with triggering release mechanisms. *J. Mater. Chem.* **17**, 3987-4001 (2007).

172 Liu, J. *et al.* pH-Sensitive nano-systems for drug delivery in cancer therapy. *Biotechnol. Adv.* **32**, 693-710 (2014).

173 Manchun, S., Dass, C. R. & Sriamornsak, P. Targeted therapy for cancer using pH-responsive nanocarrier systems. *Life Sci.* **90**, 381-387 (2012).

174 Cho, Y. W., Kim, J. D. & Park, K. Polycation gene delivery systems: escape from endosomes to cytosol. *J. Pharm. Pharmacol.* **55**, 721-734 (2003).

175 Yessine, M. A. & Leroux, J. C. Membrane-destabilizing polyanions: interaction with lipid bilayers and endosomal escape of biomacromolecules. *Adv. Drug Deliv. Rev.* **56**, 999-1021 (2004).

176 Ko, J. *et al.* Tumoral acidic extracellular pH targeting of pH-responsive MPEG-poly (beta-amino ester) block copolymer micelles for cancer therapy. *J. Control. Release* **123**, 109-115 (2007).

177 Hsiue, G. H. *et al.* Environmental-sensitive micelles based on poly(2-ethyl-2-oxazoline)-b-poly(L-lactide) diblock copolymer for application in drug delivery. *Int. J. Pharm.* **317**, 69-75 (2006).

178 Mao, B. W. *et al.* Controlled one-pot synthesis of pH-sensitive self-assembled diblock copolymers and their aggregation behavior. *Polymer* **46**, 10045-10055 (2005).

179 Jacquin, M. *et al.* Chemical analysis and aqueous solution properties of charged amphiphilic block copolymers PBA-b-PAA synthesized by MADIX((c)). *J. Colloid Interface Sci.* **316**, 897-911 (2007).

180 Bendejacq, D. D. & Ponsinet, V. Double-polyelectrolyte, like-charged amphiphilic diblock copolymers: Swollen structures and pH- and salt-dependent lyotropic behavior. *J. Phys. Chem. B* **112**, 7996-8009 (2008).

181 Murthy, N. *et al.* A Novel Strategy for Encapsulation and Release of Proteins: Hydrogels and Microgels with Acid-Labile Acetal Cross-Linkers. *J. Am. Chem. Soc.* **124**, 12398-12399 (2002).

182 Chan, Y. *et al.* Acid-cleavable polymeric core-shell particles for delivery of hydrophobic drugs. *J. Control. Release* **115**, 197-207 (2006).

183 Bulmus, V. *et al.* Synthesis and characterization of degradable p(HEMA) microgels: Use of acid-labile crosslinkers. *Macromol. Biosci.* **7**, 446-455 (2007).

184 Zhang, L. *et al.* Acid-Degradable Core-Crosslinked Micelles Prepared from Thermosensitive Glycopolymers Synthesized via RAFT Polymerization. *Macromol. Rapid Commun.* **29**, 123-129 (2008).

185 Themistou, E. & Patrickios, C. S. A Cleavable Network Based on Crosslinked Star Polymers Containing Acid-Labile Diacetal Crosslinks: Synthesis, Characterization and Hydrolysis. *Macromolecular Chemistry and Physics* **209**, 1021-1028 (2008).

186 Chan, Y. *et al.* Acid-Labile Core Cross-Linked Micelles for pH-Triggered Release of Antitumor Drugs. *Biomacromolecules* **9**, 1826-1836 (2008).

187 Lu, J. *et al.* Acetals moiety contained pH-sensitive amphiphilic copolymer self-assembly used for drug carrier. *Polymer* **51**, 1709-1715 (2010).

188 Gillies, E. R. & Frechet, J. M. J. pH-responsive copolymer assemblies for controlled release of doxorubicin. *Bioconjugate Chem.* **16**, 361-368 (2005).

189 Masson, C. *et al.* pH-sensitive PEG lipids containing orthoester linkers: new potential tools for nonviral gene delivery. *J. Control. Release* **99**, 423-434 (2004).

190 Heller, J. *et al.* Poly(ortho esters): synthesis, characterization, properties and uses. *Adv. Drug Deliv. Rev.* **54**, 1015-1039 (2002).

191 Bruyère, H., Westwell, A. D. & Jones, A. T. Tuning the pH sensitivities of orthoester based compounds for drug delivery applications by simple chemical modification. *Bioorganic & Medicinal Chemistry Letters* **20**, 2200-2203 (2010).

192 Lin, S. *et al.* An Acid-Labile Block Copolymer of PDMAEMA and PEG as Potential Carrier for Intelligent Gene Delivery Systems. *Biomacromolecules* **9**, 109-115 (2008).

193 Tang, R., Ji, W. & Wang, C. Amphiphilic Block Copolymers Bearing Ortho Ester Side-Chains: pH-Dependent Hydrolysis and Self-Assembly in Water. *Macromol. Biosci.* **10**, 192-201 (2010).

194 Yang, X. *et al.* Tumor-Targeting, pH-Responsive, and Stable Unimolecular Micelles as Drug Nanocarriers for Targeted Cancer Therapy. *Bioconjugate Chem.* **21**, 496-504 (2010).

195 Lee, Y. *et al.* Synthesis, Characterization, Antitumor Activity of Pluronic Mimicking Copolymer Micelles Conjugated with Doxorubicin via Acid-Cleavable Linkage. *Bioconjugate Chem.* **19**, 525-531 (2008).

196 Hrubý, M., Koňák, Č. & Ulbrich, K. Polymeric micellar pH-sensitive drug delivery system for doxorubicin. *J. Control. Release* **103**, 137-148 (2005).

197 Bae, Y. *et al.* Design of environment-sensitive supramolecular assemblies for intracellular drug delivery: Polymeric micelles that are responsive to intracellular pH change. *Angew. Chem.-Int. Edit.* **42**, 4640-4643 (2003).

198 Burkoth, A. K. & Anseth, K. S. MALDI-TOF Characterization of Highly Cross-Linked, Degradable Polymer Networks. *Macromolecules* **32**, 1438-1444 (1999).

199 Ding, C. *et al.* Preparation of Multifunctional Drug Carrier for Tumor-Specific Uptake and Enhanced Intracellular Delivery through the Conjugation of Weak Acid Labile Linker. *Bioconjugate Chem.* **20**, 1163-1170 (2009).

200 Shi, L. & Berkland, C. Acid-Labile Polyvinylamine Micro- and Nanogel Capsules. *Macromolecules* **40**, 4635-4643 (2007).

201 Hu, J. *et al.* Stimuli-responsive tertiary amine methacrylate-based block copolymers: Synthesis, supramolecular self-assembly and functional applications. *Prog. Polym. Sci.* **39**, 1096-1143 (2014).

202 Schmaljohann, D. Thermo- and pH-responsive polymers in drug delivery. *Adv. Drug Deliv. Rev.* **58**, 1655-1670 (2006).

203 Gao, W., Chan, J. M. & Farokhzad, O. C. pH-Responsive Nanoparticles for Drug Delivery. *Molecular Pharmaceutics* **7**, 1913-1920 (2010).

204 Huang, X. N. *et al.* Novel acid-labile, thermoresponsive poly(methacrylamide)s with pendent ortho ester moieties. *Macromol. Rapid Commun.* **28**, 597-603 (2007).

205 Huang, X. *et al.* Stereochemical Effect of Trans/Cis Isomers on the Aqueous Solution Properties of Acid-Labile Thermoresponsive Polymers. *Macromolecules* **41**, 5433-5440 (2008).

206 Huang, X. *et al.* Acid-Sensitive Polymeric Micelles Based on Thermoresponsive Block Copolymers with Pendent Cyclic Orthoester Groups. *Macromolecules* **42**, 783-790 (2009).

207 Qiao, Z. Y. *et al.* Polymersomes from Dual Responsive Block Copolymers: Drug Encapsulation by Heating and Acid-Triggered Release. *Biomacromolecules* **14**, 1555-1563 (2013).

208 Du, F.-S. *et al.* Aqueous Solution Properties of the Acid-Labile Thermoresponsive Poly(meth)acrylamides with Pendent Cyclic Orthoester Groups. *Macromolecules* **43**, 2474-2483 (2010).

209 Qiao, Z.-Y. *et al.* Biocompatible Thermoresponsive Polymers with Pendent Oligo(ethylene glycol) Chains and Cyclic Ortho Ester Groups. *Macromolecules* **43**, 6485-6494 (2010).

210 Qiao, Z.-Y. *et al.* Multi-responsive nanogels containing motifs of ortho ester, oligo(ethylene glycol) and disulfide linkage as carriers of hydrophobic anti-cancer drugs. *J. Control. Release* **152**, 57-66 (2011).

211 Schacht, E. *et al.* Polyacetal and poly(ortho ester)–poly(ethylene glycol) graft copolymer thermogels: Preparation, hydrolysis and FITC-BSA release studies. *J. Control. Release* **116**, 219-225 (2006).

212 Tang, R. *et al.* Poly(ortho ester amides): Acid-Labile Temperature-Responsive Copolymers for Potential Biomedical Applications. *Biomacromolecules* **10**, 722-727 (2009).

213 Tang, R. P. *et al.* Block copolymer micelles with acid-labile ortho ester side-chains: Synthesis, characterization, and enhanced drug delivery to human glioma cells. *J. Control. Release* **151**, 18-27 (2011).

214 Gillies, E. R. & Frechet, J. M. J. A new approach towards acid sensitive copolymer micelles for drug delivery. *Chem. Commun.*, 1640-1641 (2003).

215 Morinaga, H. *et al.* Amphiphilic Copolymer Having Acid-Labile Acetal in the Side Chain as a Hydrophobe: Controlled Release of Aldehyde by Thermoresponsive Aggregation−Dissociation of Polymer Micelles. *Macromolecules* **42**, 2229-2235 (2009).

216 Heath, F. *et al.* 'Isothermal' phase transitions and supramolecular architecture changes in thermoresponsive polymers via acid-labile side-chains. *Polym. Chem.* **1**, 1252-1262 (2010).

217 Klaikherd, A., Nagamani, C. & Thayumanavan, S. Multi-Stimuli Sensitive Amphiphilic Block Copolymer Assemblies. *J. Am. Chem. Soc.* **131**, 4830-4838 (2009).

218 Pelletier, M. *et al.* Investigation of a New Thermosensitive Block Copolymer Micelle: Hydrolysis, Disruption, and Release. *Langmuir* **24**, 12664-12670 (2008).

219 Huang, X.-N. *et al.* Acid-labile, thermoresponsive (meth)acrylamide polymers with pendant cyclic acetal moieties. *Journal of Polymer Science Part A: Polymer Chemistry* **46**, 4332-4343 (2008).

220 Deslongchamps, P., Dory, Y. L. & Li, S. The Relative Rate of Hydrolysis of a Series of Acyclic and Six-Membered Cyclic Acetals, Ketals, Orthoesters, and Orthocarbonates. *Tetrahedron* **56**, 3533-3537 (2000).

221 Monge, S. *et al.* Poly(tris(hydroxymethyl)acrylamidomethane)-based copolymers: a new class of acid-labile thermosensitive polymers. *Polym. Chem.* **3**, 2502-2507 (2012).

222 Zou, Y. Q., Brooks, D. E. & Kizhakkedathu, J. N. A novel functional polymer with tunable LCST. *Macromolecules* **41**, 5393-5405 (2008).

223 Vanparijs, N. *et al.* Transiently responsive protein-polymer conjugates via a grafting-from RAFT approach: for intracellular co-delivery of proteins and immune-modulators. *Chem. Commun.* (2015).

224 Yang, J. *et al.* Synthesis of Y-shaped poly(solketal acrylate)-containing block copolymers and study on the thermoresponsive behavior for micellar aggregates. *J. Colloid Interface Sci.* **352**, 405-414 (2010).

225 Zhang, Q. L. *et al.* Dual pH- and temperature-responsive RAFT-based block co-polymer micelles and polymer-protein conjugates with transient solubility. *Polym. Chem.* **5**, 1140-1144 (2014).

226 Zhang, Q. *et al.* Acid-Labile Thermoresponsive Copolymers That Combine Fast pH-Triggered Hydrolysis and High Stability under Neutral Conditions. *Angewandte Chemie International Edition* **54**, 10879-10883 (2015).

227 Louage, B. *et al.* Degradable Ketal-Based Block Copolymer Nanoparticles for Anticancer Drug Delivery: A Systematic Evaluation. *Biomacromolecules* **16**, 336-350 (2015).

228 Shinde, V. S. & Pawar, V. U. Synthesis of thermosensitive glycopolymers containing D-glucose residue: Copolymers with N-isopropylacrylamide. *J. Appl. Polym. Sci.* **111**, 2607-2615 (2009).

229 Dhumure, A. B. *et al.* Thermoresponsive copolymers with pendant D-galactosyl 1,2,3-triazole groups: synthesis, characterization and thermal behavior. *New J. Chem.* **39**, 8179-8187 (2015).

230 Samanta, S. *et al.* Polyacetals: Water-Soluble, pH-Degradable Polymers with Extraordinary Temperature Response. *Macromolecules* **49**, 1858-1864 (2016).

231 McClelland, R. A. & Somani, R. Kinetic analysis of the ring opening of an N-alkyloxazolidine. Hydrolysis of 2-(4-methylphenyl)-2,3-dimethyl-1,3-oxazolidine. *The Journal of Organic Chemistry* **46**, 4345-4350 (1981).

232 Sélambarom, J. *et al.* Stereoelectronic control of oxazolidine ring-opening: structural and chemical evidences. *Tetrahedron* **58**, 9559-9566 (2002).

233 Cui, Q., Wu, F. & Wang, E. Novel amphiphilic diblock copolymers bearing acid-labile oxazolidine moieties: Synthesis, self-assembly and responsive behavior in aqueous solution. *Polymer* **52**, 1755-1765 (2011).

234 Cui, Q., Wu, F. & Wang, E. Thermosensitive Behavior of Poly(ethylene Glycol)-Based Block Copolymer (PEG-b-PADMO) Controlled via Self-Assembled Microstructure. *The Journal of Physical Chemistry B* **115**, 5913-5922 (2011).

235 Hruby, M. *et al.* New bioerodable thermoresponsive polymers for possible radiotherapeutic applications. *J. Control. Release* **119**, 25-33 (2007).

236 Murray, B. S. *et al.* Reactive thermoresponsive copolymer scaffolds. *Chem. Commun.* **46**, 8651-8653 (2010).

237 Sugiyama, K. & Sono, K. Characterization of photo- and thermoresponsible amphiphilic copolymers having azobenzene moieties as side groups. *J. Appl. Polym. Sci.* **81**, 3056-3063 (2001).

238 Shimoboji, T. *et al.* Photoresponsive polymer–enzyme switches. *Proceedings of the National Academy of Sciences* **99**, 16592-16596 (2002).

239 Kroger, R., Menzel, H. & Hallensleben, M. L. Light controlled solubility change of polymers - copolymers of n,n-dimethylacrylamide and 4-phenylazophenyl acrylate. *Macromolecular Chemistry and Physics* **195**, 2291-2298 (1994).

240 Desponds, A. & Freitag, R. Synthesis and characterization of photoresponsive N-isopropylacrylamide cotelomers. *Langmuir* **19**, 6261-6270 (2003).

241 Tang, X. D. *et al.* Water-Soluble Triply-Responsive Homopolymers of N,N-Dimethylaminoethyl methacrylate with a Terminal Azobenzene Moiety. *J. Polym. Sci. Pol. Chem.* **48**, 2564-2570 (2010).

242 Lim, S.-J. *et al.* Multifunctional photo- and thermo-responsive copolymer nanoparticles. *Dyes and Pigments* **89**, 230-235 (2011).

243 Sumaru, K. *et al.* Characteristic Phase Transition of Aqueous Solution of Poly(N-isopropylacrylamide) Functionalized with Spirobenzopyran. *Macromolecules* **37**, 4949-4955 (2004).

244 Enomoto, R., Kousaka, S. & Yusa, S. Preparation of a Thermo- and Photoresponsive Water-soluble Polymer. *Chem. Lett.* **44**, 1491-1493 (2015).

245 Nargeot, J. *et al.* Time course of the increase in the myocardial slow inward current after a photochemically generated concentration jump of intracellular cAMP. *Proceedings of the National Academy of Sciences* **80**, 2395-2399 (1983).

246 Adams, S. R., Kao, J. P. Y. & Tsien, R. Y. Biologically useful chelators that take up calcium(2+) upon illumination. *J. Am. Chem. Soc.* **111**, 7957-7968 (1989).

247 Jiang, J., Tong, X. & Zhao, Y. A New Design for Light-Breakable Polymer Micelles. *J. Am. Chem. Soc.* **127**, 8290-8291 (2005).

248 Jiang, J. *et al.* Toward Photocontrolled Release Using Light-Dissociable Block Copolymer Micelles. *Macromolecules* **39**, 4633-4640 (2006).

249 Babin, J. *et al.* A New Two-Photon-Sensitive Block Copolymer Nanocarrier. *Angewandte Chemie International Edition* **48**, 3329-3332 (2009).

250 Ionov, L. & Diez, S. Environment-Friendly Photolithography Using Poly(N-isopropylacrylamide)-Based Thermoresponsive Photoresists. *J. Am. Chem. Soc.* **131**, 13315-13319 (2009).

251 Jiang, X. *et al.* Multiple Micellization and Dissociation Transitions of Thermo- and Light-Sensitive Poly(ethylene oxide)-b-poly(ethoxytri(ethylene glycol) acrylate-co-o-nitrobenzyl acrylate) in Water. *Macromolecules* **41**, 2632-2643 (2008).

252 Wu, Y. *et al.* Thermo- and Light-Regulated Formation and Disintegration of Double Hydrophilic Block Copolymer Assemblies with Tunable Fluorescence Emissions. *Langmuir* **29**, 3711-3720 (2013).

253 Nowak, A. P. *et al.* Rapidly recovering hydrogel scaffolds from self-assembling diblock copolypeptide amphiphiles. *Nature* **417**, 424-428 (2002).

254 Hartgerink, J. D., Beniash, E. & Stupp, S. I. Self-Assembly and Mineralization of Peptide-Amphiphile Nanofibers. *Science* **294**, 1684-1688 (2001).

255 Yokoi, H., Kinoshita, T. & Zhang, S. Dynamic reassembly of peptide RADA16 nanofiber scaffold. *Proc. Natl. Acad. Sci. U. S. A.* **102**, 8414-8419 (2005).

256 Petka, W. A. *et al.* Reversible Hydrogels from Self-Assembling Artificial Proteins. *Science* **281**, 389-392 (1998).

257 Aggeli, A. *et al.* Responsive gels formed by the spontaneous self-assembly of peptides into polymeric [beta]-sheet tapes. *Nature* **386**, 259-262 (1997).

258 Klok, H.-A. Protein-Inspired Materials: Synthetic Concepts and Potential Applications. *Angewandte Chemie International Edition* **41**, 1509-1513 (2002).

259 Wang, H. *et al.* GABAA-receptor-associated protein links GABAA receptors and the cytoskeleton. *Nature* **397**, 69-72 (1999).

260 Gezimati, J., Singh, H. & Creamer, L. K. Heat-Induced Interactions and Gelation of Mixtures of Bovine β-Lactoglobulin and Serum Albumin. *Journal of Agricultural and Food Chemistry* **44**, 804-810 (1996).

261 Hoffmann, M. A. M. & van Mil, P. J. J. M. Heat-Induced Aggregation of β-Lactoglobulin: Role of the Free Thiol Group and Disulfide Bonds. *Journal of Agricultural and Food Chemistry* **45**, 2942-2948 (1997).

262 Urry, D. W. Entropic elastic processes in protein mechanisms. I. Elastic structure due to an inverse temperature transition and elasticity due to internal chain dynamics. *Journal of Protein Chemistry* **7**, 1-34.

263 Urry, D. W. Free energy transduction in polypeptides and proteins based on inverse temperature transitions. *Progress in Biophysics and Molecular Biology* **57**, 23-57 (1992).

264 Urry, D. W. Physical Chemistry of Biological Free Energy Transduction As Demonstrated by Elastic Protein-Based Polymers. *The Journal of Physical Chemistry B* **101**, 11007-11028 (1997).

265 Meyer, D. E. & Chilkoti, A. Quantification of the Effects of Chain Length and Concentration on the Thermal Behavior of Elastin-like Polypeptides. *Biomacromolecules* **5**, 846-851 (2004).

266 McPherson, D. T., Xu, J. & Urry, D. W. Product Purification by Reversible Phase Transition FollowingEscherichia coliExpression of Genes Encoding up to 251 Repeats of the Elastomeric Pentapeptide GVGVP. *Protein Expression and Purification* **7**, 51-57 (1996).

267 Meyer, D. E. & Chilkoti, A. Purification of recombinant proteins by fusion with thermally-responsive polypeptides. *Nat. Biotechnol.* **17**, 1112-1115 (1999).

268 Meyer, D. E., Trabbic-Carlson, K. & Chilkoti, A. Protein purification by fusion with an environmentally responsive elastin-like polypeptide: Effect of polypeptide length on the purification of thioredoxin. *Biotechnol. Prog.* **17**, 720-728 (2001).

269 Hassouneh, W., Christensen, T. & Chilkoti, A. Elastin-like Polypeptides as a Purification Tag for Recombinant Proteins. *Current protocols in protein science / editorial board, John E. Coligan ... [et al.]* **CHAPTER**, Unit-6.11 (2010).

270 Cappello, J. *et al.* In-situ self-assembling protein polymer gel systems for administration, delivery, and release of drugs. *J. Control. Release* **53**, 105-117 (1998).

271 Megeed, Z., Cappello, J. & Ghandehari, H. Genetically engineered silk-elastinlike protein polymers for controlled drug delivery. *Adv. Drug Deliv. Rev.* **54**, 1075-1091 (2002).

272 Morihara, Y. *et al.* Thermosensitive gel formation of novel polypeptides containing a collagen-derived pro-hyp-gly sequence and an elastin-derived val-pro-uy-val-gly sequence. *J. Polym. Sci. Pol. Chem.* **43**, 6048-6056 (2005).

273 Chilkoti, A. *et al.* Targeted drug delivery by thermally responsive polymers. *Adv. Drug Deliv. Rev.* **54**, 613-630 (2002).

274 Mart, R. J. *et al.* Peptide-based stimuli-responsive biomaterials. *Soft Matter* **2**, 822-835 (2006).

275 Dreher, M. R. *et al.* Evaluation of an elastin-like polypeptide–doxorubicin conjugate for cancer therapy. *J. Control. Release* **91**, 31-43 (2003).

276 Chilkoti, A., Dreher, M. R. & Meyer, D. E. Design of thermally responsive, recombinant polypeptide carriers for targeted drug delivery. *Adv. Drug Deliv. Rev.* **54**, 1093-1111 (2002).

277 Roweton, S., Huang, S. J. & Swift, G. Poly(aspartic acid): Synthesis, biodegradation, and current applications. *J. Environ. Polym. Degrad.* **5**, 175-181 (1997).

278 Nakato, T., Kusuno, A. & Kakuchi, T. Synthesis of poly(succinimide) by bulk polycondensation of L-aspartic acid with an acid catalyst. *J. Polym. Sci. Pol. Chem.* **38**, 117-122 (2000).

279 Cho, J. Y. *et al.* Thermosensitive PEGylated Polypeptides. *Macromol. Rapid Commun.* **25**, 964-967 (2004).

280 Cho, J. Y. *et al.* pH/temperature sensitive poly(aspartic acid)-g-poly(propylene glycol). *J. Drug Deliv. Sci. Technol.* **16**, 71-76 (2006).

281 Tachibana, Y. *et al.* Biodegradable thermoresponsive poly(amino acid)s. *Chem. Commun.*, 106-107 (2003).

282 Tachibana, Y. *et al.* Thermoresponsive Hydrogels Based on Biodegradable Poly(amino acid)s. *Chem. Lett.* **32**, 374-375 (2003).

283 Takeuchi, Y. *et al.* Injectable thermoreversible hydrogels based on amphiphilic poly(amino acid)s. *Journal of Polymer Science Part A: Polymer Chemistry* **44**, 671-675 (2006).

284 Tachibana, Y. *et al.* Thermo- and pH-Responsive Biodegradable Poly(α-N-substituted γ-glutamine)s. *Biomacromolecules* **4**, 1132-1134 (2003).

285 Shimokuri, T. *et al.* Preparation and Thermosensitivity of Naturally Occurring Polypeptide Poly(γ-glutamic acid) Derivatives Modified by Propyl Groups. *Macromol. Biosci.* **4**, 407-411 (2004).

286 Chen, C., Wang, Z. & Li, Z. Thermoresponsive Polypeptides from Pegylated Poly-l-glutamates. *Biomacromolecules* **12**, 2859-2863 (2011).

287 Oh, H. J. *et al.* Secondary Structure Effect of Polypeptide on Reverse Thermal Gelation and Degradation of l/dl-Poly(alanine)–Poloxamer–l/dl-Poly(alanine) Copolymers. *Macromolecules* **41**, 8204-8209 (2008).

288 Choi, Y. Y. *et al.* Significance of secondary structure in nanostructure formation and thermosensitivity of polypeptide block copolymers. *Soft Matter* **4**, 2383-2387 (2008).

289 Jeong, Y. *et al.* Enzymatically degradable temperature-sensitive polypeptide as a new in-situ gelling biomaterial. *J. Control. Release* **137**, 25-30 (2009).

290 Lahasky, S. H., Hu, X. & Zhang, D. Thermoresponsive Poly(α-peptoid)s: Tuning the Cloud Point Temperatures by Composition and Architecture. *ACS Macro Lett.* **1**, 580-584 (2012).

291 Tao, X. *et al.* Polypeptoids with tunable cloud point temperatures synthesized from N-substituted glycine N-thiocarboxyanhydrides. *Polym. Chem.* **6**, 3164-3174 (2015).

292 Yoshida, T. *et al.* Newly designed hydrogel with both sensitive thermoresponse and biodegradability. *J. Polym. Sci. Pol. Chem.* **41**, 779-787 (2003).

293 Yeh, J.-C. *et al.* Synthesis and characteristics of biodegradable and temperature responsive polymeric micelles based on poly(aspartic acid)-g-poly(N-isopropylacrylamide-co-N,N-dimethylacrylamide). *Colloids and Surfaces A: Physicochemical and Engineering Aspects* **421**, 1-8 (2013).

294 Kim, S. *et al.* Synthetic MMP-13 degradable ECMs based on poly(N-isopropylacrylamide-co-acrylic acid) semi-interpenetrating polymer networks. I. Degradation and cell migration. *J. Biomed. Mater. Res. Part A* **75A**, 73-88 (2005).

295 Katayama, Y., Sonoda, T. & Maeda, M. A Polymer Micelle Responding to the Protein Kinase A Signal. *Macromolecules* **34**, 8569-8573 (2001).

296 Kim, T.-i. & Kim, S. W. Bioreducible polymers for gene delivery. *Reactive and Functional Polymers* **71**, 344-349 (2011).

297 Wu, C. *et al.* Interplay of Chemical Microenvironment and Redox Environment on Thiol–Disulfide Exchange Kinetics. *Chemistry – A European Journal* **17**, 10064-10070 (2011).

298 Anderson, M. E. Glutathione: an overview of biosynthesis and modulation. *Chemico-Biological Interactions* **111–112**, 1-14 (1998).

299 Jones, D. P. *et al.* Glutathione measurement in human plasma: Evaluation of sample collection, storage and derivatization conditions for analysis of dansyl derivatives by HPLC. *Clinica Chimica Acta* **275**, 175-184 (1998).

300 Yan, Y. *et al.* Cellular Association and Cargo Release of Redox-Responsive Polymer Capsules Mediated by Exofacial Thiols. *Advanced Materials* **23**, 3916-+ (2011).

301 Phillips, D. J. & Gibson, M. I. Degradable thermoresponsive polymers which display redox-responsive LCST Behaviour. *Chem. Commun.* **48**, 1054-1056 (2012).

302 Phillips, D. J. & Gibson, M. I. Biodegradable Poly(disulfide)s Derived from RAFT Polymerization: Monomer Scope, Glutathione Degradation, and Tunable Thermal Responses. *Biomacromolecules* **13**, 3200-3208 (2012).

303 Zhang, Q. *et al.* Dual Temperature and Thiol-Responsive POEOMA-Multisegmented Polydisulfides: Synthesis and Thermoresponsive Properties. *Macromol. Rapid Commun.* **33**, 1528-1534 (2012).

304 Rahimian-Bajgiran, K. *et al.* Tuning LCST with thiol-responsiveness of thermoresponsive copolymers containing pendant disulfides. *Chem. Commun.* **49**, 807-809 (2013).

305 Chan, N. *et al.* Dual Redox and Thermoresponsive Double Hydrophilic Block Copolymers with Tunable Thermoresponsive Properties and Self-Assembly Behavior. *Macromol. Rapid Commun.* **35**, 752-757 (2014).

306 Lee, J. *et al.* Temperature-Sensitive Biodegradable Poly(ethylene glycol). *Journal of Biomaterials Science-Polymer Edition* **20**, 957-965 (2009).

307 Gupta, M. K. *et al.* Cell Protective, ABC Triblock Polymer-Based Thermoresponsive Hydrogels with ROS-Triggered Degradation and Drug Release. *J. Am. Chem. Soc.* **136**, 14896-14902 (2014).

308 Hu, J. *et al.* Nitric Oxide (NO) Cleavable Biomimetic Thermoresponsive Double Hydrophilic Diblock Copolymer with Tunable LCST. *Macromolecules* **48**, 3817-3824 (2015).

# PART II

## Design of protein-reactive nanoparticles

# Chapter 3

# Synthesis of protein-reactive polymers via RAFT polymerization

In collaboration with

**Prof. Wim E. Hennink** from Utrecht University, Netherlands

**Prof. Richard Hoogenboom** from Ghent University, Belgium

Parts of this chapter were published in:

**Polymer-protein conjugation via a 'grafting to' approach - a comparative study of the performance of protein-reactive RAFT chain transfer agents**

N. Vanparijs, S. Maji, B. Louage, L. Voorhaar, D. Laplace, Q. Zhang, Y. Shi, W. E. Hennink, R. Hoogenboom, B. G. De Geest, *Polymer Chemistry* **2015**, 6, 5602-5614

## Abstract

In this chapter we aimed at preparing well-defined polymers for conjugation to proteins by reversible addition-fragmentation chain transfer (RAFT) polymerization of both acrylates and methacrylamides with protein-reactive chain transfer agents (CTAs). These RAFT agents contained either a N-hydroxysuccinimide (NHS) or pentafluorophenyl (PFP) ester moiety that can be conjugated to lysine residues, and alternatively a maleimide (MAL) or pyridyl disulfide (PDS) moiety that can be conjugated to cysteine residues. The polymerization kinetics of these RAFT agents were investigated for the polymerization of a model hydrophilic acrylate monomer 2-hydroxyethylacrylate (HEA) and methacrylamides with biomedical relevance, i.e. 2-hydroxypropylmethacrylamide (HPMAm) and its thermo-responsive dilactate derivative (HPMAm-$Lac_2$).

## Introduction

Polymer-protein conjugation strategies have received increasing interest owing to the ability to engineer proteins with a wide variety of properties, by simply coupling protein-reactive polymers to certain amino acid residues.[1-5] For example the conjugation of linear poly(ethylene glycol) to proteins, commonly known as PEGylation, results in prolonged body-residence time and a reduction of protein immunogenicity by blocking the adhesion of opsonins present in blood serum. In this way the proteins are masked from phagocytic cells and opsonization is strongly reduced.[6-8]

Controlled radical polymerization offers an excellent tool to synthesize polymers with well-defined composition, chain length, narrow dispersity and functional end groups that can be used for protein conjugation.[9,10] This significantly increases versatility and reproducibility compared to classical free radical polymerization, which is important with respect to both the design of multifunctional polymeric architectures as well as towards regulatory affairs. Reversible addition-fragmentation chain transfer (RAFT) polymerization in particular, has shown to be tolerant to many chemical groups and offers a straightforward route to synthesize polymers with a protein-reactive end-group via the use of a functional chain transfer agent (CTA).[11,12]

Sumerlin *et al.* reported on the use of a N-hydroxysuccinimide containing RAFT agent to synthesize poly(N-isopropylacrylamide) or p(NIPAAm) with a protein-reactive end-group that allowed conjugation to lysine residues.[13] Depending on the polymer to protein ratio, multi-site attachment (i.e. multiple polymer chains grafted onto one protein chain) can be obtained. However, for some applications, single site attachment, i.e. one polymer chain per protein molecule, might be more advantageous. In this regard, Velonia and co-workers used a protected maleimide functionalized RAFT CTA that can react with less abundantly present free cysteine residues.[14] Alternatively, the Maynard group used a pyridyl disulfide group to introduce reversibility into conjugate bonds.[15] In addition to these conventional protein-reactive groups, increasing synthetic effort is dedicated to develop newly emerging conjugation chemistries based on reactive moieties such as thiazolidine-2-thione[16], pentafluorophenyl[17,18] and dibromomaleimide[19]. However, no direct comparison of these different conjugation strategies had been reported.

In this chapter, 4 different protein-reactive RAFT CTAs are prepared containing either a N-hydroxysuccinimide (NHS) or pentafluorophenyl (PFP) ester moiety that can conjugate to lysine residues, and alternatively a maleimide or pyridyl disulfide (PDS) moiety for conjugation to cysteine residues. The polymerization kinetics of these RAFT agents are investigated for the polymerization of a model hydrophilic acrylate monomer 2-hydroxyethylacrylate (HEA) and methacrylamides with biomedical relevance, i.e. 2-hydroxypropylmethacrylamide (HPMAm) and its thermo-responsive dilactate derivative (HPMAm-$Lac_2$). These monomers are currently intensively studied for biomedical applications, in particular for anti-cancer drug formulations.[20-24]

## Material and methods

### *Materials*

Organic solvents dichloromethane (DCM, anhydrous and HPLC grade), toluene, methanol, chloroform, hexane, ethylacetate, dimethylacetamide (DMA, anhydrous), dimethylformamide (DMF, anhydrous) and chemicals N-hydroxysuccinimide, pentafluorophenol, mercaptoethanol, furan, 2-(2-amino-ethoxy)-ethanol), $MgSO_4$ and $NaSO_4$ were obtained from Sigma Aldrich and used without purification. Azobisisobutyronitrile

(AIBN, 98%, Aldrich) was recrystallized from MeOH (twice) and stored in a freezer. 2-Hydroxyethyl acrylate (HEA, 96%, Aldrich) was destabilized by passing the monomer over a column with inhibitor remover (Aldrich) prior to polymerization. The RAFT agent 4-cyano-4-[(dodecylsulfanylthiocarbonyl)sulfanyl]pentanoic acid (CDTPA) was purchased from Sigma Aldrich whilst 2-propanoic acid butyl trithiocarbonate (PABTC) and 4-cyano-4-[(ethylsulfanylthiocarbonyl)sulfanyl]pentanoic acid (CETPA) were prepared according to established procedures.[25,26] Chemicals 2,2'-dipyridyl disulfide, 4-dimethylaminopyridine (DMAP), 1-(3-dimethylaminopropyl)-3-ethylcarbodiimide (EDC) and N,N'-diisopropylcarbodiimide (DIC) were purchased from TCI Europe. Maleic anhydride from Merck Germany was used as received. 2-Hydroxypropylmethacrylamide (HPMAm) was obtained from Polysciences, whilst HPMAm-dilactate was synthesized according to established procedures.[27]

***Instrumentation***

Kinetic studies of the RAFT polymerizations were performed using a Chemspeed ASW2000 automated synthesizer equipped with 16 parallel reactors of 13 mL, a Huber Petite Fleur thermostat for heating/cooling, a Huber Ministat 125 for reflux and a Vacuubrand PC 3000 vacuum pump following a recently reported protocol.[28,29] Stock solutions of all components were prepared and bubbled with argon for at least 30 minutes before being introduced into the robot system and then kept under argon atmosphere. The reactors were degassed through ten vacuum-argon cycles and subsequently flushed with argon to ensure an inert atmosphere. The hood of the automated synthesizer was continuously flushed with nitrogen. Stock solutions were transferred to the reactors using the syringe of the automated synthesizer while the reactors were cooled to 10°C, after which the reactors were heated to 70°C to start the polymerizations. During the reactions samples were taken at preset time intervals for GC, SEC and NMR analysis. The polymerizations were stopped by cooling the reactors to 10°C.

Gas chromatography was performed on a 7890A from Agilent Technologies with an Agilent J&W Advanced Capillary GC column (30 m, 0.320 mm, and 0.25 µm). Injections were performed with an Agilent Technologies 7693 auto sampler. Detection was done with a FID detector. The injector and detector temperatures were kept constant at 250 and 280°C, respectively. The column was initially set at 50°C, followed by two heating stages: from 50°C

to 100°C with a rate of 20°C /min and from 100°C to 300°C with a rate of 50°C /min, and then held at this temperature for 0.5 minutes. Conversion of HEA was determined based on the integration of the monomer peak using DMA as internal standard.

Size exclusion chromatography was carried out on an Agilent 1260 system, equipped with an 1260 ISO-pump, an 1260 diode array detector (DAD) and an 1260 refractive index detector (RID). Measurement were done in DMA containing 50 mM LiCl at 50°C and with a flow rate of 0.593 mL/min. The two PL gel 5 µm mixed-D columns were calibrated with poly(methylmethacrylate) (PMMA) standards (Polymer standards service) in a molecular weight (Mn) range of 1980 Da to 372000 Da.

$^{1}$H-NMR an $^{19}$F-NMR spectra were recorded on a Bruker 300 MHz FT-NMR spectrometer using $CDCl_3$ as solvent.

Column chromatography was performed on a Grace Reveleris X2 flash chromatography system using silica Reveleris flash cartridges.

***Synthesis of N-hydroxysuccinimide containing CTA***

N-hydroxysuccinimide (NHS) PABTC was synthesized as reported by Sumerlin *et al*.[13] PABTC (1.430 g, 6 mmol) and NHS (690.54 mg, 6 mmol) were introduced in a round-bottom flask and dissolved in anhydrous dichloromethane (DCM, 50 mL). The reaction mixture was cooled to 0°C in an ice bath and a solution of DIC (757 mg, 6 mmol) in anhydrous DCM (10 mL) was added drop-wise while vigorously stirring. The reaction mixture was stirred in an ice bath for 2h and subsequently at room temperature overnight. The resulting solution was filtered (whatman grade 2), and the solvent was evaporated under vacuum. The crude product was purified by column chromatography on silica gel with a mobile phase of EtOAc/hexane 1/1 (v/v). The first fraction was collected and the solvent was removed under reduced pressure to obtain the product as a yellow oil (986 mg, yield 49%, **Figure 1**).

***Synthesis of pentafluorophenol containing CTA***

Pentafluorophenol (PFP) PABTC was synthesized as described by Stenzel *et al*.[17] PABTC (1.192 g, 5 mmol), PFP (1.012 g, 5.5 mmol) and DMAP (61 mg, 0.5 mmol) were introduced into a round-bottom flask and dissolved in anhydrous dichloromethane (DCM, 50 mL). The reaction mixture was cooled to 0°C in an ice bath and a solution of DIC (694 mg, 5.5 mmol) in DCM (10 mL) was added drop-wise while vigorously stirring. The reaction mixture

was stirred in an ice bath for 2h and subsequently at room temperature overnight. The resulting solution was filtered (whatman grade 2), and the solvent was evaporated under vacuum. The crude product was purified by column chromatography on silica gel using chloroform as eluent. The first fraction was collected and the solvent was removed under reduced pressure to obtain the product as an orange/red oil (1.490 g, yield 67%, **Figure 2**). The same procedure was used to functionalize CDTPA (yield 67%, **Figure 3**) and CETPA (yield 64%, **Figure 4**) with PFP.

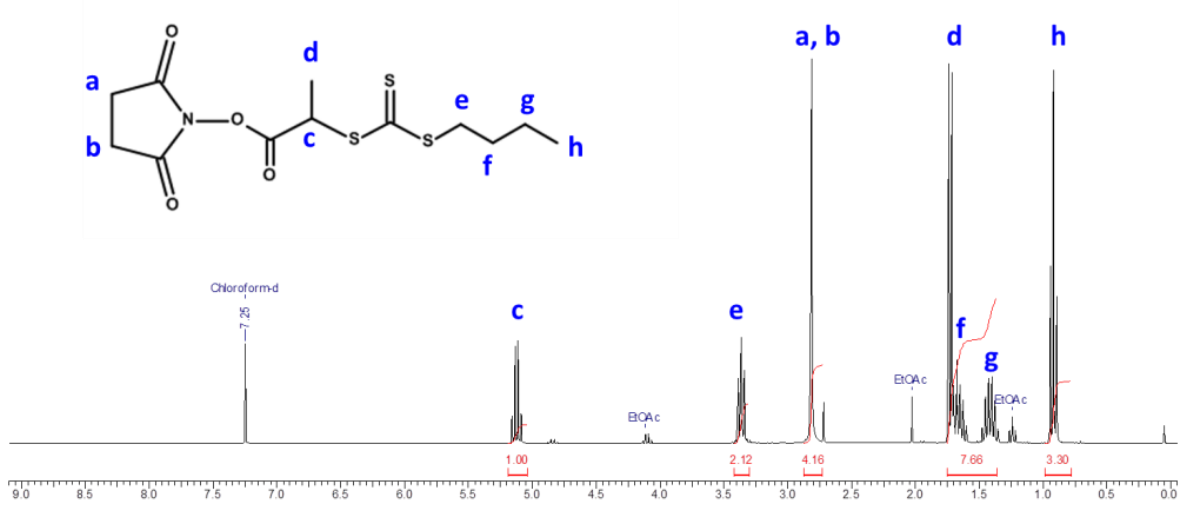


**Figure 1**. $^{1}$H-NMR of NHS PABTC (300 MHz, $CDCl_3$) δ (ppm): 5.13 (q, *J* = 7.5, 1H, -C***H***$CH_3$), 3.36 (t, *J* = 7.4 Hz, 2 H, -SC***H*****$_2$**-), 2.82 (s, 4 H, -COC***H*****$_2$**C***H*****$_2$**CO-), 1.73 (d, *J* = 7.5 Hz, 3 H, -CHC***H*****$_3$**), 1.68 (tt, *J* = 7.4 Hz, 2 H, -$SCH_2$C***H*****$_2$**-), 1.42 (app. sext, *J* = 7.4 Hz, -C***H*****$_2$**$CH_3$), 0.92 (t, *J* = 7.4 Hz, 3H, -$CH_2$C***H*****$_3$**).

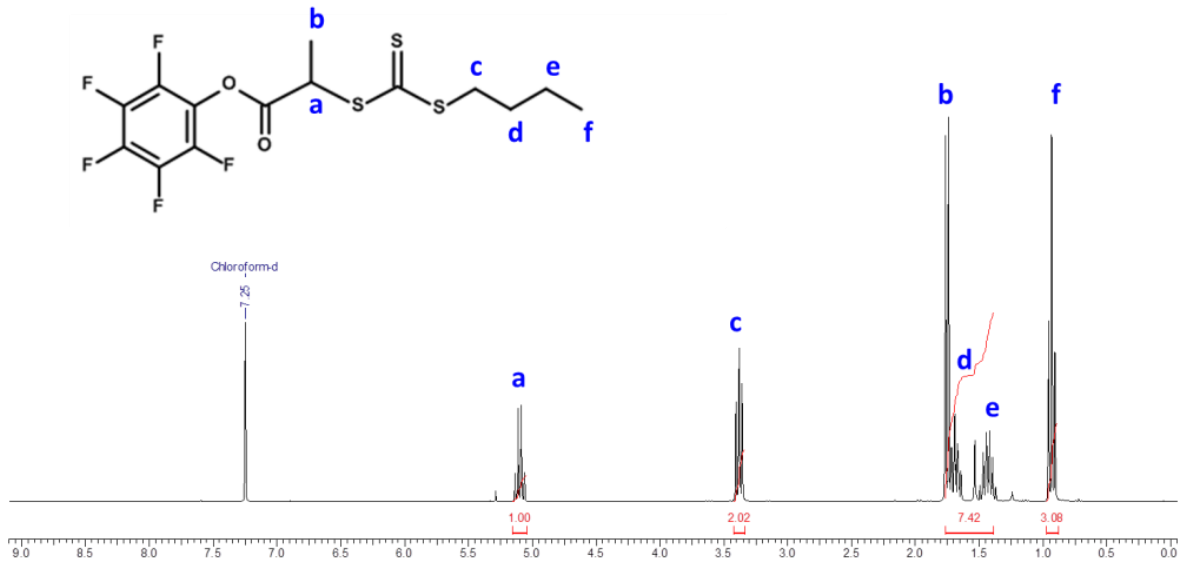


**Figure 2**. $^{1}$H-NMR of PFP PABTC (300 MHz, $CDCl_3$) δ (ppm): 5.10 (q, *J* = 7.4, 1H, -C***H***$CH_3$), 3.38 (t, *J* = 7.4 Hz, 2 H, -SC***H*****$_2$**-), 1.76 (d, *J* = 7.4 Hz, 3 H, -CHC***H*****$_3$**), 1.69 (tt, *J* = 7.4 Hz, 2 H, -$SCH_2$C***H*****$_2$**-), 1.44 (app. sext, *J* = 7.4 Hz, -C***H*****$_2$**$CH_3$), 0.93 (t, *J* = 7.4 Hz, 3H, -$CH_2$C***H*****$_3$**). Not shown: $^{19}$F-NMR (300 MHz, $CDCl_3$) δ (ppm): -152.27 (d, 2 F), -157.40 (t, 1 F), -162.07 (t, 2F)

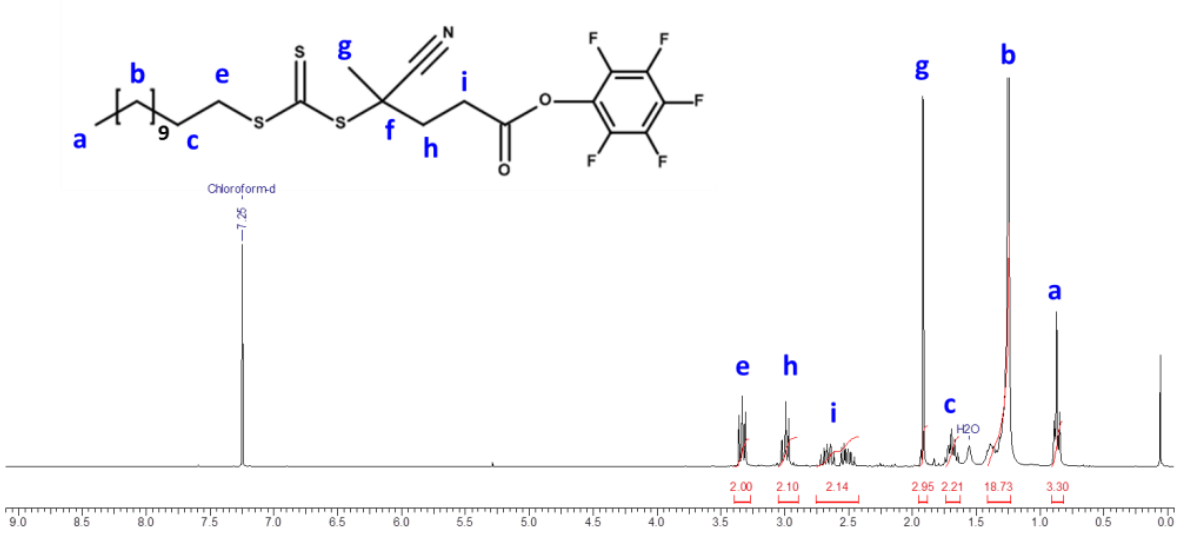


**Figure 3.** $^{1}$H-NMR of PFP CDTPA (300 MHz, $CDCl_3$) δ (ppm): 3.33 (t, *J* = 7.4 Hz, -SC***H*****$_2$**-), 3.03-2.96 (band, 2 H, -CC***H*****$_2$**-), 2.73-2.45 (band, 2 H, -COC***H*****$_2$**-), 1.92 (s, 3 H, -CC***H*****$_3$**), 1.75-1.64 (band, 2 H, -$SCH_2$C***H*****$_2$**-), 1.44-1.21 (band 18 H, -$C_9$***H*****$_{18}$**$CH_3$) 0.87 (t, *J* = 6.4 Hz, 3 H, -$CH_2$C***H*****$_3$**). Not shown: $^{19}$F-NMR (300 MHz, $CDCl_3$) δ (ppm): -152.49 (d, 2 F), -157.29 (t, 1 F), -161.86 (t, 2F).

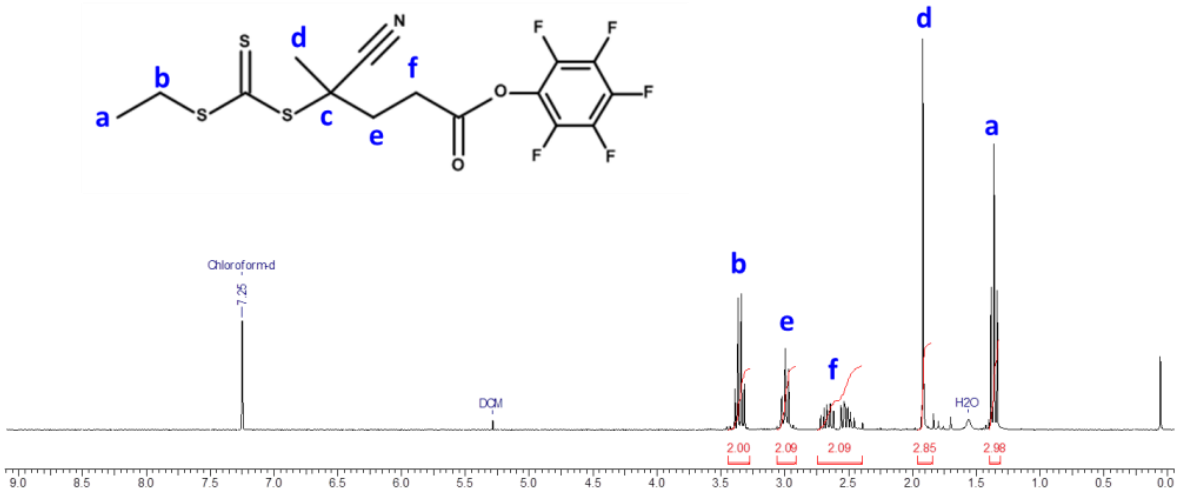


**Figure 4.** $^{1}$H-NMR of PFP CETPA (300 MHz, $CDCl_3$) δ (ppm): 3.36 (q, *J* = 7.4 Hz, 2 H, -C***H*****$_2$**$CH_3$), 3.03-2.97 (band, 2 H, -CC***H*****$_2$**-), 3.75-2.45 (band, 2 H, -COC***H*****$_2$**-), 1.92 (s, 3 H, -CC***H*****$_3$**), 1.36 (t, *J* = 7.4 Hz, 3 H, -$CH_2$C***H*****$_3$**). Not shown: $^{19}$F-NMR (300 MHz, $CDCl_3$) δ (ppm): -152.49 (d, 2 F), -157.29 (t, 1 F), -161.86 (t, 2F).

### *Synthesis of the pyridyl disulfide containing CTA*

*Synthesis of hydroxyethyl pyridyl disulfide*

Hydroxyethyl pyridyl disulfide (HEPDS) was synthesized as described by Thayumanavan *et al.*[30] 2,2'-dipyridyl disulfide (25 g, 113 mmol) was dissolved in 120 mL of methanol containing 1.7 mL of glacial acetic acid. A solution of mercaptoethanol (4.434 g, 57 mmol) in methanol (25 mL) was added drop-wise at room temperature while vigorously stirring. The reaction was continued at room temperature for additional 3 hours. The

resulting solution was filtered (whatman grade 2), and the solvent was evaporated under vacuum. The crude product was purified by column chromatography on silica gel with a gradient of EtOAc/hexane 30/70-50/50 (v/v). The second fraction was collected and the solvent was removed under reduced pressure to obtain the product as a colorless oil (7.5 g, yield 70%, **Figure 5**).

*Synthesis of pyridyl disulfide containing CTA*

HEPDS was used to synthesize the pyridyl disulfide (PDS) RAFT agent as reported by Maynard *et al*.[15] PABTC (2.86 g, 12 mmol) and HEPDS (1.87 g, 10 mmol) were introduced into a round-bottom flask and dissolved in anhydrous dichloromethane (DCM, 50 mL). The reaction mixture was cooled to 0°C in an ice bath while vigorously stirring. EDC (2.12 mL, 12 mmol) and DMAP (122 mg, 1 mmol) were then added in one portion. The reaction was stirred in an ice bath for 2h and subsequently at room temperature overnight. The resulting solution was filtered (whatman grade 2), and the solvent was evaporated under vacuum. The crude product was purified by column chromatography on silica gel with a mobile phase of EtOAc/hexane 1/2 (v/v). The second fraction was collected and the solvent was removed under reduced pressure to obtain the product as a yellow oil (2.287 g, yield 56%, **Figure 6**). The same procedure was used to functionalize CETPA with PDS (yield 46%, **Figure 7**).

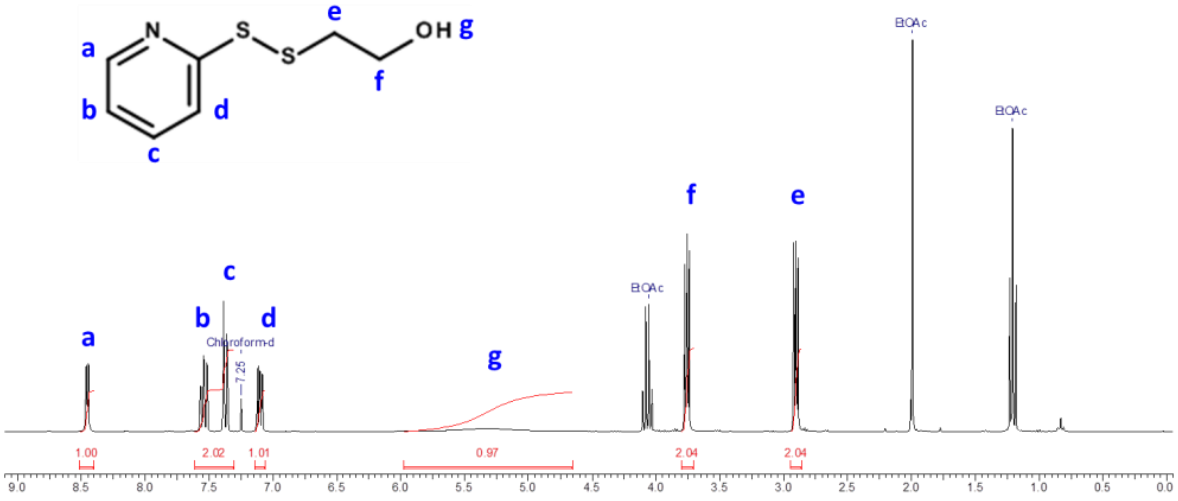


**Figure 5.** $^{1}$H-NMR of HEPDS (300 MHz, $CDCl_3$) δ (ppm): 8.45 (m, 1H, $\boldsymbol{H_{ortho\text{-}N}}$), 7.55 (m, 1H, $\boldsymbol{H_{meta\text{-}N}}$), 7.37 (m, 1H, $\boldsymbol{H_{para\text{-}N}}$), 7.10 (ddd, *J* = 1.1, 5.2 and 7.4 Hz, 1H, $\boldsymbol{H_{ortho\text{-}disulfide}}$), 5.98-4.65 (m, 1H, -O***H***), 3.76 (t, *J* = 5.2 Hz, 2H, -C$\boldsymbol{H_2}$OH), 2.91 (t, *J* = 5.2, 2H, -C$\boldsymbol{H_2}$C$H_2$OH)

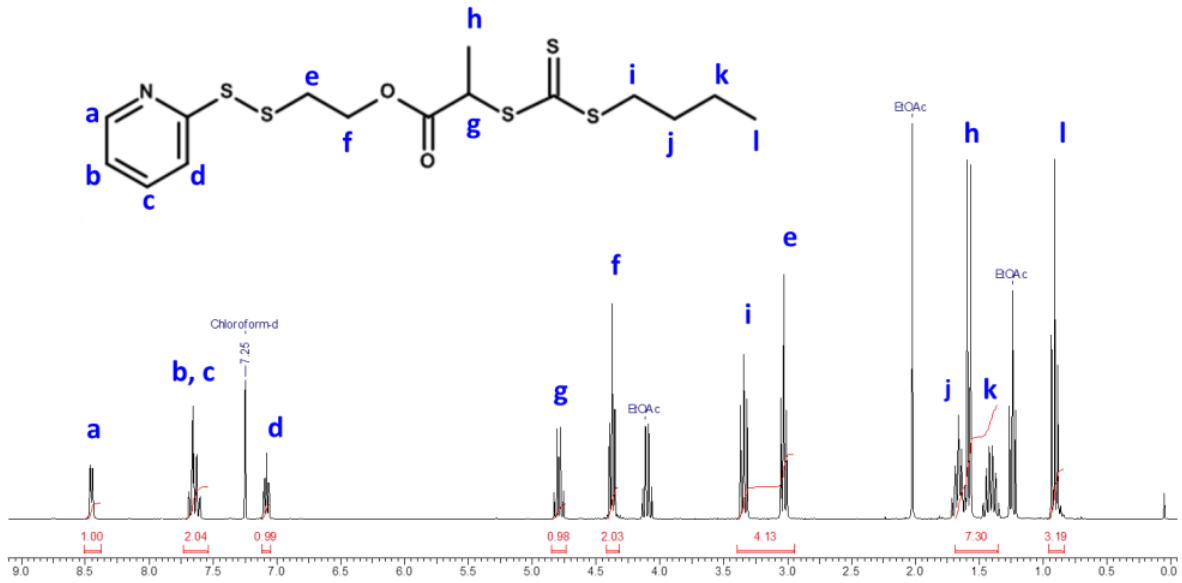


**Figure 6.** $^{1}$H-NMR of PDS PABTC (300 MHz, $CDCl_3$) δ (ppm): 8.46 (m, 1 H, $\boldsymbol{H_{ortho\text{-}N}}$), 7.70-7.60 (band, 2 H, $\boldsymbol{H_{meta\text{-}N}}$ and $\boldsymbol{H_{para\text{-}N}}$), 7.09 (ddd, *J* = 1.7, 4.9 and 6.6 Hz, 1 H, $\boldsymbol{H_{ortho\text{-}disulfide}}$), 4.80 (q, *J* = 7.4 Hz, 1 H, -C***H***$CH_3$), 4.38 (t, *J* = 6.4 Hz, 2 H, -OC$\boldsymbol{H_2}$-), 3.34 (t, *J* = 7.3 Hz, 2 H, -SC$\boldsymbol{H_2}C_3H_7$ ), 3.03 (t, *J* = 6.4 Hz, 2 H, -C$\boldsymbol{H_2}CH_2O$-), 1.66 (app. quint, *J* = 7.3 Hz, 2 H, -$SCH_2C\boldsymbol{H_2}$-), 1.57 (d, *J* = 7.4 Hz, 3 H, -CHC$\boldsymbol{H_3}$), 1.41 (app. sext, *J* = 7.3 Hz, -C$\boldsymbol{H_2}CH_3$-), 0.91(t, *J* = 7.3 Hz, 3H, -$CH_2C\boldsymbol{H_3}$).

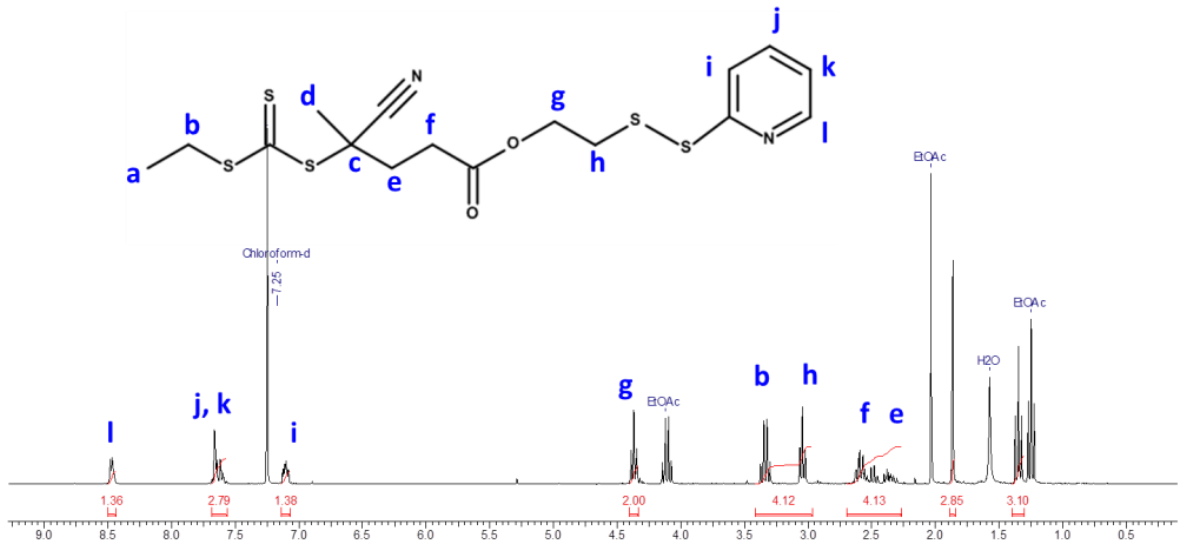


**Figure 7.** $^{1}$H-NMR of PDS CETPA (300 MHz, $CDCl_3$) δ (ppm): 8.50-8.45 (m, 1 H, $\boldsymbol{H_{ortho\text{-}N}}$), 7.68-7.56 (band, 2 H, $\boldsymbol{H_{meta\text{-}N}}$ and $\boldsymbol{H_{para\text{-}N}}$), 7.14-7.07 (m, 1 H, $\boldsymbol{H_{ortho\text{-}disulfide}}$), 4.37 (t, *J* = 6.4 Hz, 2 H, -OC$\boldsymbol{H_2}$-), 3.34 (q, *J* = 7.4 Hz, 2 H, -C$\boldsymbol{H_2}CH_3$), 3.04 (t, *J* = 6.4 Hz, 2 H, -$OCH_2C\boldsymbol{H_2}$-), 2.65-2.45 (band, 2 H, -$COCH_2C\boldsymbol{H_2}$-), 2.41-2.21 (band, 2 H, -COC$\boldsymbol{H_2}$-), 1.86 (s, 3 H, -CC$\boldsymbol{H_3}$), 1.35 (t, *J* = 7.4 Hz, 3 H, -$CH_2C\boldsymbol{H_3}$)

***Synthesis of the (furan protected) maleimide containing CTA***

*Synthesis of 4,10-Dioxatricyclo[5.2.1.0(2,6)]dec-8-ene-3,5-dione [1]*

4,10-Dioxatricyclo[5.2.1.0(2,6)]dec-8-ene-3,5-dione was synthesized as reported by Velonia *et al*.[14] Maleic anhydride (30.0 g, 306 mmol) was suspended in 150 mL of toluene and the mixture was warmed to 80 °C in an oil bath. Furan (33.4 mL, 459 mmol) was added via syringe while vigorously stirring and the resulting turbid solution was stirred for 6 h. The mixture was then cooled to ambient temperature and the stirring was stopped. After 1 h, the formed white crystals were collected by filtration and washed with 30 mL of hexane to obtain the product as small white crystals (44 g, yield 87%, **Figure 8**)

*Synthesis of 4-[2-(2-Hydroxy-ethoxy)-ethyl]-10-oxa-4-aza-tricyclo[5.2.1.0(2,6)]dec-8-ene-3,5-dione [2]*

The anhydride [1] (16.00 g, 96.3 mmol) was suspended in methanol (250 mL) and the mixture was cooled in an ice bath. A solution of 2-(2-amino-ethoxy)-ethanol (9.64 mL, 96.3 mmol) in 20 mL of methanol was subsequently added dropwise (15 min) while vigorously stirring. Next, the reaction was stirred at ambient temperature for 30 min and finally refluxed for 4 h. After cooling the mixture to ambient temperature, the solvent was removed under reduced pressure, and the residue was dissolved in 2 x 150 mL of DCM (in two portions) and washed with 2 x 100 mL of water separately. The organic layers were combined, dried over $MgSO_4$ and filtered. Removal of the solvent under reduced pressure yielded the product as a highly viscous yellow residue (6.88 g, yield 28%, **Figure 9**).

*Synthesis of 2-butylsulfanylthiocarbonylsulfanyl-propionic acid 2-[2-(3,5-dioxo-10-oxa-4-aza-tricyclo[5.2.1.0(2,6)]dec-8-en-4-yl)-ethoxy]-ethyl ester [3]*

A solution of compound [2] (2.5 g, 9.87 mmol) and PABTC (2.82 g, 11.8 mmol) in dichloromethane (20 mL) was cooled in an ice bath while vigorously stirring. Solutions of EDC (1.84 g, 11.8 mmol) and DMAP (0.15 g, 1.18 mmol) in DCM were then added drop-wise via syringe over 10 minutes. The reaction was stirred in an ice bath for 2h and subsequently at room temperature overnight. The product was diluted with dichloromethane (100 mL), washed with distilled water (3x100 mL), dried with sodium sulfate ($Na_2SO_4$), filtered and finally dried under reduced pressure to get product [3]. Finally the product was purified by column chromatography on silica gel using a mobile phase of EtOAC/hexane 1/1 (v/v). The third fraction was collected and the solvent was removed under reduced pressure to obtain the product as a yellow oil (2.24 g, yield 48%, **Figure 10**).

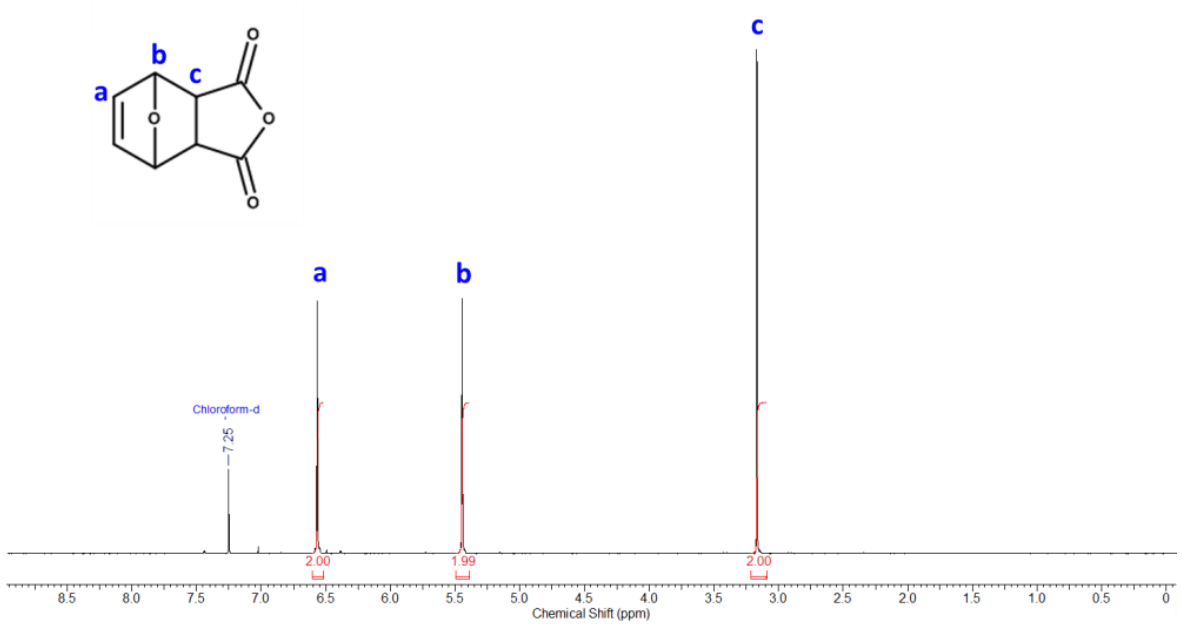


**Figure 8.** $^{1}$H-NMR of compound [1] (300 MHz, $CDCl_3$) δ (ppm): 6.57 (t, *J* = 0.9 Hz, 2H, -C***H***$_{vinyl}$-), 5.45 (t, *J* = 0.9 Hz, 2H, -C***H***O-), 3.17 (s, 2H, -C***H***-).

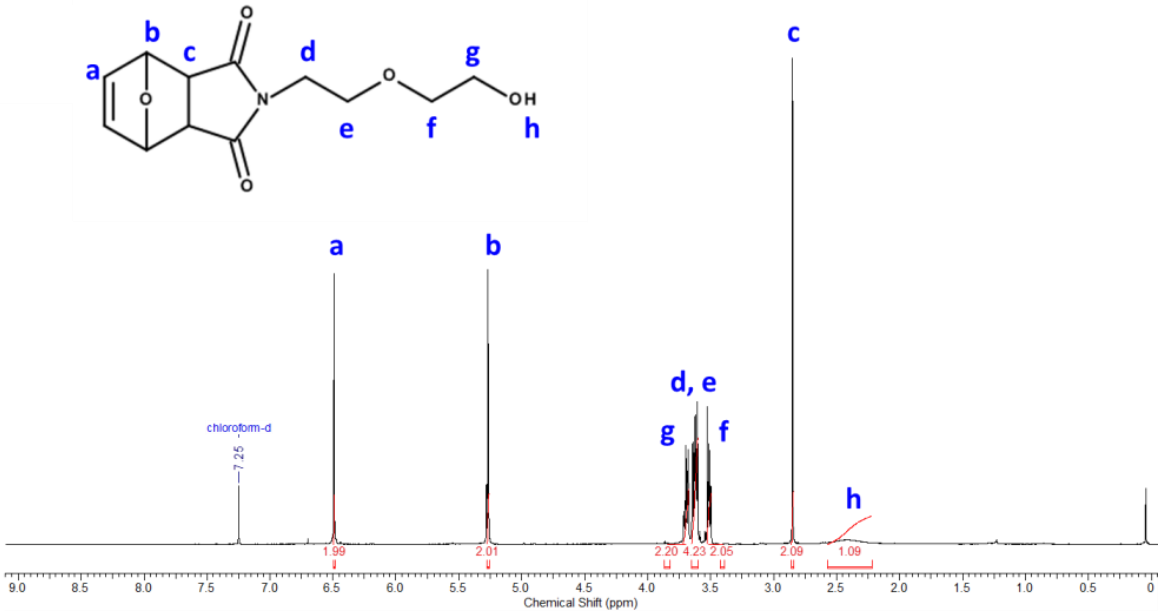


**Figure 9.** $^{1}$H-NMR of compound [2] (300 MHz, $CDCl_3$) δ (ppm): 6.49 (t, *J* = 0.9 Hz, 2H, -C***H***$_{vinyl}$-), 5.27 (t, *J* = 0.9 Hz, 2H, -C***H***O-), 3.71-3.67 (band, 2 H, -C***H***$_2$OH), 3.65-3.60 (band, 4 H, -NC***H***$_2$C***H***$_2$-), 3.53-3.50 (band, 2 H, -C***H***$_2$CH$_2$OH), 2.85 (s, 2H, -C***H***-), 2.57-2.22 (m, 1 H, -O***H***).

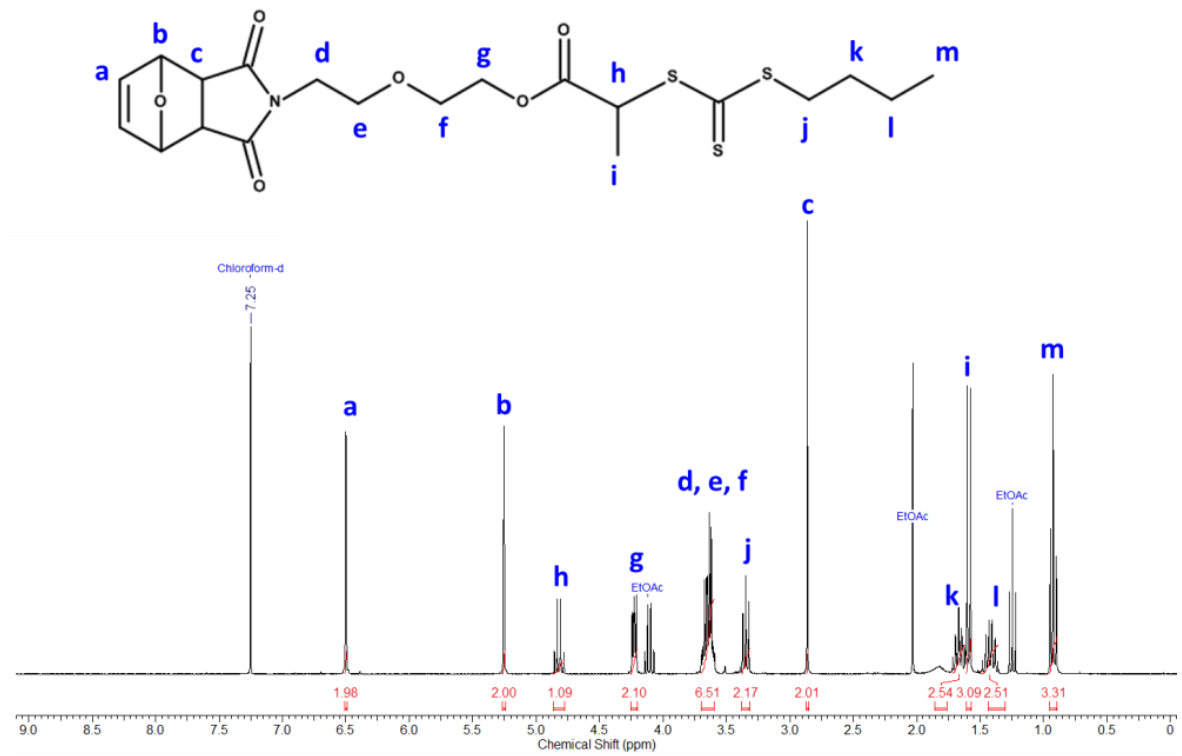


**Figure 10.** $^{1}$H-NMR of compound [3] (300 MHz, $CDCl_3$) δ (ppm): 6.50 (t, *J* = 0.8 Hz, 2 H, -C***H***$_{vinyl}$-), 5.25 (t, *J* = 0.8 Hz, 2H, -C***H***O-), 4.82 (q, *J* = 7.3, 1H, -C***H***$CH_3$), 4.23 (m, 2 H, -COOC***H***$_2$-), 3.70-3.59 (band, 6 H, -NC***H***$_2$C***H***$_2$OC***H***$_2$-), 3.35 (m, 2 H, -SC***H***$_2$-), 2.86 (s, 2H, -C***H***CON-), 1.67 (app. quint, *J* = 7.4, 2 H, -$SCH_2$C***H***$_2$-), 1.59 (d, *J* = 7.3 Hz, 3 H, -CHC***H***$_3$), 1.42 (app. sext, *J* = 7.4 Hz, -C***H***$_2CH_3$-), 0.92 (t, *J* = 7.3 Hz, 3H, -$CH_2$C***H***$_3$).

### *RAFT polymerization of HEA with the protein-reactive CTA's*

*Kinetic study in Chemspeed robot*

The functionalized PABTC CTAs were used for the RAFT polymerization of HEA in DMF (2.5M) at 70°C, using AIBN as initiator at a HEA:CTA:AIBN ratio of 100:1:0.2 or 100:1:0.1, respectively. Samples were taken at various time points (T0 = 0 min, T1= 10 min, T2 = 20 min, T3 = 30 min, T4 = 40 min, T5 = 50 min, T6 = 60 min, T7 = 90 min, T8 = 120 min, T9 = 150 min, T10 =180 min) and were evaluated via GC to follow HEA conversion and SEC to follow the number average molecular weight ($M_n$) and dispersity (Đ) of the polymers in time.

*Synthesis of functional poly(2-hydroxyethylacrylate) for protein conjugation*

The HEA:CTA:AIBN ratio was kept at 100:1:0.1 and polymerizations were stopped after 30 min (MAL CTA), 90 min (PFP CTA) and 120 min (NHS and PDS CTA). An example RAFT polymerization was as follows. HEA (10 mmol, 1.149 mL), CTA (0.1 mmol) and AIBN (0.01 mmol, 1.642 mg) were transferred into a schlenktube and dissolved in anhydrous DMF (2.9 mL, 2.5M). After bubbling with nitrogen for 30 min., the solution was heated at 70°C in an oil bath for the predetermined time before being quenched by cooling it in an ice water bath

and exposing the polymerization solution to air. The reaction solutions were diluted with DCM in a 1:1 ratio, and the polymeric product was precipitated into hexane and dried under vacuum to yield protein-reactive polymers.

*Deprotection of the furan-protected maleimide group*

Deprotection was accomplished by a retro Diels-Alder reaction.[14] After precipitation, the polymer was dissolved in dioxane (1g / 25 mL) and the solution was heated to 110°C in an oil bath. Next, dioxane was removed under reduced pressure to give the final polymer. As a control, the trithiocarbonate polymer end-group was cleaved into a thiol by aminolysis. After 30 minutes of polymerization, the reaction mixture was cooled to room temperature and an excess of propylamine in molar ratio of 1:30 CTA:Propylamine was added to the schlenktube. The solution was stirred for 2 hours at room temperature and the formed product was precipitated 3 times in hexane. Next, the same deprotection procedure was performed as described above.

***RAFT polymerization of HPMAm with the protein-reactive CTA's***

*Kinetic study in Chemspeed robot*

The functionalized PFP CDTPA and PFP CETPA CTA's were used for the RAFT polymerization of HPMAm in DMAc (2M) at 70°C, using AIBN as initiator at a HPMAm:CTA:AIBN ratio of 100:1:0.2 or 200:1:0.2, respectively. This rather high AIBN concentration was required to allow efficient initiation of the RAFT polymerization of HPMAm. Stock solution of AIBN, CTA and monomer were bubbled with nitrogen for 30 min. and the polymerization reactions were performed in the reactors of the Chemspeed robot under argon atmosphere. Samples were taken at various time points (T0 = 0 min, T1= 30 min, T2 = 60 min, T3 = 90 min, T4 = 120 min, T5 = 180 min, T6 = 240 min, T7 = 300 min, T8 = 360 min, T9 = 480 min, T10 =600 min) and were evaluated via $^{1}$H-NMR spectroscopy to follow monomer conversion and SEC to follow the number average molecular weight ($M_n$) and dispersity (Đ) of the polymers in time. The conversion of HPMAm was determined according to literature by comparing the $^{1}$H-NMR integration areas of resonances from the vinyl protons of HPMAm at 5.30 ppm and the methine protons of HPMAm at 3.65 ppm of the crude reaction mixture.[31]

*Synthesis of functional poly(N-hydroxypropylmethacrylamide) for protein conjugation*

An example RAFT polymerization with PDS CETPA CTA was as follows. HPMAm (6.98 mmol, 1 g), CTA (0.07 mmol for DP100; 0.035 mmol for DP200) and AIBN (0.014 mmol for DP100; 0.007 mmol for DP200) were transferred into a schlenktube and dissolved in anhydrous DMAc (3.5 mL, 2M). After bubbling with nitrogen for 30 min., the solution was heated at 70°C in an oil bath for 10h. The polymers were isolated by precipitation in diethyl ether and dried under vacuum. The same conditions were used to polymerize HPMAm-$Lac_2$.

## Results and discussion

### *Synthesis of protein-reactive CTAs for acrylate RAFT polymers*

Four different trithiocarbonate-based CTAs for acrylate/acrylamide RAFT polymerization bearing a protein-reactive functional group at the R-position were synthesized. This was done by carbodiimide-mediated esterification of the carboxylic acid group of 2-(n-butyltrithiocarbonylthio) propionic acid (PABTC) with either N-hydroxysuccinimide (NHS), pentafluorophenol (PFP), hydroxethylpyridyldisulfide (HEPDS) or 4-[2-(2-Hydroxy-ethoxy)-ethyl]-10-oxa-4-aza-tricyclo[5.2.1.0(2,6)]dec-8-ene-3,5-dione. The latter contains a furan-protected maleimide that requires deprotection, revealing the maleimide, prior to protein-conjugation. Note that the furan protection group is required to avoid side-reactions by radical addition to the maleimide during RAFT polymerization. **Scheme 1** summarizes the synthesis of these different CTAs, and illustrates how they conjugate to either lysine or cysteine residues to afford protein conjugation. For the sake of clarity the respective CTAs will be further denoted as NHS-PABTC, PFP-PABTC, PDS-PABTC and FpMAL-PABTC (Fp: furan-protected). Further on, the polymer with a deprotected maleimide group will be referred to as MAL.

### *RAFT polymerization of HEA with protein-reactive CTAs*

The respective CTAs with a protein-reactive functional group were subsequently used for RAFT polymerization of 2-hydroxyethylacrylate (HEA) (**Scheme 1**) with a targeted degree of polymerization (DP) of 100. Note that this DP was chosen arbitrary, and in future work we are aiming at investigating the influence of polymer chain length on the conjugation

efficiency of the respective functional RAFT polymers. Polymerization kinetics were studied using an automated synthesis robot that allows to run multiple polymerization reactions, including sampling, in parallel. This set-up minimizes the experimental error and batch-to-batch variation. Polymerizations were run in duplicate at 70°C and with two different AIBN to CTA (i.e 0.1 and 0.2) ratios. Although it is well-documented that polymerization of acrylate monomers at 70°C can cause side reactions (e.g. backbiting)[32], we have chosen work conditions that have been reported in literature to provide good control over the polymerization.[33,34]

Samples were analyzed by gas chromatography (GC) for monomer conversion (**Figure 11**) and by size exclusion chromatography (SEC, **Figure 12**) for their molecular weight and dispersity. The kinetic data depict that NHS-, PFP- and PDS-PABTC provide, for both AIBN/CTA ratios, good control over the polymerization as indicated by the linear pseudo-first order kinetic plots and the linear growth of molecular weight with monomer conversions. A double molar mass shoulder in the SEC elugrams was only observed above 90% conversion, indicative of termination by chain coupling as commonly observed for radical polymerization at high monomer conversion. As expected, the RAFT polymerization kinetics are, within experimental error, independent of the CTA as the initiating fragments are very similar. Furthermore, using more AIBN results in faster polymerization due to the higher concentration of radicals. However, it should be noted that in case of FpMAL-PABTC, side-reactions were observed above 50% conversion, as witnessed by the emergence of a multimodal distribution in the SEC elugrams and an increase in dispersity. This is probably due to in situ deprotection of the maleimide at the polymerization temperature of 70°C and its subsequent incorporation into the polymer chains by radical addition. This issue could not be fully solved by using V70 initiator (10 hour half-life at 30°C) and performing the polymerization reaction at 50°C (data not shown), which suggests other side reactions might underlie the reduced control over RAFTpolymerization using this FpMAL-PABTC.

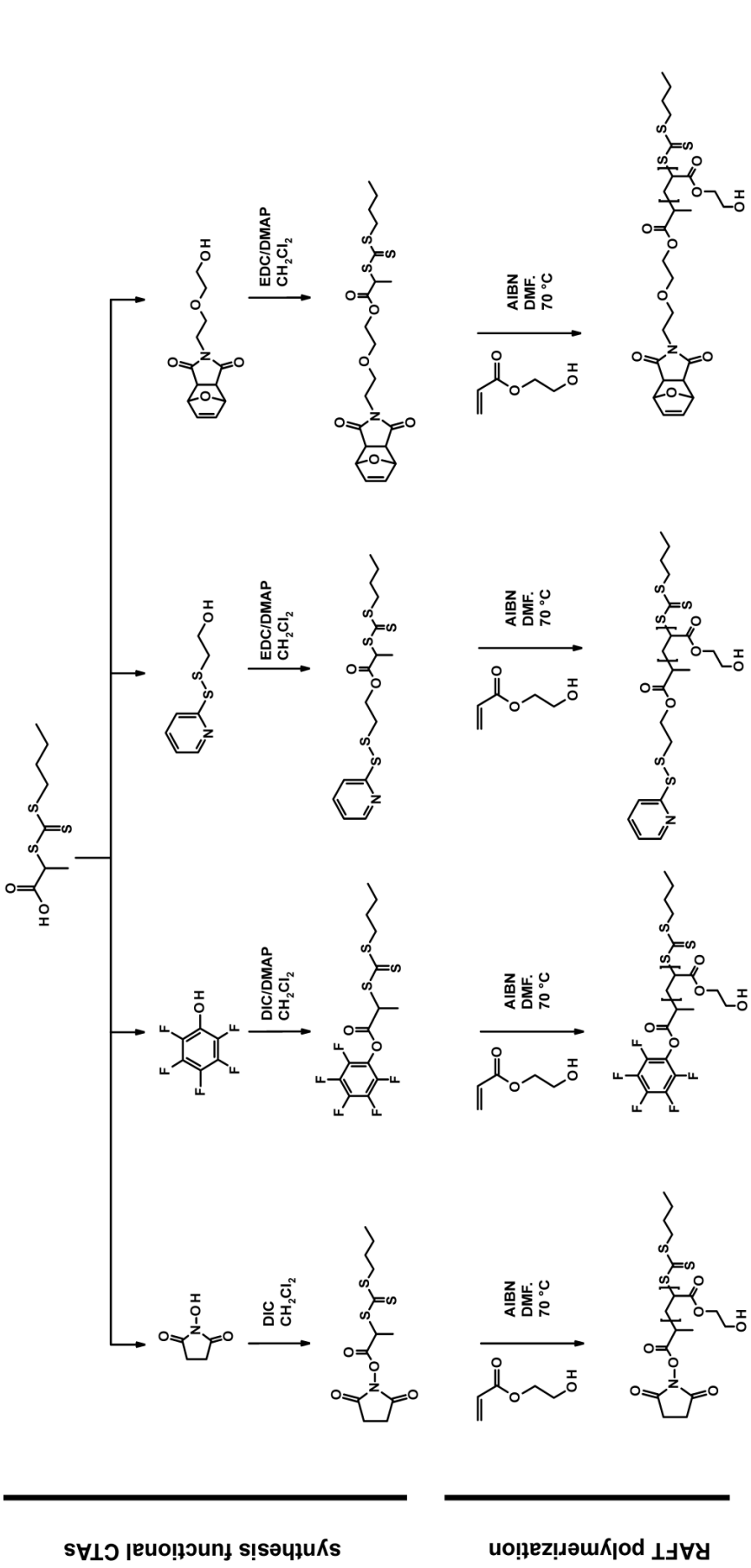


**Scheme 1.** Synthesis of the different functional PABTC CTAs used in this work for RAFT polymerization of 2-hydroxyethylacrylate. From left to right: N-hydroxysuccinimide (NHS) and pentafluorophenyl (PFP) esters that can conjugate to lysine residues, and alternatively a pyridyl disulfide (PDS) and maleimide (MAL) for conjugation to cysteine residues.

Next, a larger amount of p(HEA) was synthesized with the different RAFT CTAs and, based on the kinetic data, conversion was stopped at 90 % when using NHS-PABTC, PFP-PABTC and PDS-PABTC as chain transfer agent and 50 % when using FpMAL-PABTC to obtain well-defined polymers for further polymer-protein conjugation studies. The obtained polymers were purified by threefold precipitation and drying under high vacuum, followed by storage at -20 °C under nitrogen prior to further use. The properties of the polymers are listed in **Table 1**. All polymers had narrow molecular weight distributions (PDI < 1.2), indicative of a well-controlled RAFT polymerization process. Note that the molecular weights ($M_n$) determined by SEC are largely overestimated, due to differences in hydrodynamic volume with respect to the PMMA standards.

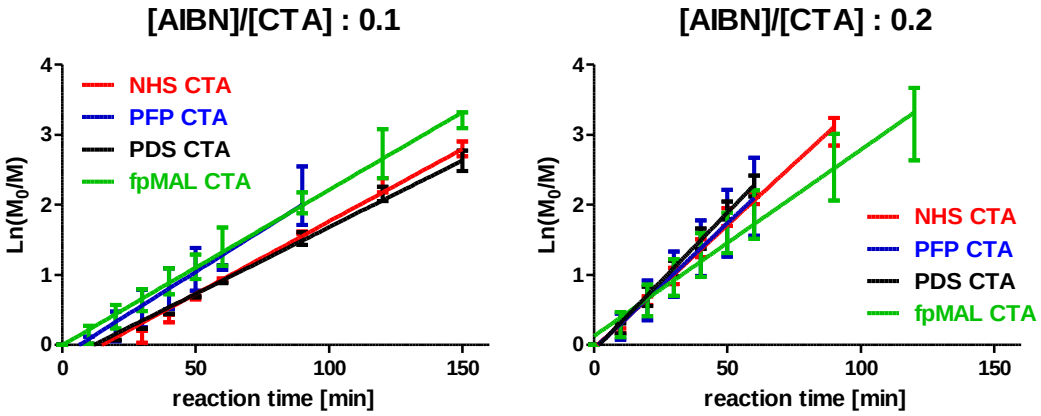


**Figure 11.** Kinetic curve *versus* RAFT polymerization time of HEA, using 4 different protein-reactive CTAs in DMF at 70°C with a HEA:CTA:AIBN molar ratio of 100:1:0.1 (left graph) or 100:1:0.2 (right graph).

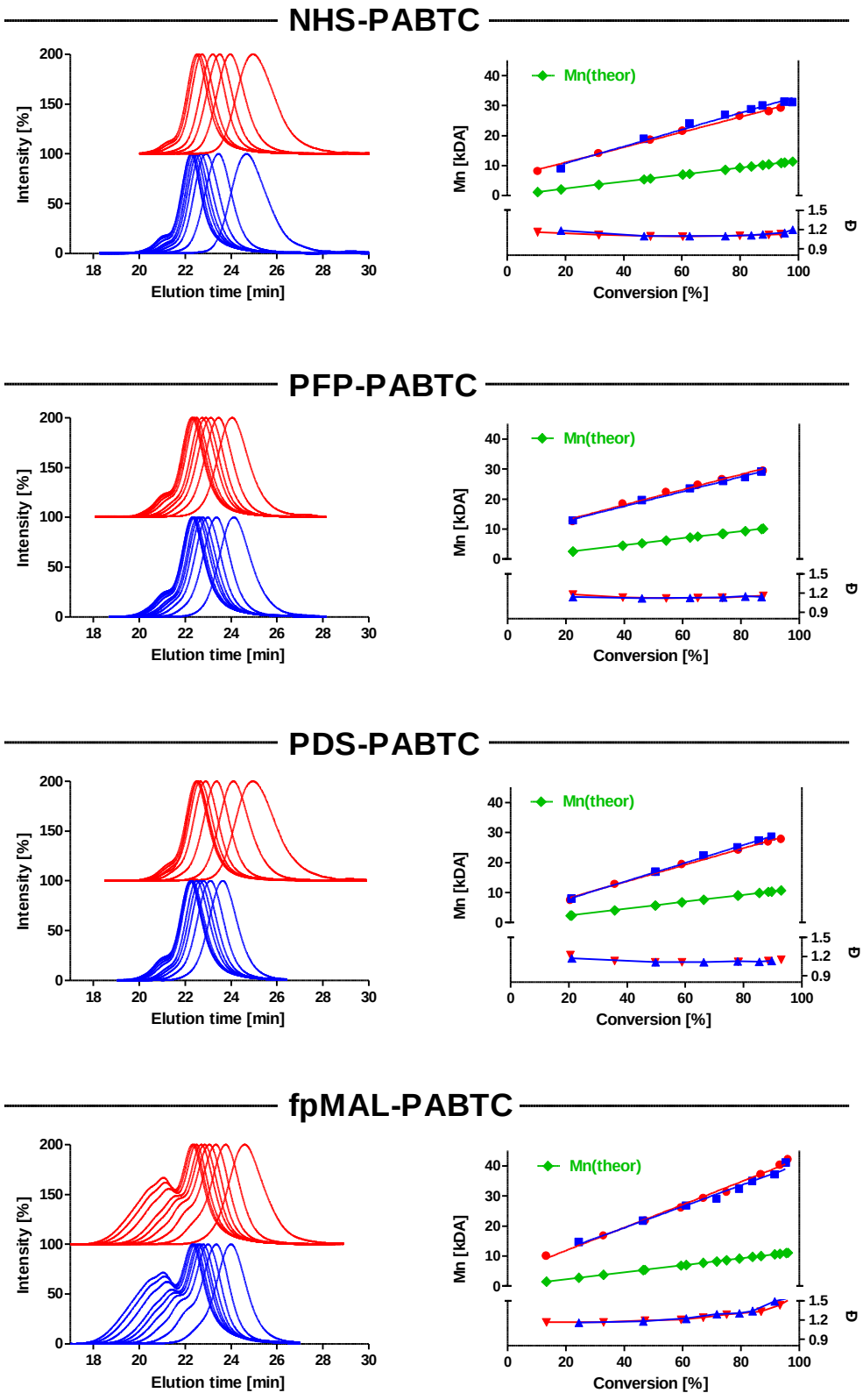


**Figure 12.** RAFT polymerization of HEA, using 4 different protein-reactive CTAs in DMF at 70°C with a HEA:CTA:AIBN molar ratio of 100:1:0.1 (red curves) or 100:1:0.2 (blue curves). SEC traces at different timepoints (left), and molecular weight ($M_n$) and PDI (Đ) of the polymers *versus* monomer conversion (right). The green curve illustrates the theoretical molecular weight ($M_n$(theor)) based off of monomer conversion.

**Table 1.** Protein-reactive p(HEA) polymers, synthesized in DMF at 70°C with AIBN as an initiator and functionalized PABTC as a RAFT CTA.

| CTA | [HEA]/[CTA] | $t_{reaction}$ | $DP^{GC}$ | $M_n^{GC}$ | $M_n^{SEC}$ | Đ |
|---|---|---|---|---|---|---|
| NHS-PABTC | 100 | 120 min | 94 | 10.9 kDa | 32 kDa | 1.18 |
| PFP-PABTC | 100 | 90 min | 94 | 10.9 Da | 29 kDa | 1.16 |
| PDS-PABTC | 100 | 120 min | 93 | 10.8 kDa | 28 kDa | 1.15 |
| FpMAL-PABTC | 100 | 30 min | 56 | 6.5 kDa | 21 kDa | 1.20 |
| MAL-PABTC | - | - | - | - | 25 kDa | 1.20 |

In case of p(HEA) synthesized using Fp-MAL-PABTC as chain transfer agent, the maleimide group needed to be deprotected prior to protein-conjugation. This was done by refluxing the purified polymer in dioxane at 110 °C. Note that in literature this reaction is mostly reported in toluene[14], however this was not possible due to the insolubility of p(HEA) in this solvent. SEC analysis (**Figure 13A**) shows that the polymer could be recovered without alteration in the molecular weight and dispersity, while $^1$H-NMR analysis revealed the disappearance of the signal from the furan moiety (**Figure 13B**). To investigate the effect of cleavage of the trithiocarbonate end-group, we have converted this group into a thiol by aminolysis (i.e. addition of propylamine), followed by threefold precipitation and high vacuum to remove the propylamine. When subsequently the deprotection of the maleimide was performed, a multimodal elugram was observed by SEC analysis (Figure 2A). This suggests that under the conditions used for deprotection of maleimide end-group, the trithiocarbonate moiety at the other polymer chain end most likely remains intact, which is essential to obtain well-defined MAL-p(HEA).

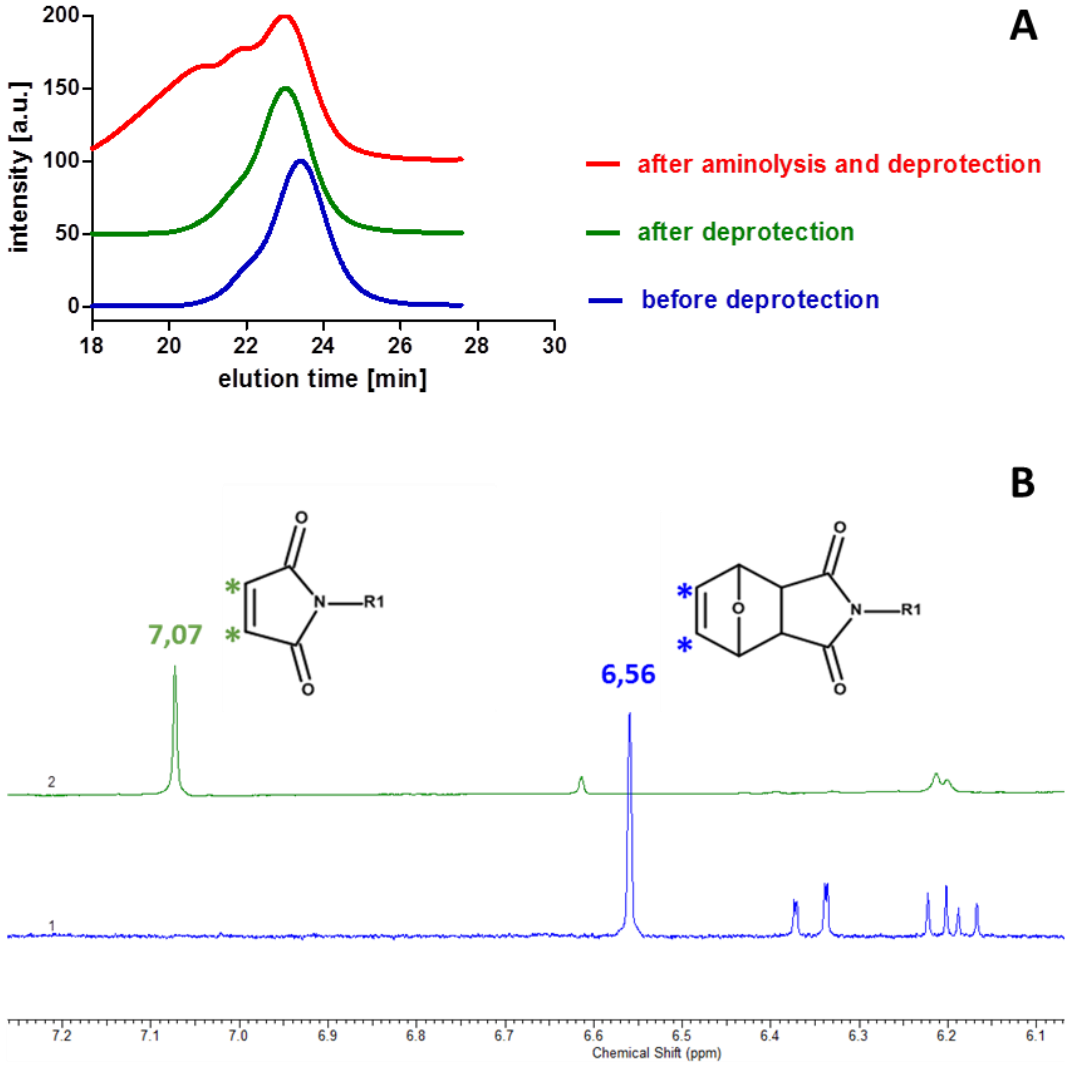


**Figure 13.** Deprotection of fpMAL-p(HEA). **(A)** SEC elugram of p(HEA) synthesized using fpMAL-PABTC as chain transfer agent before (blue curve) and after deprotection (green curve) of the maleimide end-group. As control, the trithiocarbonate end-group was cleaved into a thiol prior to the deprotection reaction, leading to a multimodal distribution (red curve). **(B)** $^{1}$H-NMR (500 MHz, DMSO) of fpMAL-p(HEA) (blue curve) and after deprotection (green curve) where the peak of the furan vinyl protons (6.56 ppm) diminishes and the maleimide vinyl protons appear (7.07 ppm).

***Synthesis of protein-reactive CTA's for methacrylamide RAFT polymers***

Next we explored the applicability of the PFP and PDS containing RAFT agents to obtain protein-reactive poly(N-hydroxypropylmethacrylamide) or p(HMPA) (**scheme 2**), which is a highly relevant polymer in view of biomedical applications.[20,21] In addition we also evaluated the polymerization of N-hydroxypropylmethacrylamide-dilactate, which yields temperature responsive polymers (phase transition temperature $T_{cp}$= 10 °C) that witness a gradual increase in $T_{cp}$ upon degradation of the dilactate side chains and which are currently under investigation for a number of biomedical applications, including anti-cancer drug delivery and tissue engineering.[22-24,35] Successful application of the RAFT process requires the appropriate selection of a RAFT agent for a particular monomer.[9] Indeed, it has been reported that RAFT polymerization of methacrylates and methacrylamides requires the presence of a cyano moiety adjacent to the thiocarbonate moiety.[36] This was confirmed by us as well, as PABTC was found incapable of yielding well defined pHMPA.

Several groups have reported on RAFT of p(HMPA) using trithio- and dithiocarbonate based chain transfer agents.[31,37] In our present work we opted for a cyanotrithiocarbonate CTA for its reported higher hydrolytic stability[38,39] and its lower susceptibility to retardation at the initial phase of the polymerization[40]. Hennink and co-workers used the commercially available 4-cyano-4- [(dodecylsulfanylthiocarbonyl)sulfanyl]pentanoic acid (CDTPA) CTA for the polymerization of HPMAm.[31] However, to minimize in future studies the contribution of the aliphatic dodecyl chain to potential self-assembly behavior in aqueous medium by hydrophobic interaction, we compared the performance of this CTA to 4-cyano-4-[(ethylsulfanylthiocarbonyl)sulfanyl]pentanoic acid (CETPA) which might be preferred due to the shorter ethyl chain length of the Z-group. CETPA was successfully functionalized with respectively PFP and PDS by carbodiimide chemistry.

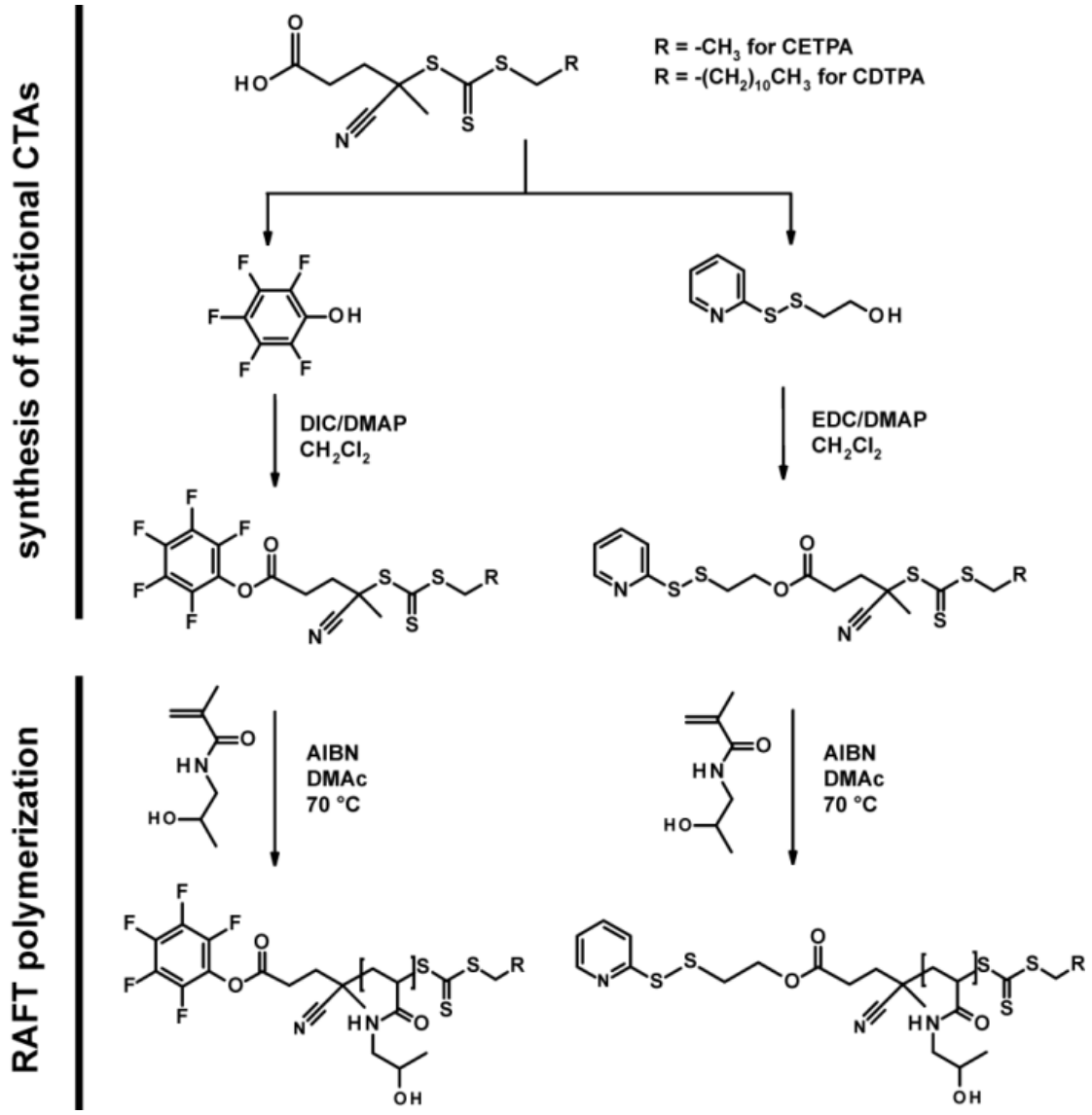


**Scheme 2.** Synthesis of the different functional CTAs used in this work for RAFT polymerization of N-hydroxypropylmethacrylamide (HPMAm).

### *RAFT polymerization of HPMAm with protein-reactive CTAs*

Kinetic studies of HPMAm polymerization carried out in an automated synthesis robot showed for both the PFP-CDTPA and PFP-CETPA chain transfer agents high control over the polymerization reaction with linear pseudo-first order kinetic plots and a linear growth of molecular weight with monomer conversions (**Figure 14**). Overall, conversions were significantly lower than for HEA polymerization, which can be likely ascribed to the lower reactivity of methacrylamides versus acrylates. Therefore, we also investigated higher DP values, i.e. DP=200, to obtain higher molecular weight polymers at similar conversions. As

shown in **Figure 14**, this was found to be successful. These polymerization conditions were then used to synthesize well defined PFP- and PDS- p(HPMAm) and PDS-p(HPMAm-$Lac_2$) using functionalized CETPA as RAFT agent. The specifications of the synthesized polymers are listed in **Table 2**. Note that the molecular weights ($M_n$) determined by SEC are largely overestimated, due to differences in hydrodynamic volume with respect to the PMMA standards.

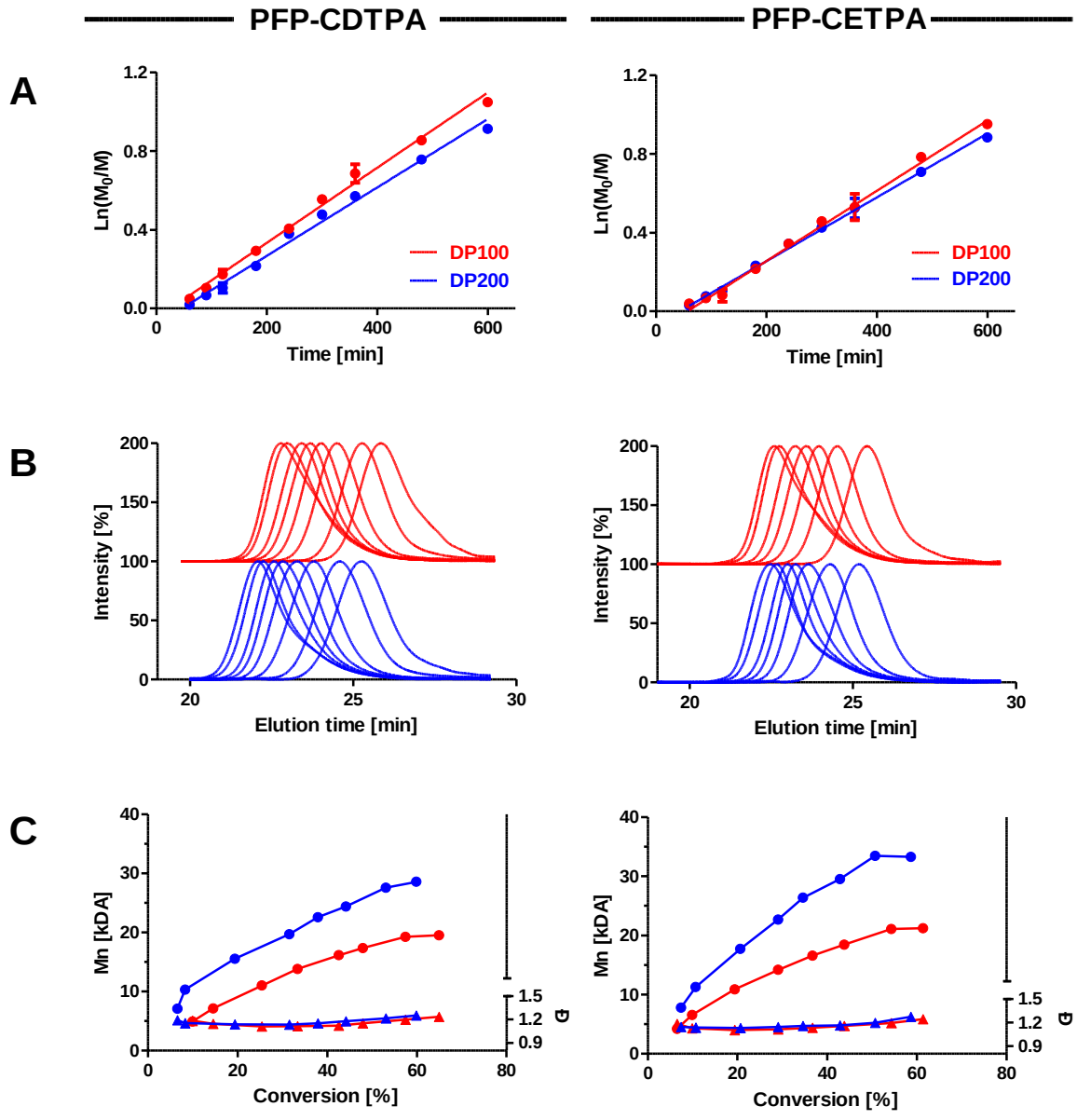


**Figure 14.** RAFT polymerization of HPMAm using PFP-CDTPA (left) and PFP-CETPA (right) in DMAc at 70°C with a HPMAm:CTA:AIBN molar ratio of 100:1:0.2 (red curves) or 200:1:0.2 (blue curves). **(A)** Kinetic curve *versus* polymerization time. **(B)** SEC traces at different timepoints. **(C)** Molecular weight ($M_n$) and PDI of the polymers *versus* monomer conversion.

**Table 2.** Protein-reactive p(HPMAm) and poly(HPMAm-$Lac_2$) polymers synthesized in DMAc at 70°C with AIBN as an initiator and functionalized CETPA as a CTA.

| PR CTA | Monomer | [M]/[CTA] | $t_{reaction}$ | $DP^{NMR}$ | $M_n^{NMR}$ | $M_n^{SEC}$ | PDI |
|---|---|---|---|---|---|---|---|
| **PFP** | HPMAm | 100 | 10 h | 59 | 8.4 kDa | 21 kDa | 1.24 |
| **PFP** | HPMAm | 200 | 10 h | 123 | 17.6 kDa | 33 kDa | 1.27 |
| **PDS** | HPMAm | 100 | 10 h | 30 | 4.3 kDa | 13 kDa | 1.20 |
| **PDS** | HPMAm | 200 | 10 h | 46 | 6.6 kDa | 16 kDa | 1.24 |
| **PDS** | HPMAm-**$Lac_2$** | 100 | 10 h | 33 | 4.7 kDa | 13 kDa | 1.19 |

## Conclusions

A series of RAFT chain transfer agents for both acrylates and methacrylamides were functionalized with different reactive moieties that can be conjugated to either lysine or cysteine residues to afford polymer-protein conjugates. RAFT polymerization with these protein-reactive CTA's provided high control over the polymerization with linear pseudo-first order kinetic plots and a linear growth of molecular weight with monomer conversions, for both acrylates and methacrylamides. The chain transfer agent bearing a (protected) maleimide, however, was prone to side-reactions and therefore, polymerization had to be stopped at 50% conversion to be able to obtain well-defined polymers. This can probably be attributed to deprotection of the maleimide during polymerization, inducing its participation in the polymerization process. Moreover, an additional deprotection step is necessary to activate the protein-reactive maleimide group. These setbacks make the maleimide group a less attractive conjugation strategy.

## References


1 Duncan, R. The dawning era of polymer therapeutics. *Nat. Rev. Drug Discov.* **2**, 347-360 (2003).

2 Broyer, R. M., Grover, G. N. & Maynard, H. D. Emerging synthetic approaches for protein-polymer conjugations. *Chem. Commun.* **47**, 2212-2226 (2011).

3 Lutz, J. F. & Borner, H. G. Modern trends in polymer bioconjugates design. *Prog. Polym. Sci.* **33**, 1-39 (2008).

4 González-Toro, D. C. & Thayumanavan, S. Advances in polymer and polymeric nanostructures for protein conjugation. *European Polymer Journal* **49**, 2906-2918 (2013).

5 Johnson, R. P., John, J. V. & Kim, I. Recent developments in polymer–block–polypeptide and protein–polymer bioconjugate hybrid materials. *European Polymer Journal* **49**, 2925-2948 (2013).

6 Owens, D. E. & Peppas, N. A. Opsonization, biodistribution, and pharmacokinetics of polymeric nanoparticles. *Int. J. Pharm.* **307**, 93-102 (2006).

7 Roberts, M. J., Bentley, M. D. & Harris, J. M. Chemistry for peptide and protein PEGylation. *Adv. Drug Deliv. Rev.* **54**, 459-476 (2002).

8 Veronese, F. M. & Pasut, G. PEGylation, successful approach to drug delivery. *Drug Discov. Today* **10**, 1451-1458 (2005).

9 Braunecker, W. A. & Matyjaszewski, K. Controlled/living radical polymerization: Features, developments, and perspectives. *Prog. Polym. Sci.* **32**, 93-146 (2007).

10 Chiefari, J. *et al.* Living free-radical polymerization by reversible addition-fragmentation chain transfer: The RAFT process. *Macromolecules* **31**, 5559-5562 (1998).

11 Nicolas, J., Mantovani, G. & Haddleton, D. M. Living radical polymerization as a tool for the synthesis of polymer-protein/peptide bioconjugates. *Macromol. Rapid Commun.* **28**, 1083-1111 (2007).

12 Moad, G., Rizzardo, E. & Thang, S. H. Living Radical Polymerization by the RAFT Process – A Third Update. *Australian Journal of Chemistry* **65**, 985-1076 (2012).

13 Li, H. M. *et al.* Protein conjugation of thermoresponsive amine-reactive polymers prepared by RAFT. *Polym. Chem.* **2**, 323-327 (2011).

14 Mantovani, G. *et al.* Design and synthesis of N-maleimido-functionalized hydrophilic polymers via copper-mediated living radical polymerization: A suitable alternative to PEGylation chemistry. *J. Am. Chem. Soc.* **127**, 2966-2973 (2005).

15 Heredia, K. L. *et al.* Reversible siRNA-polymer conjugates by RAFT polymerization. *Chem. Commun.*, 3245-3247 (2008).

16 Tao, L. *et al.* Synthesis and bioactivity of poly(HPMA)-lysozyme conjugates: the use of novel thiazolidine-2-thione coupling chemistry. *Org. Biomol. Chem.* **7**, 3481-3485 (2009).

17 Scarano, W. *et al.* Folate Conjugation to Polymeric Micelles via Boronic Acid Ester to Deliver Platinum Drugs to Ovarian Cancer Cell Lines. *Biomacromolecules* **14**, 962-975 (2013).

18 Roth, P. J. *et al.* Synthesis of Reactive Telechelic Polymers Based on Pentafluorophenyl Esters. *Macromolecules* **41**, 8513-8519 (2008).

19 Robin, M. P. *et al.* Dibromomaleimide End Functional Polymers by RAFT Polymerization Without the Need of Protecting Groups. *ACS Macro Lett.* **1**, 222-226 (2012).

20 Talelli, M. *et al.* Micelles based on HPMA copolymers. *Adv. Drug Deliv. Rev.* **62**, 231-239 (2010).

21 Kopecek, J. & Kopeckova, P. HPMA copolymers: Origins, early developments, present, and future. *Adv. Drug Deliv. Rev.* **62**, 122-149 (2010).

22 Soga, O., van Nostrum, C. F. & Hennink, W. E. Poly(N-(2-hydroxypropyl) methacrylamide mono/di lactate): A new class of biodegradable polymers with tuneable thermosensitivity. *Biomacromolecules* **5**, 818-821 (2004).

23 Talelli, M. *et al.* Core-crosslinked polymeric micelles with controlled release of covalently entrapped doxorubicin. *Biomaterials* **31**, 7797-7804 (2010).

24 Talelli, M. *et al.* Synthesis and Characterization of Biodegradable and Thermosensitive Polymeric Micelles with Covalently Bound Doxorubicin-Glucuronide Prodrug via Click Chemistry. *Bioconjugate Chem.* **22**, 2519-2530 (2011).

25 Ferguson, C. J. *et al.* Ab initio emulsion polymerization by RAFT-controlled self-assembly. *Macromolecules* **38**, 2191-2204 (2005).

26 Convertine, A. J. *et al.* Development of a novel endosomolytic diblock copolymer for siRNA delivery. *J. Control. Release* **133**, 221-229 (2009).

27 Neradovic, D. *et al.* Degradation mechanism and kinetics of thermosensitive polyacrylamides containing lactic acid side chains. *Macromolecules* **36**, 7491-7498 (2003).

28 Becer, C. R. *et al.* Protocol for Automated Kinetic Investigation/Optimization of the RAFT Polymerization of Various Monomers. *QSAR & Combinatorial Science* **27**, 977-983 (2008).

29 Voorhaar, L. *et al.* Cu(0)-mediated polymerization of hydrophobic acrylates using high-throughput experimentation. *Polym. Chem.* **5**, 4268-4276 (2014).

30 Ghosh, S., Basu, S. & Thayumanavan, S. Simultaneous and reversible functionalization of copolymers for biological applications. *Macromolecules* **39**, 5595-5597 (2006).

31 Shi, Y. *et al.* Reversible Addition-Fragmentation Chain Transfer Synthesis of a Micelle-Forming, Structure Reversible Thermosensitive Diblock Copolymer Based on the N-(2-Hydroxy propyl) Methacrylamide Backbone. *ACS Macro Lett.* **2**, 403-408 (2013).

32 Junkers, T. & Barner-Kowollik, C. The Role of Mid-Chain Radicals in Acrylate Free Radical Polymerization: Branching and Scission. *J. Polym. Sci. Pol. Chem.* **46**, 7585-7605 (2008).

33 Steinhauer, W. *et al.* Block and Gradient Copolymers of 2-Hydroxyethyl Acrylate and 2-Methoxyethyl Acrylate via RAFT: Polymerization Kinetics, Thermoresponsive Properties, and Micellization. *Macromolecules* **46**, 1447-1460 (2013).

34 Steinhauer, W. *et al.* Copolymerization of 2-Hydroxyethyl Acrylate and 2-Methoxyethyl Acrylate via RAFT: Kinetics and Thermoresponsive Properties. *Macromolecules* **43**, 7041-7047 (2010).

35 Ulbrich, K. *et al.* Polymeric drugs based on conjugates of synthetic and natural macromolecules I. Synthesis and physico-chemical characterisation. *J. Control. Release* **64**, 63-79 (2000).

36 Benaglia, M. *et al.* Searching for More Effective Agents and Conditions for the RAFT Polymerization of MMA: Influence of Dithioester Substituents, Solvent, and Temperature. *Macromolecules* **38**, 3129-3140 (2005).

37 Scales, C. W. *et al.* Direct, controlled synthesis of the nonimmunogenic, hydrophilic polymer, poly(N-(2-hydroxypropyl)methacrylamide) via RAFT in aqueous media. *Biomacromolecules* **6**, 1846-1850 (2005).

38 Albertin, L. *et al.* Effect of an added base on (4-cyanopentanoic acid)-4-dithiobenzoate mediated RAFT polymerization in water. *Polymer* **47**, 1011-1019 (2006).

39 Thomas, D. B. *et al.* Hydrolytic susceptibility of dithioester chain transfer agents and implications in aqueous RAFT polymerizations. *Macromolecules* **37**, 1735-1741 (2004).

40 Saricilar, S. *et al.* Reversible addition fragmentation chain transfer polymerization of 3-tris(trimethylsilyloxy) silyl propyl methacrylate. *Polymer* **44**, 5169-5176 (2003).

# Chapter 4

# Polymer-protein conjugation via a ‘grafting-to’ approach

In collaboration with

**Prof. Richard Hoogenboom** from Ghent University, Belgium

Parts of this chapter were published in:

**Dual pH- and temperature-responsive RAFT-based block co-polymer micelles and polymer-protein conjugates with transient solubility**
Q. L. Zhang, N. Vanparijs, B. Louage, B. G. De Geest, R. Hoogenboom, *Polymer Chemistry* **2014**, 5, 1140-1144

**Polymer-protein conjugation via a 'grafting to' approach - a comparative study of the performance of protein-reactive RAFT chain transfer agents**
N. Vanparijs, S. Maji, B. Louage, L. Voorhaar, D. Laplace, Q. Zhang, Y. Shi, W. E. Hennink, R. Hoogenboom, B. G. De Geest, *Polymer Chemistry* **2015**, 6, 5602-5614

**Solvent-free mechanochemical synthesis of a bicyclononyne tosylate: a fast route towards bioorthogonal clickable poly(2-oxazoline)s**
M. Glassner, S. Maji, V. R. de la Rosa, N. Vanparijs, K. Ryskulova, B. G. De Geest, R. Hoogenboom, *Polymer Chemistry* **2015**, 6, 8354-8359 .

## Abstract

In this chapter, the bioconjugation efficiency of polymers with different protein-reactive groups was investigated as a function of stoichiometry, polymer molecular weight, and protein pre-conditioning. First, RAFT-derived polymers were used that contained either a N-hydroxysuccinimide (NHS) or pentafluorophenyl (PFP) ester moiety that can be conjugated to lysine residues, and alternatively a maleimide (MAL) or pyridyl disulfide (PDS) moiety that can be conjugated to cysteine residues. Some of these protein-reactive polymers were thermoresponsive and required optimized conjugation conditions. Protein modification with N-succinimidyl-S-acetylthiopropionate (SATP) was performed to introduce sulfhydryl groups onto primary amines and increase the conjugation efficiency with MAL- and PDS-containing polymers. Alternatively, bicyclononyne (BCN) functionalized poly(2-ethyl-2-oxazoline) or p(EtOx) was conjugated to azide-substituted proteins via copper-free strain-promoted azide-alkyne cycloaddition (SPAAC) reactions.

## Introduction

As discussed earlier, polymer-protein conjugation strategies have received increasing interest owing to the ability to engineer proteins with a wide variety of properties.[1-5] Different approaches have been proposed to design polymer-protein conjugates (**Scheme 1**) including the 'grafting-to' method, where a pre-formed reactive polymer is conjugated to a protein; and the 'grafting-from' method, where the polymer chain is grown from a protein macroinitiator (or macroCTA).[6] Both strategies can be followed using protein-reactive RAFT agents such as the ones prepared in **Chapter 3**.[7-9] The advantage of 'grafting-to' is the use of pre-synthesized polymer, which allows thorough characterization of the polymer and avoids exposure of the protein to potentially denaturing polymerization conditions. An additional limitation of the 'grafting-from' method is the possible sterical hindrance during polymerization, leading to a substantial amount of unreacted protein-bound CTA. However, a major advantage of the 'grafting-from' approach is that the prepared conjugates only need to be purified from low molecular weight compounds (i.e. unreacted monomer, initiator, etc…). This can easily be done by dialysis, unlike the removal of unreacted polymer, involved

in 'grafting-to', which is often tedious and requires preparative gel filtration chromatography.

An alternative approach to conventional conjugation chemistries is the use of so-called orthogonal handles, e.g. copper(I)-catalyzed cyclo-addition (CuAAC) between an azide and an alkyne[6] (i.e. the Huisgen-Sharpless 'click' reaction[10]). This involves a two-step modification strategy where the protein is first modified with an orthogonal (i.e. a group that does not interfere with any of the amino acid residues) functional group, that is then in a second step used to conjugate to the functional end-group of a polymer in a 'grafting-to' manner. Different groups described the synthesis of an azide-functionalized RAFT agent that can couple to alkyne-modified biomolecules.[11,12] As the use of CuAAC in living systems is limited by the toxicity of copper(I), Bertozzi and coworkers sought to activate alkynes by a method other than metal catalysis, namely by ring strain.[13] This led to the discovery of strain-promoted azide–alkyne cycloadditions (SPAAC) between azides and cyclooctyne derivatives, that do not require cytotoxic copper as a catalyst.[14] Among the various cyclooctynes that have been developed for SPAAC reactions, derivatives of bicyclo[6.1.0]non-4-yne (BCN) can be prepared with the least synthetic effort.[15]

In this chapter, we first performed a head-to-head comparison of four different protein-reactive RAFT CTAs in their bioconjugation efficiency to two types of serum albumin (i.e. avian and bovine) via a 'grafting-to' approach. These CTAs contained either a N-hydroxysuccinimide (NHS) or pentafluorophenyl (PFP) ester moiety that can conjugate to lysine residues, and alternatively a maleimide or pyridyl disulfide (PDS) moiety for conjugation to cysteine residues (**Chapter 3**). The proteins were also modified with N-succinimidyl-S-acetylthiopropionate (SATP) to introduce sulfhydryl groups onto primary amines and increase the conjugation efficiency with MAL- and PDS-containing polymers. In addition to model hydrophilic RAFT-based polymers containing these protein-reactive groups, we also conjugated transiently thermoresponsive polymers (**Chapter 2**) to proteins and investigated whether this provided the protein with dual temperature- and pH-responsive properties. In a second part of this chapter, we introduced azide-based orthogonal handles onto BSA, allowing subsequent bioconjugation to BCN-functional poly(2-ethyl-2-oxazoline) or p(EtOx) via copper-free SPAAC.

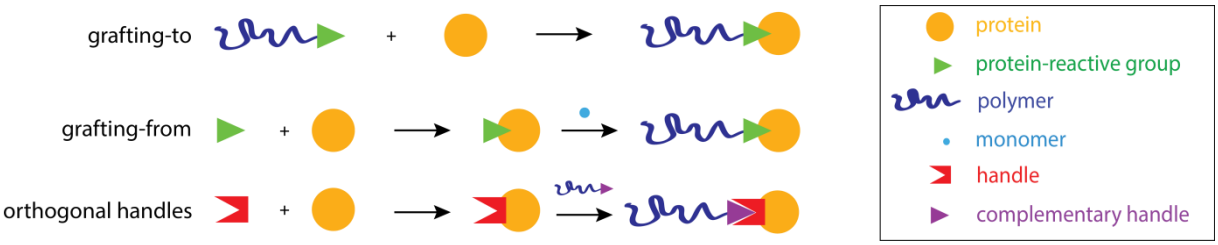


**Scheme 1.** Schematic overview of the different RAFT-based strategies that are available for designing polymer-protein conjugates.

## Material and methods

### *Materials*

Chemicals bovine serum albumin (BSA), $NaHCO_3$, NaSCN, hydroxylamine-HCl, ethylenediaminetetraacetic acid (EDTA) and ninhydrin reagent (2% solution) were obtained from Sigma Aldrich and used without purification. Ovalbumin (OVA) was purchased from Worthington, whilst N-succinimidyl-S-acetylthiopropionate (SATP) and NHS-$PEG_4$-$N_3$ were obtained from Thermo Scientific. Sodium dodecyl sulfate-polyacrylamide gel electrophoresis (SDS-PAGE) was performed with a 4-20% polyacrylamide gradient gel, using the Mini-PROTEAN Tetra Cell from Bio-Rad.

The synthesis and characterization of the employed protein-reactive homopolymers containing 2-hydroxyethylacrylate (HEA), 2-hydroxypropylmethacrylamide (HPMAm) and its thermoresponsive dilactate derivative (HPMAm-$Lac_2$) have been discussed in **Chapter 3.** The synthesis and characterization of NHS-containing P33 and P32 polymers (6 kDa and 18 kDa respectively) and of bicyclononyne (BCN) functional poly(2-ethyl-2-oxazoline) (PEtOx) was performed by the Hoogenboom group and has been discussed in the corresponding papers.[16,17]

### *Conjugation of RAFT-based protein-reactive polymers to OVA and BSA*

An example conjugation procedure is as follows. Stock solutions of protein (1.16 x 10-4 M, 5 mg OVA or 7.7 mg BSA / mL) and polymer (10 mg/mL) were prepared in a bicarbonate buffer (0.1M, pH 8.2). The stock solutions were combined to obtain a molar ratio of protein:polymer 1:10 or 1:20. Subsequently, the reaction mixture was diluted with buffer solution to obtain a protein concentration of 9.30 x $10^{-6}$ M. For conjugation reactions with

SATP-modified protein, a deacetylation solution (0.5 M hydroxylamine-HCl / 25 mM EDTA in PBS) was added to the reaction in a 300-fold molar excess of hydroxylamine to protein. For conjugation reactions with p(HPMAm-$Lac_2$), a 1M NaSCN solution was used to enhance polymer solution by "salting in". Next, the mixture was incubated overnight at room temperature (or on ice for HPMAm-$Lac_2$) with continuous stirring. Conjugation efficiency was evaluated by native SDS-PAGE. β-Mercaptoethanol was used to check reversibility of the PDS- and MAL-conjugates. Quantification of protein conjugation was done by automated integration of optical density by ImageJ software and calculating the ratio of bound protein to total protein content per lane (**Figure 1**).

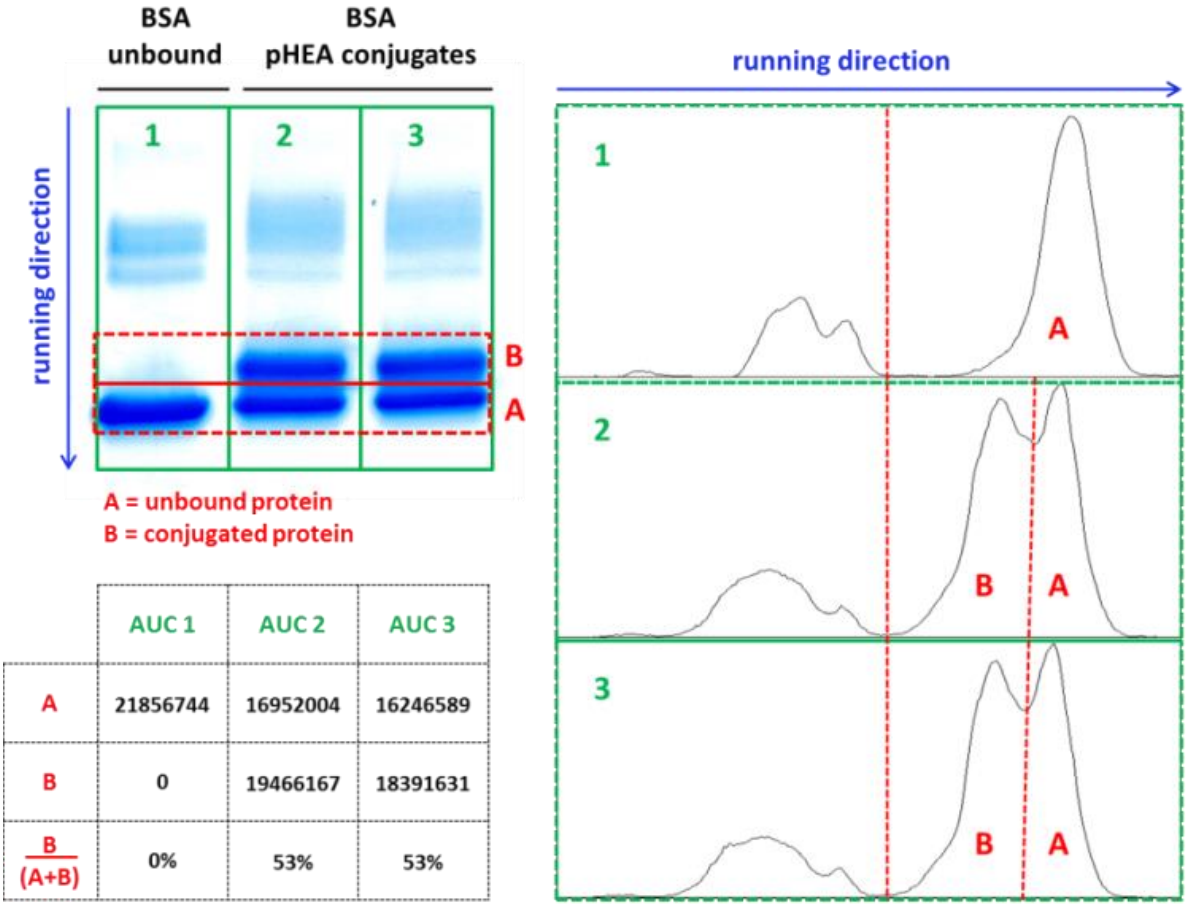


| | AUC 1 | AUC 2 | AUC 3 |
|---|---|---|---|
| A | 21856744 | 16952004 | 16246589 |
| B | 0 | 19466167 | 18391631 |
| B / (A+B) | 0% | 53% | 53% |

**Figure 1.** Quantification of protein conjugation by automated integration of optical density by ImageJ software and calculating the ratio of conjugated protein (B) to total protein content per lane (A+B). As BSA forms high molecular weight aggregates, these bands were excluded from the calculations. For OVA, aggregation did not occur.

### *SATP-modification of OVA and BSA*

Prior to conjugation, part of the lysines of OVA and BSA was modified with N-Succinimidyl S-Acetylthiopropionate (SATP) (**Scheme 2**). SATP (20 mg/mL in anhydrous DMSO) was added to a stock solution of OVA and BSA (120 µM in PBS) in a molar ratio of protein:SATP 1:20. The mixture was incubated at room temperature for 45 min. and unreacted SATP was removed using a disposable PD10 desalting column (Sigma). After freeze-drying, the degree of modification was calculated by determination of the moles of free amines per mol of protein before and after SATP modification using the ninhydrin assay.[18]

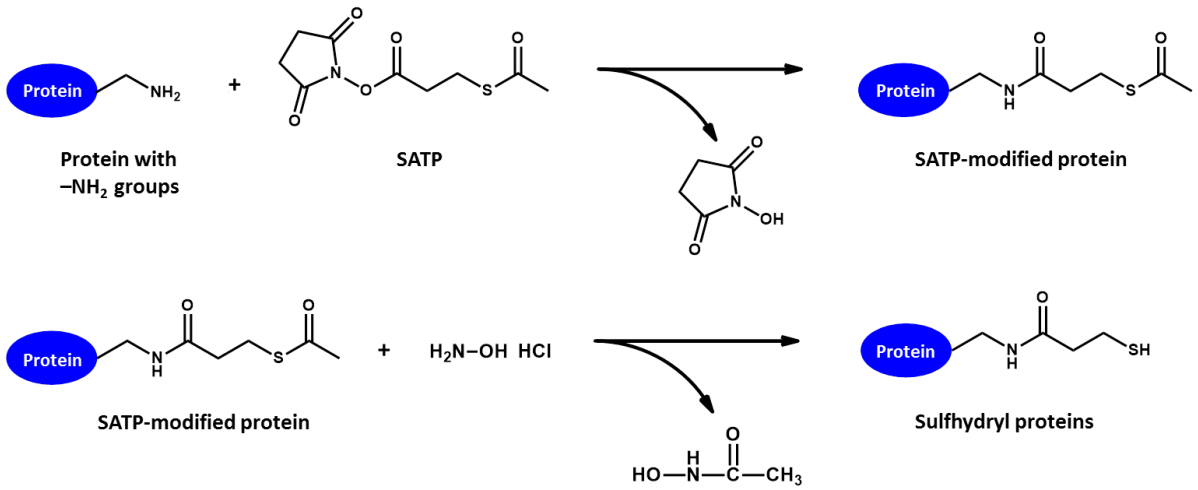


**Scheme 2.** Reaction scheme for the modification of protein amino groups with SATP. First, primary amines on the protein react and form an amide bond with N-succinimidyl-S-acetylthiopropionate (SATP), which contains a protected sulfhydryl. Next, hydroxylamine is used to deacetylate the sulfur and yield a sulfhydryl group.

### *Conjugation of RAFT-based NHS-containing thermopresponsive polymers to lysozyme*

A typical conjugation procedure for NHS-P33 (6 kDa) and NHS-P32 (18 kDa) was as follows. A lysozyme (from hen egg white, Sigma) solution in DI water (0.25 mL, $8.56 \times 10^{-5}$ mmol, 5 mg/mL) was added to different volumes of polymer solution in DI water (10 mg/mL for NHS-P33 and 20 mg/mL for NHS-P32), respectively in a 1:1, 1:10 and 1:20 molar ratio. The total volume was brought to 2 mL with a 0.1 M sodium bicarbonate buffer of pH 8.3. The solutions were kept at room temperature with gentle shaking overnight. Polymer solution without lysozyme was included as a control. Moreover half of the conjugation mixture was brought to pH 3 with 0.1 M HCl and kept in a heating block at 56°C overnight, in order to

hydrolyse the polymer under accelerated conditions. The undiluted conjugation mixtures were analyzed by SDS-PAGE. To confirm thermoresponsive behaviour, native page was performed at room temperature and at 45°C by placing the PAGE set-up in an oven.

***Conjugation of PEtOx-BCN to NHS-PEG$_4$-N$_3$ modified BSA***

Stock solutions of BSA (1.16 x $10^{-4}$ M, 7.7 mg/mL in PBS pH 7.4) and NHS-PEG$_4$-N$_3$ (2.57 x $10^{-2}$ M, 10 mg/mL in DMSO) were prepared. BSA (1.16 x $10^{-4}$ mmol, 1 mL) was modified with a 5-, 10- or 20-fold molar excess of NHS-PEG$_4$-N$_3$ (22.5, 45 or 90 µL respectively). After overnight reaction, the protein solution were dialyzed against DI water (6 x 5L) for 2 days using a MWCO of 8000 Da and freeze-dried. Stock solutions of BSA-PEG$_4$-N$_3$ (1.16 x $10^{-4}$ M, 7.7 mg/mL in PBS pH 7.4) and PEtOx-BCN (3.33 x $10^{-3}$ M, 10 mg/mL in PBS pH 7.4) were combined to obtain a molar ratio of protein:polymer 1:10 or 1:20. The reaction mixtures were diluted with PBS to obtain a final protein concentration of 1.16 x $10^{-5}$ M and incubated overnight at room temperature with continuous stirring. Conjugation efficiency was evaluated by SDS-PAGE. Quantification of protein conjugation was done by automated integration of optical density by ImageJ software (**Figure 1**).

## Results and discussion

***Protein conjugation using protein-reactive p(HEA)***

In the first part of this chapter we aimed at evaluating the performance of the respective functional polymeric end-groups prepared in **Chapter 3** with respect to protein conjugation. **Scheme 3** gives an overview of the respective conjugation chemistries. For this purpose, ovalbumin (OVA) and bovine serum albumin (BSA) were chosen as model proteins. The reason for choosing OVA is due to the availability of a large number of *in vitro* and *in vivo* immune-biological assays for OVA-based formulations.[19-21] This makes OVA a useful model vaccine antigen for screening of the adjuvant effect of (stimuli-responsive) polymer conjugation to OVA. BSA was used as reference protein, as it has been extensively reported in literature for the evaluation of polymer-protein conjugation.[7,9,22] The properties of both proteins, including the number of lysine and cysteine residues respectively, are summarized in **Table 1**.

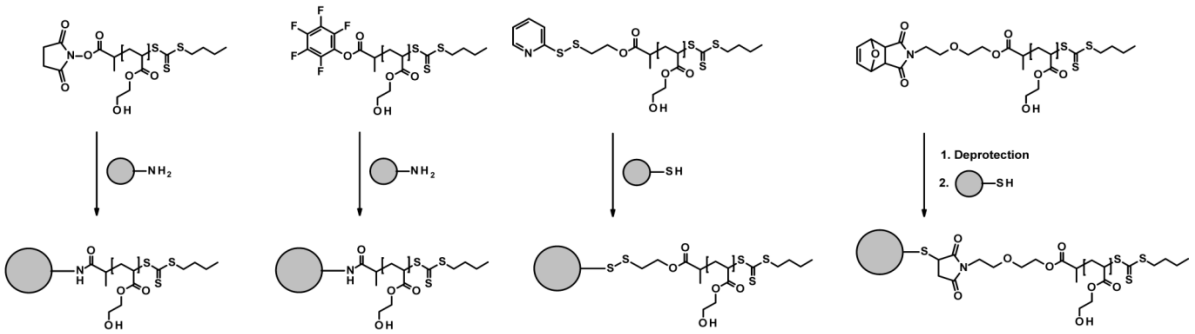


**Scheme 3.** Overview of the applied conjugation chemistries for protein conjugation. From left to right: N-hydroxysuccinimide (NHS) and pentafluorophenyl (PFP) esters that can conjugate to lysine residues, and alternatively a pyridyl disulfide (PDS) and maleimide (MAL) for conjugation to cysteine residues.

**Bovine Serum Albumine (BSA)**

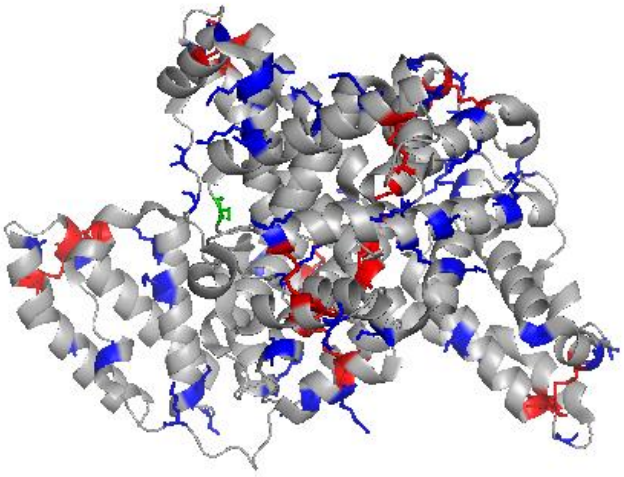

66.5 kDa

17 disulfide bridges (red)

1 free cysteine residue (green)

59 lysine residues (blue)

**Ovalbumine (OVA)**

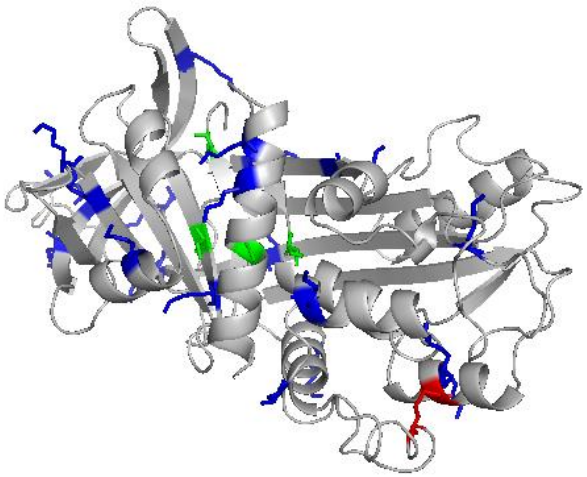

44 kDa

1 disulfide bridge (red)

4 free cysteine residues (green)

20 lysine residues (blue)

**Table 1.** Structural properties of BSA and OVA.

All conjugation reactions were performed in a 0.1 M sodium bicarbonate buffer of pH 8.2. This buffer has been reported by various groups as being an optimal conjugation buffer for the respective functional groups[23-25]. OVA and BSA were incubated in aqueous medium with the different functional p(HEA)'s in a protein-to-polymer molar ratio of 1:10 or 1:20, respectively. After overnight reaction, the conjugates were analyzed by SDS-PAGE and after staining, the gels were imaged and processed by ImageJ software. In the Materials and Methods section, the quantitative analysis of the SDS-PAGE data by ImageJ is explained into detail. Note that to preserve the disulfide bonds that are formed between the PDS-p(HEA) and the proteins, SDS-PAGE was run under non-reductive conditions (in absence of β-mercaptoethanol).

For OVA, conjugation efficacy was relatively low, especially when using activated ester functionalized polymers. Of these two activated ester containing polymers (i.e. bearing NHS, respectively PFP as end-group), the PFP-functional polymers appeared to perform the best. This can likely be ascribed to the higher hydrolytic stability of PFP-esters versus NHS-esters.[26,27] This would provide more opportunity for the PFP-esters to react with lysine moieties, whereas the NHS-esters will be more prone to rapid hydrolysis in aqueous medium into carboxylic acid moieties. The best performing functional group for OVA appeared to be the PDS which afforded over 50 % of the protein to become conjugated (**Figure 2**). This can be attributed to the 4 free cysteine residues within the OVA protein sequence.

For BSA, the overall conjugation efficacies were higher and PFP was the best performing functional group, allowing over 80% of the protein to become conjugated. The limited increase in protein-binding when doubling the polymer-to-protein ratio from 10:1 to 20:1 highlights the current limitations of the 'grafting-to' approach. This offers a window of opportunity for either elaborating onto alternative strategies (e.g. 'grafting from') or to develop more quantitatively strategies involving more reactive orthogonal groups, e.g. in combination with recombinant protein engineering to introduce complimentary reactive groups on a well-accessible site on the protein periphery. As BSA contains only one free cysteine residue, lower conjugation efficiency with thiol-reactive moieties (i.e. PDS and MAL) was expected.

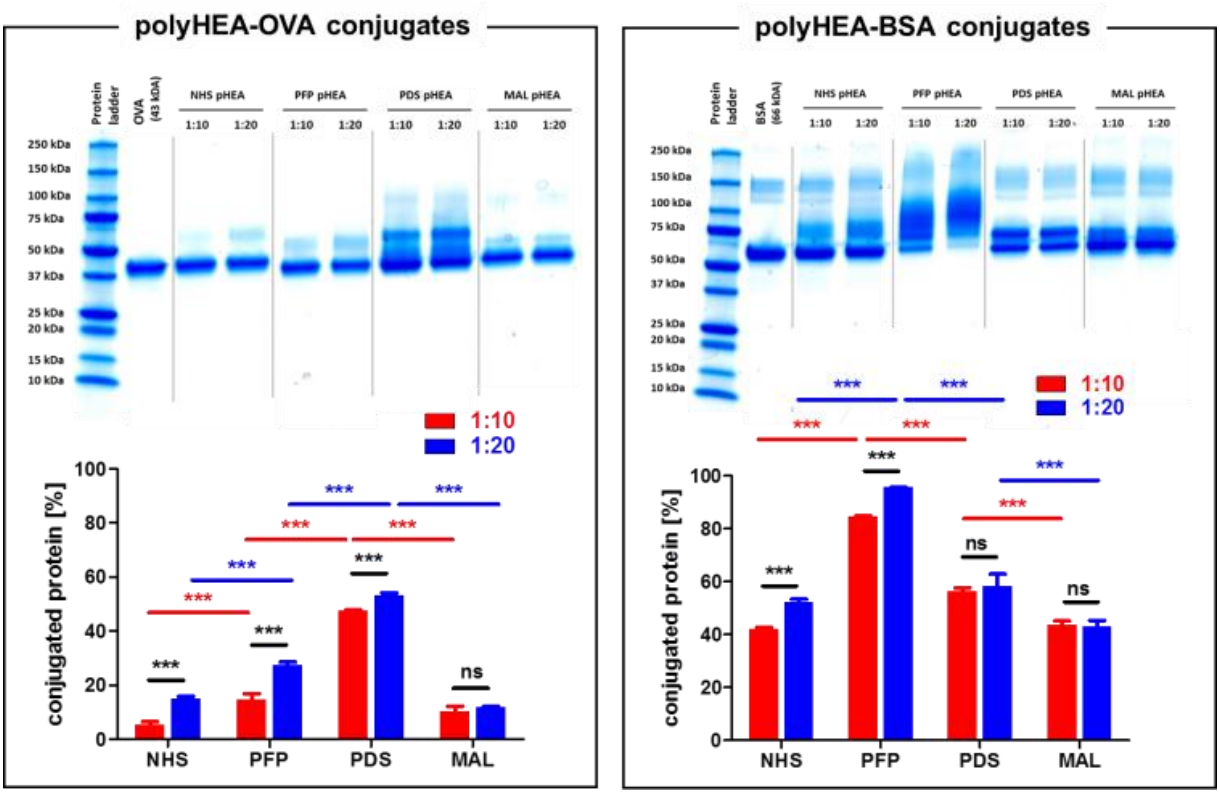


**Figure 2.** SDS-PAGE results from the conjugation of OVA (43 kDa) and BSA (66 kDa) with protein-reactive p(HEA) polymers (NHS, PFP, PDS and MAL) in a molar ratio of protein:polymer 1:10 and 1:20. (Mean ± SD, *n* = 3, *** $p < 0.0001$; one-way ANOVA)

To evaluate the reversibility of the PDS- and MAL-conjugates, reductive SDS-PAGE in presence of β-mercaptoethanol was performed. As expected, the disulfide bonds formed between the proteins and the PDS-p(HEA) were fully cleaved upon reduction (**Figure 3**). For MAL, the BSA conjugates remained intact in the presence of β-mercaptoethanol. Although it is common knowledge that a thio-ether bond by Michael-type addition is irreversible, some recent findings have suggested limited stability of thiol-maleimide bonds under physiological conditions.[28] Similar results were observed for OVA (results not shown). It should be noted that the protein retention by SDS-PAGE was slightly increased with the use of β-mercaptoethanol.

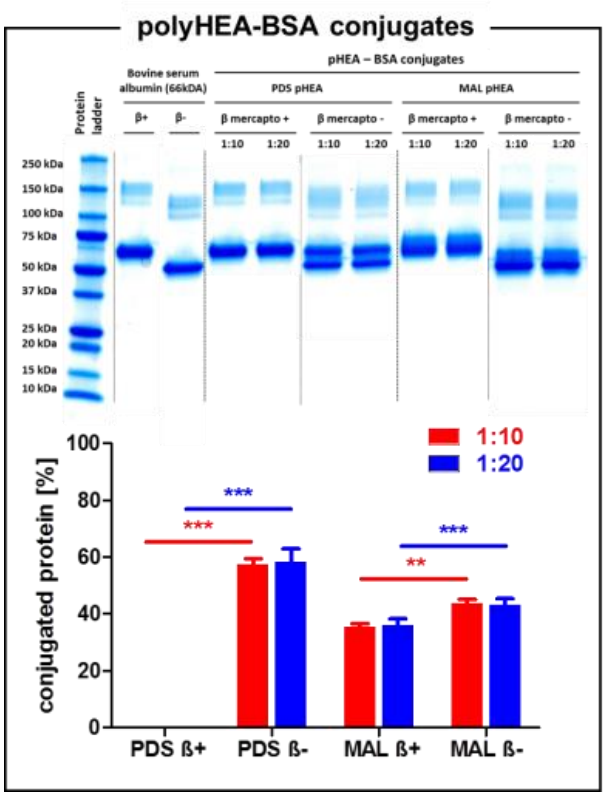


**Figure 3. S**DS-PAGE results from the conjugation of BSA with PDS- and MAL-containing p(HEA) with and without β-mercaptoethanol, in a molar ratio of protein:polymer 1:10 and 1:20. β+ = reductive SDS-AGE, β- = native SDS-PAGE. (Mean ± SD, *n* = 3, *** p < 0.0001, ** p < 0.001, one-way ANOVA)

To further enhance the conjugation efficiency for PDS- and MAL-moieties, OVA and BSA were modified with SATP, which adds sulfhydryl groups onto primary amines (i.e., lysine residues and the N-terminus) of proteins in a protected form. Deprotection by deacylation to generate a free sulfhydryl is accomplished by treatment with an excess of hydroxylamine. Quantification of the free amines before and after SATP modification (molar ratio 1:20) by ninhydrin assay showed a conversion of 79% and 78% for BSA and OVA respectively. Due to the extensive modification of the lysine residues, staining of the gels became less efficient as coommassie dyes have a high complexation affinity for lysine moieties.[29] Nonetheless, SDS-PAGE analysis revealed that the introduction of sulfhydryl groups onto primary amines groups of proteins strongly increases conjugation efficiency with PDS and MAL containing p(HEA) (**Figure 4**). PDS-p(HEA) reaches 100% of conjugation for both OVA and BSA, even at a protein-to-polymer ratio of 1:10.

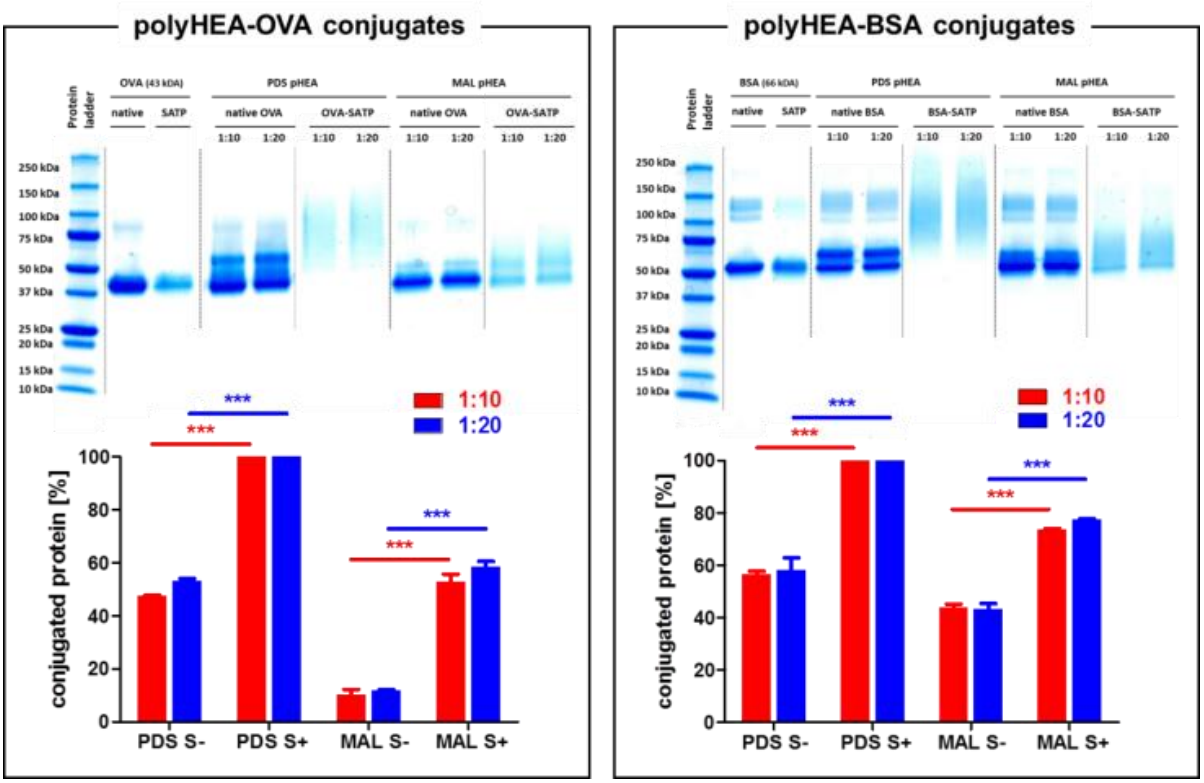


**Figure 4.** SDS-PAGE results from the conjugation of SATP-modified OVA and BSA with PDS- and MAL-containing p(HEA) in a molar ratio of protein:polymer 1:10 and 1:20. S- = native protein, S+ = SATP-modified protein. (Mean ± SD, *n* = 3, *** $p < 0.0001$; one-way ANOVA)

### *Protein conjugation using protein-reactive p(HPMAm) and p(HPMAm-Lac$_2$)*

In analogy with the protein-conjugation experiments with p(HEA), we now used PFP-p(HMPA) and PDS-p(HMPA) of different molecular weights to conjugate to OVA and BSA, in a 1:10 and 1:20 protein-to-polymer ratio. Protein conjugation was performed under identical conditions as described earlier for p(HEA). Interestingly, SDS-PAGE analysis (**Figure 5**) of the reaction mixture yielded similar trends as observed for the conjugation experiments with p(HEA). Again, conjugation of PFP-functionalized polymer was much more efficient for BSA conjugation than for OVA conjugation, whereas PDS-p(HPMAm) was much more efficient in conjugating to OVA than to BSA. This points out that differences in conjugation efficiency are most likely due to differences in protein structure, especially the availability of reactive groups rather than polymer chemistry, at least for the systems studied in this work. Moreover, the conjugation products with PFP-p(HPMAm) of DP123 clearly exhibited an increase in molecular weight as compared to those with PFP-p(HPMAm) of DP59. For the PDS-p(HPMAm) polymers this effect was less clear, due to the smaller difference in molecular weight.

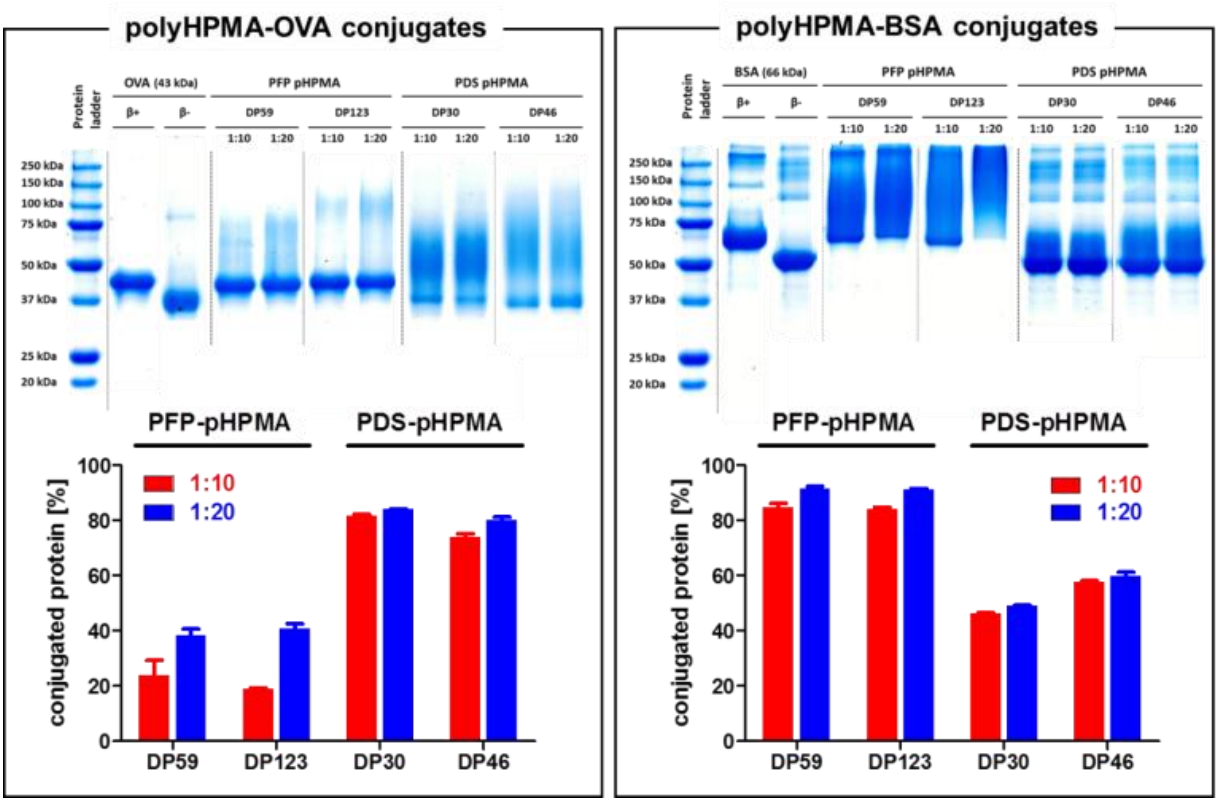


**Figure 5.** SDS-PAGE results from the conjugation of OVA and BSA with PFP- and PDS-containing p(HPMAm) of different molecular weights, in a molar ratio of protein:polymer 1:10 and 1:20. (Mean ± SD, *n* = 3)

For conjugation experiments with the thermoresponsive p(HPMAm-Lac$_2$), we found that performing conjugation below the $T_{cp}$ of the polymer (i.e. at 0°C) did not yield polymer-protein conjugation, while performing the conjugation reaction at room temperature (i.e. above the $T_{cp}$) with the polymer in collapsed state was unsuccessful too. To address this issue we added sodium thiocyanate (NaSCN) which is known from the Hofmeister series to exert a strong 'salting in effect' and is capable of increasing the phase transition temperature of polymers.[30,31] We observed that in presence of 1M NaSCN p(HMPA-Lac$_2$) became fully soluble in an ice bath and the consequent conjugation efficiency of PDS- p(HMPA-Lac$_2$) to OVA was found to be drastically improved (**Figure 6**). These results indicate that even though p(HPMAm-Lac$_2$) is soluble at 0°C, the polymer end group is inaccessible for conjugation in the absence of NaSCN.

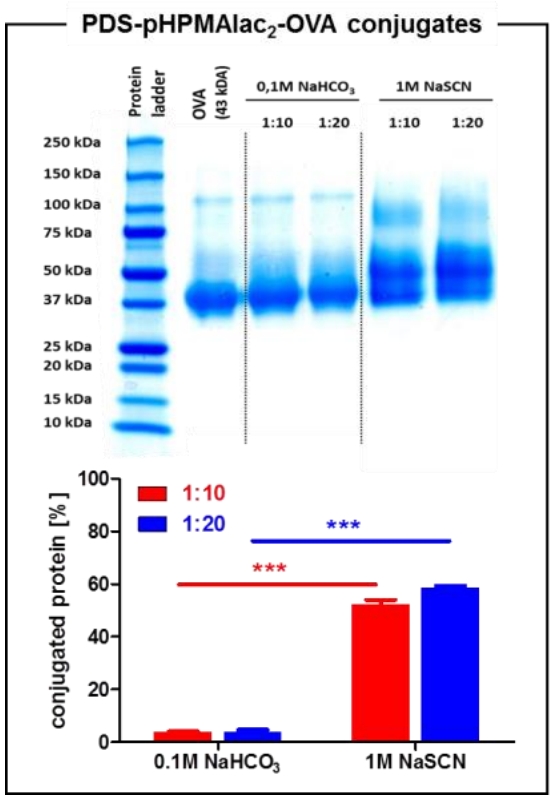


**Figure 6**. SDS-PAGE results from the conjugation of OVA with PDS-containing p(HPMAm-Lac$_2$) in a molar ratio of protein:polymer 1:10 and 1:20 in the standard 0.1M $NaHCO_3$ conjugation buffer and in a 1M NaSCN "salting in" solution. (Mean ± SD, *n* = 3, *** p < 0.0001; one-way ANOVA)

### *Protein conjugation using NHS-containing thermoresponsive polymers*

In addition to PDS-containing p(HPMAm-Lac$_2$), we investigated whether low temperature aqueous conjugation of transiently thermoresponsive NHS-containing polymers to proteins, allowed modulation of the solution behavior of the polymer-protein conjugates by altering temperature and/or pH. Therefore, copolymers of HEA and (2,2-dimethyl-1,3-dioxolane-4-yl)methyl acrylate (DMDMA) were synthesized by the Hoogenboom lab using an NHS-containing RAFT CTA **(Scheme 3).** Copolymerization with DMDMA was reported to allow 'à la carte' tuning of the $T_{cp}$ below physiological temperature by varying the monomer ratio.[16] Importantly, the acetal groups of the DMDMA are acid-labile,[32] thereby hydrolyzing into hydrophilic glycerol acrylate moieties at low pH. Copolymers of two different molecular weights, i.e. 6 (NHS-P32) and 18 kDa (NHS-P33), were synthesized that exhibited a $T_{cp}$ of 24.2 $^{o}$C and 31 $^{o}$C respectively.

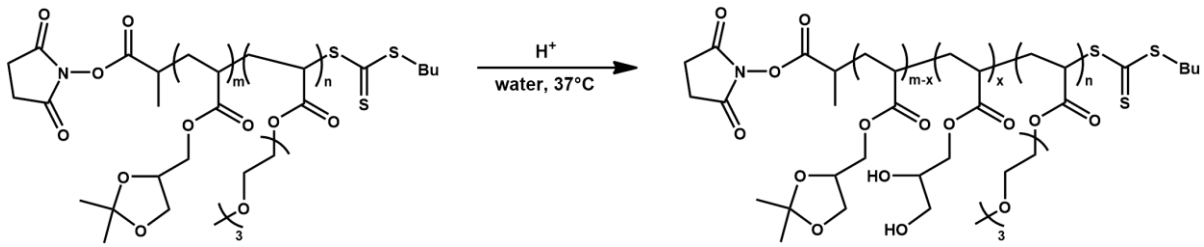


**Scheme 3.** Molecular structure and (partial) hydrolysis of NHS-containing, pH degradable, temperature-responsive copolymers containing HEA and DMDMA. P33-NHS = p(DMDMA$_{28}$-*co*-mTEGA$_{56}$) and P32-NHS = p(DMDMA$_{7}$-*co*-mTEGA$_{22}$).

Lysozyme was used as model protein and the polymers were conjugated below their $T_{cp}$ in aqueous medium buffered, at pH 8.3. SDS-PAGE (**Figure 7**) demonstrated that, relative to native lysozyme (lane 2), the polymer-protein conjugates (lane 3 to 8) exhibited an increase in molecular weight, indicating successful bio-conjugation. As expected, the 6 kDa polymer yielded lower MW conjugates than the 18 kDa polymer. Increasing the molar ratio of polymer to lysozyme resulted in a larger amount of protein becoming conjugated, likely with multiple chains attached. Control samples (polymer incubated without lysozyme) were not visible on the gel and proteins mixed with unreactive copolymers without NHS-ester end-group did not induce a delay in gel migration (data not shown).

To assess whether copolymer conjugation provides the protein with dual temperature- and pH-responsive properties, we measured the electrophoretic mobility of the conjugates by SDS-PAGE below and above the $T_{cp}$ of the copolymers and before and after acid-triggered hydrolysis. As the presence of SDS in the PAGE experiment would strongly increases the $T_{cp}$ of the copolymers, we performed PAGE under so-called 'native' non-reducing conditions excluding SDS. As shown in **Figure 8**, when PAGE was performed below the $T_{cp}$ of the copolymers, no difference in electrophoretic mobility was observed between non-hydrolyzed and hydrolyzed conjugates. Contrary, when PAGE was performed above the $T_{cp}$ of the copolymers, the non-hydrolyzed conjugates did not migrate on the gel whereas the hydrolyzed conjugates migrated on the gel, independently of temperature. These data clearly demonstrate that the copolymer-protein conjugates have dual-responsive properties. Indeed, the conjugates are water soluble below the $T_{cp}$, precipitate from solution above the $T_{cp}$ while regaining full solubility upon hydrolysis of the acetals into hydrophilic glycerol moieties.

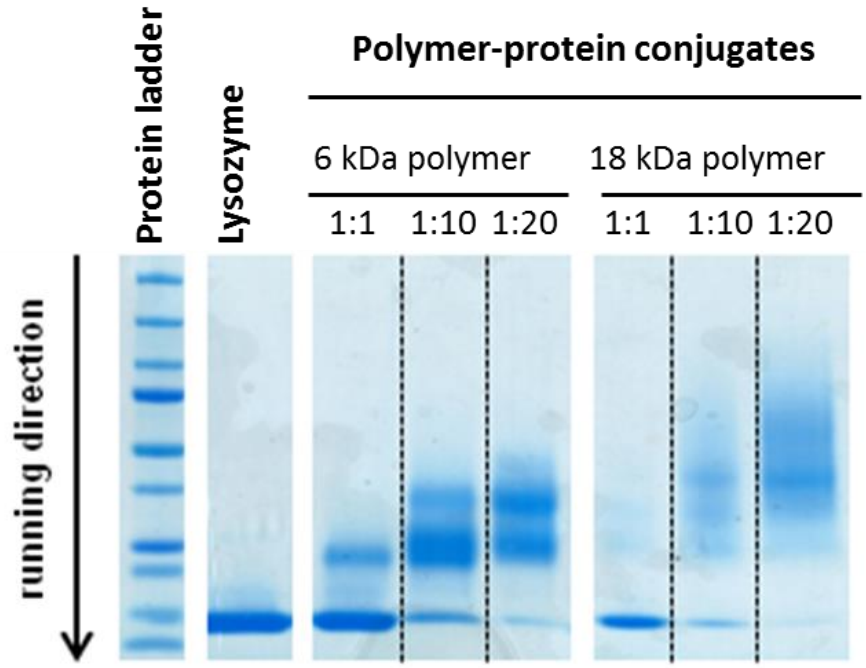


**Figure 7.** SDS-PAGE analysis of the conjugation mixtures. (Lane 2) Native lysozyme. (Lane 3 to 5) Lysozyme - 6 kDa polymer (NHS-P32) conjugates in a ratio 1:1, 1:10 and 1:20 (Lane 6 to 8) Lysozyme - 18 kDa polymer (NHS-P33) conjugates in a ratio 1:1, 1:10 and 1:20.

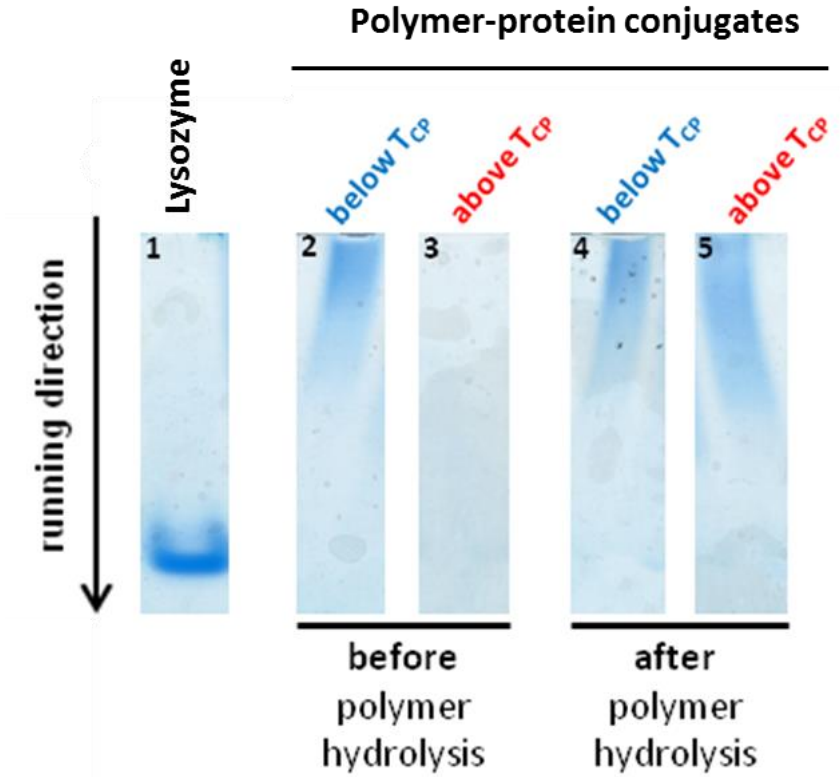


**Figure 8**. Native PAGE of primary and hydrolyzed protein-polymer conjugates (18 kDa copolymer, ratio 20:1). Below $T_{cp}$ there is no clear difference between both samples. Above $T_{cp}$, however, the intact polymer conjugates are not visible on the gel due to precipitation in the well.

***Protein conjugation using BCN-functional PEtOx***

As an alternative to the conventional 'grafting-to' conjugation approach, we also evaluated the use of so-called orthogonal handles for strain-promoted azide–alkyne cycloaddition (SPAAC) between azide-functional proteins and cyclooctyne-functional polymers. The Hoogenboom lab synthesized poly(2-ethyl-2-oxazoline) or p(EtOx) via cationic ring-opening polymerization (CROP) using a bicyclononyne (BCN) tosylate initiator, yielding a 5 kDa BCN-functional PEtOx polymer (**Scheme 4**). Unlike the copper(I)-catalyzed cyclo-addition (CuAAC) between an azide and an alkyne[6], ring strain in cyclooctyne derivatives allows for copper-free 'click' reactions.[14] Bovine serum albumin (BSA) was modified with respectively a 5-, 10- or 20-fold molar excess NHS-$PEG_4$-$N_3$, followed by extensive dialysis to remove unreacted azide. In this step, lysine residues are substituted with azides that contain a tetraethyleneglycol spacer, through amide bond formation. In a second step, PEtOx-BCN is conjugated to BSA via SPAAC using a protein to polymer molar ratio of 1:10 or 1:20. After overnight reaction, the conjugates were analyzed by SDS-PAGE (**Figure 9A**). Integration of the optical density of the gels (**Figure 9B**), reveals a clear shift in molecular weight for the BSA-$PEG_4$-$N_3$ towards higher molecular weight species, demonstrating successful conjugation. This shift depends both on the extent of azide modification of BSA in the first step and on the excess of PEtOx-BCN added in the second step.

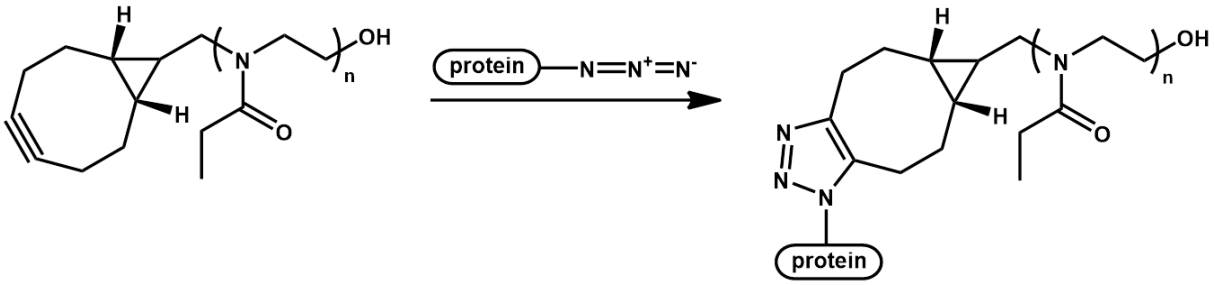


**Scheme 4**. Conjugation of bicyclononyne (BCN)-functional poly(2-ethyl-2-oxazoline) or p(EtOx) to azide-functionalized protein.

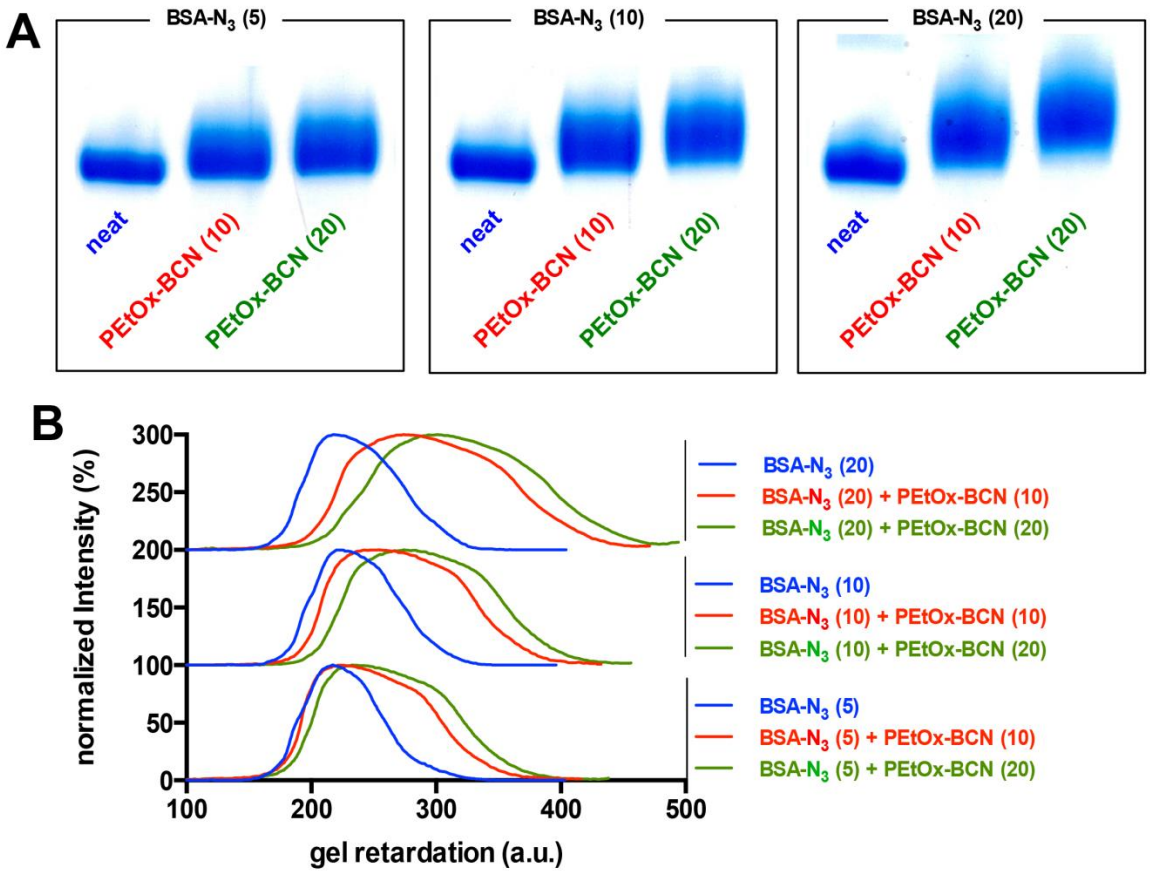


**Figure 9. (A)** SDS-PAGE analysis of the conjugation of PEtOx-BCN to azide-modified BSA. **(B)** Quantification of PEtOx-BCN to BSA conjugation by integration of the optical density.

## Conclusions

In summary, the conjugation efficiency of acrylate and methacrylamide polymers with different protein-reactive moieties to two types of serum albumin (i.e. avian and bovine) was investigated. These include N-hydroxysuccinimide (NHS) or pentafluorophenyl (PFP) ester moieties that can be conjugated to lysine residues, and alternatively maleimide (MAL) or pyridyl disulfide (PDS) moieties that can be conjugated to cysteine residues. PFP- and PDS-containing polymers exhibited the highest conjugation efficiency with BSA and OVA respectively, as observed for both p(HEA) and p(HPMAm), and therefore are the preferred conjugation chemistries for BSA and OVA respectively. The disulfide bond in the PDS-polymer-protein conjugates was fully cleaved upon reduction, whereas MAL-based conjugates remained intact under reductive conditions. Introduction of additional thiol moieties by converting lysine residues with SATP, strongly increased protein-conjugation efficiencies for both PDS- and MAL-containing polymers. This can be exploited for PDS-

polymer-BSA conjugates, when a reversible disulfide bond is preferred to the stable amide bonds obtained with PFP-containing polymers. Additionally, we were also able to conjugate transiently thermoresponsive RAFT-based polymers to proteins. The dilactate derivative of HPMAm (i.e. HPMAm-$Lac_2$) could be reacted with OVA via a PDS CTA when using a 'salting-in' approach. Conjugating lysozyme to NHS-containing thermoresponsive and acid-degradable polymers yielded polymer-protein conjugates with dual-responsive properties. Finally, copper-free 'click' chemistry was successfully used to conjugate BCN-functional PEtOx to azide-modified BSA.

## References


1 Duncan, R. The dawning era of polymer therapeutics. *Nat. Rev. Drug Discov.* **2**, 347-360 (2003).

2 Broyer, R. M., Grover, G. N. & Maynard, H. D. Emerging synthetic approaches for protein-polymer conjugations. *Chem. Commun.* **47**, 2212-2226 (2011).

3 Lutz, J. F. & Borner, H. G. Modern trends in polymer bioconjugates design. *Prog. Polym. Sci.* **33**, 1-39 (2008).

4 González-Toro, D. C. & Thayumanavan, S. Advances in polymer and polymeric nanostructures for protein conjugation. *European Polymer Journal* **49**, 2906-2918 (2013).

5 Johnson, R. P., John, J. V. & Kim, I. Recent developments in polymer–block–polypeptide and protein–polymer bioconjugate hybrid materials. *European Polymer Journal* **49**, 2925-2948 (2013).

6 Nicolas, J., Mantovani, G. & Haddleton, D. M. Living radical polymerization as a tool for the synthesis of polymer-protein/peptide bioconjugates. *Macromol. Rapid Commun.* **28**, 1083-1111 (2007).

7 Boyer, C. *et al.* Well-defined protein-polymer conjugates via in situ RAFT polymerization. *J. Am. Chem. Soc.* **129**, 7145-7154 (2007).

8 Li, M. *et al.* Thermoresponsive Block Copolymer-Protein Conjugates Prepared by Grafting-from via RAFT Polymerization. *Macromol. Rapid Commun.* **32**, 354-359 (2011).

9 De, P. *et al.* Temperature-regulated activity of responsive polymer-protein conjugates prepared by grafting-from via RAFT polymerization. *J. Am. Chem. Soc.* **130**, 11288-+ (2008).

10 Rostovtsev, V. V. *et al.* A stepwise Huisgen cycloaddition process: Copper(I)-catalyzed regioselective "ligation" of azides and terminal alkynes. *Angew. Chem.-Int. Edit.* **41**, 2596-+ (2002).

11 Boyer, C. *et al.* Direct synthesis of well-defined heterotelechelic polymers for bioconjugations. *Macromolecules* **41**, 5641-5650 (2008).

12 Li, M. *et al.* Responsive polymer-protein bioconjugates prepared by RAFT polymerization and copper-catalyzed azide-alkyne click chemistry. *Macromol. Rapid Commun.* **29**, 1172-1176 (2008).

13 Sletten, E. M. & Bertozzi, C. R. Bioorthogonal Chemistry: Fishing for Selectivity in a Sea of Functionality. *Angew. Chem.-Int. Edit.* **48**, 6974-6998 (2009).

14 Agard, N. J., Prescher, J. A. & Bertozzi, C. R. A Strain-Promoted [3 + 2] Azide–Alkyne Cycloaddition for Covalent Modification of Biomolecules in Living Systems. *J. Am. Chem. Soc.* **126**, 15046-15047 (2004).

15 Dommerholt, J. *et al.* Readily Accessible Bicyclononynes for Bioorthogonal Labeling and Three-Dimensional Imaging of Living Cells. *Angew. Chem.-Int. Edit.* **49**, 9422-9425 (2010).

16 Zhang, Q. L. *et al.* Dual pH- and temperature-responsive RAFT-based block co-polymer micelles and polymer-protein conjugates with transient solubility. *Polym. Chem.* **5**, 1140-1144 (2014).

17 Glassner, M. *et al.* Solvent-free mechanochemical synthesis of a bicyclononyne tosylate: a fast route towards bioorthogonal clickable poly(2-oxazoline)s. *Polym. Chem.* **6**, 8354-8359 (2015).

18 Moore, S. Amino acid analysis - aqueous dimethyl sulfoxide as solvent for ninhydrin reaction. *J. Biol. Chem.* **243**, 6281-& (1968).

19 De Geest, B. G. *et al.* Polymeric Multilayer Capsule-Mediated Vaccination Induces Protective Immunity Against Cancer and Viral Infection. *ACS Nano* **6**, 2136-2149 (2012).

20 De Koker, S. *et al.* Polyelectrolyte Microcapsules as Antigen Delivery Vehicles To Dendritic Cells: Uptake, Processing, and Cross-Presentation of Encapsulated Antigens. *Angew. Chem.-Int. Edit.* **48**, 8485-8489 (2009).

21 De Geest, B. G. *et al.* Surface-Engineered Polyelectrolyte Multilayer Capsules: Synthetic Vaccines Mimicking Microbial Structure and Function. *Angew. Chem.-Int. Edit.* **51**, 3862-3866 (2012).

22 Heredia, K. L. *et al.* Synthesis of Heterotelechelic Polymers for Conjugation of Two Different Proteins. *Macromolecules* **42**, 2360-2367 (2009).

23 Li, H. M. *et al.* Protein conjugation of thermoresponsive amine-reactive polymers prepared by RAFT. *Polym. Chem.* **2**, 323-327 (2011).

24 Heredia, K. L. *et al.* Reversible siRNA-polymer conjugates by RAFT polymerization. *Chem. Commun.*, 3245-3247 (2008).

25 Brinkley, M. A brief survey of methods for preparing protein conjugates with dyes, haptens, and cross-linking reagents. *Bioconjugate Chem.* **3**, 2-13 (1992).

26 Imming, P. & Jung, M. H. Pentafluorophenyl esters of dicarboxylic-acids. *Arch. Pharm.* **328**, 87-91 (1995).

27 Lockett, M. R. *et al.* A tetrafluorophenyl activated ester self-assembled monolayer for the immobilization of amine-modified oligonucleotides. *Langmuir* **24**, 69-75 (2008).

28 Shen, B. Q. *et al.* Conjugation site modulates the in vivo stability and therapeutic activity of antibody-drug conjugates. *Nat. Biotechnol.* **30**, 184-189 (2012).

29 Demoreno, M. R., Smith, J. F. & Smith, R. V. Mechanism studies of coomassie blue and silver staining of proteins. *J. Pharm. Sci.* **75**, 907-911 (1986).

30 Suwa, K. *et al.* Effects of salt on the temperature and pressure responsive properties of poly(N-vinylisobutyramide) aqueous solutions. *Colloid Polym. Sci.* **276**, 529-533 (1998).

31 Bloksma, M. M. *et al.* The Effect of Hofmeister Salts on the LCST Transition of Poly(2-oxazoline)s with Varying Hydrophilicity. *Macromol. Rapid Commun.* **31**, 724-728 (2010).

32 Murthy, N. *et al.* A novel strategy for encapsulation and release of proteins: Hydrogels and microgels with acid-labile acetal cross-linkers. *J. Am. Chem. Soc.* **124**, 12398-12399 (2002).

# Chapter 5

# Polymer-protein conjugates via a 'grafting-from' approach for the delivery of immune-modulators

Parts of this chapter were published in:

**Transiently responsive protein-polymer conjugates via a 'grafting-from' RAFT approach for intracellular co-delivery of proteins and immune-modulators**
N. Vanparijs, R. De Coen, D. Laplace, B. Louage, S. Maji, L. Lybaert, R. Hoogenboom and B. G. De Geest, *Chemical Communications* **2015**, 51, 13972-13975.

## Abstract

In this chapter, a 'grafting-from' strategy was evaluated as an alternative for the 'grafting-to' approach, to prepare transiently responsive protein-polymer conjugates. The 'grafting-from' approach should avoid the need for large molar excesses of protein-reactive polymer to obtain high protein conjugation efficiency. The model protein bovine serum albumin (BSA) was modified with a chain transfer agent to allow 'grafting-from' RAFT polymerization of a dioxolane-containing acrylamide. The resulting protein-polymer conjugates were thermoresponsive, and self-assembled into nanoparticles at physiological temperature and pH. Acidic triggered hydrolysis of the dioxolane units into diol moieties rendered the conjugates fully water soluble, irrespective of temperature. Additionally, these thermoresponsive and acid-labile protein-polymer conjugates were used for the intracellular delivery of proteins and hydrophobic molecules. Via solvent displacement, the amphiphilic conjugates could be loaded with hydrophobic molecules, including a fluorescent dye and an immune-modulating compound that holds potential for vaccine delivery. The efficacy of these protein-polymer conjugates as intracellular delivery vehicles was demonstrated by *in vitro* experiments in dendritic cells.

## Introduction

Efficient polymer-protein conjugation is a crucial step in the design of many therapeutic protein formulations including vaccine nanoformulations and antibody-drug conjugates.[1,2] Particulary covalent modification with stimuli-responsive polymers is of interest, to confer the responsive properties of these polymers to the attached protein molecules. For example, temperature-responsive polymers conjugated to proteins can self-assemble into nanoparticles above the cloud point temperature ($T_{cp}$), due to their amphiphilic character.[3,4] This controlled and reversible aggregation of proteins into nanoparticles could be exploited for vaccine delivery.

Whereas soluble antigen is predominantly presented by dendritic cells (DCs; the most potent class of antigen presenting cells) to CD4 T cells, antigen in the form of nano- and microparticles becomes presented to both CD4 and CD8 T cells. This process of cross-presentation occurs because exogenous antigens in particulate form mimic the morphology

of micro-organisms and can thus be better recognized by DCs as being potentially dangerous, thereby altering the route of internalization and antigen presentation (**Chapter 1**).[5-9] MHCI-peptide stimulated CD8 T cells will differentiate into cytotoxic T cells, that possess the unique capacity to recognize and kill infected or transformed cells. This path of the immune response is termed cellular immunity and is thought to be crucial for effective vaccination against intracellular pathogens such as HIV, malaria, tuberculosis and for anti-cancer immune therapy.[10,11]

The cross-presentation pathway can be further improved by co-encapsulation of immune-modulators that shape the direction and strength of the adaptive immune response.[12,13] In this context, agonists of Toll-like receptors (TLRs) are under intensive investigation as adjuvants for vaccination[14] or as agents for anti-cancer immunotherapy.[15] In addition, ultra-small nanoparticles and albumin-binding amphiphiles, are efficiently transported via the interstitial flow and lymphatic capillaries to the draining lymph nodes where they are taken up by dendritic cells (DCs).[16-18]

As discussed in **Chapter 2**, Kizhakkedathu and co-workers described the synthesis and polymerization of [(2,2-dimethyl-1,3-dioxolane)methyl]acrylamide (DMDOMAm), yielding temperature-responsive polymers with acid-labile dioxolane side groups.[19] Gradual hydrolysis of these dioxolane groups into diol moieties increases the $T_{cp}$ of the polymers from below room temperature upwards until they become fully water soluble, irrespective of temperature. Such transiently responsive homopolymers are also expected to possess a better predictable behavior than combining multiple co-monomers yielding temperature- and pH-responsive polymers, e.g. the HEA/DMDMA copolymer system (**Chapter 2 and 4**).[20,21]

Amongst the different controlled radical polymerization techniques,[22,23] reversible addition-fragmentation chain transfer (RAFT) polymerization in particular, has shown to be tolerant to many chemical groups, solvent media and offers a straightforward route to synthesize polymers with a protein-reactive end-group via the use of a functional chain transfer agent (CTA).[4,24,25] In the previous chapter we reported on a head-to-head evaluation of several protein-reactive RAFT CTAs for protein-polymer conjugation via a 'grafting-to' approach.[26] The advantage of the 'grafting-to' approach is the use of pre-synthesized polymer, which allows for thorough characterization of the polymer and avoids exposure of the protein to potentially denaturing polymerization conditions. However, we found that a

large molar excess (up to 20-40 fold) of protein-reactive polymer is required to obtain full protein conjugation.

An alternative approach is a 'grafting-from' approach, where the polymer chain is grown directly from a protein that is modified with a CTA.[27-29] The major advantage is that the prepared conjugates only need to be purified from low molecular weight compounds (i.e. unreacted monomer, initiator, …). This can easily be done by dialysis, unlike the removal of unreacted polymer, involved in 'grafting-to', which is often tedious and requires preparative gel filtration chromatography. However, possible steric hindrance during polymerization can lead to a substantial amount of unreacted protein-bound CTA.

In this chapter, we design transiently thermoresponsive protein-polymer conjugates via a 'grafting-from' RAFT approach. Bovine serum albumin (BSA) is modified with pentafluorophenyl (PFP) CTA moieties, allowing 'grafting-from' RAFT polymerization of DMDOMAm. The resulting conjugates can change from a soluble to aggregated state in response to temperature; but become fully soluble, irrespective of temperature, by acid triggered hydrolysis. These conjugates are intended to be responsive to the acidic endosomal milieu where nanoparticles are usually stored upon phagocytosis.[30] These features are essential for clearance of the polymeric carrier from the body, to avoid long-term accumulation. In addition, we establish an *in vitro* proof-of-concept showing that p(DMDOMAm)-conjugation can be used for intracellular co-delivery of proteins and small hydrophobic molecules loaded into the hydrophobic domains of the p(DMDOMAm) above its $T_{cp}$. Fluorescently labeled BSA-p(DMDOMAm) conjugates are encapsulated with a hydrophobic dye to evaluate the uptake in DCs by flow cytometry. Analogously, unlabeled conjugates are loaded with an immune-modulating TLR agonist to induce maturation in bone marrow DCs.

## Material and methods

### *Materials*

Unless otherwise noted all chemicals were purchased from Sigma-Aldrich. 2.2'-azobis[2-(2-imidazolin-2-yl)propane] dihydrochloride (VA-044) was purchased from Wako Chemicals. The pentafluorophenyl modified 4-cyano-4-[(ethylsulfanylthiocarbonyl)sulfanyl]

pentanoic acid (PFP-CETPA) RAFT agent was synthesized as reported earlier.[26] The [(2,2-dimethyl-1,3-dioxolane)methyl] acrylamide (DMDOMAm) was synthesized according to literature.[19] Cyanine5-NHS (Cy5-NHS) and cyanine3-alkyne (Cy3-alkyne) were purchased from Lumiprobe. CL075 was purchased from Invivogen. The immortalized dendritic cell line DC2.4 was a kind gift from Dr. Kenneth Rock.[31] Bone marrow derived dendritic cells were obtained as previously reported.[32] Cell culture medium and supplements, Hoechst and Cholera Toxin Subunit B, Alexa Fluor® 488 Conjugate (CTB-AF488) were purchased from Life Technologies. FC block, MHCII-FITC, CD11c-APC and CD86-PE were obtained from BD Pharmingen.

***Conjugation of BSA with pentafluorophenyl CTA to obtain macroCTA***

BSA (3.2 g; 48.4 µmol; 1 equiv.) was dissolved in phosphate buffered saline (PBS; 413 mL; pH 7.4) in a 1 L round bottom flask, equipped with a magnetic stir bar. The solution was purged with nitrogen for 40 min. A solution of the PFP-CETPA (415.6 mg, 968 µmol, 20 equiv.) in DMF (17 mL) was added dropwise, and the solution was stirred at room temperature overnight. The reaction mixture was centrifuged twice (4000 rpm, 10 min, 5 °C) to remove the excess of PFP CTA. Subsequently, the supernatant was dialyzed against deionized (DI) water (6 x 15 L) for 2 days, using a MWCO of 8000 Da, and then lyophilized to isolate the BSA macroCTA.

***UV-Vis analysis BSA macroCTA***

UV-Vis spectroscopy was carried out on a Shimadzu UV-1650PC UV-Vis double beam spectrophotometer. PFP-CETPA was dissolved in methanol to obtain a 3 mg/mL (7 mM) concentrated stock solution that was used to make a two-fold dilution series ranging from 6 µg/mL to 48 µg/mL. The absorbance of each solution was measured at 306 nm ($\lambda_{max}$ of the PFP-CETPA) to obtain a linear plot of CTA concentration *versus* absorbance. The CTA extinction coefficient was determined to be $\varepsilon$ = 9875 $M^{-1}$ $cm^{-1}$, and this value was used to calculate the concentration of the CTA content within the BSA macroRAFT agent.

***RAFT homopolymerization of DMDOMAm***

DMDOMAm (15 mmol), PFP-CETPA (0.075 mmol for a DP 200) and AIBN (0.015 mmol) were transferred into a Schlenk tube and dissolved in anhydrous DMF (2M monomer

concentration). After bubbling with nitrogen for 30 min, the solution was heated at 70°C in an oil bath for 4 h. The polymers were isolated by precipitation in hexane and dried under vacuum. Monomer conversion was measured by $^{1}$H-NMR and calculated to be 92% ($DP^{NMR}$ = 184, $Mw^{NMR}$ = 34.4 kDa). The purified polymer was characterized by SEC analysis ($Mn^{SEC}$ = 26,3 kDa, PDI = 1.15).

$^{1}$H-NMR spectra were recorded on a Bruker 300 MHz FT-NMR spectrometer using $CDCl_3$ as solvent. Size exclusion chromatography was carried out on Shimadzu Prominence GPC system equipped with a LC-20AD isocratic pump and a RID-20A refractive index detector. Measurement were done in DMA containing 50 mM LiCl at 50°C and with a flow rate of 0.593 mL/min. The two PL gel 5 µm mixed-D columns were calibrated with poly(methylmethacrylate) (PMMA) standards (Polymer standards service) in a molecular weight (Mn) range of 1980 Da to 372000 Da.

***RAFT polymerization of DMDOMAm with BSA macroCTA***

A 'grafting-from' RAFT polymerization of DMDOMAm from the BSA macroCTA with an aimed degree of polymerization (DP) of 200 was conducted as follows. DMDOMAm (185 mg, 1 mmol), BSA macroCTA (65 mg, 1 µmoL of protein, which contained 5 µmol of CTA functionality, as determined by UV-Vis), VA-044 (2 mg, 6.5 µmol) and phosphate buffer pH 6 (PB, 3.8 mL) were sealed in a Schlenk vial equipped with a magnetic stir bar. The solution was degassed by 5 cycles of freeze-vacuum-thaw, prior to immersing the Schlenk vial into a preheated oil bath at 25°C. For a DP of 100, the [DMDOMAm]:[$CTA_{functionality}$] ratio was kept at 100:1 instead of 200:1. VA-044 was employed in a [VA-044]:[$CTA_{functionality}$] ratio of 1.3:1.

After 16 h reaction the polymerization mixture had become turbid, indicative of polymerization-induced self-assembly (PISA). Time samples before ($T_0$) and after ($T_e$) polymerization were analyzed on SDS-PAGE and DLS. Half of the reaction mixture was diluted with DI water and dialyzed against DI water (6 x 5L; 4°C) for 2 days using a MWCO of 8000 Da. The other half was first diluted 3 times with a 0.1 M bicarbonate buffer pH 8.2 and fluorescently labeled with the Cy5-NHS (stock solution in DMSO, molar ratio BSA:Cy5-NHS = 1:10). After overnight reaction, the fluorescently labeled BSA-p(DMDOMAm) conjugates were dialyzed against DI water (10 x 5 L, 4°C). The resulting solutions were lyophilized to obtain the unlabeled and Cy5-labeled protein-polymer conjugates respectively.

***Sodium Dodecyl Sulfate-polyacrylamide Gel Electrophoresis (SDS-PAGE)***

SDS-PAGE was performed with a 4-20 % polyacrylamide gradient gel using the Mini-PROTEAN Tetra Cell from Bio-Rad, at 175 V for 45 min. The polymerization time point samples were diluted 20 times with ice-cold phosphate buffer at pH 6 and were further diluted with 4x Laemmli sample buffer in a 3:1 ratio before loading on the SDS-PAGE gels. Staining was accomplished with Coomassie Blue. Integration of the protein bands was done by ImageJ software as reported earlier.[26]

***Dynamic Light Scattering (DLS)***

DLS measurements of polymerization time point samples were conducted with a Malvern Zetasizer Nano-S. Both $T_0$ and $T_e$ were measured below (3°C) and above (30°C) the $T_{cp}$ of the protein-polymer conjugates.

***Cloud Point Temperature ($T_{cp}$) measurements***

The phase transition temperature of the protein-polymer conjugates was determined by DLS measurements at 1°C intervals ranging from 5 to 40°C. The purified BSA-p(DMDOMAm) conjugates were dissolved in ice-cold PBS (2.5 mg/mL) and filtered through a 0.45 µm syringe filter prior to measurements. The $T_{cp}$ was defined as the temperature where the mean volume and derived count rate abruptly shifted to higher values.

***Determination of the Critical Micellar Concentration (cmc)***

Similar to a previously reported protocol, the cmc of the BSA-p(DMDOMAm) conjugates were determined by fluorescence microscopy using pyrene as a fluorescent probe.[21] First, 5 mL of protein-polymer conjugate solutions were prepared in ice-cold PBS with concentrations ranging from 0.001 to 1 mg/mL. The samples were kept on ice and a pyrene working solution in acetone (16.67 µL, 36 µg/mL) was added under continuous stirring and heating above the $T_{cp}$. After overnight evaporation of the acetone, fluorescence excitation spectra were collected at 25°C on a Cary Eclipse fluorescence spectrophotometer (Agilent Technologies) equipped with a Varian Cary Temperature Controller. The cmc was quantified based on the change in excitation intensity ratio at 338 and 333 nm upon dilution

***Hydrolysis of dioxolane side groups***

A solution of the BSA-p(DMDOMAm) conjugates (2.5 mg/mL in ice-cold PBS) was filtered through a 0.45 µm syringe filter and 475 µL was transferred into a DLS cuvette. The sample was measured on DLS at 37°C, followed by addition of an HCl stock solution (25 µL, 1M) to obtain an 50 mM HCl final concentration. The evolution of particle size and light scattering intensity was followed in function of time by DLS at 37°C. To confirm that the evolution in particle size is due to hydrolysis of the p(DMDOMAm) dioxolane side groups rather that degradation of the BSA itself, several control experiments were included. Both soluble BSA and the BSA-p(DMDOMAm) conjugates (2.5 mg/mL) treated with 50 mM HCl were compared with untreated samples by SDS-PAGE.

***Loading of BSA-p(DMDOMAm) nanoparticles with hydrophobic molecules***

A typical solvent displacement loading protocol for the BSA-p(DMDOMAm) particles was as follows. The protein-polymer conjugates were dissolved in ice-cold PBS buffer (2.5 mg/mL) and a stock solution of the hydrophobic compound in ethanol was added under continuous stirring and heating above the $T_{cp}$. After overnight evaporation of ethanol at 37°C, the non-encapsulated hydrophobic compound was removed by filtration (0.45 µm syringe filter). In this way, Cy5-labeled BSA-p(DMDOMAm) conjugates (1 mL, 2.5 mg/mL in PBS) were loaded with Cy3-alkyne (5 µL, 1 mg/mL in ethanol) and unlabeled BSA-p(DMDOMAm) conjugates (0.5 mL, 2.5 mg/mL in PBS) were loaded with CL075 (15 µL, 5 mg/mL in ethanol). As a control, the same procedure was repeated for solutions of PBS buffer and (Cy5-)BSA macroCTA.

***In vitro uptake experiment by DC2.4 cells***

DC2.4 cells (immortalized dendritic cell line) were cultured in RPMI-glutamax, supplemented with 10% FBS, 1 mM sodium pyruvate, 10 mM HEPES buffer, 0.05 mM 2-mercaptoethanol, MEM NEAA and antibiotics (50 units/mL penicillin and 50 µg/mL streptomycin). Cells were incubated at 37 °C in an controlled, sterile environment of 95% relative humidity and 5% CO2. DC2.4 cells were seeded into 24-well titer plates (250 000 cells per well, suspended in 0.95 mL of culture medium) and incubated overnight to allow cell sedimentation and subsequent adhesion to the bottom of the wells. Next, 50 µL of the Cy3-alkyne loaded Cy5-BSA-p(DMDOMAm) particles (2.5 mg/mL, *cfr. supra*) was added to

the cells (conjugate concentration in wells of 0.125 mg/mL), followed by 24 h of incubation to allow cellular uptake. The same procedure was followed for Cy3-alkyne loaded PBS and Cy5-BSA macroCTA control samples. After overnight incubation, the wells were aspirated, washed with 1 mL of PBS and incubated with 500 µL of Cell Dissociation Buffer (15 min., 37°C). The cell suspensions were transferred into Eppendorf tubes and immediately centrifuged (350 g, 10 min., 5 °C). Finally, the supernatant was aspirated and the cell pellets were suspended in 200 µL of PBS and kept on ice to maintain cell integrity. FACS was performed on a BD Accuri C6 (BD Biosciences). The data were processed by FlowJo software.

***Confocal microscopy on DC2.4 cells***

DC2.4 cells were plated out on Willco-Dish glass bottom dishes (50 000 cells, suspended in 200 µL of culture medium) and incubated overnight. Next, 10 µL of the Cy3-alkyne loaded Cy5-BSA-p(DMDOMAm) particles (2.5 mg/mL, *cfr. supra*) was added, followed by 24 h of incubation. Hoechst and CTB-AF488 staining was carried out simultaneously on fixed cells. In summary, culture medium was aspirated and cells were washed with PBS. Next, 200 µL of 4 % paraformaldehyde was added and allowed to fixate for 30 min. A staining solution was prepared by adding Hoechst (10 µL of a 1 mg/mL stock in DMSO) and CTB-AF488 (5 µL of a 1 mg/mL stock in PBS) to a PBS buffer containing 1% of BSA (2.5 mL). After aspiration and washing, 200 µL of this staining solution was added to the fixed cells and incubated for 40 minutes at room temperature. Finally, the samples were washed with 1% BSA PBS buffer. Confocal microscopy was carried out on a Leica DMI6000 B inverted microscope equipped with an oil immersion objective (Leica, 63x, NA 1.40) and attached to an Andor DSD2 confocal scanner. Images were processed with ImageJ software.

***In vitro maturation experiment in murine bone marrow derived DCs***

Mouse bone-marrow-derived DCs (BM-DCs) were generated using a modified Inaba protocol.[33] Bone marrow was flushed from the femurs and tibias obtained from euthanized C57BL/6 mice with complete RPMI. The cell suspension was filtered through a 100 µm cell strainer and incubated for 3−5 min in red blood cell lysis buffer on ice. The cells were subsequently seeded into a 24 well plate at a density of $1.5 \times 10^5$ cells/mL in complete RPMI containing 20 ng/mL of GM-CSF and incubated at 37 °C / 5 % $CO_2$ for 7 days. To ensure optimal BM-DC growth, fresh medium containing 20 ng/mL GM-CSF was added on day 3,

and on day 6 the medium was refreshed at 10 ng/mL GM-CSF. Day 7 BM-DCs were incubated with 25 µL of the CL075 loaded BSA-p(DMDOMAm) particles (2.5 mg/mL, *cfr. supra*). CL075 loaded PBS and BSA macroCTA were included as control samples. After overnight incubation, the cell suspensions were transferred into Eppendorf tubes and immediately centrifuged (350 g, 10 min., 5 °C). The supernatant was aspirated and the cell pellets were suspended in 50 µL of an antibody cocktail solution containing Fc block (diluted 200x), MHCII-FITC (diluted 500x), CD11c-APC (diluted 200x) and CD86-PE (diluted 200x) in PBS buffer. After 30 min. of incubation on ice, 200 µL of PBS was added to the samples prior to centrifugation (350 g, 10 min., 5 °C). Finally, the supernatant was aspirated and the cell pellets were suspended in 200 µL of PBS and kept on ice to maintain cell integrity. FACS was performed on a BD Accuri C6 (BD Biosciences). The data were processed by FlowJo software. **Figure 1** illustrates the applied gating strategy, where the CD11c mouse DC surface marker is used to distinguish the dendritic cells from other bone morrow derived cell types.

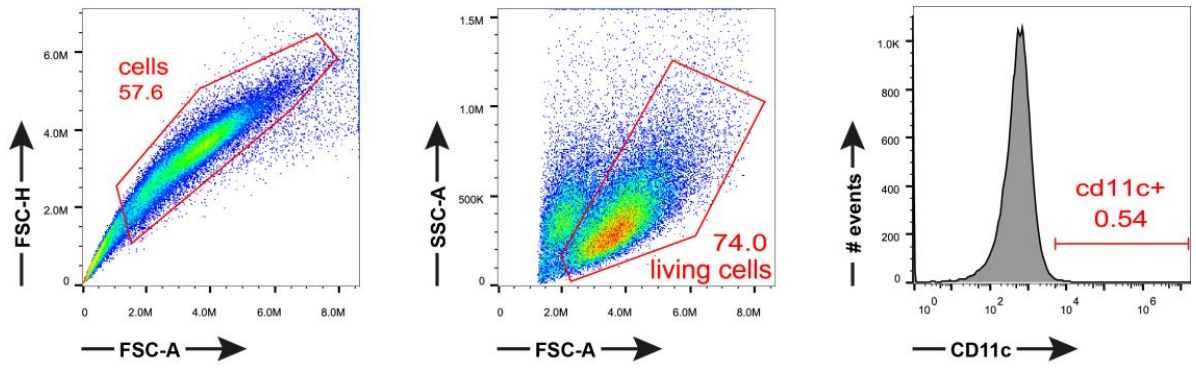


**Figure 1.** Flow cytometry gating strategy on unstained control samples to select DCs from bone marrow cultures.

## Results and discussion

In this chapter, transiently soluble polymer-protein conjugates were prepared via a 'grafting-from' RAFT approach (**Scheme 1**). Bovine serum albumin (BSA), used as model protein, was reacted with a 20-fold molar excess of a pentafluorophenyl (PFP) functionalized trithiocarbonate RAFT CTA. The choice for PFP as activated ester moiety to modify lysine residues is based on our previous work where we showed that PFP outperformed the more widespread NHS esters in terms of protein-conjugation efficiency, likely due to increased hydrolytic stability.[26] UV-Vis analysis of the obtained protein macroCTA ($\lambda_{max}$ of the PFP-CTA

is at 306 nm) revealed an average of 5 CTA molecules grafted per BSA molecule (**Figure 2**). Polymerization of DMDOMAm at a targeted DP (degree of polymerization) of respectively 100 and 200 was conducted at 25°C in phosphate buffer pH 6 using the water-soluble azo initiator VA-044 as radical source.[28] Overnight reaction yielded a turbid mixture, indicating self-assembly to occur during the polymerization reaction. Such phenomenon has been termed by several groups as polymerization-induced self-assembly (PISA).[34-36] SDS-PAGE analysis clearly proved that polymers were grown from the protein backbone, as the protein bands had shifted to higher molecular weights (**Figure 3**). As expected, the protein-polymer band for the targeted DP of 200 was visible at higher molecular weights than the one for DP 100. Integration by ImageJ software, indicated that approximately 30% of the protein remained unmodified. This can likely be attributed to uneven distribution of the CTA units over the different BSA molecules, and/or BSA molecules with too sterically hindered CTA moieties that do not allow for 'grafting-from' polymerization.

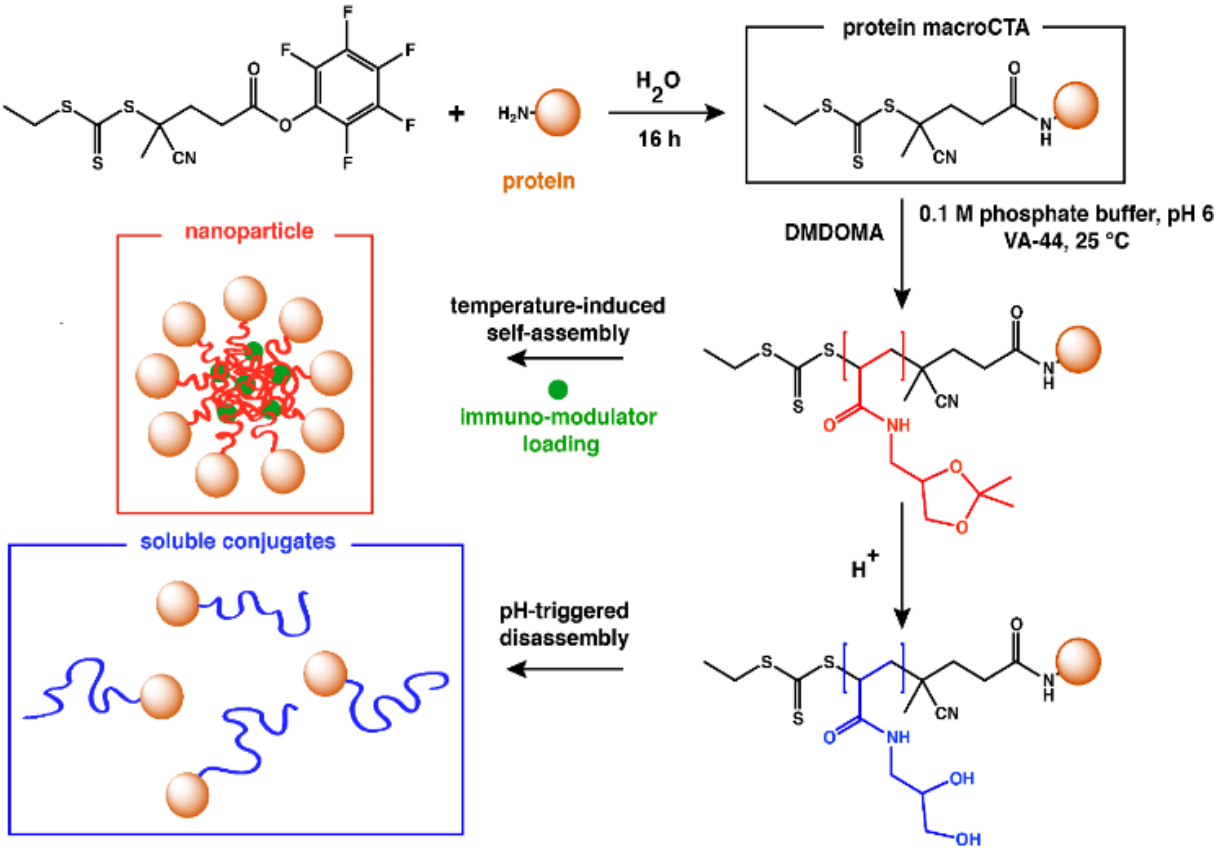


**Scheme 1.** Molecular structure and schematic representation of the synthesis, self-assembly and disassembly of transiently responsive protein-polymer conjugates via 'grafting from' RAFT polymerization and loading of hydrophobic molecules in their core.

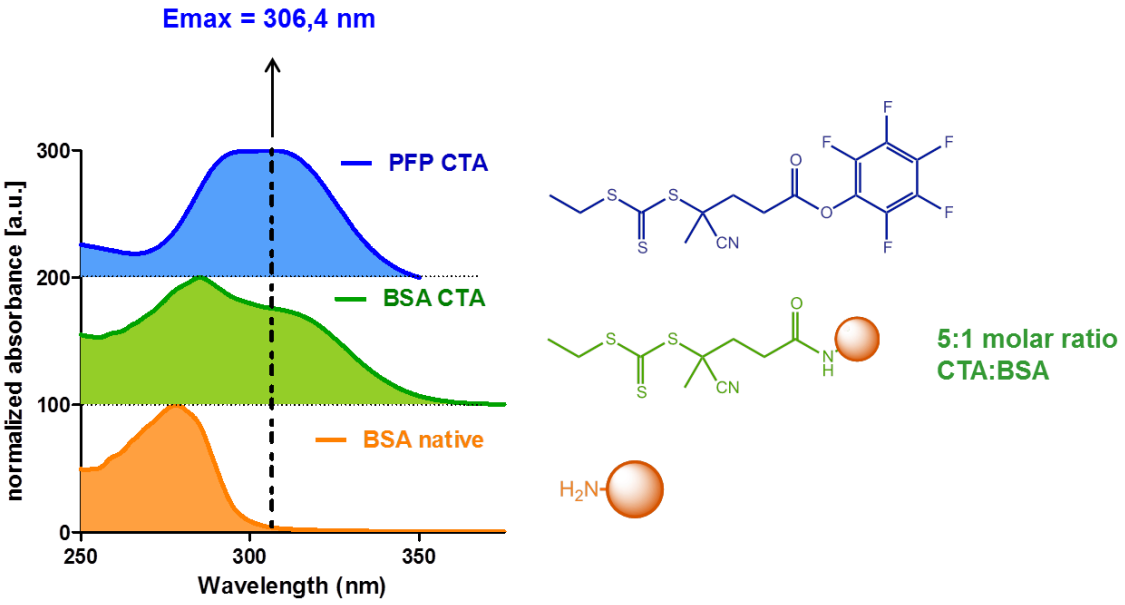


**Figure 2.** UV-Vis spectra of native BSA (orange), CTA-modified BSA (green) and PFP CTA (blue). In the spectra of the CTA-modified BSA (green) a second peak appears around the $\lambda_{max}$ value of the PFP CTA, indicating successful modification of the BSA molecules with CETPA.

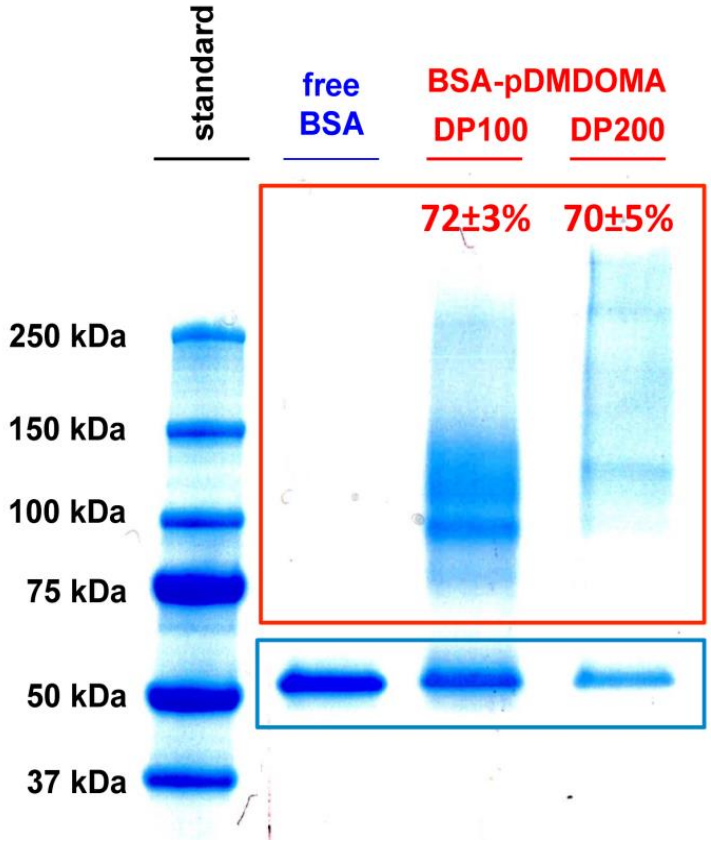


**Figure 3.** SDS-PAGE analysis of BSA-p(DMDOMAm) conjugates with a targeted DP for DMDOMAm of 100 and 200.

DLS analysis of the reaction mixture before ($T_0$) and after ($T_e$) polymerization clearly proofs the formation of temperature-responsive conjugates (**Figure 4**). Before the onset of polymerization, there is no significant difference in size upon increase in temperature. After polymerization, DLS analysis indicates the presence of temperature-responsive behavior, with a $T_{cp}$ of 27°C and 19°C for BSA-p(DMDOMAm)$^{DP100}$ and BSA-p(DMDOMAm)$^{DP200}$ respectively (**Figure 5**). This difference in $T_{cp}$ could be expected as a shorter p(DMDOMAm) chain length will yield less hydrophobic polymer moieties on the conjugates. Below the $T_{cp}$, a slight increase in size (from 7.25 nm to 8.79 nm and from 6.93 nm to 13.18 nm for BSA-p(DMDOMAm)$^{DP100}$ and BSA-p(DMDOMAm)$^{DP200}$ respectively) is observed. This can be attributed to the presence of grafted polymer chains on the protein which increase the hydrodynamic radius. Above the $T_{cp}$, the protein-polymer conjugates form particles of approximately 48 and 187 nm for BSA-p(DMDOMAm)$^{DP100}$ and BSA-p(DMDOMAm)$^{DP200}$ respectively. This temperature-reversible transition between globules and fully soluble unimers suggests that no significant crosslinking occurred during polymerization. The critical micellar concentration (cmc) was in the same order of magnitude for both conjugates: 48 µg/mL and 51 µg/mL for BSA-p(DMDOMAm)$^{DP100}$ and BSA-p(DMDOMAm)$^{DP200}$ respectively (**Figure 6**).

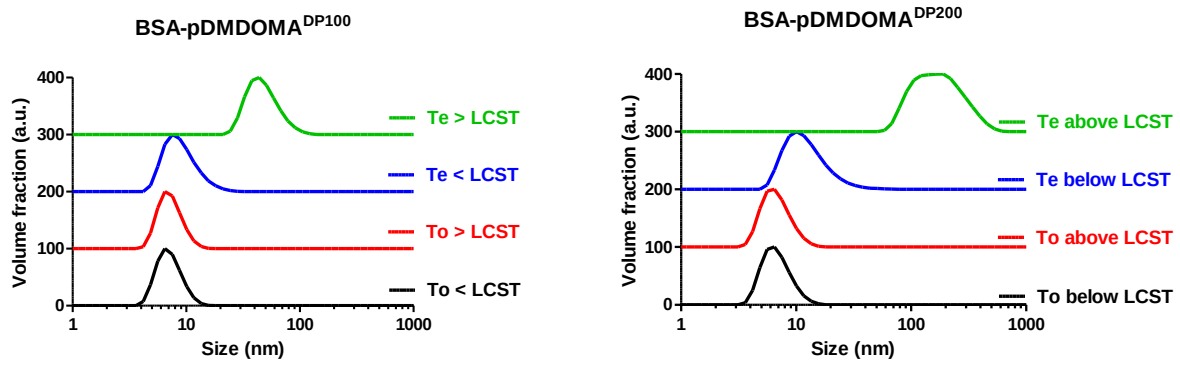


**Figure 4** Size distribution measured by DLS of the BSA-p(DMDOMAm) reaction mixtures before (T0) and after (Te) polymerization for a targeted DP of 100 and 200.

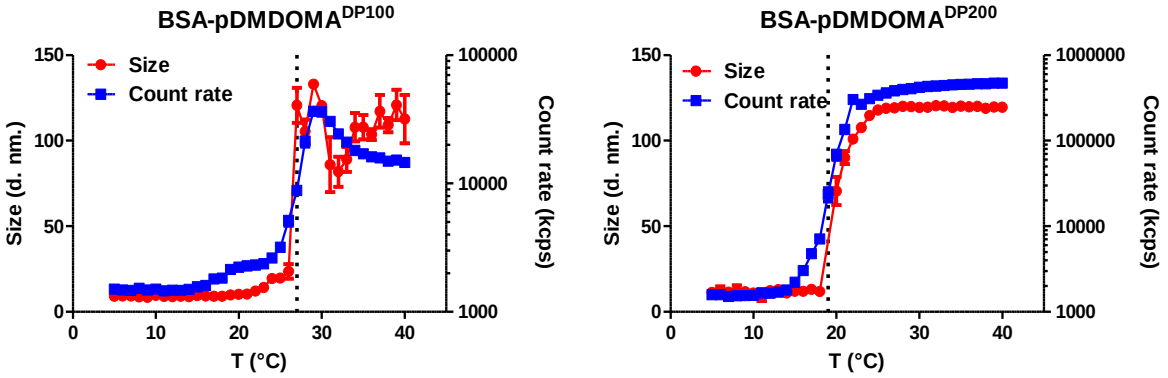


**Figure 5.** Volume mean diameter (red data points) and count rate (a measure for the light scattering intensity) (blue data points) of the BSA-p(DMDOMAm) conjugates as function of temperature, measured by DLS.

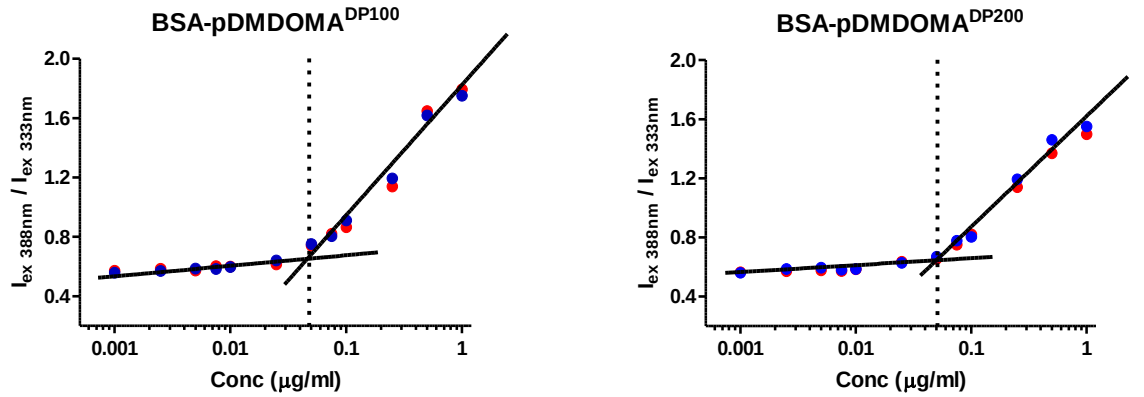


**Figure 6.** Intensity ratio of pyrene at 338 nm ($I_3$) and 333 nm ($I_1$) as function of the BSA-p(DMDOMAm) concentration determined by fluorescence spectroscopy at 25°C. The CMC was similar for BSA-p(DMDOMAm) conjugates with different polymer chain lengths: 48 µg/mL for DP100 and 51 µg/mL for DP200.

To investigate whether the dioxolane moieties allow the polymer-protein conjugates to undergo pH-triggered transition from amphiphilic structures into fully water soluble structures, we exposed the conjugates to acidic medium (50 mM HCl as proof of concept) at 37 °C and monitored the evolution of particle size and light scattering intensity by DLS. As shown in **Figure 7**, the light scattering intensity drops as function of time, indicating the hydrolysis of the hydrophobic dioxolane moieties into hydrophilic diol moieties resulted in a gradual dissolution of the self-assembled conjugates. In addition, **Figure 7** confirms that the protein-polymer conjugates lose their self-assembly capacities after hydrolysis, as their size at 37 °C returns to that of the non-hydrolyzed conjugates below their $T_{cp}$.

SDS-PAGE (**Figure 8**) and $^{1}$H-NMR (**Figure 9**) analysis of BSA, p(DMDOMAm) or BSA-p(DMDOMAm) suggests that hydrolysis of the ketal moieties and not protein hydrolysis is responsible for the pH-triggered transition from globules to unimers of the BSA-p(DMDOMAm) conjugates. No significant changes in gel retardation or lower molecular weight protein fractions that could result from protein hydrolysis were observed. By contrast, the $^{1}$H-NMR analysis of the p(DMDOMAm) homopolymer clearly revealed removal of the dimethyl groups on the dioxolane moieties after treatment with 50 mM HCl.

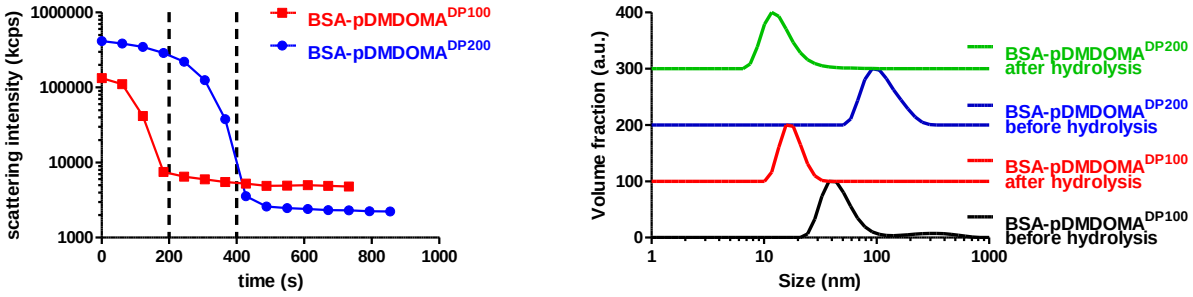


**Figure 7.** Light scattering intensity measured by DLS as function of time during the acid-catalyzed hydrolysis of the BSA-p(DMDOMAm) conjugates at 37 °C (left) and the corresponding size distribution curves before and after hydrolysis measured at 37 °C (right).

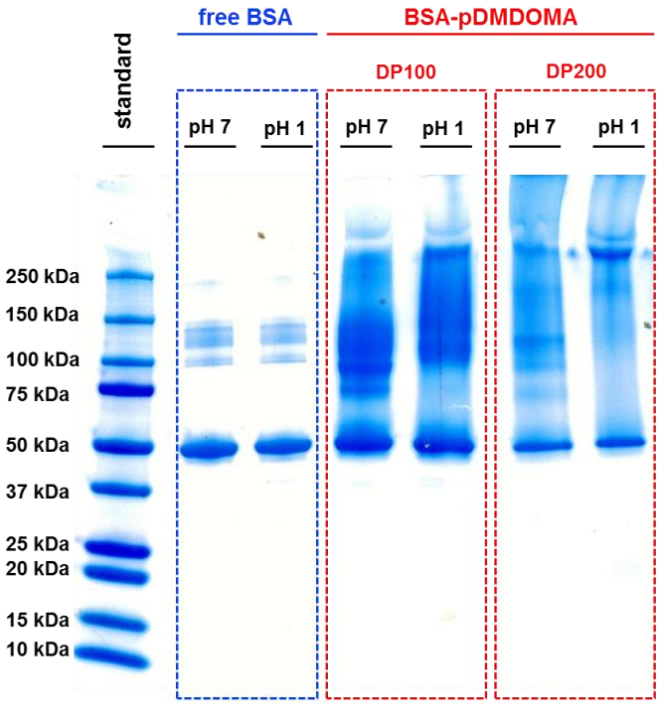


**Figure 8.** SDS-PAGE analysis of free BSA and BSA-p(DMDOMAm) conjugates treated with 50 mM HCl (pH 1), compared with corresponding untreated samples (pH 7).

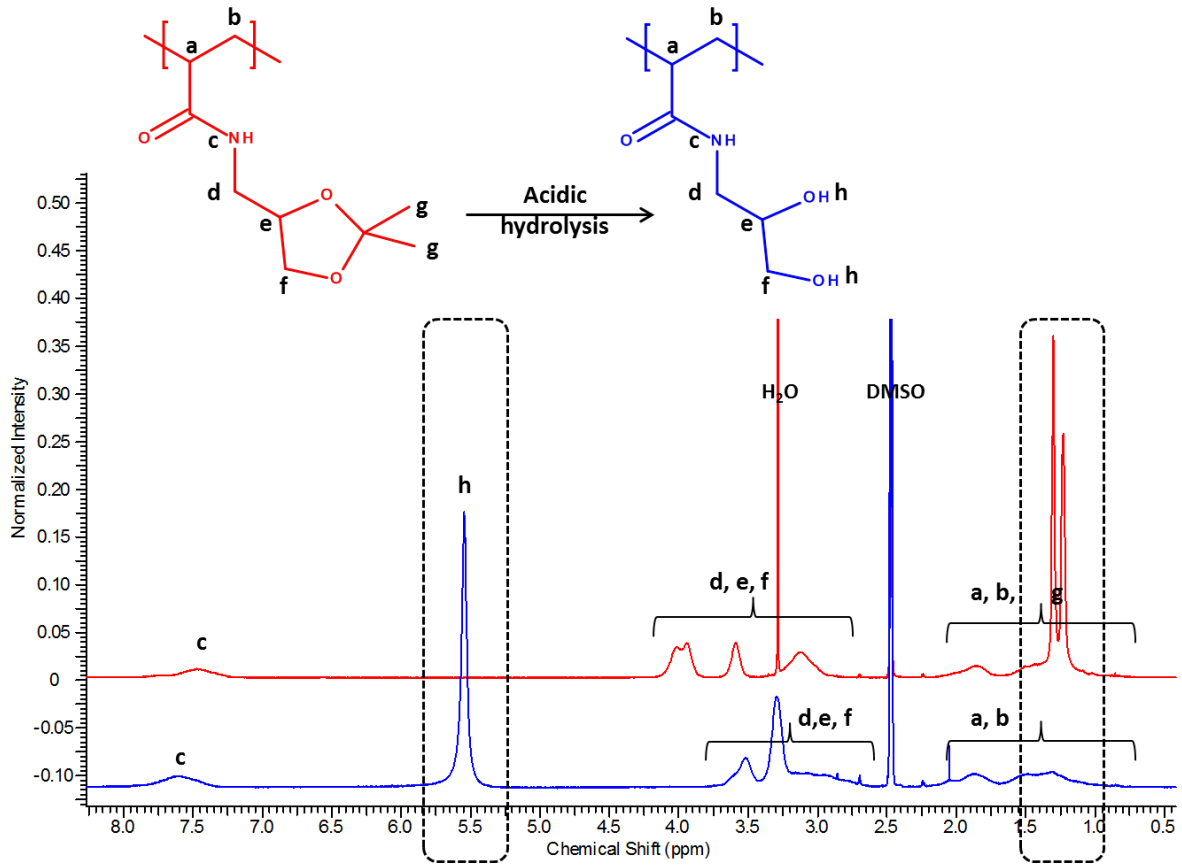


**Figure 9.** $^{1}$H-NMR spectra in $(CD_3)_2SO$ of p(DMDOMAm) before (red curve) and after (blue curve) treatment with 50 mM HCl. The spectra clearly show the removal of the dimethyl groups (g) on the dioxolane moieties by acidic hydrolysis, yielding hydroxyl groups (h).

In a second part of this chapter, we establish an *in vitro* proof-of-concept showing that p(DMDOMAm)-conjugation can be used for intracellular co-delivery of proteins and small hydrophobic molecules, loaded into the hydrophobic domains of the p(DMDOMAm) above its $T_{cp}$ (**Scheme 1**). For this purpose we used dendritic cells (DCs). These are the most potent class of antigen presenting cells of the immune system and a key target cell population for vaccination and immune-therapy.[9] First, the BSA-p(DMDOMAm) conjugates were fluorescently labeled with Cy5-NHS, that can bind to the lysine residues in the BSA backbone. Next the Cy5-BSA-p(DMDOMAm) particles were loaded via solvent displacement from ethanol with the fluorescent dye Cy3-alkyne, as a model hydrophobic molecule. Non-encapsulated Cy3-alkyne (i.e. precipitated particulates) was removed by filtration. As a control, the same procedure was repeated for PBS buffer and soluble BSA macroCTA.

Dendritic cells (immortalized DC2.4 cell line) were pulsed with the conjugates, and after overnight incubation analyzed by flow cytometry. **Figure 10** shows that particulate Cy5-BSA-p(DMDOMAm) is taken up more efficiently than soluble Cy5-BSA, as the mean fluorescence of the Cy5 channel is significantly higher for the Cy5-BSA-p(DMDOMAm) conjugates. Also the mean fluorescence in the Cy3 channel clearly indicates that formulation of the hydrophobic Cy3-alkyne dye with Cy5-BSA-p(DMDOMAm) conjugates results in higher cell uptake. To confirm whether the conjugates are internalized by the cells, rather than sticking to the cell surface, confocal microscopy imaging was performed. **Figure 11** shows that the Cy5-BSA-p(DMDOMAm) particles loaded with the Cy3-alkyne are indeed internalized by the dendritic cells. Additionally, a strong co-localization of the Cy3 and Cy5 channel is observed, suggesting that the BSA-p(DMDOMAm) conjugates act as delivery carrier for the hydrophobic Cy3-alkyne dye.

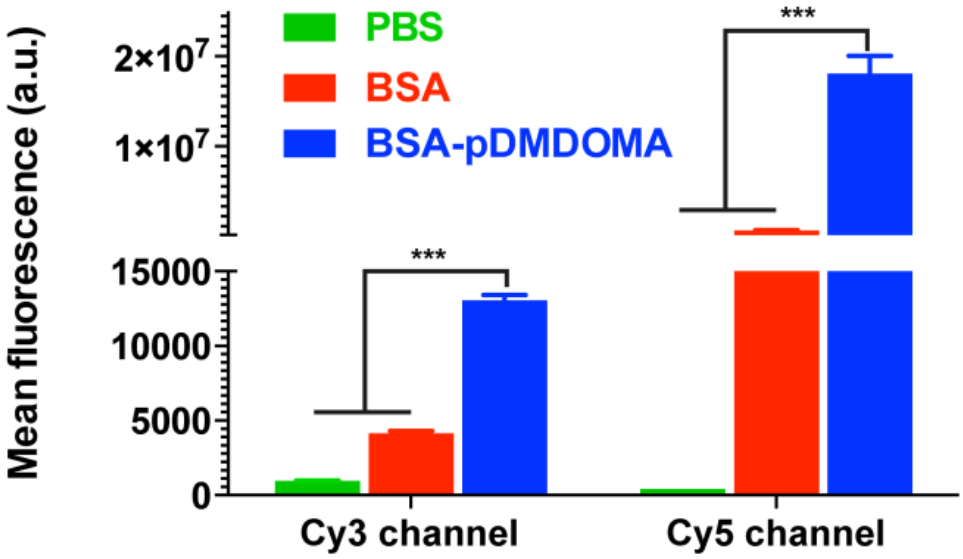


**Figure 10.** Mean cell fluorescence in Cy3 and Cy5 channel measured by flow cytometry of DC2.4 cells pulsed with Cy3-alkyne formulated in PBS, Cy5-BSA or Cy5-BSA-p(DMDOMAm).

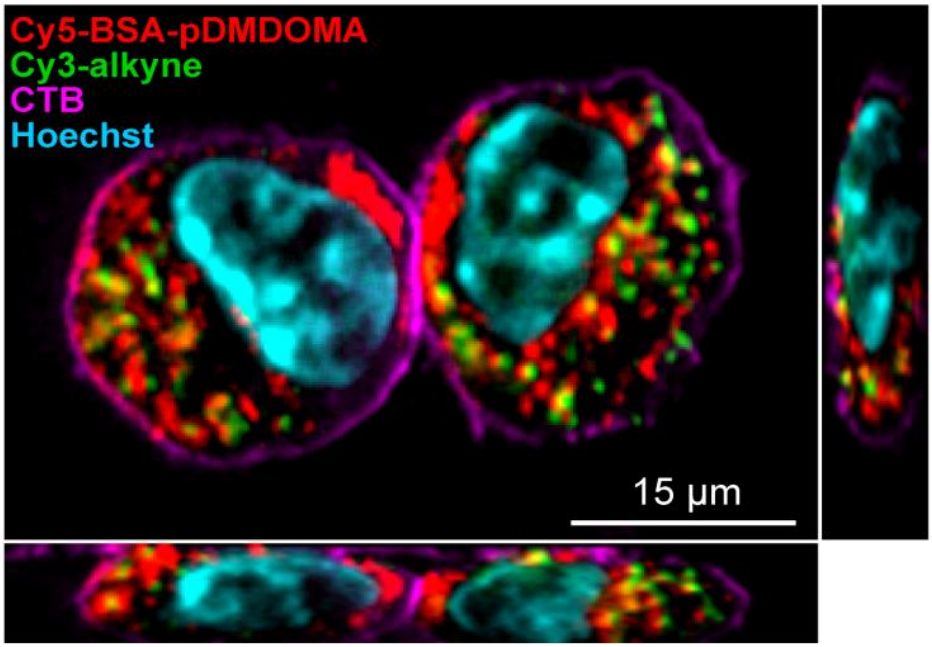


**Figure 11.** Confocal microscopy image of DC2.4 cells pulsed with Cy3-alkyne formulated in Cy5-BSA-p(DMDOMAm). The cell nucleus and cell membrane are stained with Hoechst and CTB respectively.

Next, we aimed at utilizing the BSA-p(DMDOMAm) system to deliver the hydrophobic immune-stimulatory molecule CL075.[37] CL075 triggers the Toll-like receptor 7, present on endosomes of DCs, and boosts cellular immune responses against tumors and intracellular pathogens.[38] CL075 is water-insoluble and precipitates from solution upon solvent displacement from ethanol into water. Formulation was performed similarly as for the model compound Cy3-alkyne. Samples were added to mouse bone marrow derived dendritic cells (BM-DCs) followed by analysis of the induction of the cell surface maturation markers MHCII and CD86 by flow cytometry. Control samples included PBS buffer and BSA macroCTA with and without CL075, as well as unloaded BSA-p(DMDOMAm) conjugates. Although the basal expression level of MHCII was already high for PBS treated DCs, only DC's treated with CL075 formulated in BSA-p(DMDOMAm) nanoparticles exhibited a significant further increase in MHCII expression. Similar, and even more outspoken, was the effect of CL075 formulated in BSA-p(DMDOMAm) nanoparticles on CD86 expression and on the co-expression of both MHCII and CD86 (**Figure 12**). These findings indicate that relative to PBS and native BSA, the BSA-p(DMDOMAm) conjugates possess sufficient amphiphilicity to encapsulate the hydrophobic CL075, while still allowing it to exert its biological activity on DCs.

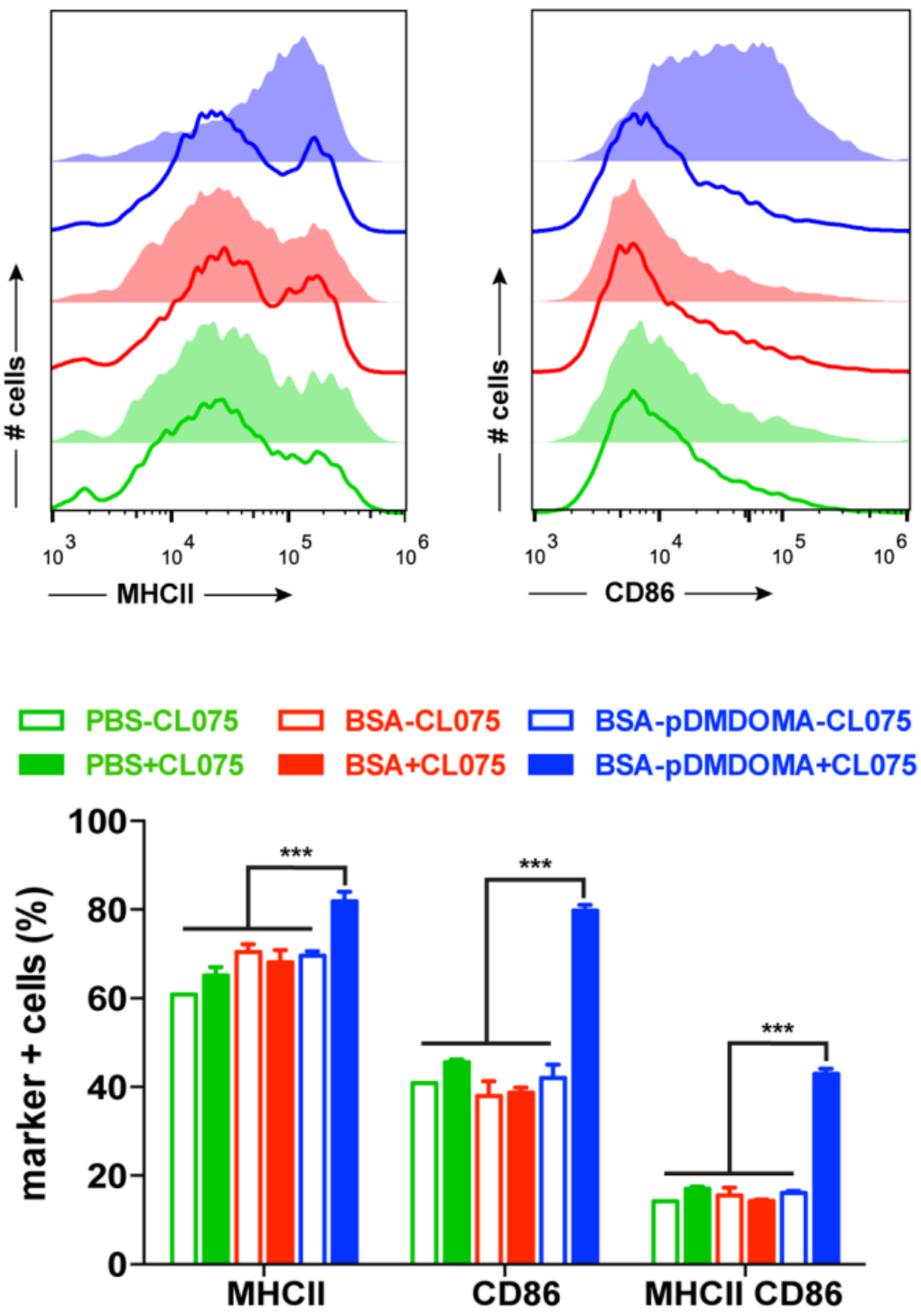


**Figure 12.** Flow cytometry histograms (top) and quantification (bottom) of maturation marker MHCII and CD86 in DCs pulsed with CL075 formulated in PBS, BSA and BSA-p(DMDOMAm) and the corresponding negative controls. (***; p<0,001)

## Conclusions

In conclusion, we have demonstrated that transiently soluble and acid-degradable polymer-protein conjugates could be synthesized via a 'grafting-from' RAFT approach. Bovine serum albumin (BSA) was reacted with a pentafluorophenyl (PFP) functionalized CTA which allowed polymerization of the acid-labile DMDOMAm monomer from this protein macroCTA, as evidenced by SDS-PAGE. The resulting protein-polymer conjugates exhibited thermoresponsive behavior and self-assembled into nanoparticles above their $T_{cp}$. When the conjugates were exposed to acidic medium, hydrolysis of the dioxolane moieties allowed the polymer-protein conjugates to undergo pH-triggered transition from nanoparticulates into fully water soluble structures. In addition, we have demonstrated these transiently soluble and acid-degradable polymer-protein conjugates can be used for intracellular delivery of proteins and hydrophobic molecules. *In vitro* cell experiments in DCs demonstrated that particulate BSA-p(DMDOMAm) was taken up more efficiently than soluble BSA. Formulating the hydrophobic Cy3-alkyne within the hydrophobic core of these BSA-DMDOMAm conjugates resulted in higher cell uptake of the dye. Analogously, the immune-stimulatory molecule CL075 was loaded into the protein-polymer conjugates to induce maturation in BM-DCs. A significant up-regulation of maturation markers MHCII and CD86 was only observed when CL075 was formulated in BSA-p(DMDOMAm) nanoparticles.

## References


1 Pelegri-O'Day, E. M., Lin, E. W. & Maynard, H. D. Therapeutic Protein-Polymer Conjugates: Advancing Beyond PEGylation. *J. Am. Chem. Soc.* **136**, 14323-14332 (2014).

2 Elsabahy, M. & Wooley, K. L. Design of polymeric nanoparticles for biomedical delivery applications. *Chem. Soc. Rev.* **41**, 2545-2561 (2012).

3 Boyer, C. *et al.* An overview of protein-polymer particles. *Soft Matter* **7**, 1599-1614 (2011).

4 Li, H. M. *et al.* Protein conjugation of thermoresponsive amine-reactive polymers prepared by RAFT. *Polym. Chem.* **2**, 323-327 (2011).

5 Hubbell, J. A., Thomas, S. N. & Swartz, M. A. Materials engineering for immunomodulation. *Nature* **462**, 449-460 (2009).

6 Moon, J. J., Huang, B. & Irvine, D. J. Engineering Nano- and Microparticles to Tune Immunity. *Advanced Materials* **24**, 3724-3746 (2012).

7 De Koker, S. *et al.* Designing polymeric particles for antigen delivery. *Chem. Soc. Rev.* **40**, 320-339 (2011).

8 Kasturi, S. P. *et al.* Programming the magnitude and persistence of antibody responses with innate immunity. *Nature* **470**, 543-547 (2011).

9 Banchereau, J. *et al.* Immunobiology of dendritic cells. *Annu. Rev. Immunol.* **18**, 767-811 (2000).

10 Rappuoli, R. From Pasteur to genomics: progress and challenges in infectious diseases. *Nat Med* **10**, 1177-1185 (2004).

11 Parmiani, G. *et al.* Cancer Immunotherapy With Peptide-Based Vaccines: What Have We Achieved? Where Are We Going? *Journal of the National Cancer Institute* **94**, 805-818 (2002).

12 Moon, J. J. *et al.* Interbilayer-crosslinked multilamellar vesicles as synthetic vaccines for potent humoral and cellular immune responses. *Nat. Mater.* **10**, 243-251 (2011).

13 Scott, E. A. *et al.* Dendritic cell activation and T cell priming with adjuvant- and antigen-loaded oxidation-sensitive polymersomes. *Biomaterials* **33**, 6211-6219 (2012).

14 Coffman, R. L., Sher, A. & Seder, R. A. Vaccine Adjuvants: Putting Innate Immunity to Work. *Immunity* **33**, 492-503 (2010).

15 Narayan, R. *et al.* Immunomodulation by Imiquimod in Patients with High-Risk Primary Melanoma. *J. Invest. Dermatol.* **132**, 163-169 (2012).

16 Reddy, S. T. *et al.* Exploiting lymphatic transport and complement activation in nanoparticle vaccines. *Nat. Biotechnol.* **25**, 1159-1164 (2007).

17 Liu, H. P. *et al.* Structure-based programming of lymph-node targeting in molecular vaccines. *Nature* **507**, 519-522 (2014).

18 Kwon, Y. J. *et al.* In vivo targeting of dendritic cells for activation of cellular immunity using vaccine carriers based on pH-responsive microparticles. *Proc. Natl. Acad. Sci. U. S. A.* **102**, 18264-18268 (2005).

19 Zou, Y. Q., Brooks, D. E. & Kizhakkedathu, J. N. A novel functional polymer with tunable LCST. *Macromolecules* **41**, 5393-5405 (2008).

20 Zhang, Q. L. *et al.* Dual pH- and temperature-responsive RAFT-based block co-polymer micelles and polymer-protein conjugates with transient solubility. *Polym. Chem.* **5**, 1140-1144 (2014).

21 Louage, B. *et al.* Degradable Ketal-Based Block Copolymer Nanoparticles for Anticancer Drug Delivery: A Systematic Evaluation. *Biomacromolecules* **16**, 336-350 (2015).

22 Braunecker, W. A. & Matyjaszewski, K. Controlled/living radical polymerization: Features, developments, and perspectives. *Prog. Polym. Sci.* **32**, 93-146 (2007).

23 Nicolas, J., Mantovani, G. & Haddleton, D. M. Living radical polymerization as a tool for the synthesis of polymer-protein/peptide bioconjugates. *Macromol. Rapid Commun.* **28**, 1083-1111 (2007).

24 Chiefari, J. *et al.* Living free-radical polymerization by reversible addition-fragmentation chain transfer: The RAFT process. *Macromolecules* **31**, 5559-5562 (1998).

25 Heredia, K. L. *et al.* Reversible siRNA-polymer conjugates by RAFT polymerization. *Chem. Commun.*, 3245-3247 (2008).

26 Vanparijs, N. *et al.* Polymer-protein conjugation via a 'grafting to' approach - a comparative study of the performance of protein-reactive RAFT chain transfer agents. *Polym. Chem.* (2015).

27 De, P. *et al.* Temperature-regulated activity of responsive polymer-protein conjugates prepared by grafting-from via RAFT polymerization. *J. Am. Chem. Soc.* **130**, 11288-+ (2008).

28 Boyer, C. *et al.* Well-defined protein-polymer conjugates via in situ RAFT polymerization. *J. Am. Chem. Soc.* **129**, 7145-7154 (2007).

29 Gao, W. P. *et al.* In situ growth of a stoichiometric PEG-like conjugate at a protein's N-terminus with significantly improved pharmacokinetics. *Proc. Natl. Acad. Sci. U. S. A.* **106**, 15231-15236 (2009).

30 Canton, I. & Battaglia, G. Endocytosis at the nanoscale. *Chem. Soc. Rev.* **41**, 2718-2739 (2012).

31 Shen, Z. H. *et al.* Cloned dendritic cells can present exogenous antigens on both MHC class I and class II molecules. *J. Immunol.* **158**, 2723-2730 (1997).

32 De Koker, S. *et al.* Polyelectrolyte Microcapsules as Antigen Delivery Vehicles To Dendritic Cells: Uptake, Processing, and Cross-Presentation of Encapsulated Antigens. *Angew. Chem.-Int. Edit.* **48**, 8485-8489 (2009).

33 Randolph, G. J. *et al.* Differentiation of Phagocytic Monocytes into Lymph Node Dendritic Cells In Vivo. *Immunity* **11**, 753-761 (1999).

34 Charleux, B. *et al.* Polymerization-Induced Self-Assembly: From Soluble Macromolecules to Block Copolymer Nano-Objects in One Step. *Macromolecules* **45**, 6753-6765 (2012).

35 Ladmiral, V. *et al.* Polymerization-Induced Self-Assembly of Galactose-Functionalized Biocompatible Diblock Copolymers for Intracellular Delivery. *J. Am. Chem. Soc.* **135**, 13574-13581 (2013).

36 Karagoz, B. *et al.* Polymerization-Induced Self-Assembly (PISA) - control over the morphology of nanoparticles for drug delivery applications. *Polym. Chem.* **5**, 350-355 (2014).

37 Mancini, R. J. *et al.* Directing the Immune System with Chemical Compounds. *ACS Chem. Biol.* **9**, 1075-1085 (2014).

38 Spranger, S. *et al.* Generation of Th1-Polarizing Dendritic Cells Using the TLR7/8 Agonist CL075. *J. Immunol.* **185**, 738-747 (2010).

# Chapter 6

# Hydrogel nanocapsules for lymph node targeted vaccine delivery

In collaboration with

**Prof. Frank Caruso** from the University of Melbourne, Australia

**Dr. Lorenzo Albertazzi** from the Institute for Bioengineering of Catalonia, Spain and Eindhoven University of Technology, Netherlands

Parts of this chapter were published in:

**Engineering hydrogel nanocapsules for lymph node targeted vaccine delivery**
S. De Koker,* J. W. Cui,* N. Vanparijs,* L. Albertazzi, J. Grooten, F. Caruso, B. G. De Geest
*Angewandte Chemie-International Edition* **2016**, 55, 1334-1339

**Super Resolution Imaging of Nanoparticles Cellular Uptake and Trafficking**
D. van der Zwaag,* N. Vanparijs,* S. Wijnands, R. De Rycke, B. G. De Geest, L. Albertazzi, *ACS Applied Materials & Interfaces* **2016**, 8, 6391-6399

* these authors contributed equally as first author

## Abstract

The induction of antigen-specific adaptive immunity exclusively occurs in lymphoid organs. As a consequence, the efficacy by which vaccines reach these tissues strongly affects the potency of the vaccine. In this respect, small nanoparticles have shown to rapidly reach the lymph nodes through passive drainage via the lymphatics. Therefore, nanoparticles were prepared by the Caruso lab by infiltrating mesoporous silica particles (ca. 200 nm) with poly(methacrylic acid), followed by disulfide-based crosslinking and template removal. PEGylation of these nanoparticles did not affect their cellular association *in vitro*, but dramatically improved their lymphatic drainage *in vivo*. In this chapter we will discuss the interaction between the hydrogel nanoparticles and DCs *in vitro* and provide an overview of our main findings *in vivo*. Additionally, a head-to-head comparison of TEM, STORM and confocal microscopy was performed, for their applicability in intracellular imaging of such nanomedicines.

## Introduction

Modulating T and B cell immunity not only is key to the development of improved and new vaccines against pathogens, but also holds great promise to treat malignancies, autoimmune diseases and allergies.[1,2] Priming of T cell responses requires the presentation of antigens by dendritic cells (DCs), in the format of processed peptide fragments loaded onto major histocompatibility complexes. Priming of B cells and their differentiation into antibody secreting plasma cells, relies on surface triggering of the B cell receptor (BCR) by antigens. As mentioned in **Chapter 1** and **5**, priming of naïve T and B cells can be dramatically enhanced by delivering antigens formulated as nano- or microparticles.[1-5] Compared to soluble antigens, particulate vaccines enhance the quality and the magnitude of the adaptive immune response by acting on different levels. At the level of the DC, particulate vaccines increase antigen uptake and improve antigen presentation to T cells qualitatively and quantitatively. Peptide fragments of particulate antigens are loaded onto MHCII and MHCI molecules and thus can evoke both CD4 and CD8 T cell responses. By contrast, soluble antigens are almost exclusively presented via MHCII molecules, resulting in an immune response restricted to CD4 T cells. At the level of the B cell, the display of multiple antigen

copies at the particle surface dramatically increases activation of B cells by simultaneous triggering of multiple BCRs on the B cell surface.[6]

T cell and B cell priming exclusively occur in secondary lymphoid organs. As a consequence, the efficacy with which vaccine carriers reach these sites constitutes a critical determinant of their efficacy to induce adaptive immunity and thus ultimately affects the protective efficacy of the vaccine.[7-10]As vaccines are commonly delivered by intramuscular or subcutaneous injection, lymph nodes are the lymphoid organs vaccines need to target. To move from the site of injection to lymph nodes, vaccines must be either transported actively to the lymph nodes by tissue DCs; or they need to move along the interstitial flow, across the extracellular matrix, into the lymphatics.[11] As the latter process does not involve cellular uptake for transport, it is called passive drainage. The way particles drain to lymph nodes, and the efficacy with which they reach antigen-presenting cells, mainly depends on their *in situ* mobility after injection.

Particles that show limited mobility in the extracellular matrix, rely on local DCs recruited to the injection site for uptake and transport. Such particles become surrounded by fibrous tissue and become engulfed predominantly by tissue macrophages. As a consequence, only a minor fraction of particle-delivered antigens will reach the lymph nodes and contribute to the induction of the antigen-specific immune response. Moreover, the long-term presence of particles at the injection site creates an antigen depot that could cause exhausted T cell responses, and could hamper vaccine elicited protection.[12,13] By contrast, particles with high mobility in the extracellular matrix can move along the interstitial flow and thus have better potential to reach the lymph nodes, either after uptake by tissue DCs or after passive entry into the lymphatics. Similar requirements are needed for nanomaterial-based sentinel lymph node mapping.[14] However, there is much debate on the size and physicochemical properties of particles that is required to ensure optimal lymph node targeting. Moreover, particle uptake *in vitro* often is a poor predictor of in vivo particle mobility.

In this context, PEGylation [i.e. surface modification with poly(ethyleneglycol)] might improve the mobility of nanocarriers in the extracellular matrix following subcutaneous injection. PEGylation has shown to be a successful strategy to increase the half-life of proteins and nanoparticles in systemic circulation after intravenous injection, by reducing the interaction with macrophages and serum proteins.[15] To assess the impact of PEGylation

on the lymphatic drainage properties of reduction-sensitive hydrogel nanoparticles and its influence on the subsequent priming of T cells, the Caruso group prepared PEGylated hydrogel nanoparticles. In this chapter, we will discuss the *in vitro* cell experiments and the main *in vivo* data that were obtained, and highlight the potential of engineered hydrogel nanoparticles for the lymphatic delivery of antigens and immune-modulating compounds. Additionally, we will elaborate on the use of Two-color Stochastic Optical Reconstruction Microscopy (STORM) for the direct visualization of the nanoparticle uptake mechanism and the intracellular tracking of nanoparticles by dendritic cells.

## Materials and methods

### *Materials*

Unless otherwise noted, all chemicals were purchased from Sigma-Aldrich. The PEGylated hydrogel nanoparticles were synthesized by our collaborators according to previously reported methods[16-18] and is discussed in the corresponding paper.[19] The immortalized dendritic cell line DC2.4 was a kind gift from Dr. Kenneth Rock (Dana Farber Cancer Institute, now at University of Massachusetts Medical School).[20] Bone marrow derived dendritic cells were obtained as previously reported.[21] Cell culture medium and supplements, Hoechst and Cholera Toxin Subunit B, Alexa Fluor® 647 Conjugate (CTB-AF647) were purchased from Life Technologies.

### *Microscopy*

Confocal images were recorded on a Leica DMI6000B inverted microscope equipped with a 10 X and 63x (1.40 NA) oil immersion objective, and coupled to an Andor DSD2 confocal scanner. Transmission electron microscopy images were viewed on a 1010 (JEOL, Tokyo, Japan).

STORM images were acquired using a Nikon N-STORM 427 system configured for total internal reflection fluorescence (TIRF) imaging. Fluorophores were excited by illuminating the sample with the 647 nm (~160 mW), 561 nm 431(~80 mW), and 488 nm (~80 mW) laser lines built into the microscope. Fluorescence was collected by means of a Nikon 100x, 1.4NA oil immersion objective and passed through a quad-band-pass dichroic

filter (97335 Nikon). Images were recorded onto a 256 × 256 pixel region (pixel size 170 nm) of a EMCCD camera (ixon3, Andor). Single molecules localization movies were analyzed with NIS element 437Nikon software.

***In vitro cell uptake of PEGylated hydrogel nanoparticles***

DC2.4 cells (immortalized dendritic cell line) were cultured in RPMI-glutamax, supplemented with 10% FBS, 1 mM sodium pyruvate, 10 mM HEPES buffer, 0.05 mM 2-mercaptoethanol, MEM NEAA and antibiotics (50 units/mL penicillin and 50 µg/mL streptomycin). Cells were incubated at 37 °C in an controlled, sterile environment of 95% relative humidity and 5% CO2. For FACS experiments, DC2.4 cells were seeded into 24-well titer plates (250 000 cells per well, suspended in 0.95 mL of culture medium) and incubated overnight to allow cell sedimentation and subsequent adhesion to the bottom of the wells. Next, 50 µL of the PMA based particles (5E9 particles/mL) was added to the cells (1000 particles per cell) on ice or at 37°C respectively. After 3h incubation, the wells were aspirated, washed with 1 mL of PBS and incubated with 500 µL of Cell Dissociation Buffer (15 min., 37°C). The cell suspensions were transferred into Eppendorf tubes and immediately centrifuged (350 g, 10 min., 5 °C). Finally, the supernatant was aspirated and the cell pellets were suspended in 200 µL of PBS and kept on ice to maintain cell integrity. FACS was performed on a BD Accuri C6 (BD Biosciences). The data were processed by FlowJo software.

For confocal and STORM microscopy, DC2.4 cells were seeded into Willco-Dish glass bottom dishes (50 000 cells, suspended in 200 µL of culture medium) and incubated for 3h (confocal) and overnight (STORM) respectively. Next, 10 µL of the of the PMA based particles (5E9 particles/mL) was added to the cells (1000 particles per cell), followed by 24 h of incubation. Hoechst (only for confocal, not for STORM) and CTB-AF647 staining was carried out simultaneously on fixed cells. In summary, culture medium was aspirated and cells were washed with PBS. Next, 200 µL of 4 % paraformaldehyde was added and allowed to fixate for 30 min. A staining solution was prepared by adding Hoechst (10 µL of a 1 mg/mL stock in DMSO) and CTB-AF647 (5 µL of a 1 mg/mL stock in PBS) to a PBS buffer containing 1% of BSA (2.5 mL). After aspiration and washing, 200 µL of this staining solution was added to the fixed cells and incubated for 40 minutes at room temperature. Finally, the samples were washed with 1% BSA PBS buffer.

***Performance comparison of TEM, STORM and confocal microscopy***

To compare the performance of 3 different microscopy techniques, DCs were incubated with a mixture of (i) 300 nm Alexa647-labeled OVA-coated NPs; (ii) 80 nm Alexa647-labeled carboxylic acid NPs; and (iii) 300 nm Cy3-labeled amino beads, followed by STORM, confocal microscopy and TEM imaging. These nanoparticles (NP) were prepared by the Albertazzi lab and is described in the corresponding paper.[22] The samples for STORM and confocal microscopy were prepared in a similar manner as described in the previous paragraph. For TEM, DC2.4 cells were seeded into 24-well plates containing glass coverslips inside the wells (250 000 cells, suspended in 1 mL of culture medium) and cultured overnight at 37 °C and 5% CO2. Next, NP solution was added, followed by 24 h of culturing at 37° and 5% CO2. Culture medium was aspirated, and cells were washed with PBS. Next, 1 mL of a fixing solution containing 4% paraformaldehyde and 2.5% glutaraldehyde in 0.1 m sodium cacodylate buffer (pH 7.2) was added and allowed to fixate for 4 h at room temperature, followed by fixation overnight at 48 °C. After washing three times for 20 min with buffer solution, cells were dehydrated through a graded ethanol series, including a bulk staining with 1% uranylacetate at the 50% ethanol step followed by embedding in Spurr's resin. Ultrathin sections of a gold interference color were cut using an ultramicrotome (ultracut E/ 464 Reichert-Jung), followed by a poststaining with uranyl acetate and lead citrate in a Leica ultrastainer, and collected on Formvar-coated copper slot grids.

## Result and discussion

Mesoporous silica (MS) nanoparticles with an average size of 200 nm were synthesized according to a previously reported method.[16,17] Hydrogel nanoparticles are fabricated by infiltrating amine-modified MS nanoparticles with pyridine dithioethylamine (PDA)-modified poly(methacrylic acid) ($PMA^{PDA}$). Subsequently, cysteamine (SH-) modified poly(methacrylic acid) ($PMA^{SH}$) is infiltrated, leading to crosslinking by disulfide exchange (**Figure 1**).[18] To track particle uptake, fluorescent labeling was performed with Alexa Fluor 488-cadaverine (AF488) prior to dissolution of the silica template particles in buffered HF solution. Since there are both residual thiols and pyridyldisulfides remaining in the PMA nanoparticles, PEGylation was performed by grafting maleimide-functionalized

poly(ethylene glycol)($PEG^{MAL}$) and thiol-functionalized PEG ($PEG^{SH}$) onto the PMA nanoparticles.

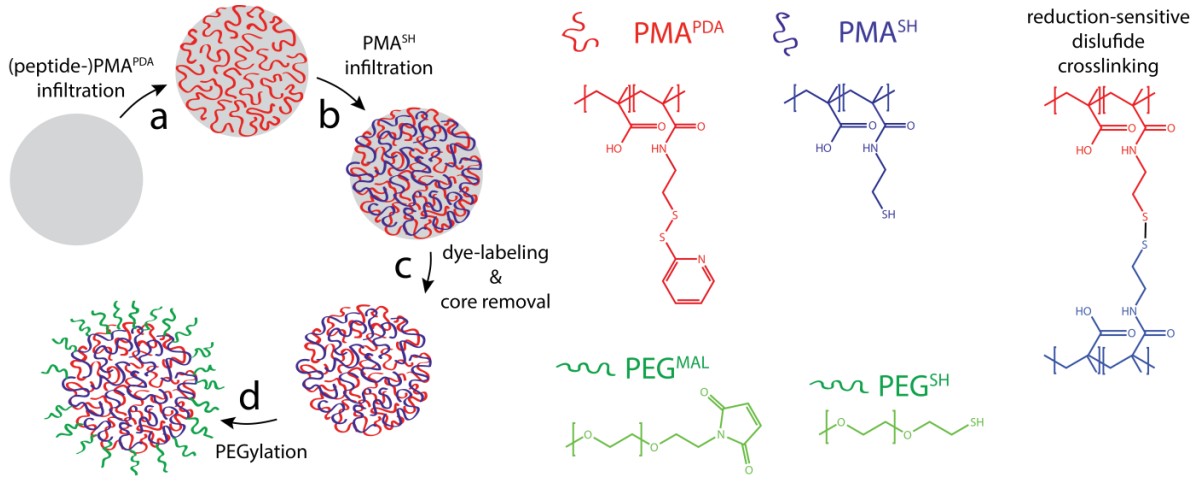


**Figure 1.** Schematic representation of the assembly of hydrogel nanoparticles. **(a)** Infiltration of MS templates (ca. 200 nm) with $PMA^{PDA}$. **(b)** Crosslinking of the $PMA^{PDA}$ by infiltration of $PMA^{SH}$ and disulfide exchange. **(c)** Template dissolution. **(d)** PEGylation with $PEG^{MAL}$ by thioether formation. In the case of non-PEGylated nanoparticles, step d is omitted.

To investigate the interaction between the hydrogel nanoparticles and DCs *in vitro*, we incubated DCs with PMA and PEG-PMA nanoparticles, followed by confocal microscopy and quantitative analysis using flow cytometry (FACS). Confocal microscopy **(Figure 2A)** of the cell membrane, stained by AlexaFluor647-conjugated cholera toxin subunit B (AF647-CTB), demonstrated massive internalization of the nanoparticles by DCs. No obvious differences in cell interaction between both types of nanoparticles were observed from these images. **Figure 2B** shows flow cytometry data in terms of the percentage of nanoparticle-associated cells (B1) and their mean fluorescence (B2). Nanoparticle uptake appears to proceed in an energy-dependent fashion, since minimal cellular association occurred at 4 °C, but significantly increased at 37 °C without any difference in nanoparticle–cell association between PMA and PEG-PMA nanoparticles.

To gain more insight into the intracellular localization of the nanoparticles by DCs, we used stochastic optical reconstruction microscopy (STORM), a super-resolution microscopy technique that allows sub-diffraction-limited features to be resolved.[23] **Figure 3A** and **B** show a whole DC and part of a DC, respectively, whereas **Figure 3C** depicts a series of relevant events during the internalization process of the nanoparticles. These pictures show at high resolution the engulfment of the nanoparticles by the plasma membrane (**Figure 3C1**), lipid

raft-mediated routing (**Figure 3C2**) and finally storage of the nanoparticles in endo/lysosomal vesicles (**Figure 3C3**). The most striking feature of these images is that they enable imaging at single-particle and single-endo/phago/lysosome resolution. CTB specifically binds to the ganglioside GM1 that is present on the plasma membrane of DCs, in particular at sites that are involved in lipid raft-mediated endocytosis.[24] In this case, it also provides an avenue for labeling lipid rafts and becomes incorporated in endo/lysosomal membranes, as shown in **Figure 3C**. This set of data is, to the best of our knowledge, amongst the first showing the potential of super-resolution microscopy for assessing the intracellular fate of nanoparticles. Note that trafficking of antigen in intracellular vesicles does not hamper efficient antigen presentation.[25]

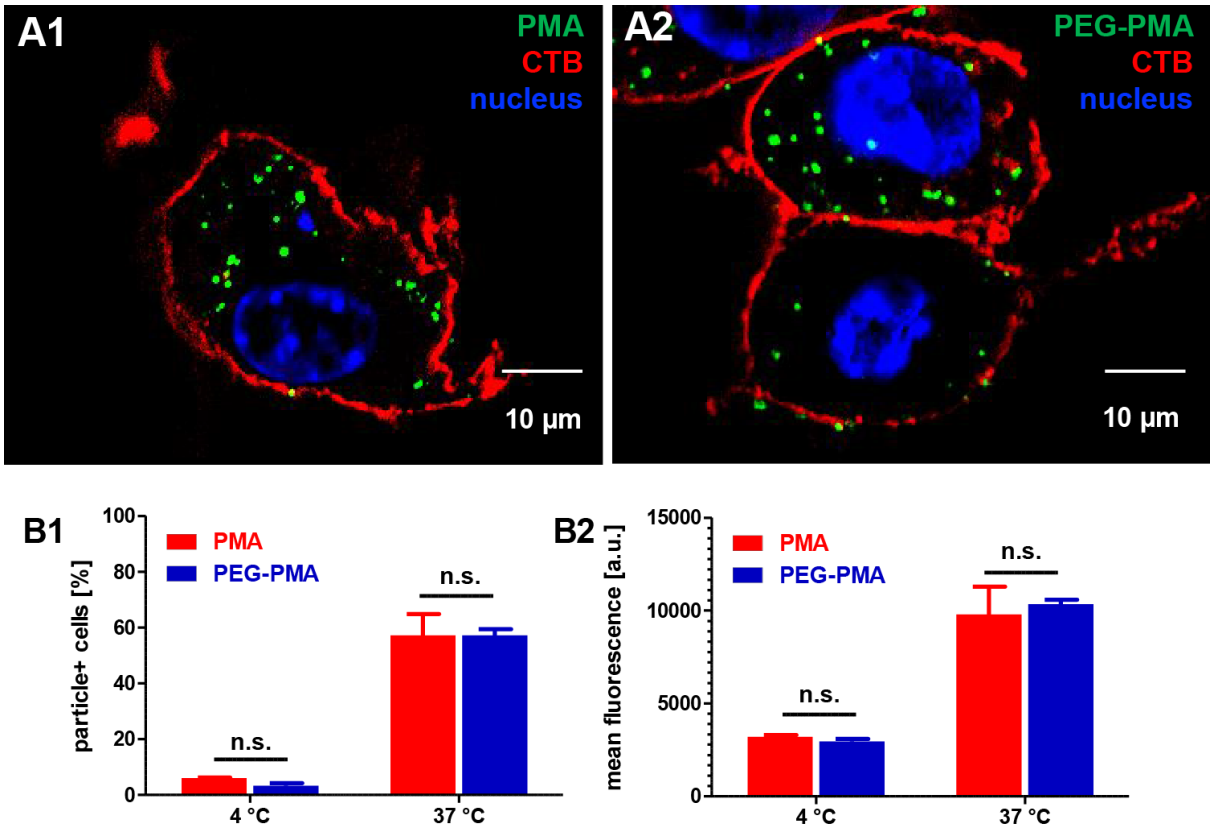


**Figure 2.** In vitro uptake of nanoparticles by DCs. **(A)** Confocal microscopy and **(B)** flow cytometry data of DCs pulsed with PMASH and PEGPMA nanoparticles (n=3). Particles are labelled with AF488, the cell membrane is stained by AF647-CTB and cell nuclei were stained with Hoechst.

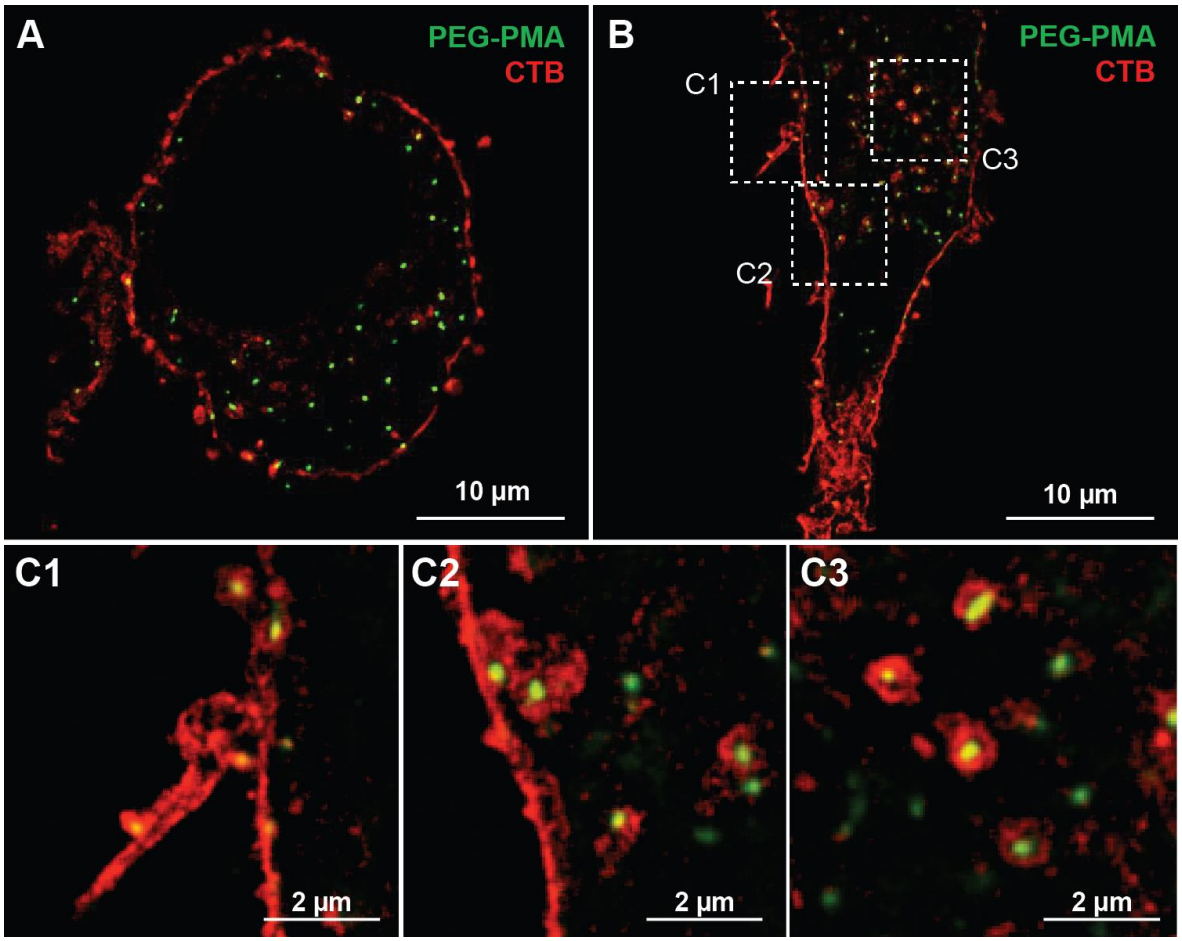


**Figure 3**. STORM data of PEGPMA nanoparticles internalized by DCs as illustrated for **(A)** an entire DC and **(B)** part of a DC. Panels **(C1–3)** highlight different stages during the internalization process of the nanoparticles: **(C1)** Engulfment of nanoparticles by the plasma membrane. **(C2)** Intracellular routing and **(C3)** storage in endo/lysosomal vesicles. Particles are labelled with AF488 and the cell membrane is stained by AF647-CTB.

Although PEGylation did not affect the uptake of 200 nm sized PMA and PEG-PMA nanoparticles by DCs *in vitro*, it might significantly enhance their mobility and lymph node drainage behavior *in vivo*. Therefore, *in vivo* experiments in mice were performed. Subcutaneous administration of nanoparticles in the footpad resulted in a strongly improved lymph node transportation of PEGylated hydrogel nanoparticles compared to their non-PEGylated counterparts. Significantly more nanoparticle-positive DCs and B cells were measured in the draining lymph nodes, and the number of particles on a cell-per-cell basis dramatically increased, especially within the migratory DCs population that originates from the injection site. This enhanced lymphatic transportation of PEG-PMA nanoparticles can clearly be appreciated from the tissue section of the draining popliteal lymph nodes shown in **Figure 4**. The increased presence of particles in the lymph nodes resulted in increased

priming of antigen-specific T cells when a CD8 peptide epitope was covalently attached to the nanoparticles. We will not elaborate on these data in the current chapter, but they are thoroughly discussed in the corresponding paper.[19]

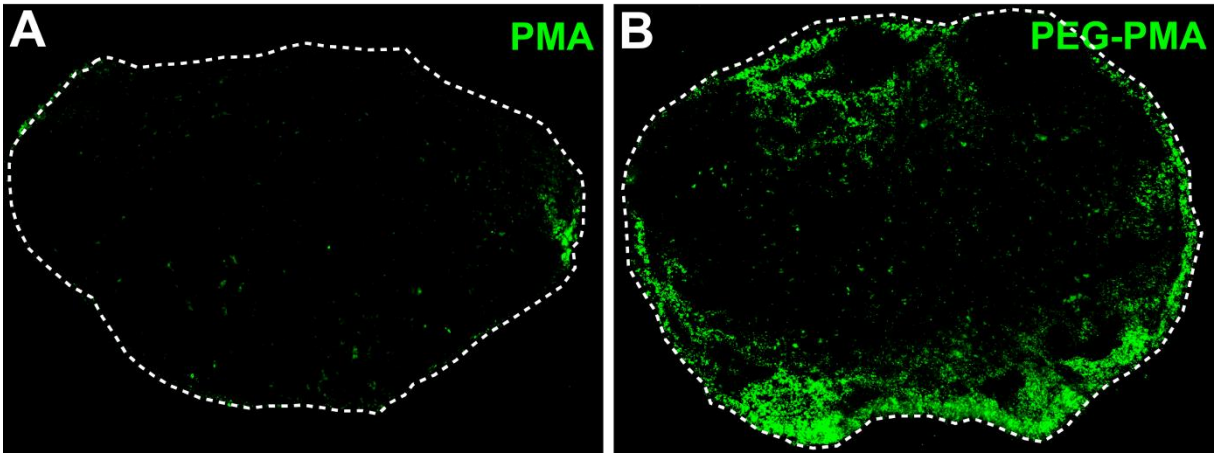


**Figure 4.** Fluorescence microscopy of lymph nodes of mice injected with **(A)** PMA and **(B)** PEG-PMA nanoparticles, respectively. The dashed white lines are drawn to distinguish the contours of the lymph nodes.[19]

To fully appreciate the benefit STORM can offer for intracellular imaging of nanomedicines, we designed an experiment to be challenging for confocal and electron microscopy. DCs were incubated with a mixture of (i) 300 nm Alexa647-labeled OVA-coated NPs; (ii) 80 nm Alexa647-labeled carboxylic acid NPs; and (iii) 300 nm Cy3-labeled amino beads, followed by STORM, confocal microscopy, and TEM imaging as shown schematically in **Figure 5A**. The mixture of these three species represents a good benchmark to evaluate the ability of the different techniques to resolve differences in NP size and color. **Figure 5B** shows TEM, STORM, and confocal images of NP-pulsed dendritic cells; and demonstrates that for all the techniques it is possible to visualize particle internalization.

Whereas TEM does yield a high resolution, albeit with some issues for soft materials that have limited contrast upon uranyl acetate or osmium tetrachloride staining, TEM does not yield any information on the nanoparticle color and thus surface-functionalization. This is showcased in the lower panel of **Figure 5B**. The excellent resolution of TEM allows for discriminating between particles of different sizes, while at the same time solving the morphologies of the cellular structures in the surroundings, e.g. endosomal vesicles or plasma membrane. However, particles of the same size but different chemical functionality are not distinguishable.

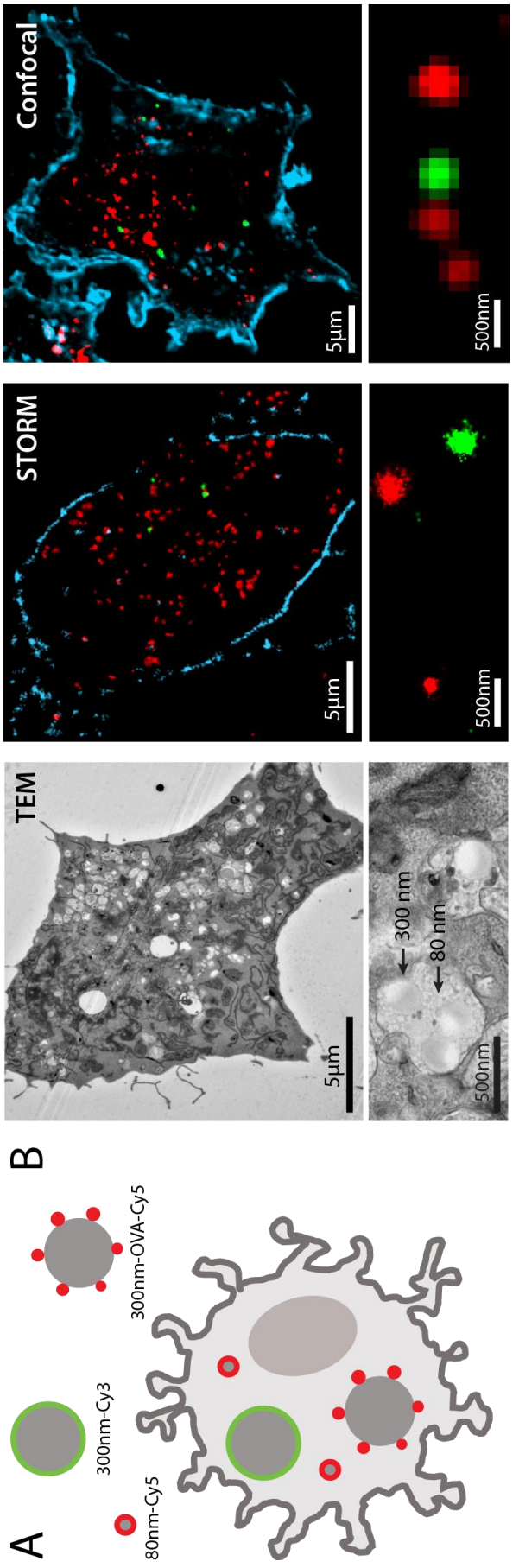


**Figure 5**. **(A)** Schematic representation of the experiment used to compare TEM, STORM, and confocal microscopy. Three different nanoparticles (varying in size and color) are administered to DCs prior to fixation and imaging. **(B)** TEM (left), STORM (middle), and confocal imaging (right) of the different nanoparticles inside DCs. Bottom panels are magnifications demonstrating the ability of the different techniques to image NPs of varying size and color.

On the contrary, both confocal and STORM can differentiate between particles with different labeling. However, confocal microscopy is unable to discriminate between 300 and 80 nm particles as they fall below the diffraction limit. Importantly, STORM microscopy succeeds in distinguishing both particles varying in size and surface functionality, although not at the same resolution of TEM. Notably, confocal and STORM microscopy can be applied to live cell samples, a great advantage in the study of dynamic phenomena involving nanoparticles in living cells. In this regard, the development of live cell STORM for nanoparticles will represent a significant advance toward the understanding of nanoparticle trafficking in cells.

## Conclusion

In conclusion we found that PEGylation of hydrogel nanoparticles does not affect their cellular association *in vitro*, but dramatically improves their lymphatic drainage *in vivo*. These findings emphasize that *in vitro* data are not always a legitimate indicator for *in vivo* outcomes. More importantly, it highlights the necessity for nanoparticles to possess a low-fouling surface to efficiently reach the draining lymph nodes. These findings have provided us with a rational basis for optimal vaccine nanoparticle design, as described in the next chapter. Furthermore, we have shown the potential of super-resolution microscopy for assessing the intracellular fate of nanoparticles. Overall, STORM can fill the gap between electron and confocal microscopy, and the development of correlative techniques able to superimpose STORM and TEM images can be of further use to the nanomedicine field.[26]

## References


1 Moon, J. J., Huang, B. & Irvine, D. J. Engineering Nano- and Microparticles to Tune Immunity. *Advanced Materials* **24**, 3724-3746 (2012).

2 Hubbell, J. A., Thomas, S. N. & Swartz, M. A. Materials engineering for immunomodulation. *Nature* **462**, 449-460 (2009).

3 De Koker, S. *et al.* Designing polymeric particles for antigen delivery. *Chem. Soc. Rev.* **40**, 320-339 (2011).

4 De Geest, B. G. *et al.* Surface-Engineered Polyelectrolyte Multilayer Capsules: Synthetic Vaccines Mimicking Microbial Structure and Function. *Angew. Chem.-Int. Edit.* **51**, 3862-3866 (2012).

5 De Geest, B. G. *et al.* Polymeric Multilayer Capsule-Mediated Vaccination Induces Protective Immunity Against Cancer and Viral Infection. *ACS Nano* **6**, 2136-2149 (2012).

6 Kasturi, S. P. *et al.* Programming the magnitude and persistence of antibody responses with innate immunity. *Nature* **470**, 543-547 (2011).

7 Moon, J. J. *et al.* Interbilayer-crosslinked multilamellar vesicles as synthetic vaccines for potent humoral and cellular immune responses. *Nat. Mater.* **10**, 243-251 (2011).

8 Liu, H. P. *et al.* Structure-based programming of lymph-node targeting in molecular vaccines. *Nature* **507**, 519-522 (2014).

9 Jewell, C. M., Lopez, S. C. B. & Irvine, D. J. In situ engineering of the lymph node microenvironment via intranodal injection of adjuvant-releasing polymer particles. *Proc. Natl. Acad. Sci. U. S. A.* **108**, 15745-15750 (2011).

10 Reddy, S. T. *et al.* Exploiting lymphatic transport and complement activation in nanoparticle vaccines. *Nat. Biotechnol.* **25**, 1159-1164 (2007).

11 Randolph, G. J., Angeli, V. & Swartz, M. A. Dendritic-cell trafficking to lymph nodes through lymphatic vessels. *Nat. Rev. Immunol.* **5**, 617-628 (2005).

12 Wherry, E. J. & Kurachi, M. Molecular and cellular insights into T cell exhaustion. *Nat. Rev. Immunol.* **15**, 486-499 (2015).

13 Hailemichael, Y. *et al.* Persistent antigen at vaccination sites induces tumor-specific CD8(+) T cell sequestration, dysfunction and deletion. *Nature Medicine* **19**, 465-+ (2013).

14 Kim, S. *et al.* Near-infrared fluorescent type II quantum dots for sentinel lymph node mapping. *Nat. Biotechnol.* **22**, 93-97 (2004).

15 Harris, J. M. & Chess, R. B. Effect of pegylation on pharmaceuticals. *Nat. Rev. Drug Discov.* **2**, 214-221 (2003).

16 Cui, J. *et al.* Templated Assembly of pH-Labile Polymer-Drug Particles for Intracellular Drug Delivery. *Advanced Functional Materials* **22**, 4718-4723 (2012).

17 Cui, J. *et al.* Engineering Poly(ethylene glycol) Particles for Improved Biodistribution. *ACS Nano* **9**, 1571-1580 (2015).

18 Cui, J. *et al.* Mechanically Tunable, Self-Adjuvanting Nanoengineered Polypeptide Particles. *Advanced Materials* **25**, 3468-3472 (2013).

19 De Koker, S. *et al.* Engineering Polymer Hydrogel Nanoparticles for Lymph Node-Targeted Delivery. *Angew. Chem.-Int. Edit.* **55**, 1334-1339 (2016).

20 Shen, Z. H. *et al.* Cloned dendritic cells can present exogenous antigens on both MHC class I and class II molecules. *J. Immunol.* **158**, 2723-2730 (1997).

21 De Koker, S. *et al.* Polyelectrolyte Microcapsules as Antigen Delivery Vehicles To Dendritic Cells: Uptake, Processing, and Cross-Presentation of Encapsulated Antigens. *Angew. Chem.-Int. Edit.* **48**, 8485-8489 (2009).

22 van der Zwaag, D. *et al.* Super Resolution Imaging of Nanoparticles Cellular Uptake and Trafficking. *ACS Applied Materials & Interfaces* **8**, 6391-6399 (2016).

23 Rust, M. J., Bates, M. & Zhuang, X. W. Sub-diffraction-limit imaging by stochastic optical reconstruction microscopy (STORM). *Nat. Methods* **3**, 793-795 (2006).

24 Blank, N. *et al.* Cholera toxin binds to lipid rafts but has a limited specificity for ganglioside GM1. *Immunol. Cell Biol.* **85**, 378-382 (2007).

25 Houde, M. *et al.* Phagosomes are competent organelles for antigen cross-presentation. *Nature* **425**, 402-406 (2003).

26 Kim, D. *et al.* Correlative Stochastic Optical Reconstruction Microscopy and Electron Microscopy. *PLoS ONE* **10**, e0124581 (2015).

# Chapter 7

# Covalently crosslinked nanogels for immune activation and antigen conjugation

In collaboration with

**Prof. Heather D. Maynard** from the University of California Los Angeles, U.S.

**Prof. Sunil A. David** from the University of Minnesota, Minneapolis, U.S.

Parts of this chapter were published in:

**pH-degradable imidazoquinoline-ligated nanogels for lymph node focused immune activation**
L. Nuhn, N. Vanparijs, A. De Beuckelaer, L. Lybaert, G. Verstraete, K. Deswarte, S. Lienenklaus, N.M. Shukla, A.C.D. Salyer, B.N. Lambrecht, J. Grooten, S.A. David, S. De Koker, B.G. De Geest, *Proceedings of the National Academy of Sciences* **2016**, 113(29), 8098-8103

**Core and shell reactive nanogels for protein conjugation via a combination of RAFT polymerization and vinyl sulfone post-modification**
N. Vanparijs, L. Nuhn, S. Paluck, H.D. Maynard, B.G. De Geest, *Nanomedicine* **2016**, in press

## Abstract

In this chapter, we report on the macromolecular engineering of polymer-based nanogels for immune activation and protein conjugation respectively. Polymers containing a solvophobic poly(pentafluorophenyl) (PFP) block and a solvophilic poly(methoxytriethylene glycol) block were synthesized via RAFT polymerization. Self-assembly in DMSO yielded nanoparticles through hydrophobic interaction between the PFP moieties. Additionally, the activated PFP esters allowed for core-cross linking and conversion of the nanoparticle into a hydrophilic nanogels by amide bond formation with primary amines. This chemistry was exploited to covalently ligate a small molecule imidazoquinoline-based TLR7/8 agonist into the nanogel core, which are potent activators of the innate immune system. Importantly, the imidazoquinoline-ligated nanogels focused the *in vivo* immune-activation on the draining lymph nodes, whilst dramatically reducing systemic inflammation. This unique feature also promoted antigen-specific humoral and cellular immune responses against an admixed protein antigen. Alternatively, these nanogels were equipped with protein-reactive vinyl sulfone moieties to allow for antigen conjugation. Free thiols were introduced at both the polymer chain ends through aminolysis of the RAFT thiocarbonyl groups, and into the nanogel core by reacting PFP esters with cysteamine. Subsequently, these free thiols were converted into vinyl sulfone moieties. Despite sterical constraints, nanogel-associated vinyl sulfone moieties remained well accessible for protein conjugation using BSA as a model antigen.

## Introduction

As discussed earlier, formulating protein antigens as nanoparticles has proven to be a promising strategy to modulate and increase the adaptive antigen-specific CD8+ T cell response. This occurs through stimulation of the cross-presentation pathway[1-5] and enhanced lymphatic transportation of nanoparticulate species compared to soluble ones[6-8]. The cross-presentation pathway can be further improved by co-delivery of immune-modulators that shape the direction and strength of the adaptive immune response.[9,10] Agonists of Toll-like receptors (TLRs) are amongst the most potent activators of the innate immune response identified to date and thus are under intensive investigation as adjuvants

for vaccination[11] or as agents for anti-cancer immunotherapy.[12] Especially promising in this context are TLR7/8 agonists, that trigger endosomal danger receptors. These receptors typically recognize single stranded RNAs generated during viral infection[13] but can also be triggered by a synthetic class of small molecule imidazoquinolines and guanosines.[14]

Due to their pharmacokinetic profile, most molecular adjuvants rapidly diffuse after administration and evoke systemic inflammatory responses that cause dose-limiting toxicity.[15,16] In the context of vaccination, the rapid diffusion of molecular adjuvants dramatically lowers the ability of antigen and TLR agonist to reach the same antigen-presenting cells in the draining lymph node, which results in suboptimal immunity to the delivered vaccine antigen and by consequence, wasted inflammation.[17] Co-encapsulation of antigens and TLR agonists inside polymeric carriers through steric, hydrophobic, or electrostatic entrapment as means to augment B and T cell immunity has been pursued by us and others.[1,2,9,18-21] Nevertheless, the procedures applied to entrap TLR agonists inside polymeric carriers are often highly complex and yield ill-defined systems that suffer from burst releases of the TLR agonist following *in vivo* application. Covalent ligation of TLR agonists to polymeric nanoparticles might provide chemically better defined alternatives to physical (co)-encapsulation systems, as recently nicely highlighted by the Seder lab.[22]

Additionally, a robust and selective conjugation strategy needs to be employed to enable efficient antigen conjugation to polymeric nanoparticles that contain these TLR agonists. In **Chapter 3-4,** we have endeavored to use maleimide- and pyridyldisulfide-functionalized RAFT chain transfer agents to generate protein-reactive polymers, forming thioether and disulfide bonds with cysteine residues. However, maleimides are instable in the presence of primary amines used for nanogel core crosslinking, and pyridyldisulfides are prone to disulfide exchange *in vivo* with randomly encountered cysteines leading to de-conjugation. Moreover, there is recent evidence on limited stability of maleimide-generated thioethers *in vivo*.[23] Therefore, we elaborated on an alternative approach introduced by Maynard and co-workers, comprising post-polymerization modification of the thiocarbonyl end-group of RAFT polymers into a vinyl sulfone (VS) moiety. The latter can react with free cysteine moieties by Michael-type addition, affording stable thioether bonds (**Figure 1**).[24] In this approach, after polymerization the thiocarbonyl moiety of the employed RAFT chain transfer agent (CTA) was reduced via aminolysis and subsequently, the resulting thiol was trapped with a divinyl sulfone.

In this chapter, polymer nanogels were prepared by selective crosslinking of self-assembled amphiphilic reactive ester block copolymers. They are composed of a hydrophilic, poly(ethyleneglycol) or PEG-like polymer block based on methoxytriethylene glycol methacrylate (mTEGMA) and a hydrophobic polymer block based on pentafluorophenyl methacrylate (PFPMA) that can be block copolymerized by reversible addition-fragmentation chain transfer (RAFT) polymerization.[25] The PEG-like hydrophilic block was used to provide nanoparticle stability and tissue mobility as recently demonstrated by us and others.[6,9,26] The PFPMA block allowed for self-assembly into nanoparticles in polar aprotic solvents (such as DMSO), followed by functionalization and crosslinking of the PFP esters with bisamines[27] without facing competing hydrolysis reactions that would occur in aqueous medium.[28] This feature was exploited to introduce a small molecule imidazoquinoline-based TLR7/8 agonist or protein-reactive vinyl sulfone moieties into the nanogel core. At the polymer chain end, vinyl sulfone moieties were introduced upon aminolysis of the RAFT thiocarbonyl groups. Furthermore, remaining PFP esters could be converted into hydrophilic moieties to yield fully hydrated nanogels after transfer to aqueous medium.

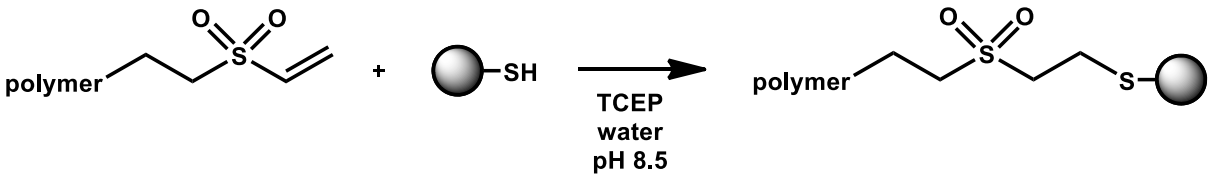


**Figure 1.** Protein conjugation of vinyl sulfone-functionalized polymers or nanogels to free cysteine moieties in protein by Michael-type addition.

## Materials and methods

### *Materials*

Unless otherwise stated, all chemicals were purchased from Sigma Aldrich and Acros Organics. 2, 2'-azobis(2-methylpropionitrile) (AIBN) as initiator was provided by Wako Chemicals and purified by recrystallization from diethyl ether prior to use. RAFT chain transfer agent 4-cyano-4-[(ethylsulfanylthiocarbonyl)sulfanyl]pentanoic acid (CETPA) and 4-cyano-4-(phenylcarbonothioylthio)pentanoic acid (CPTPA) and the monomers tri(ethylene glycol) methyl ether methacrylate (mTEGMA) and pentafluorophenyl methacrylate (PFPMA)

were synthesized according to established procedures.[27,29] Synthesis an characterization of the TLR agonist-ligated nanogels has been discussed in the corresponding paper[30] and was similar to the nanogels synthesis described in this chapter. Amicon® Ultra-15 centrifugal filters with a MWCO of 3 or 10 kDa were obtained from Merck Millipore. Spectra/Por 3 dialysis membranes with a MWCO of 1 kDa were obtained from Spectrum Labs. Sodium dodecyl sulfate-polyacrylamide gel electrophoresis (SDS-PAGE) was performed using Any kD™ Mini-PROTEAN® TGX™ precast gels from Bio-Rad. The immortalized dendritic cell line DC2.4 was a kind gift from Dr. Kenneth Rock (Dana Farber Cancer Institute, now at University of Massachusetts Medical School).[31] Bone marrow derived dendritic cells were obtained as previously reported.[32] Cell culture medium and supplements, Hoechst, Cholera Toxin Subunit B Alexa Fluor® 488 Conjugate (CTB-AF488) and tetramethylrhodamine (TMR) cadaverine were purchased from Life Technologies. The antibodies Fc block (CD16/32), MHCII-FITC, CD11c-APC and CD80-PE were obtained from BD Pharmingen.

***Instrumentation***

All $^{1}$H-, $^{13}$C-, and $^{19}$F-NMR spectra were recorded on a Bruker 300 MHz or 400 MHz FT NMR spectrometer. Chemical shifts (δ) are provided in ppm relative to TMS. Samples were prepared in given deuterated solvents and their signals referenced to residual non-deuterated signals of the solvent.

Molecular weight determination of the precursor polymers was obtained using size exclusion chromatography (SEC) in tetrahydrofuran (THF) as solvent. This system consisted of a PU 1580 pump, AS 1555 auto sampler, UV 1575 UV-detector (detection at 254 nm), RI 1530 RI-detector from JASCO. Columns were purchased at MZ-Analysentechnik: MZ-Gel SDplus 102 Å and MZ-Gel SDplus 106 Å. Calibration was done using poly(styrene) standards purchased from Polymer Standard Services.

UV-Vis spectrophotometry was performed on a Biomate 5 Thermo Spectronic spectrometer. Dynamic light scattering (DLS) analyses were performed on a Zetasizer Nano S (Malvern Instruments Ltd., Malvern, U.K.) equipped with a HeNe laser (λ = 633 nm) and detection a scattering angle of 173°. All samples were filtered through Whatman nylon syringe filters (0.45 µm pore size, GE Healthcare Life Science) prior to each measurement.

***In vitro dendritic cell uptake of TLR agonist-ligated nanogels***

*Flow cytometry*

DC2.4 cells (immortalized dendritic cell line) were cultured in RPMI-glutamax, supplemented with 10% FBS, 1 mM sodium pyruvate, 10 mM HEPES buffer, 0.05 mM 2-mercaptoethanol, MEM NEAA and antibiotics (50 units/mL penicillin and 50 µg/mL streptomycin). Cells were incubated at 37 °C in an controlled, sterile environment of 95% relative humidity and 5% CO2. DC2.4 cells were seeded into 24-well titer plates (250 000 cells per well, suspended in 0.95 mL of culture medium) and incubated overnight to allow cell sedimentation and subsequent adhesion to the bottom of the wells. Next, the cells were pulsed with 50 µL (yielding a total polymer/nanogel concentration of 80 µg/mL) of the TMR cadaverine-labeled nanogels. The same procedure was followed for soluble polymer and PBS. All samples were run in triplicate and the experiment was conducted for 4 h at 4 °C and 37 °C. Special attention was given at the samples at 4 °C, as they were put on ice 30 min prior to pulsing in order to bring their temperature down to 4 °C. After 4 h of incubation, the wells were aspirated, washed with 1 mL of PBS and incubated with 500 µL of Cell Dissociation Buffer (15 min., 37°C). The cell suspensions were transferred into Eppendorf tubes and immediately centrifuged (350 g, 10 min., 5 °C). Finally, the supernatant was aspirated and the cell pellets were suspended in 200 µL of PBS and kept on ice to maintain cell integrity. FACS was performed on a BD Accuri C6 (BD Biosciences). The data were processed by FlowJo software.

*Confocal microscopy*

DC2.4 cells were plated out on Willco-Dish glass bottom dishes (50 000 cells, suspended in 200 µL of culture medium) and incubated overnight. Next, 10 µL (yielding a total polymer/nanogel concentration of 80 µg/mL) of the respective samples that were fluorescently labeled with TMR cadaverine was added, followed by 4 h of incubation. Hoechst and CTB-AF488 staining was carried out simultaneously on fixed cells. In summary, culture medium was aspirated and cells were washed with PBS. Next, 200 µL of 4 % paraformaldehyde was added and allowed to fixate for 30 min. A staining solution was prepared by adding Hoechst (10 µL of a 1 mg/mL stock in DMSO) and CTB-AF488 (5 µL of a 1 mg/mL stock in PBS) to a PBS buffer containing 1% of BSA (2.5 mL). After aspiration and washing, 200 µL of this staining solution was added to the fixed cells and incubated for 40 minutes at room temperature. Finally, the samples were washed with 1% BSA PBS buffer.

Confocal microscopy was carried out on a Leica DMI6000 B inverted microscope equipped with an oil immersion objective (Leica, 63x, NA 1.40) and attached to an Andor DSD2 confocal scanner. Images were processed with the ImageJ software package.

***In vitro dendritic cell maturation***

Mouse bone-marrow-derived DCs (BM-DCs) were generated from C57BL/6 mice using the modified Inaba protocol described in **Chapter 5**.[33] Day 7 bone marrow derived DCs were incubated with different concentrations (i.e. total IMDQ-equivalent of 0.08, 0.4 and 2 µg/mL) of the respective samples. After overnight incubation, the cell suspensions were transferred into Eppendorf tubes and immediately centrifuged (350 g, 10 min., 5 °C). The supernatant was aspirated and the cell pellets were suspended in 50 µL of an antibody cocktail solution containing Fc block (diluted 200x), MHCII-FITC (diluted 500x), CD11c-APC (diluted 200x) and CD80-PE (diluted 200x) in PBS buffer. After 30 min. of incubation on ice, 200 µL of PBS was added to the samples prior to centrifugation (350 g, 10 min., 5 °C). Finally, the supernatant was aspirated and the cell pellets were suspended in 200 µL of PBS and kept on ice to maintain cell integrity. FACS was performed on a BD Accuri C6 (BD Biosciences). The data were processed with the FlowJo software package and the applied gating strategy is depicted in **Figure 2.**

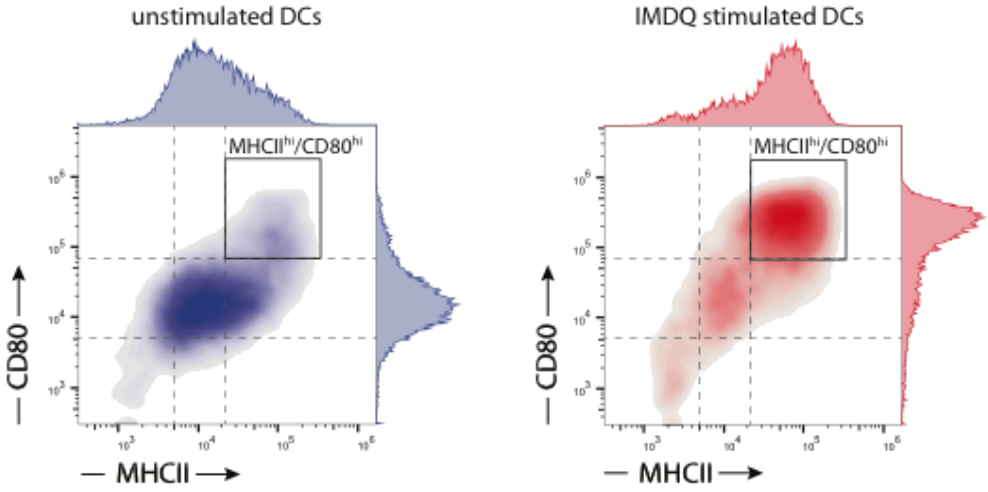


**Figure 2.** Flow cytometry gating strategy for BM-DC maturation.

### *Synthesis of p(PFPMA)$_{33}$ using CPTPA*

In analogy to earlier reports,[27] a Schlenk tube equipped with a stir bar was loaded with PFPMA (2.0 g; 7.932 mmol), CPTPA (88.5 mg; 0.317 mmol) and AIBN (5.2 mg; 0.032 mmol). All compounds were dissolved in anhydrous dioxane (2.0 mL). Following three freeze-pump-thaw cycles the tube was immersed in an oil bath at 70 ˚C for 6 h under vigorously stirring. A $^1$H-NMR sample of the reaction mixture dissolved in $CDCl_3$ was analyzed showing 50% monomer conversion. The resulting polymer was isolated by precipitation in hexane and centrifugation (the supernatant was slightly red from unreacted CTA). After re-dissolving in a few mL of dioxane, this process was repeated three times. The precipitated polymer was dried for 12 h at 40˚C under 10 mbar vacuum affording **p(PFPMA)$_{33}$** (determined by $^1$H-NMR, **Figure 3**) (889 mg; 82%) as a red powder. SEC (THF, PS-Std.): Number-average molecular weight ($M_n$) = 8,400 g/mol; Weight-average molecular weight ($M_w$) = 10,700 g/mol; Molecular weight dispersity (Đ) = 1.29.

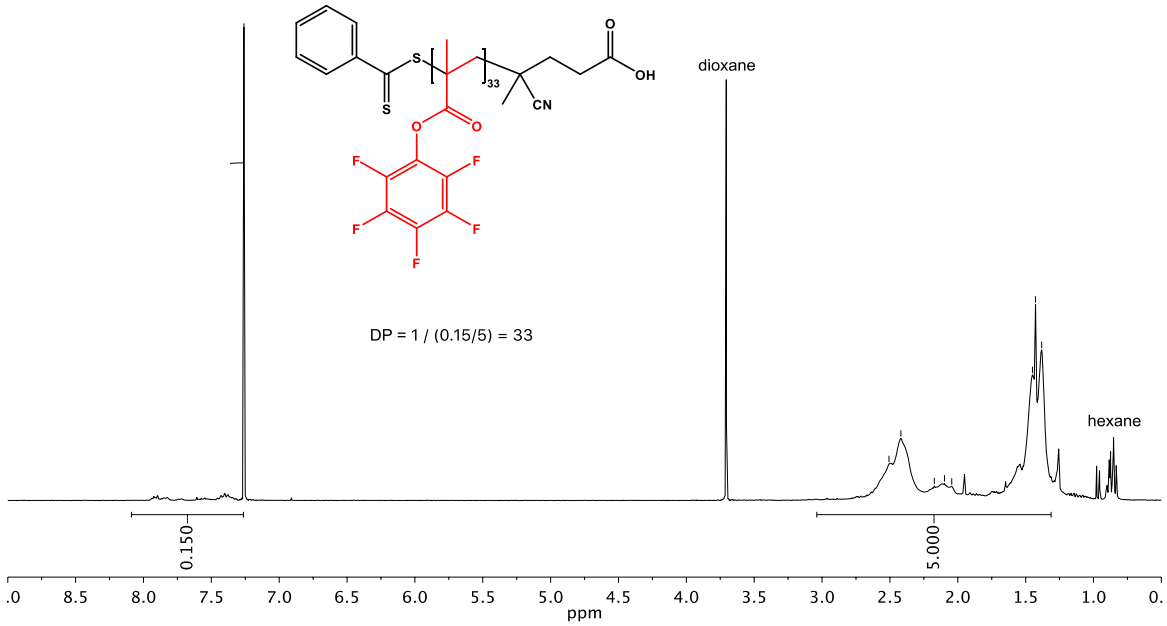


**Figure 3.** $^1$H-NMR ($CDCl_3$, 300 MHz) of **p(PFPMA)$_{33}$**: $\delta$ [ppm] = 8.20 – 7.30 (m, 5H, -C$_6$*H$_5$* CTA phenyl end group); 3.05 – 1.90 (br, 2H, -C*H$_2$*- PFPMA polymer main chain); 1.90 – 1.20 (br, 3H, -C*H$_3$* PFPMA polymer main chain).

### *Synthesis of p(PFPMA)$_{46}$ using CETPA*

In analogy to earlier reports,[27] a Schlenk tube equipped with a stir bar was loaded with PFPMA (2.0 g; 7.932 mmol), CETPA (83.6 mg; 0.317 mmol) and AIBN (5.2 mg; 0.032 mmol). All compounds were dissolved in anhydrous dioxane (2.0 mL). Following three freeze-pump-thaw cycles the tube was immersed in an oil bath at 70˚C for 6 h under vigorously stirring. A $^1$H-NMR sample of the reaction mixture dissolved in $CDCl_3$ was analyzed showing 52% monomer conversion. The resulting polymer was isolated by precipitation in hexane and centrifugation (the supernatant was slightly yellow from unreacted CTA). After re-dissolving in few mL of dioxane, this process was repeated three times. The precipitated polymer was dried for 12 h at 40˚C under 10 mbar vacuum affording **p(PFPMA)$_{46}$** (determined by $^1$H-NMR, **Figure 4**) (907 mg; 81%) as a yellow powder. SEC (THF, PS-Std.): $M_n$ = 11,800 g/mol; $M_w$ = 15,300 g/mol; Đ = 1.29.

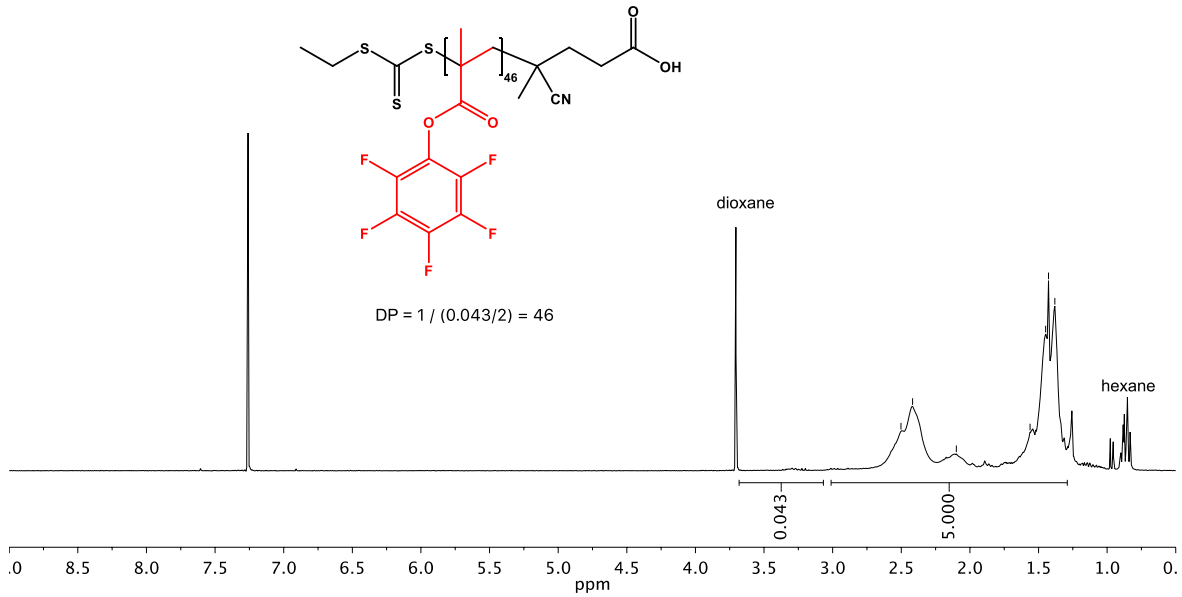


**Figure 4.** $^1$H-NMR ($CDCl_3$, 300 MHz) of **p(PFPMA)$_{46}$**: $\delta$ [ppm] = 3.60 – 3.05 (m, 2H, -S-CS-S-C$H_2$- CTA ethyl end group); 3.05 – 1.90 (br, 2H, -C$H_2$- PFPMA polymer main chain); 1.90 – 1.20 (br, 3H, -C$H_3$ PFPMA polymer main chain).

### *Synthesis of CPTPA p(PFPMA)$_{33}$-b-p(MTEGMA)$_{35}$ (1)*

In analogy to earlier reports,[27] a Schlenk tube equipped with a stir bar was loaded with mTEGMA (760 mg; 3.27 mmol), **p(PFPMA)$_{33}$** (425 mg; 0.049 mmol) and AIBN (1.1 mg; 0.07 mmol). All compounds were dissolved in anhydrous dioxane (2.34 mL). Following three

freeze-pump-thaw cycles the tube was immersed in an oil bath at 70˚C for 18 h under vigorously stirring. A $^{1}$H-NMR sample of the reaction mixture dissolved in $CDCl_3$ was analyzed showing 72% monomer conversion. The resulting polymer was isolated by precipitation in hexane and centrifugation. After re-dissolving in few mL of dioxane, this process was repeated three times. The precipitated polymer was dried for 12 h at 40˚C under 10 mbar vacuum affording **p(PFPMA)$_{33}$-*b*-p(MTEGMA)$_{35}$** (determined by $^{1}$H-NMR, **Figure 5**) (847 mg; 87%) as a slightly red powder. $^{19}$F-NMR is depicted in **Figure 6**. SEC (THF, PS-Std.): $M_n$ = 11,500 g/mol; $M_w$ = 14,000 g/mol; Đ = 1.22.

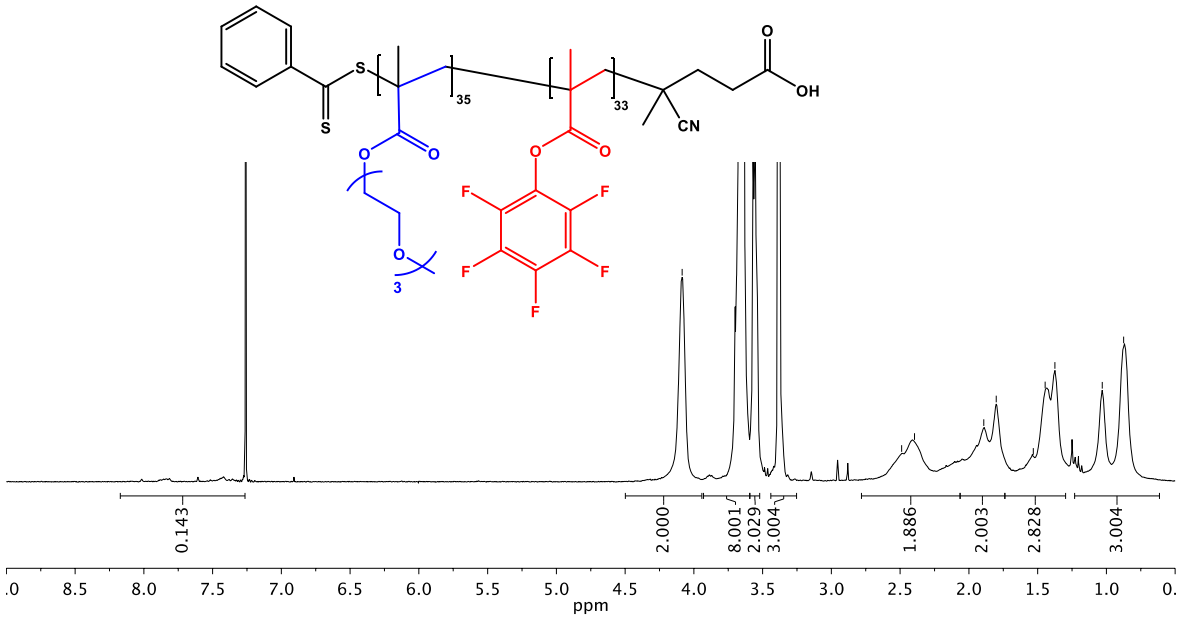


**Figure 5.** $^{1}$H-NMR ($CDCl_3$, 300 MHz) of **p(PFPMA)$_{33}$-*b*-p(MTEGMA)$_{35}$ *(1)***: $\delta$ [ppm] = 8.20 – 7.30 (m, 5H, -C$_6$*H*$_5$ CTA phenyl end group); 4.09 (br, 2H, COO-C*H*$_2$-); 3.65 (br, 8H, COO-CH$_2$-C*H*$_2$-O-C*H*$_2$-C*H*$_2$-O-C*H*$_2$-); 3.55 (br, 2H, -C*H*$_2$-O-CH$_3$); 3.38 (br, 3H, -O-C*H*$_3$); 2.85 – 2.10 (br, 2H, -C*H*$_2$- PFPMA polymer main chain); 2.10 – 1.70 (br, 2H, -C*H*$_2$- MEO$_3$MA polymer main chain); 1.70 – 1.20 (br, 3H, -C*H*$_3$ PFPMA polymer main chain) and 1.20 – 0.60 (br, 3H, -C*H*$_3$ MEO$_3$MA polymer main chain).

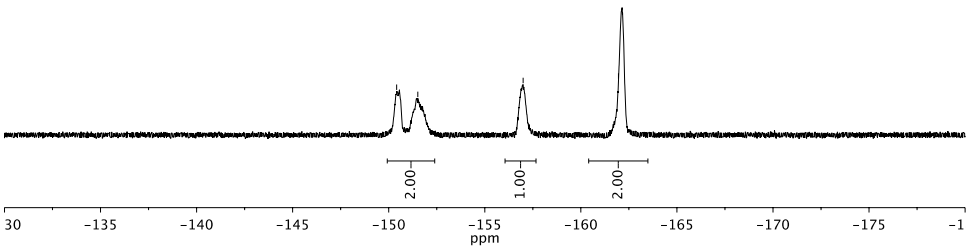


**Figure 6.** $^{19}$F-NMR ($CDCl_3$, 282 MHz) of **p(PFPMA)$_{33}$-*b*-p(MTEGMA)$_{35}$ *(1)***: $\delta$ [ppm] = -150.41 – -151.52 (br, 2F, o-Ar*F*); -157.00 (br, 1F, p-Ar*F*); 161.96 (br, 2F, m-Ar*F*).

### *Synthesis of CETPA p(PFPMA)$_{46}$-b-p(MTEGMA)$_{57}$ (2)*

In analogy to earlier reports,[27] a Schlenk tube equipped with a stir bar was loaded with mTEGMA (745 mg; 3.21 mmol), **p(PFPMA)$_{46}$** (417 mg; 0.035 mmol) and AIBN (1.0 mg; 0.006 mmol). All compounds were dissolved in anhydrous dioxane (2.30 mL). Following three freeze-pump-thaw cycles the tube was immersed in an oil bath at 70˚C for 18 h under vigorously stirring. A $^{1}$H-NMR sample of the reaction mixture dissolved in $CDCl_3$ was analyzed showing 83% monomer conversion. The resulting polymer was isolated by precipitation in hexane and centrifugation. After re-dissolving in few mL of dioxane, this process was repeated three times. The precipitated polymer was dried for 12 h at 40˚C under 10 mbar vacuum affording **p(PFPMA)$_{46}$-*b*-p(MTEGMA)$_{57}$** (determined by $^{1}$H-NMR, **Figure 7**) (865 mg; 84%) as a slightly red powder. $^{19}$F-NMR is depicted in **Figure 8**. SEC (THF, PS-Std.): $M_n$ = 19,800 g/mol; $M_w$ = 24,000 g/mol; Đ = 1.21.

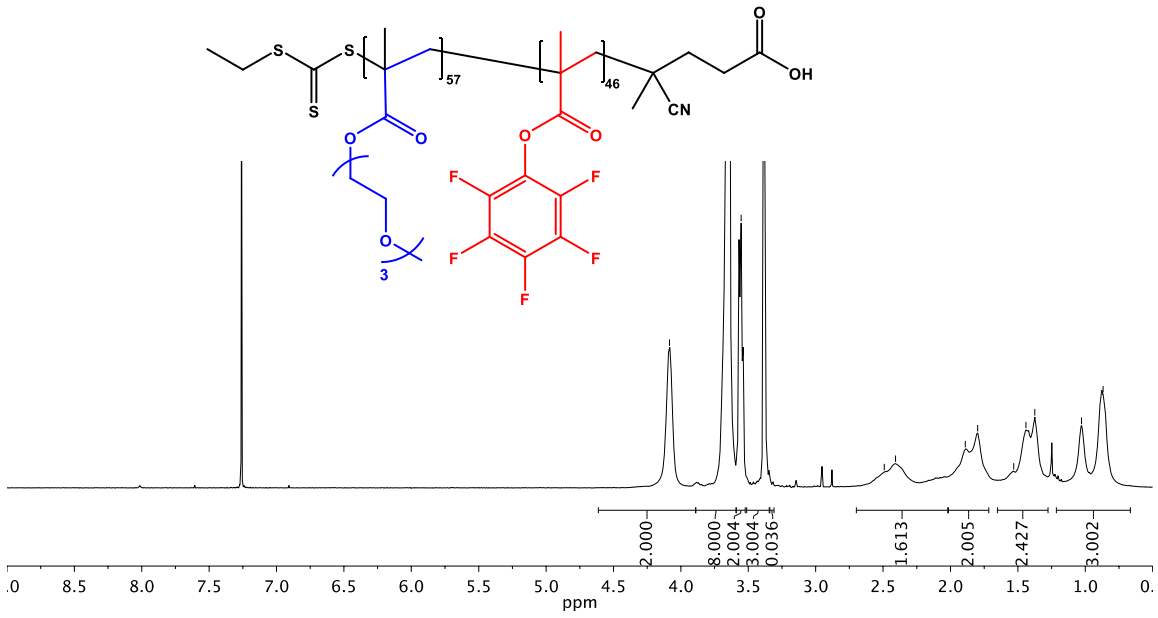


**Figure 7.** $^{1}$H-NMR ($CDCl_3$, 300 MHz) of **p(PFPMA)$_{46}$-*b*-p(MTEGMA)$_{57}$**: $\delta$ [ppm] = 4.08 (br, 2H, COO-C*H*$_2$-); 3.65 (br, 8H, COO-CH$_2$-C*H*$_2$-O-C*H*$_2$-C*H*$_2$-O-C*H*$_2$-); 3.55 (br, 2H, -C*H*$_2$-O-CH$_3$); 3.38 (br, 3H, -O-C*H*$_3$); 2.85 – 2.05 (br, 2H, -C*H*$_2$- PFPMA polymer main chain); 2.05 – 1.70 (br, 2H, -C*H*$_2$- MEO$_3$MA polymer main chain); 1.70 – 1.20 (br, 3H, -C*H*$_3$ PFPMA polymer main chain) and 1.20 – 0.60 (br, 3H, -C*H*$_3$ MEO$_3$MA polymer main chain).

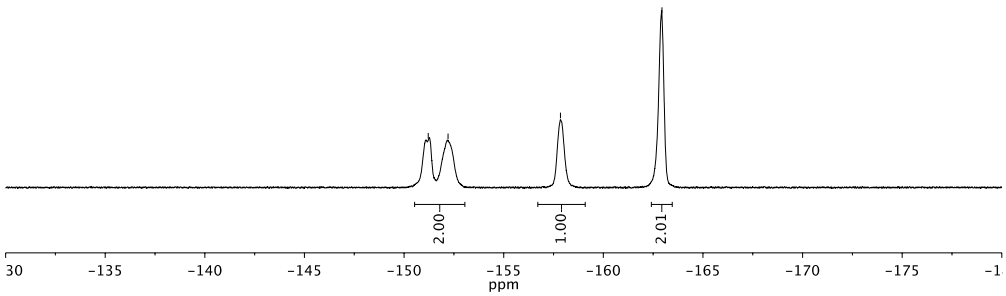


**Figure 8.** $^{19}$F-NMR ($CDCl_3$, 282 MHz) of **p(PFPMA)$_{46}$-*b*-p(MTEGMA)$_{57}$**: $\delta$ [ppm] = -151.21 – -152.21 (br, 2F, o-Ar*F*); -157.85 (br, 1F, p-Ar*F*); 162.94 (br, 2F, m-Ar*F*).

### *Nanogel synthesis*

*Crosslinking*.

A detailed example of a one-pot nanogel synthesis using CPTPA p(PFPMA)$_{33}$-*b*-p(MTEGMA)$_{35}$ ***(1)*** is provided below. The precursor block copolymer ***1*** (150 mg; 296 µmol of reactive esters; 1 eq.) was transferred into a round-bottom flask equipped with a stirring bar and dispersed at 10 mg/ml in anhydrous DMSO (15 mL) under argon atmosphere. After sonication for 2h, the resulting micellar dispersion was characterized by DLS. Crosslinking was performed by addition of 2, 2'-(ethylenedioxy)bis(ethylamine) (10.8 µL, 74 µmol, 0.25 eq.) and triethylamine (TEA) (82.6 µL, 592 µmol, 2 eq) and stirring overnight at 50˚C. This step was omitted to yield soluble control polymers with chain end ***(Polymer_1$^{VS_CE}$)*** or backbone ***(Polymer_2$^{VS_CE+BB}$)*** VS modification.

*Chain end functionalization (CE).*

Half of the crosslinked nanogel dispersions (75 mg; 4.5 µmol of CTA moieties, 148 µmol of reactive esters, 1 eq.) was used for VS shell functionalization. To guarantee complete removal of remaining PFP esters in the nanogel, the reaction mixture was quenched with excess 2-aminoethanol (26.8 µL; 445 µmol; 3 eq. relative to reactive esters) and TEA (186 µL, 1.33 mmol, 9 eq. relative to reactive esters). After 6 hours of stirring at 50˚C under argon atmosphere, an excess of 2,2'-dipyridyl disulfide (99 mg, 449 µmol, 100 eq. relative to CTA moieties) was added to the reaction mixture to cap the free thiols generated by aminolysis of the CTA moieties. After overnight reaction at 50°C, the solution was diluted 10x with deionized water and purified 5 times by spin filtration with a 40:60 water:methanol mixture to remove the excess of 2-aminoethanol, TEA and 2,2'-dipyridyl disulfide. The purified sample was diluted 1:1 with a 0.1 M bicarbonate buffer pH 8.5 and analyzed by UV-

vis spectroscopy. Subsequently the sample was added to an excess of tris(2-carboxyethyl)phosphine (TCEP, 26 mg, 89 µmol, 20 eq. relative to CTA moieties) and incubated for 15 minutes. The release of 2-pyridinethione upon cleavage of the disulfide linkages with the capped thiols was confirmed by UV-vis spectroscopy. An aliquot of this mixture was further purified by spin filtration without VS modification to yield non protein-reactive controls ***(Nanogel_1$^{SH_CE}$)*** The remaining mixture was added dropwise to an excess of divinyl sulfone (475 µL, 4.5 mmol, 1000 eq. relative to CTA moieties) and reacted for overnight under argon atmosphere at room temperature. Finally, the reaction mixture was transferred into a dialysis membrane and dialyzed against 50:50 water:methanol for three days, followed by dialysis against pure water and subsequent lyophilization ***(Nanogel_1$^{VS_CE}$).***

*Backbone functionalization (BB).*

Half of the crosslinked nanogel dispersions (75 mg, 148 µmol of reactive esters, 1 eq.) was used for VS core functionalization by the introduction of free thiol groups on the reactive ester moieties. For that purpose the crosslinked nanogels were reacted with cysteamine (8.4 mg, 74 µmol, 0.5 eq.) and TEA (82 µL, 592 µmol, 4 eq.) for 6 hours under argon atmosphere at 50°C. To guarantee complete removal of remaining PFP esters in the nanogel, the reaction mixture was quenched with excess 2-aminoethanol (26.8 µL; 445 µmol; 3 eq.) and TEA (186 µL, 1.33 mmol, 9 eq.). In addition, an excess of 2,2'-dipyridyl disulfide (408 mg, 1.8 mmol, 12.5 eq.) was added to cap the free thiols originating from the introduced cysteamine moieties. After overnight reaction at 50°C, the solution was purified by spin filtration and analyzed by UV-vis spectroscopy as described for the shell functionalized nanogels. Subsequently the sample was added to an excess of TCEP (212 mg, 741 µmol, 5 eq.) and incubated for 15 minutes. Again the release of pyridyl disulfide upon cleavage of the disulfide linkages with the capped thiols was confirmed by UV-vis spectroscopy. An aliquot of this mixture was further purified by spin filtration without VS modification to yield non protein-reactive controls ***(Nanogel_1$^{SH_CE+BB}$).*** The remaining mixture was then added dropwise to an excess of divinyl sulfone (784 µL, 7.4 mmol, 50 eq.) and reacted for overnight under argon atmosphere at room temperature. Finally, the reaction mixture was transferred into a dialysis membrane and dialyzed against 50:50 water:methanol for three days, followed by dialysis against pure water and subsequent lyophilization ***(Nanogel_1$^{VS_CE+BB}$).***

***Conjugation of VS-functionalized nanogels to BSA***

An example conjugation procedure is as follows. Stock solutions of BSA (1.16 x 10-4 M, 7.7 mg/mL), TCEP (0.1 M, 30 mg/mL) and nanogels (20 mg/mL) were prepared in a bicarbonate buffer (0.1 M, pH 8.2). The TCEP stock was combined with the BSA solution in a 1:10 ratio and allowed to react for 15 min. Subsequently, the BSA and polymer stock solutions were combined to obtain a molar ratio of protein:polymer 1:40. Then the reaction mixture was diluted with buffer solution to obtain a protein concentration of 1.51 x 10-5 M. Next, 10% of DMSO was added and the mixture was incubated overnight at 20 °C in a thermoshaker. Conjugation efficiency was evaluated by reducing SDS-PAGE using β-Mercaptoethanol as a reducing agent. Quantification of protein conjugation was done by automated integration of optical density by ImageJ software and calculating the ratio of bound protein to total protein content per lane as described in **Chapter 4**.

## Result and discussion

***In vitro and in vivo evaluation of TLR agonist-ligated nanogels***

**Scheme 1** schematically represents the supramolecular design and chemical synthesis of the degradable TLR agonist-ligated nanogels. Self-assembly of well-defined p(MTEGMA-*b*-PFPMA) block copolymers in DMSO yielded nanoparticles with a mean size of around 50 nm. Detailed synthesis procedures and characterization data are provided in the corresponding paper.[30] Subsequently, the TLR7/8 agonist 1-(4-(aminomethyl)benzyl)-2-butyl-1H-imidazo[4,5-c]quinolin-4-amine (IMDQ)[34] was covalently ligated into the core of the nanoparticles, through amide bond formation between the primary amine of IMDQ and the activated PFP esters. Core-crosslinking was performed by addition of the bis-amino-ketal 2,2-bis(aminoethoxy)propane, which installs pH-sensitive ketal moieties that renders the crosslinks susceptible to acid hydrolysis.[35,36] Subsequently, the remaining unreacted PFP-esters were converted to hydrophilic repeating units by addition of excess 2-aminoethanol. The latter in combination with the degradable crosslinker affords terminal degradation of the nanogels into fully soluble polymers, that can be excreted from the body and thus avoids long-term accumulation. As controls, non-crosslinked polymers were prepared by omitting the crosslinking step. Fluorescently labeled batches were prepared by adding the primary

amine-bearing fluorescent dye AlexaFluor488-cadaverine (AF488) or tetra-methylrhodamine cadaverine (TMR) prior to IMDQ ligation and crosslinking.

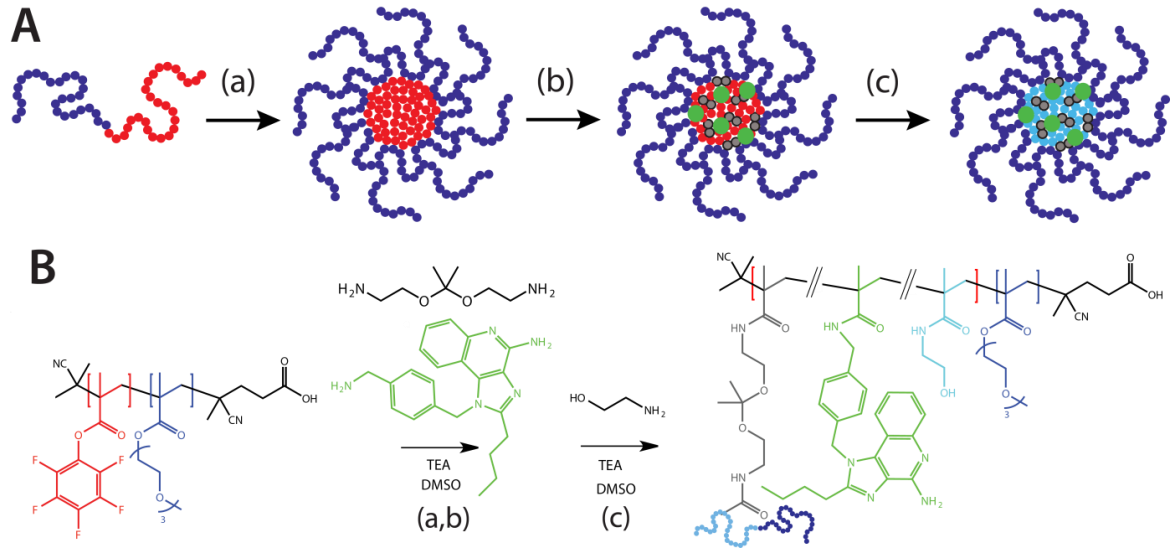


**Scheme 1.** Assembly of degradable immune-stimulatory nanogels. **(A)** Schematic overview and **(B)** corresponding chemical structures of nanogel assembly. (a) Block copolymers self-assemble in DMSO into nanoparticles. (b) Covalent ligation of TLR7/8 agonist (green) and cross-linking. (c) Conversion of residual PFP ester with 2-ethanolamine yielding fully hydrated nanogels after transfer to the aqueous phase

An extensive *in vitro* evaluation was performed to determine to which extent the IMDQ-ligated nanogels could activate bone marrow-derived dendritic cells (BM-DCs) *in vitro*. DCs represent the most potent antigen presenting cells and thus constitute the primary target of any adjuvant. As TLR7/8 is localized on the endosomal membrane of DCs, nanogels must be internalized by DCs in order for IMDQ to reach its target receptor. To address internalization, we pulsed DCs with fluorescently labeled nanogels and soluble (non-crosslinked) polymer at 4 °C and 37 °C respectively, followed by flow cytometry (FACS) analysis and confocal microscopy. At 37 °C, FACS analysis revealed a more profound association of DCs with nanogels compared to soluble polymer (**Figure 9**), a feature that can be attributed to the known preference of DCs to ingest particulate material.[28] At 4 °C by contrast, no cellular association upon incubation was observed. This indicates an energy-dependent uptake mechanism, since active endocytosis is abolished at 4 °C and only cell surface receptor binding or aspecific binding is expected. Confocal microscopy confirmed that both nanogels and soluble polymer were indeed internalized by DCs at 37°C and were not merely attached to the cell surface (**Figure 10**).

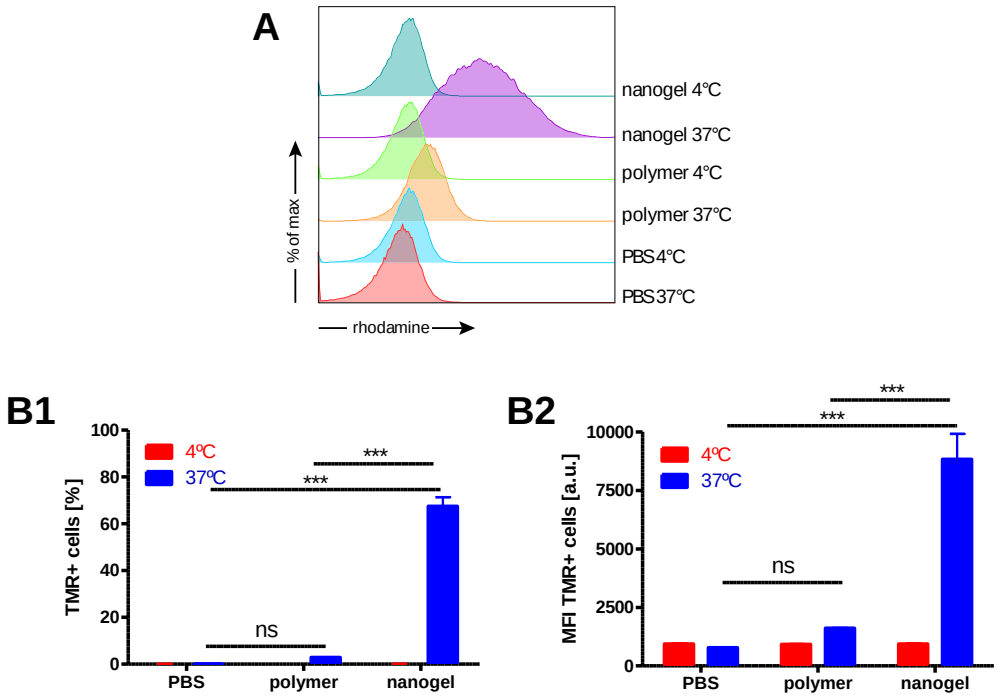


**Figure 9**. Cellular association between TMR-labeled polymer and nanogels with DCs at 4 °C and 37 °C. **(A)** Flow cytometry histogram, **(B1)** percentage of positive cells and **(B2)** mean cellular fluorescence intensity (MFI). (n=3)

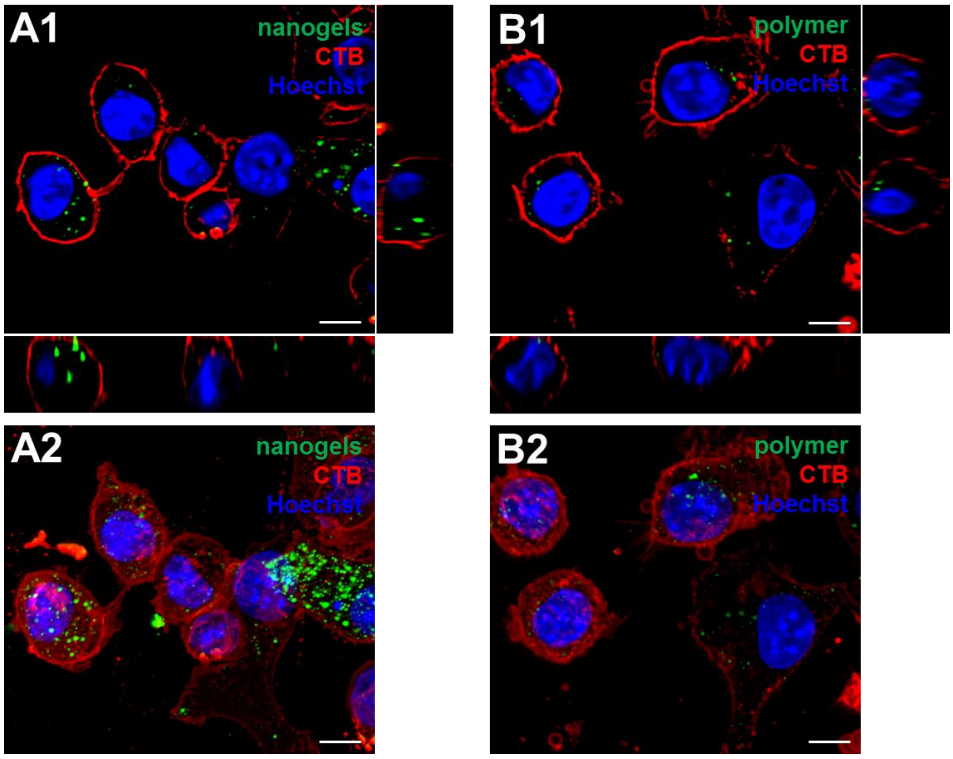


**Figure 10.** Confocal microscopy images of DCs pulsed at 37 °C with TMR-labeled (green channel) **(A)** nanogels and **(B)** non-crosslinked polymer. Cell membranes were labeled with AF647-cholera toxin B (red channel) and cell nuclei were labeled with Hoechst (blue channel). The panels **(1)** depict a confocal xy-section with the corresponding orthogonal xz- and yz-planes. The panels **(2)** depict maximum intensity projections (MIP) of the full recorded Z-stack. The images were recorded using identical settings for excitation power, detection sensitivity and contrast. Scale bar represents 10 µm.

In a subsequent series of experiments, we set out to determine whether nanogel-ligated and non-crosslinked polymer-ligated IMDQ was still capable of activating its receptor *in vitro*. For this purpose, we pulsed mouse BM-DCs with either soluble IMDQ, polymer-ligated IMDQ, or nanogel-ligated IMDQ. Control samples were left untreated or pulsed with polymer or nanogels without IMDQ. The extent of DC activation was quantified by flow cytometric (FACS) measurement of the surface expression of major histocompatibility complex class II (MHCII) and the co-stimulatory molecule CD80. The corresponding histograms and graphs are depicted in **Figure 11** and **Figure 12** respectively. FACS analysis showed, firstly, that control polymer and nanogels (without ligated IMDQ) did not activate DCs, suggesting that these are inherently non-immunogenic, at least under the experimental conditions utilized in these experiments. Second, polymer- and nanogel-ligated IMDQ was still capable of activating DCs, albeit to a lesser extent than the equivalent amount of soluble IMDQ at low doses. This is in analogy with previous findings by the David group, who reported that covalent modification of the primary amine of IMDQ with small molecules induced a reduction of its capacity to stimulate TRL7/8.[34] Nevertheless, in our setting, macromolecular modification of IMDQ still provided access to its receptor and allowed potent DC activation. Note that the discrepancy between uptake (**Figure 9**) and DC activation (**Figure 11**) - i.e. TMR-labeled polymer is barely internalized by DCs, whereas polymer-ligated IMDQ is only slightly less potent than nanogel-ligated IMDQ - is likely due to the shorter incubation time used in the DC uptake study and the more hydrophobic nature of polymer-ligated IMDQ which could enhance DC uptake in the DC activation study.

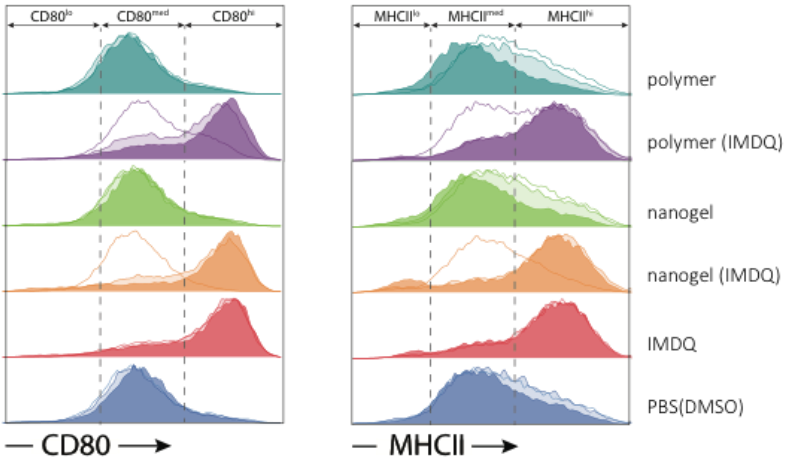


**Figure 11.** Flow cytometry histogram obtained from BM-DCs treated with crosslinked nanogels and soluble polymers, conjugated with and without IMDQ at 0.08 µg/mL (non-filled), 0.40 µg/mL (light-filled) and 2.00 µg/mL (filled).

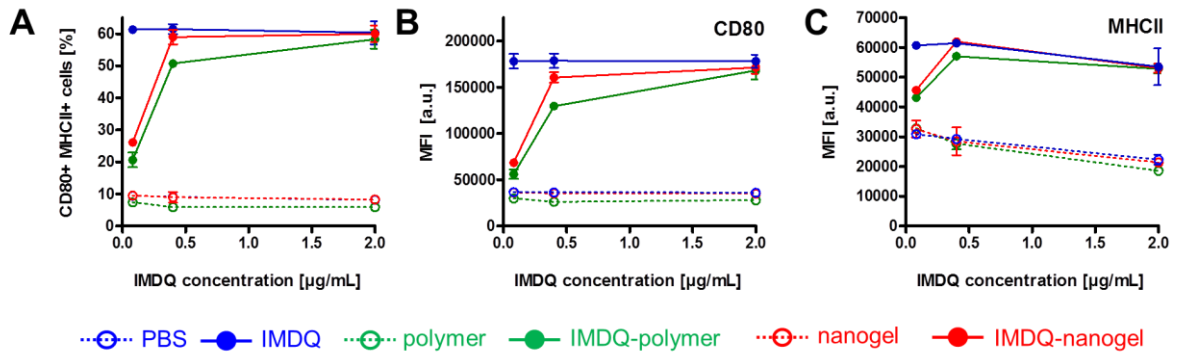


**Figure 12.** FACS analysis of the induction of DC maturation by soluble IMDQ (blue), IMDQ-ligated polymer (green) and IMDQ-ligated nanogels (red) for different concentrations of IMDQ (filled bars). The corresponding non-IMDQ-ligated controls are depicted by the hollow bars and correspond to the same concentration of DMSO to solubilize IMDQ in PBS and the same concentration of polymer, respectively nanogels as in the IMDQ-ligated samples. Data are expressed as **(A)** the percentage of $MHCII^{hi}$ & $CD80^{hi}$ cells and the mean MFI of the DCs in the **(B)** MHCII and **(C)** CD80 gate. (n=3)

In subsequent *in vivo* studies in mice we found that the nanogel-mediated delivery of IMDQ focuses innate immune activation to the site of injection and its draining lymph node (DLN), a feature closely linked to adjuvant potency and minimized toxicity. This was demonstrated in IFN-β reporter mice, in which a firefly luciferase encoding sequence had been placed under the control of the IFN-β promoter.[37] TLR7/8 agonists are indeed very potent inducers of type I IFN (including IFN-β), which are required for the adjuvant properties of TLR7/8 agonists but are also a cause of severe inflammatory toxicity when induced systemically.[12,14] Whole-body imaging in IFN-β reporter mice enables a precise, spatiotemporal analysis of IFN-β induction *in vivo*, and can therefore be a useful predictive marker in estimating tissue disposition of the adjuvant, but also in assessing systemic exposure. As depicted in **Figure 13A**, soluble IMDQ rapidly induced a systemic IFN-β response that coincided with a profound expression of IFN-β in the neck and abdomen of the injected mice. This early systemic production of type I IFN is most likely the consequence of the rapid diffusion of the injected IMDQ from the footpad to the circulation. In contrast to soluble IMDQ, nanogel-ligated IMDQ induced a luciferase signal largely confined to the footpad and the draining popliteal LN at 4 h post injection.

To confirm that IMDQ-nanogels restrict the inflammatory response to the local DLN, the acute cellular inflammatory infiltrate in the DLN of soluble IMDQ and IMDQ-nanogel injected mice were compared. As depicted in **Figure 13B**, nanogels by themselves did not

increase the total cellularity of the draining lymph node, while soluble IMDQ induced a weak increase in cellularity at the local DLN. IMDQ-nanogels by contrast caused a two-fold increase in total DLN cellularity, indicating the locally confined release of type I IFN and subsequent recruitment of inflammatory cells. In case of soluble IMDQ, type I IFN are produced more systemically and even at higher levels in distant sites such as the neck and abdomen, a phenomenon that probably diverts inflammatory cells to these sites instead.

Confocal microscopy of a DLN tissue section upon footpad injection of AF488-labeled nanogels demonstrate that the nanogels reach the draining lymph nodes and localize to the subcapsular and medullary sinuses of the lymph node, a distribution typically observed when nanoparticles reach the lymph nodes by passive flow along the lymphatics (**Figure 13C**). As mentioned earlier, particles with a size range between 10-200 nm indeed enter lymphatic vessels by direct diffusion through lymphatic endothelial cell junctions and thus can reach the draining lymph nodes without prior cellular uptake.[6]

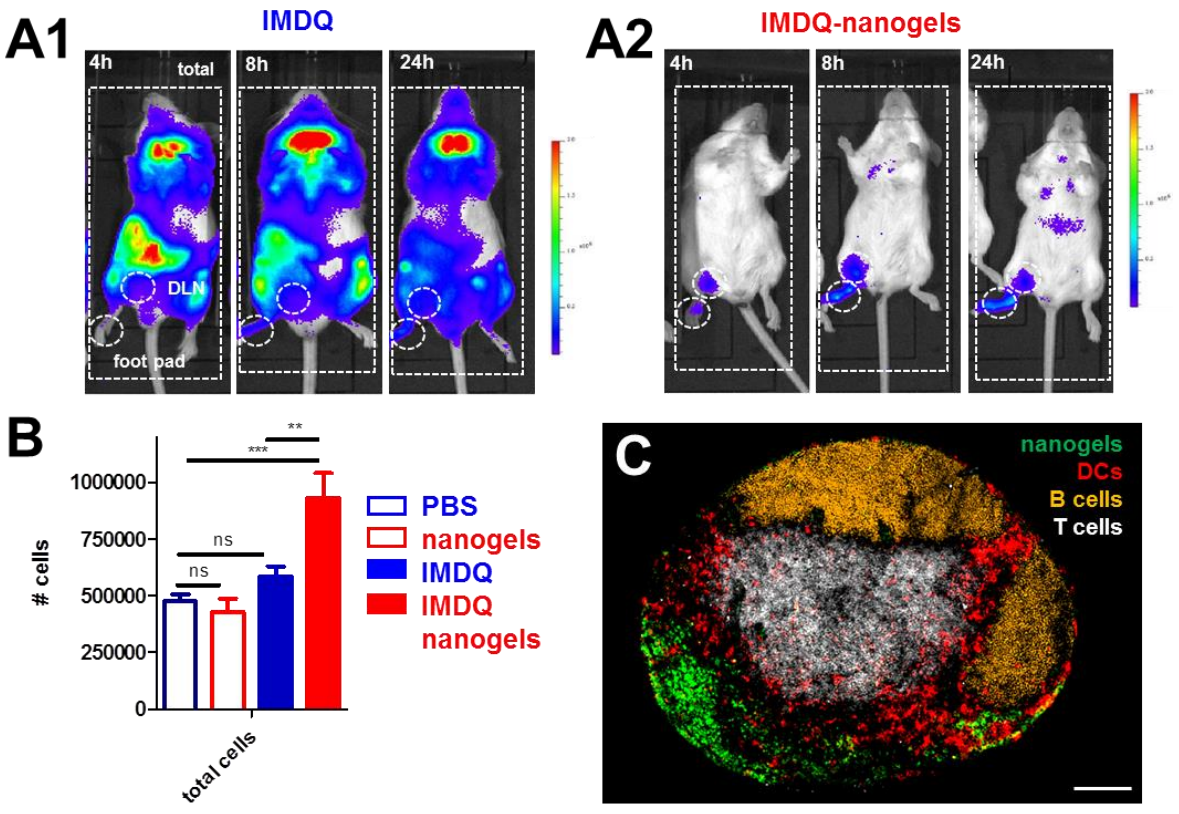


**Figure 13. (A)** *In vivo* luminescence in IFN-β reporter mice. Images recorded after 4, 8 and 24 h post injection of (A1) soluble and (A2) nanogel-ligated IMDQ in the footpad (each at 10 µg IMDQ equivalents). **(B)** FACS analysis of the DLN, depicting the total cell count (n=3). **(C)** Confocal images of the draining popliteal lymph nodes (DLN) of mice injected with IMDQ-nanogels (at 10 µg IMDQ equivalents). Scale bar represents 100 µm.[30]

These data indicate that ligation of IMDQ to the nanogels prevents systemic distribution of IMDQ, and instead restricts its action to the injection spot and its draining lymph nodes, which should result in a strongly improved therapeutic index. Additionally, the functional impact of localized IMDQ activity, by means of nanogel ligation, on the adaptive immune response against an admixed antigen was investigated. In this study, nanogel-ligated IMDQ was shown to outperform soluble IMDQ in terms of cellular and humoral responses. We will not elaborate on these data in the current chapter, but a thorough discussion including experimental sections for all the above mentioned *in vivo* studies can be found in the corresponding paper.[30] Importantly, the covalent ligation of selected peptides and antigens to the nanogels could further unveil the potential of these IMDQ-nanogels as adjuvants for vaccination. Therefore we aimed at further engineering this nanogel platform by introducing protein-reactive moieties that enable antigen conjugation.

***Design of protein-reactive nanogels***

The design strategy for protein-reactive nanogels is depicted in **Scheme 2**. In a first step, block copolymers composed of p(PFPMA) and p(mTEGMA) were prepared via RAFT polymerization using respectively 4-cyano-4-(phenylcarbonothioylthio)pentanoic acid (CPTPA) and 4-cyano-4-[(ethylsulfanylthiocarbonyl)sulfanyl]pentanoic acid (CETPA) as a chain transfer agent (CTA) and AIBN as radical initiator. We started with polymerizing PFPMA affording p(PFPMA) polymers with either a dithiobenzoate end group [$p(PFPMA)_{33}$ generated by CPTPA] or an ethyl trithiocarbonate end group [$p(PFPMA)_{46}$ generated by CETPA] that could both be used as a macroCTA for the polymerization of mTEGMA. The reason for choosing this sequence, i.e. first polymerizing PFPMA and then mTEGMA, is because we desired to obtain block copolymers with the thiocarbonyl RAFT end group at the hydrophilic chain end for further post-modification into a cysteine-reactive vinyl sulfone moiety. **Table 1** summarizes the synthesis conditions and polymer characteristics of well-defined block copolymers **$p(PFPMA)_{33}$-*b*-$p(MTEGMA)_{35}$** and **$p(PFPMA)_{46}$-*b*-$p(MTEGMA)_{57}$**, further denoted as ***1*** and ***2***. Size exclusion chromatography (SEC) elugrams with THF as eluent are shown in **Figure 14**, and $^{1}H$- and $^{19}F$ NMR spectra can be found in the *Materials and Methods* section.

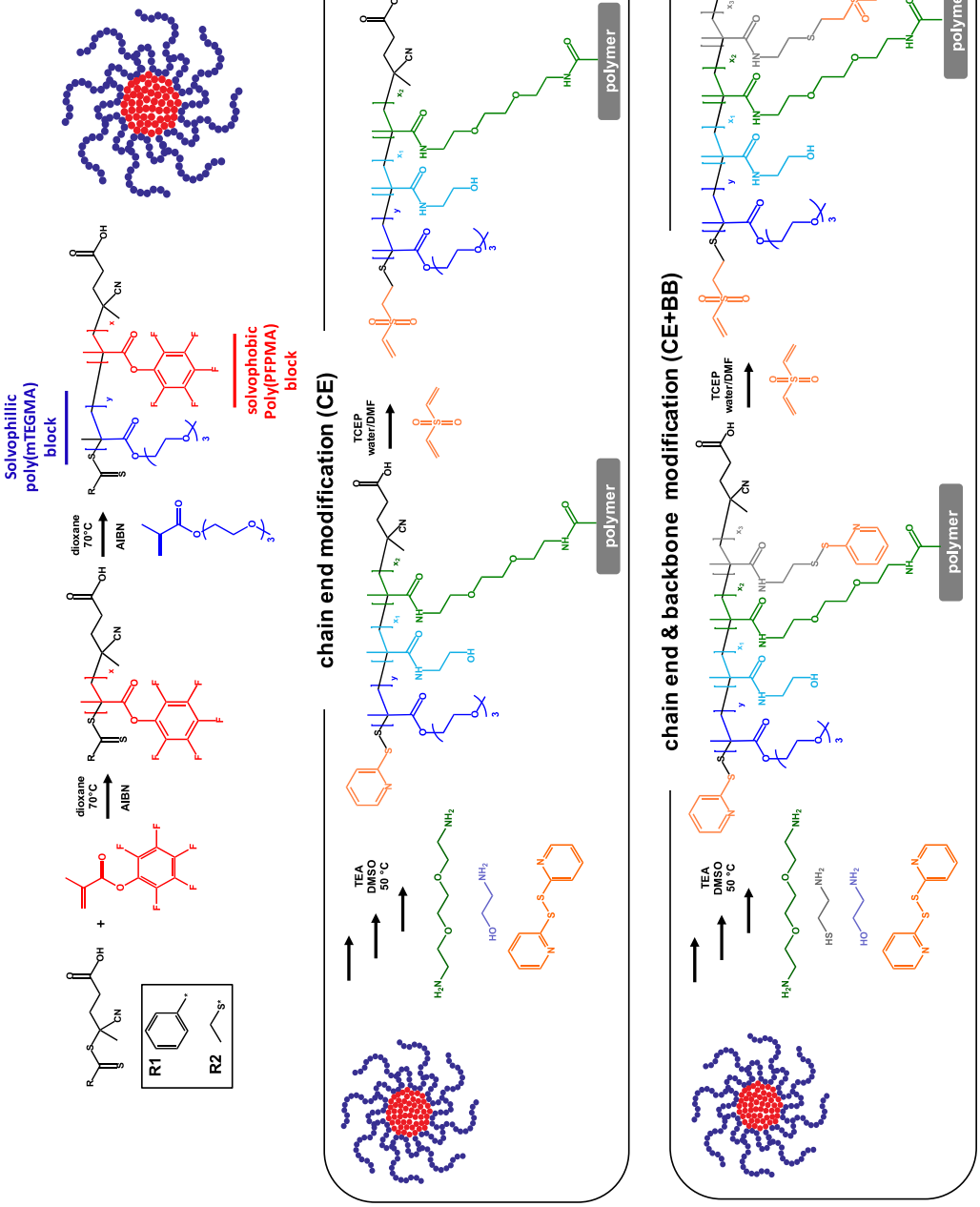


**Scheme 2.** Design strategy for protein-reactive nanogels. RAFT block copolymerization of PFPMA and mTEGMA was performed using CPTPA (R1) or CETPA (R2) as CTAs. Following self-assembly in DMSO, the block copolymer micelles were crosslinked by addition 2,2'-(ethylenedioxy)bis(ethylamine). The residual PFP esters were quenched with 2-ethanolamine, which also reacts with the thiocarbonyl group producing free thiols to allow chain end functionalization **(CE)**. Alternatively, after crosslinking, the remaining PFP esters were treated with cysteamine to allow for backbone functionalization prior to quenching with 2-ethanolamine **(BB)**. Free thiols were converted into pyridyldisulfide moieties, followed by transformation into vinyl sulfone.

**Table 1.** Results of RAFT homo and block copolymerization of PFPMA and mTEGMA.

| | CTA | [M]:[CTA] :[AIBN] | t (h) | p (%) | DP (NMR) | $M_{NMR}$ (g/mol) | $M_n$ (g/mol) | $M_w$ (g/mol) | Đ |
|---|---|---|---|---|---|---|---|---|---|
| **$(PFPMA)_{33}$** | CPTPA | 25:1:0.1 | 6 | 50 | 33 | 8,600 | 8,400 | 10,700 | 1.29 |
| **$p(PFPMA)_{46}$** | CETPA | 25:1:0.1 | 6 | 52 | 46 | 11,900 | 11,800 | 15,300 | 1.29 |
| **$p(PFPMA)_{33}$-*b*-$p(MTEGMA)_{35}$** | $p(PFPMA)_{33}$ | 65:1:0.15 | 18 | 72 | 35 | 16,700 | 11,500 | 14,000 | 1.22 |
| **$p(PFPMA_{46}$-*b*-$p(MTEGMA)_{57}$** | $p(PFPMA)_{46}$ | 90:1:0.15 | 18 | 83 | 57 | 25,100 | 19,800 | 24,000 | 1.21 |

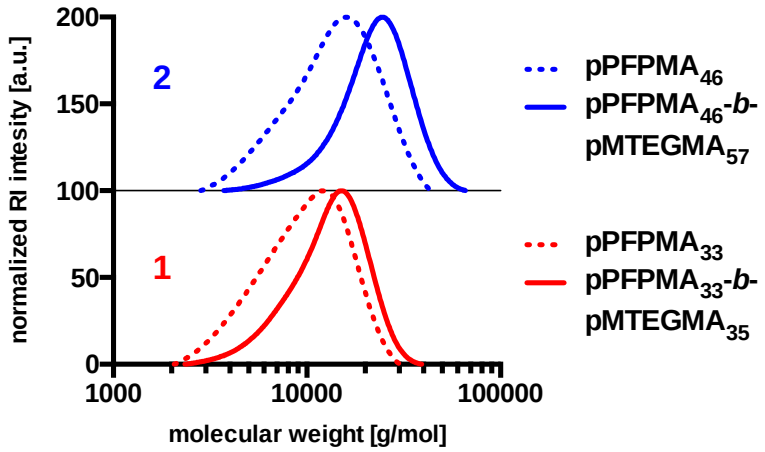


**Figure 14.** Size exclusion chromatogram (eluent: THF) of **p(PFPMA)** homo and **p(PFPMA)-*b*-p(MTEGMA)** block copolymers with their according molecular weights and distributions (based on poly(styrene) calibration).

In DMSO, both block copolymers ***1*** and ***2*** formed self-assembled nanoparticles with a mean diameter of respectively 25 and 40 nm, as measured by dynamic light scattering (DLS) (**Figure 15A**). Next, the self-assembled nanoparticles were core-crosslinked by addition of 0.25 equivalents 2, 2'-(ethylenedioxy)bis(ethylamine) in respect to reactive esters, forming stable intra- and inter-polymer amide bonds between the activated PFP-esters. For the sake of simplicity, we elaborated in this work solely on non-degradable nanogels. However, as shown for the TLR-ligated nanogels and as demonstrated in literature, this class of nanogels can easily be rendered degradable in response to endosomal pH using ketal-based bisamine crosslinkers.[28,30] As controls, we also prepared soluble polymers – instead of nanogels – by omitting this crosslinking step, which will further on in this chapter be denoted as '***polymer***', whereas crosslinked nanogels will be denoted as '***nanogel***'.

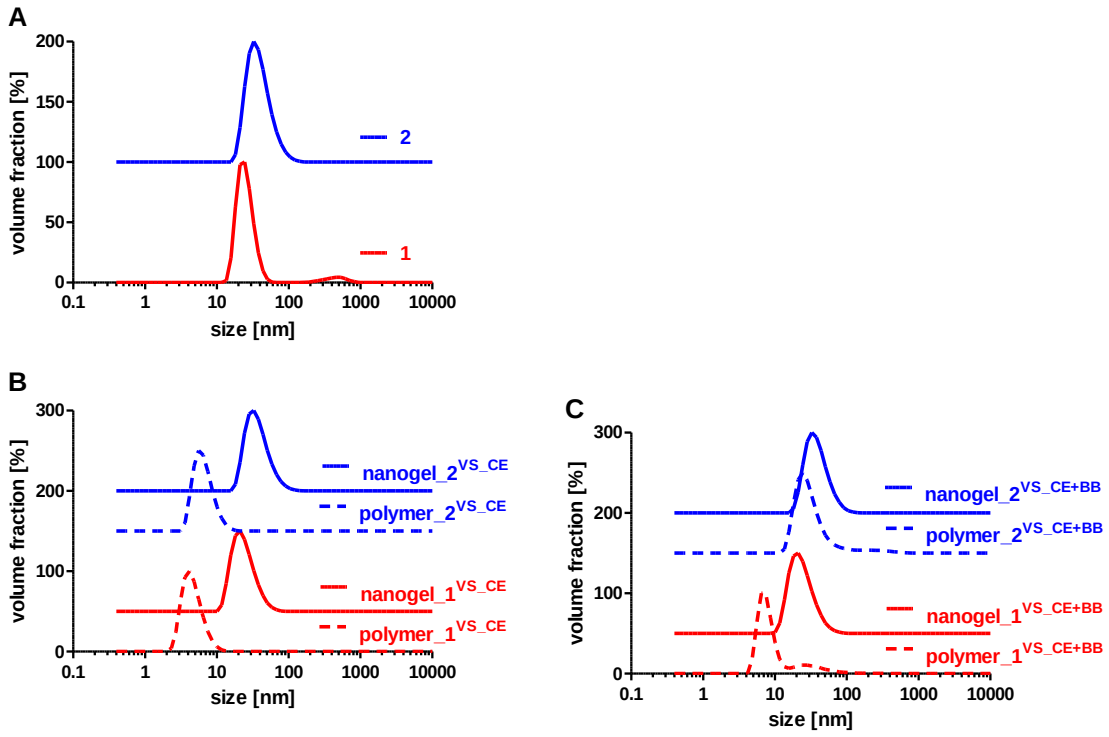


**Figure 15**. Size distribution curves (volume mean diameter) of ***1*** and ***2*** measured at 10 mg/mL **(A)** in DMSO, **(B)** after chain end functionalization, and **(C)** backbone and chain end vinyl sulfone functionalization. Crosslinked nanogels (denoted as 'nanogel') and non-crosslinked controls (denoted as 'polymer') were measured in 0.1M bicarbonate buffer pH 8.5.

Subsequently, the crosslinked nanoparticles were further engineered with cysteine-reactive moieties at either the p(mTEGMA) chain ends (CE) or both the p(mTEGMA) chain ends and the backbone (CE+BB) of the inner core polymers. For engineering cysteine-reactivity into the nanoparticles only at the chain end, after the crosslinking step, all remaining PFP-esters were converted by an excess of 2-aminoethanol. The use of 2-aminoethanol renders the inner core of the nanoparticles hydrophilic and yields fully hydrated nanogels upon transfer of the nanoparticles from DMSO to aqueous medium. To introduce cysteine-reactive moieties into the backbone of the inner core polymers, after crosslinking, the nanoparticles were first treated with 0.5 equivalents of cysteamine to convert remaining PFP-esters into mercaptoethylmethacrylamide moieties. Subsequently, the remaining unreacted PFP-esters were also converted to hydrophilic repeating units by addition of an excess 2-aminoethanol. For the sake of clarity, vinyl sulfone-functionalized nanogels and polymers will be annotated with *'VS_CE'* referring to nanogels with VS groups

only at the p(mTEGMA) chain ends, and *'**VS_CE+BB**'* referring to nanogels with VS groups both at the p(mTEGMA) chain ends and the backbone of the inner core polymer chains.

In the presence of primary amines, aminolysis of the thiocarbonyl RAFT end-groups leads to free thiols at the p(mTEGMA) chain ends. In our case, the used RAFT CTAs (CPTPA and CETPA) afforded block copolymers with either a dithiobenzoate or ethyl trithiocarbonate end group that are both suitable for conversion into free thiols by aminolysis. These chain end groups, as well as the thiols introduced into the nanogel core via cysteamine, were subsequently converted into cysteine-reactive vinyl sulfone moieties. For this purpose, the nanoparticles were transferred from DMSO to water via dialysis which also removed low molecular weight byproducts and unreacted species. Next, we attempted to react the free thiols with an excess of divinyl sulfone via a Michael-type thiol-ene reaction and in presence of TCEP, to reduce possibly formed disulfides. However, we observed that over the time course of several days during dialysis, the basic milieu that was generated for PFP-ester and RAFT end group aminolysis triggered extensive oxidation of the free thiols, which prevented subsequent Michael-type reaction with divinyl sulfone. Ellman's assay on these samples confirmed the absence of free thiols (**Figure 16**).

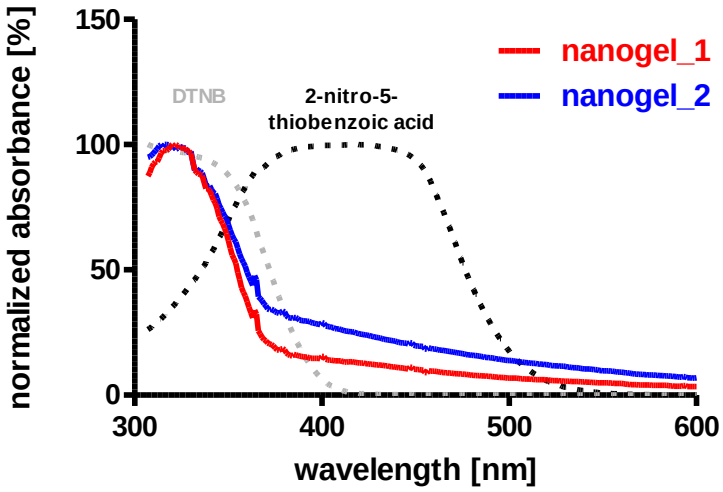


**Figure 16.** Results of an Ellman's assay for the detection of free thiols on polymer end groups in the corona of nanogel_1 and nanogel_2 prepared by block copolymer p(PFPMA)$_{33}$-*b*-p(MTEGMA)$_{35}$ (**1**) and p(PFPMA)$_{46}$-*b*-p(MTEGMA)$_{57}$ (**2**) after cross-linking with 2, 2'-(ethylenedioxy)bis(ethylamine), RAFT end group aminolysis with excess 2-aminoethanol and subsequent dialysis (no treatment with 2,2'-dipyridyl disulfide). No release of 2-nitro-5-thiobenzoic acid from the Ellman's reagent (DTNB) was found.

To circumvent this issue, immediately after PFP-ester conversion, free thiols were capped by addition of 2,2'-dipyridyldisulfide in a one-pot setting without the need for intermitted purification. Besides avoiding oxidation during further work-up, capping free thiols with 2,2'-dipyridyl disulfide also prevented unwanted inter-particle crosslinking by disulfide formation. After removal of low molecular weight by-products and the excess of unreacted species by spin filtration, free thiols were regenerated upon reduction of the disulfide linkages by TCEP, as monitored by UV-Vis spectrophotometric detection of the released pyridine-2-thione (**Figure 17** for nanogels**, Figure 18** for polymers). Note that spin filtration was preferred over dialysis to shorten the time scale of preparation and reduce the risk of unwanted oxidative side reactions. Subsequently, the free thiols were reacted with an excess of divinyl sulfone to yield cysteine-reactive vinyl sulfone (VS)-functionalized nanogels. Additionally, we also prepared control nanogels and soluble polymers by omitting the divinyl sulfone modification step. Note that in this case, due to the TCEP treatment, all pyridyldisulfide moieties at the polymer chain ends and backbone were converted into free thiols (**SH**). Finally, all samples were extensively dialyzed and obtained as a dry powder after lyophilization.

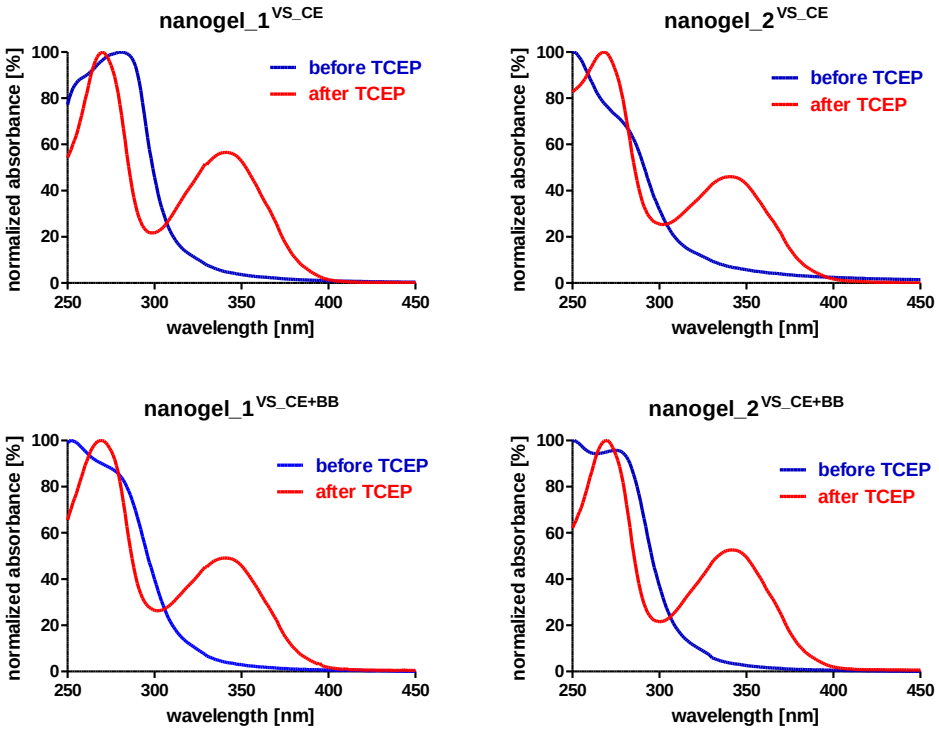


**Figure 17**. UV-Vis spectroscopy analysis of nanogels before (blue curves) and after (red curves) the addition of TCEP demonstrates the release of pyridine-2-thione ($\lambda_{max}$ = 343 nm) upon reduction of disulfide linkages, thereby generating free thiols that subsequently can be modified with divinyl sulfone.

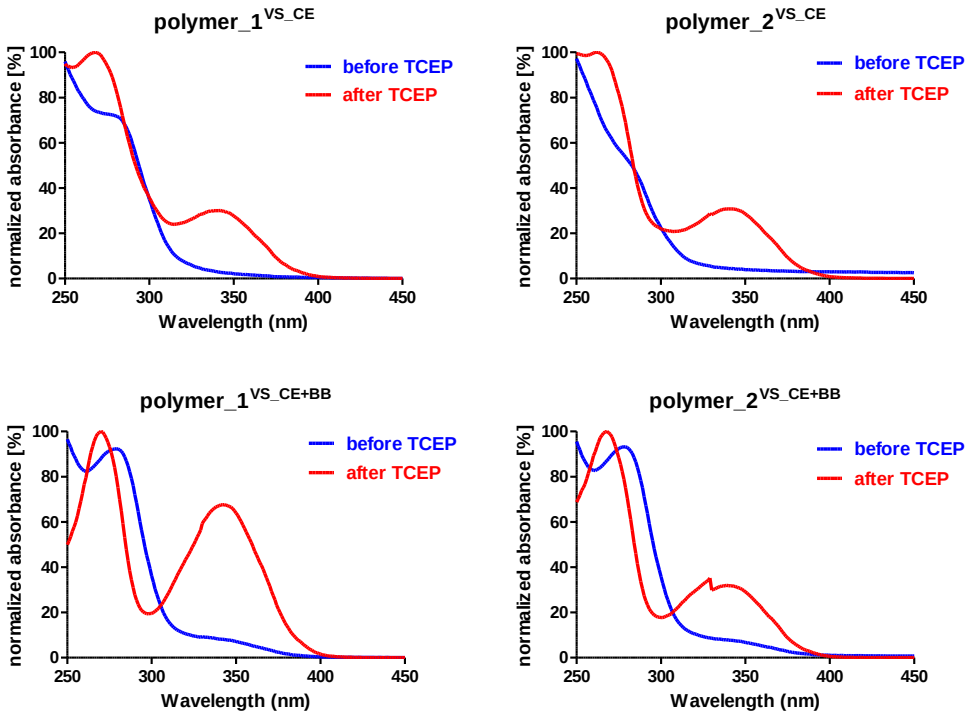


**Figure 18**. UV-Vis spectroscopy analysis of non-crosslinked polymer before (blue curves) and after (red curves) the addition of TCEP demonstrates the release of pyridine-2-thione ($\lambda_{max}$ = 343 nm) upon reduction of disulfide linkages, thereby generating free thiols that subsequently can be modified with divinyl sulfone.

DLS analysis of re-dispersed samples in aqueous medium are shown in **Figure 15B-C**. For both ***1*** and ***2***, crosslinking of the self-assembled micellar structures in DMSO (*vide supra*) with bisamines afforded the formation of nanogels with similar sizes in aqueous medium as those measured in DMSO before transformation of the PFP esters (**Figure 15A**). Contrary, when the crosslinking step was omitted, chain end vinyl sulfone functionalized polymers (i.e. ***polymer***$^{VS_CE}$) were fully water soluble due to the introduction of 2-aminoethanol onto the reactive ester moieties and exhibited unimer sizes of about 5 nm and 6.6 nm for ***1*** and ***2*** respectively. However, backbone functionalization of the polymers (i.e. ***polymer***$^{VS_CE+BB}$) with vinyl sulfone introduced new hydrophobic moieties onto the reactive ester moieties and caused some aggregate formation, in particular in case of ***2***$^{VS_CE+BB}$. To confirm the successful incorporation of vinyl sulfone, NMR analysis was performed on the non-crosslinked polymers **(Figure 19)**. For the chain end functionalized polymer (i.e. ***polymer***$^{VS_CE}$) we can clearly distinguish the vinyl sulfone proton peaks at 6.25-6.50 ppm and 6.85-7 ppm respectively. Nonetheless they are relatively weak since only one vinyl sulfone per polymer is possible. Side chain functionalized polymers (i.e. ***polymer***$^{VS_CE+BB}$) by contrast; show broader peaks

with an increased intensity due to multiple vinyl sulfones per polymer. However, in both cases peak integration was not accurate enough for quantitative analysis.

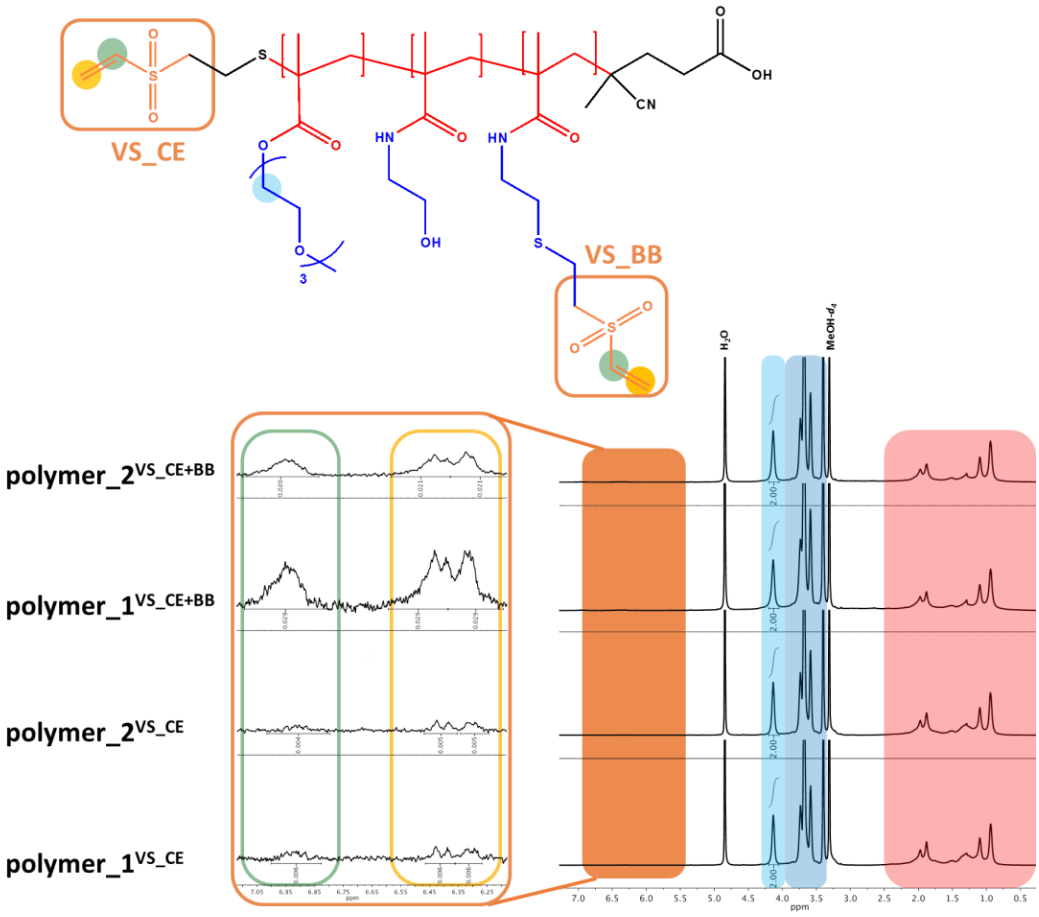


**Figure 19**. $^{1}$H-NMR (400 MHz, $CD_3OD$) δ (ppm) of non-crosslinked polymer 1 and 2 with chain end ($^{VS_CE}$) and backbone ($^{VS_CE+BB}$) vinyl sulfone functionalization.

Finally, we assessed the conjugation efficiency of the vinyl sulfone functionalized nanogels and soluble control polymers. For this purpose, we used bovine serum albumin (BSA) as model protein, and assessed conjugation efficiency by SDS-PAGE gel electrophoresis under reducing conditions in presence of β-mercaptoethanol. The reason for using BSA, is its commercial availability and widespread use as model protein. BSA contains a cysteine that does not participate in a disulfide bond (Cys-34). However, this thiol can be partially oxidized and therefore BSA was pretreated with 10 mM TCEP. Maynard and coworkers have previously demonstrated that this mild reductive treatment induces cleavage of one disulfide bond, exposing 2 additional free thiols.[38] The subsequent conjugations were performed in a 0.1 M bicarbonate buffer at pH 8.5 containing 10% DMSO to enhance

solubility of the vinyl sulfone moieties. Either 40 or 80 equivalents of nanogels/polymer to protein were added.

In a first series of conjugation experiments, we used the non-crosslinked soluble polymers, with both chain end and chain end plus backbone vinyl sulfone modification, to establish a proof-of-concept for vinyl sulfone-based conjugation for this type of polymers. The SDS-PAGE data in **Figure 20** clearly demonstrates successful conjugation of the vinyl sulfone-modified polymers to BSA. Note that SDS-PAGE was run under reducing conditions in presence of β-mercaptoethanol, which means that any disulfide formation between BSA and free thiols on the control polymers and nanogels were cleaved. Optical integration was performed to obtain semi-quantitative data, as described in **Chapter 4**. Not unexpectedly, a higher conjugation efficiency is obtained for polymers that contain vinyl sulfone moieties both at their chain end and backbone, i.e. $\boldsymbol{polymer^{VS_CE+BB}}$, as this offers multiple sites for protein conjugation per polymer chain. These $\boldsymbol{polymer^{VS_CE+BB}}$ samples also yield higher molecular weight conjugates, evidenced by the emergence of a broad band on the SDS-PAGE gel close to where the samples were loaded. Likely, this is due to multiple BSA molecules that became crosslinked by one or more polymers. With regard to the effect of the polymer to protein ratio, no significant increase in the fraction of conjugated protein is observed. These findings also point out the relatively low binding efficiency of a 'grafting to' approach when attempting to conjugate relatively large polymers to relatively large proteins. However, this drawback might be less pronounced for smaller, biologically relevant peptide antigens that are less sterically hindered, or for recombinant proteins that are engineered with readily accessible pending cysteine residues.

In a second series of experiments, BSA was conjugated to nanogels bearing vinyl sulfone moieties either at their chain ends or both their chain ends and inner core backbone. Interestingly, similar conjugation efficiencies were obtained for nanogels (**Figure 21**) as for the soluble control polymers. First of all, this means that sterical restriction induced from the crosslinking does not affect the ability of the chain end vinyl sulfone moieties to conjugate to proteins. Second, this also means that vinyl sulfone moieties located on the backbone of the inner core polymer block are also accessible for protein conjugation. This can likely be attributed to the fully hydrated nature of the nanogels, which can allow inwards diffusion of proteins; or to a more *compound micelle* like assembly, which means that both polymer

blocks are not fully phase separated, but also intermixed. Such structure would lead to a strong increase of cysteine-reactive vinyl sulfone moieties on the nanogel surface.

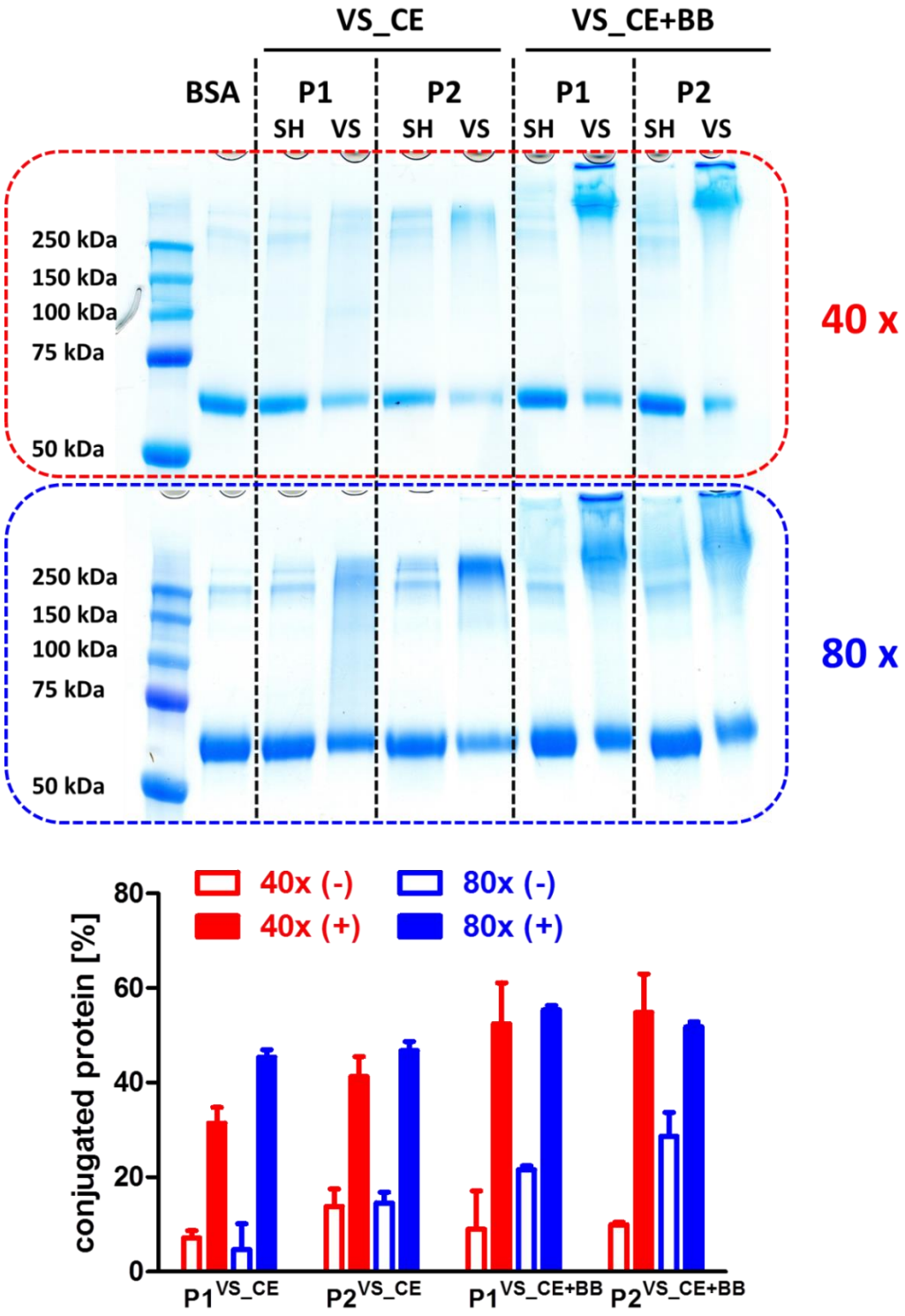


**Figure 20.** SDS-PAGE results from the conjugation of BSA (66 kDa) with chain end ***(CE)*** and backbone ***(CE+BB)*** vinyl sulfone functionalized ***(VS)*** non-crosslinked polymers P1 and P2 in a molar ratio of protein:polymer 1:40 and 1:80. Additionally, non-functionalized polymers ***(SH)*** were used as negative controls. (Mean ± SD, *n* = 3)

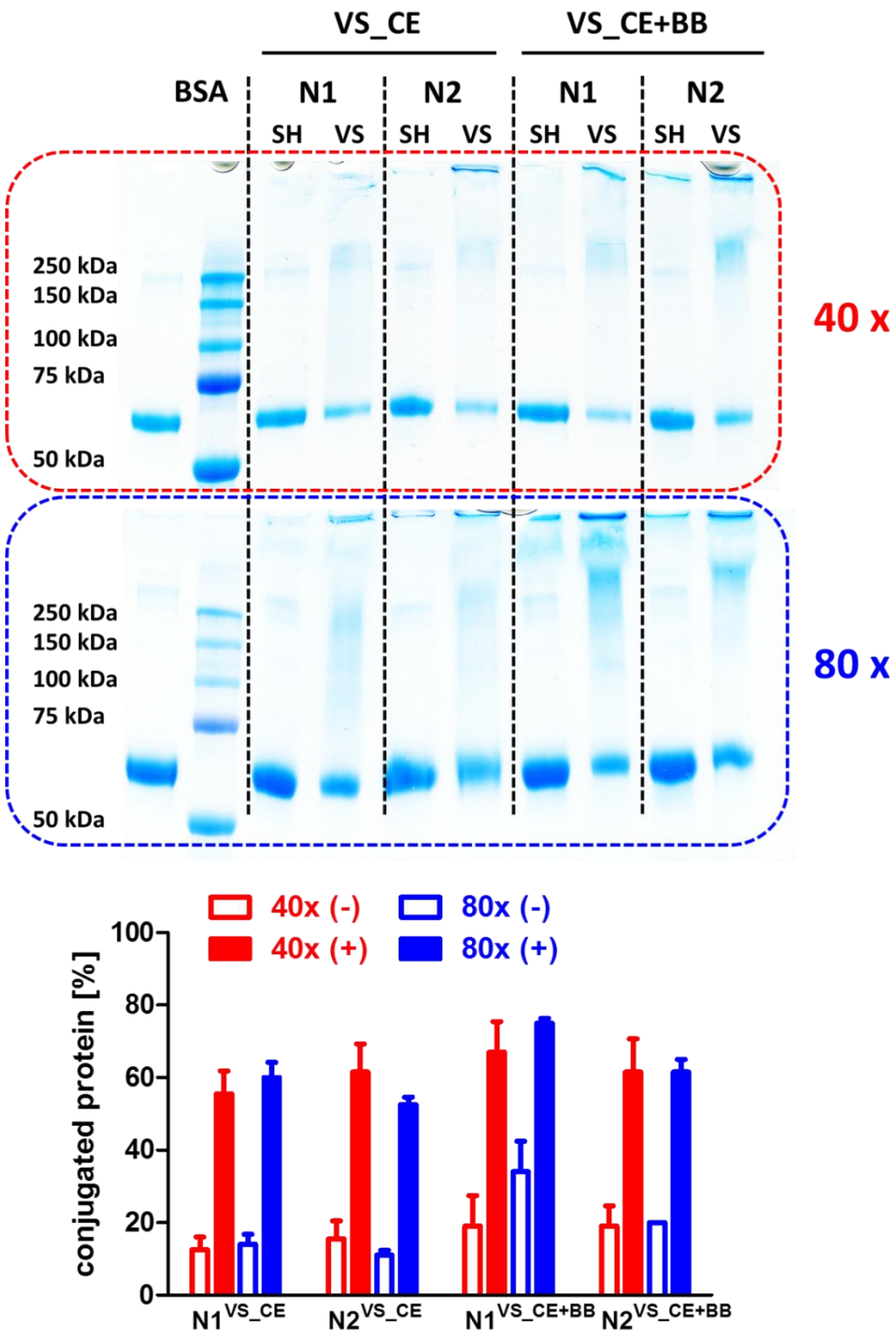


**Figure 21.** SDS-PAGE results from the conjugation of BSA (66 kDa) with chain end ***(CE)*** and backbone ***(CE+BB)*** vinyl sulfone functionalized ***(VS)*** crosslinked nanogels N1 and N2 in a molar ratio of protein:nanogel 1:40 and 1:80. Additionally, non-functionalized nanogels ***(SH)*** were used as negative controls. (Mean ± SD, *n* = 3)

## Conclusion

In summary, we have demonstrated an elegant route to engineer well-defined core-crosslinked polymeric nanogels with a small molecule imidazoquinoline-based TLR7/8 agonist or protein antigens respectively. These nanogels combine the efficient triggering of TLR7/8, with focusing immune activation to the local injection site and its draining lymph node. This is of vital importance as it limits the inflammatory toxicity associated with the use of soluble TLR agonists and thus should enable one to increase the dose and to obtain improved therapeutic efficacy. Moreover, nanogel mediated delivery of IMDQ was more potent at inducing T cell responses and antibody responses against admixed antigen when compared to soluble IMDQ. To further unveil the potential of these IMDQ-nanogels as adjuvants for vaccination, we elaborated on a strategy to covalently ligate selected peptides by introducing cysteine-reactive vinyl sulfone moieties. Importantly, when compared to non-crosslinked soluble control polymers, crosslinked nanogels exhibited similar conjugation efficiencies, pointing out that the installed vinyl sulfone moieties are well accessible for cysteine-conjugation, even to a relatively large protein as BSA (66.5 kDa). Our ongoing efforts focus on the design of engineered nanocarriers for vaccine delivery that can combine potent immune-stimulatory molecules with peptide or protein antigens, to further amplify cellular and humoral immune responses.

## References


1 Hubbell, J. A., Thomas, S. N. & Swartz, M. A. Materials engineering for immunomodulation. *Nature* **462**, 449-460 (2009).

2 Moon, J. J., Huang, B. & Irvine, D. J. Engineering Nano- and Microparticles to Tune Immunity. *Advanced Materials* **24**, 3724-3746 (2012).

3 De Koker, S. *et al.* Designing polymeric particles for antigen delivery. *Chem. Soc. Rev.* **40**, 320-339 (2011).

4 Kasturi, S. P. *et al.* Programming the magnitude and persistence of antibody responses with innate immunity. *Nature* **470**, 543-547 (2011).

5 Banchereau, J. *et al.* Immunobiology of dendritic cells. *Annu. Rev. Immunol.* **18**, 767-811 (2000).

6 Reddy, S. T. *et al.* Exploiting lymphatic transport and complement activation in nanoparticle vaccines. *Nat. Biotechnol.* **25**, 1159-1164 (2007).

7 Liu, H. P. *et al.* Structure-based programming of lymph-node targeting in molecular vaccines. *Nature* **507**, 519-522 (2014).

8 Kwon, Y. J. *et al.* In vivo targeting of dendritic cells for activation of cellular immunity using vaccine carriers based on pH-responsive microparticles. *Proc. Natl. Acad. Sci. U. S. A.* **102**, 18264-18268 (2005).

9 Moon, J. J. *et al.* Interbilayer-crosslinked multilamellar vesicles as synthetic vaccines for potent humoral and cellular immune responses. *Nat. Mater.* **10**, 243-251 (2011).

10 Scott, E. A. *et al.* Dendritic cell activation and T cell priming with adjuvant- and antigen-loaded oxidation-sensitive polymersomes. *Biomaterials* **33**, 6211-6219 (2012).

11 Coffman, R. L., Sher, A. & Seder, R. A. Vaccine Adjuvants: Putting Innate Immunity to Work. *Immunity* **33**, 492-503 (2010).

12 Narayan, R. *et al.* Immunomodulation by Imiquimod in Patients with High-Risk Primary Melanoma. *J. Invest. Dermatol.* **132**, 163-169 (2012).

13 Diebold, S. S. *et al.* Innate antiviral responses by means of TLR7-mediated recognition of single-stranded RNA. *Science* **303**, 1529-1531 (2004).

14 Hemmi, H. *et al.* Small anti-viral compounds activate immune cells via the TLR7 MyD88-dependent signaling pathway. *Nat. Immunol.* **3**, 196-200 (2002).

15 Dudek, A. Z. *et al.* First in Human Phase I Trial of 852A, a Novel Systemic Toll-like Receptor 7 Agonist, to Activate Innate Immune Responses in Patients with Advanced Cancer. *Clin. Cancer Res.* **13**, 7119-7125 (2007).

16 Weigel, B. J. *et al.* Prolonged Subcutaneous Administration of 852A, a Novel Systemic Toll-like Receptor 7 Agonist, to Activate Innate Immune Responses in Patients with Advanced Hematologic Malignancies. *Am. J. Hematol.* **87**, 953-956 (2012).

17 Wu, T. Y.-H. *et al.* Rational design of small molecules as vaccine adjuvants. *Science Translational Medicine* **6**, 263ra160-263ra160 (2014).

18 Nembrini, C. *et al.* Nanoparticle conjugation of antigen enhances cytotoxic T-cell responses in pulmonary vaccination. *Proceedings of the National Academy of Sciences* **108**, E989–E997 (2011).

19 De Geest, B. G. *et al.* Surface-Engineered Polyelectrolyte Multilayer Capsules: Synthetic Vaccines Mimicking Microbial Structure and Function. *Angew. Chem.-Int. Edit.* **51**, 3862-3866 (2012).

20 Wilson, J. T. *et al.* pH-Responsive Nanoparticle Vaccines for Dual-Delivery of Antigens and Immunostimulatory Oligonucleotides. *ACS Nano* **7**, 3912-3925 (2013).

21 Ilyinskii, P. O. *et al.* Adjuvant-carrying synthetic vaccine particles augment the immune response to encapsulated antigen and exhibit strong local immune activation without inducing systemic cytokine release. *Vaccine* **32**, 2882-2895 (2014).

22 Lynn, G. M. *et al.* In vivo characterization of the physicochemical properties of polymer-linked TLR agonists that enhance vaccine immunogenicity. *Nat Biotech* **33**, 1201-1210 (2015).

23 Lyon, R. P. *et al.* Self-hydrolyzing maleimides improve the stability and pharmacological properties of antibody-drug conjugates. *Nat. Biotechnol.* **32**, 1059-+ (2014).

24 Grover, G. N. *et al.* Trapping of Thiol-Terminated Acrylate Polymers with Divinyl Sulfone To Generate Well-Defined Semitelechelic Michael Acceptor Polymers. *Macromolecules* **42**, 7657-7663 (2009).

25 Eberhardt, M. *et al.* Synthesis of pentafluorophenyl(meth)acrylate polymers: New precursor polymers for the synthesis of multifunctional materials. *European Polymer Journal* **41**, 1569-1575 (2005).

26 De Koker, S. *et al.* Engineering Polymer Hydrogel Nanoparticles for Lymph Node-Targeted Delivery. *Angewandte Chemie International Edition*, n/a-n/a (2015).

27 Nuhn, L. *et al.* Cationic Nanohydrogel Particles as Potential siRNA Carriers for Cellular Delivery. *ACS Nano* **6**, 2198-2214 (2012).

28 Duong, H. T. T. *et al.* Acid Degradable and Biocornpatible Polymeric Nanoparticles for the Potential Codelivery of Therapeutic Agents. *Macromolecules* **44**, 8008-8019 (2011).

29 Convertine, A. J. *et al.* Development of a novel endosomolytic diblock copolymer for siRNA delivery. *J. Control. Release* **133**, 221-229 (2009).

30 Nuhn, L. *et al.* pH-degradable imidazoquinoline-ligated nanogels for lymph node focused immune activation. *Proceedings of the National Academy of Sciences* (2016).

31 Shen, Z. H. *et al.* Cloned dendritic cells can present exogenous antigens on both MHC class I and class II molecules. *J. Immunol.* **158**, 2723-2730 (1997).

32 De Koker, S. *et al.* Polyelectrolyte Microcapsules as Antigen Delivery Vehicles To Dendritic Cells: Uptake, Processing, and Cross-Presentation of Encapsulated Antigens. *Angew. Chem.-Int. Edit.* **48**, 8485-8489 (2009).

33 Randolph, G. J. *et al.* Differentiation of Phagocytic Monocytes into Lymph Node Dendritic Cells In Vivo. *Immunity* **11**, 753-761 (1999).

34 Shukla, N. M. *et al.* Structure-Activity Relationships in Human Toll-Like Receptor 7-Active Imidazoquinoline Analogues. *J. Med. Chem.* **53**, 4450-4465 (2010).

35 Duong, H. T. T. *et al.* Acid Degradable and Biocompatible Polymeric Nanoparticles for the Potential Codelivery of Therapeutic Agents. *Macromolecules* **44**, 8008-8019 (2011).

36 Binauld, S. & Stenzel, M. H. Acid-degradable polymers for drug delivery: a decade of innovation. *Chem. Commun.* **49**, 2082-2102 (2013).

37 Lienenklaus, S. *et al.* Novel Reporter Mouse Reveals Constitutive and Inflammatory Expression of IFN-beta In Vivo. *J. Immunol.* **183**, 3229-3236 (2009).

38 Heredia, K. L. *et al.* In situ preparation of protein - "Smart" polymer conjugates with retention of bioactivity. *J. Am. Chem. Soc.* **127**, 16955-16960 (2005).

# PART III

## Future perspectives

## & general conclusions

# Chapter 8

# Broader international context, relevance and future perspectives

Strategies to engineer the immune system via a materials chemistry approach, i.e. immuno-engineering, have gathered major attention the past decade. In part, this popularity is supported by the Nobel Prize in Medicine, that was awarded to Ralph Steinman in 2011 for the discovery of the dendritic cell (DC) and its role in adaptive immunity. In particular developing strategies to efficiently deliver specific signals and molecules to DCs and T cells to modulate their behaviour and/or increase to amplitude of their action, is highly attractive to design the next generation of vaccines against intracellular pathogens and to control metastatic growth by developing cancer vaccines.

In this thesis, materials chemistry is merged with immunology to develop nanoscale polymeric delivery systems for antigens and molecular adjuvants. A first approach that we have developed is the conjugation of so-called transiently thermoresponsive polymers to protein antigens. We defined transiently thermoresponsive polymers as polymer that are water soluble below a critical temperature, but precipitate from solution above this temperature; and loose this property in response to a chemical transformation in the polymer side chains or back bone, to become fully water-soluble irrespective of temperature. By conjugating such polymers to protein antigens, we envisioned to temporarily change the physicochemical state of the antigen between soluble and (nano)particulate. In this concept, the hydrophilic protein would form a stabilizing shell that prevents the transiently

thermoresponsive polymers from forming macroscopic aggregates at temperatures above their cloud point ($T_{cp}$), with the formation of micellar nanoparticles instead. In **Chapter 2** an extensive overview on transiently thermoresponsive polymers is provided, including contributions of our own research group, with a particular focus on (meth)acrylamide monomers that can be polymerized via controlled radical polymerization.

From the conceptual point of view, there is similarity with the HPMAm-$Lac_2$ technology that has been developed in the research group of Prof. Dr. Wim Hennink (Utrecht University, The Netherlands) with whom our group has an active collaboration. The HPMAm-$Lac_2$ technology provides access to poly(methacrylamide) polymers that are water soluble below roughly 10°C, and precipitate from solution above this temperature. In response to alkaline pH, the lactate esters in the polymer side chain undergo irreversible hydrolysis yielding hydrophilic HPMAm units. This feature is highly interesting for sustained release applications, but less for cell uptake triggered drug release. Indeed, upon cellular uptake, nanoparticles are typically stored in acidic vesicles (termed phagosomes, endosomes, lysosomes) that have a pH of about 5 to 6.5. Therefore, in this thesis, focus has been put on the use of ketal-based systems that are stable at alkaline and neutral pH, but degrade in response to acidic pH.

Ketal-based (co)polymers have been used in **Chapter 4-5** to prepare transiently thermoresponsive polymer-protein conjugates. In **Chapter 4** a 'grafting to' approach was elaborated on, in which polymers were synthesized with a protein reactive end-group. In **Chapter 5** a 'grafting from' approach was explored, in which proteins were functionalized with a specific group that allowed for the subsequent growth of a polymer chain. The advent of controlled radical polymerization (CRP) has triggered a boom in the development of well-defined functional polymers. CRP allows for precise control over molecular weights, with a very narrow molecular weight distribution (i.e. dispersity) by suppressing chain termination and other side-reactions. Moreover, the reduction of high-molecular-weight impurities avoids incomplete renal excretion. The two most popular controlled radical polymerization techniques are atom transfer radical polymerization (ATRP) and reversible addition-fragmentation chain transfer polymerization (RAFT). Both have been used for 'grafting to' and 'grafting from' approaches, pioneered by several groups including Maynard[1], Sumerlin[2], Boyer[3], Haddleton[4] and Matyjaszewski[5]. RAFT in particular has gained popularity in a biomedical context, due to the relatively benign reaction conditions and the tolerance to

several functional groups. Therefore, RAFT was the preferred controlled radical polymerization technique in this thesis, and major effort was devoted to the synthesis of functional RAFT chain transfer agents that bear a lysine- or cysteine-reactive moiety at their R-position (**Chapter 3**). Procedures from Sumerlin[6], Stenzel[7], Maynard[8] and Velonia[9] were used to synthesize 2-propanoic acid butyl trithiocarbonate (PABTC) bearing N-hydroxysuccinimide respectively pentafluorophenyl activated esters as lysine reactive moieties, and pyridyldisulfide respectively maleimide as cysteine-reactive moieties. Head-to-head comparison of polymers based on these RAFT CTAs with respect to their conjugation efficiency, yielded fairly large differences depending on conjugation chemistry and protein type (**Chapter 4**). The most striking observation however, which is in accordance to literature, is the very low conjugation efficiency that is obtained. For example, to achieve a nearly 100 % conjugation efficiency of BSA, a 20 fold molar excess of PFP-containing polymer is required. Taking into account the 59 lysine units in BSA plus the N terminus that could potentially be conjugated, roughly a 1000 fold excess of reactive ester end-functionalized polymers relative to lysine units is required.

Moreover, in case of lysine-based polymer-protein conjugation, a mixture of proteins conjugated with multiple polymer strands is obtained. Maleimide- and pyridyldisulfide-based conjugation strategies by contrast, are more site-specific as cysteines are generally less abundant. However, maleimides are relatively unstable in aqueous medium and need to be treated with care prior to conjugation. Moreover, maleimide-based conjugation has recently been reported to be prone to retro Michael-type addition and hydrolysis of the formed linkage.[10] Pyridyldisulfides on their hand are stable in aqueous medium, and form disulfide linkages with free thiols. The reducible nature of these disulfides can be attractive for the design of drug delivery systems, as illustrated in **Chapter 6**. However, with respect to protein conjugation, the likeliness of disulfide exchange with other thiols present in the body needs to be taken into account. In view of this hurdle, recently emerging strategies based on unnatural amino acids containing azides or alkynes - that are genetically engineered into proteins and afford subsequent alkyne-azide cycloaddition - might offer a solution due to the high reactivity of these types of reactions (**Chapter 4**).[11,12] Alternative approaches that target the modification of the N-terminus might not offer a solution to low conjugation efficiency, but could offer an important advantage with regard to site specificity.[13]

Using a 'grafting from' approach, one can largely avoid a fraction of soluble polymer as the polymer is intended to grow from a protein-based macroCTA onwards. Using this approach and BSA as model protein, we were able to synthesize transiently thermoresponsive polymer-protein conjugates and demonstrate their temperature-triggered assembly and pH-triggered irreversible disassembly (**Chapter 5**). The RAFT CTA was introduced onto lysine units, but alternative strategies targeting cysteine moieties or involving more recent approaches, such as the use of unnatural amino acids or N-terminal modification, could also be attempted. However, with respect to RAFT polymerization, it is important to use reaction conditions with a sufficiently high concentration of radical initiator to initiate the RAFT process. At very low radical concentrations, such as those when only one CTA per protein chain is present, RAFT is unlikely to proceed. In this regard, SET-LRP might be beneficial as recently reported by the Haddleton group.[14] In **Chapter 5,** the RAFT grafting from approach was used to polymerize the monomer [(2,2-dimethyl-1,3-dioxolane) methyl]acrylamide (DMDOMAm), an acrylamide reported by the Kizhakkedathu group to yield polymers with a phase transition temperature around room temperature.[15] However, a drawback of the cyclic ketals in the DMDOMAm repeating units is the relative slow degradation in mild acidic medium. Therefore, new endeavors into the synthesis of faster degrading ketal monomers is of interest. This research is currently undertaken in our research group and linear ketal crosslinkers that afford rapid degradation under mildly acidic conditions have been used for the design of core-crosslinked micelles in **Chapter 7**.

Interestingly, self-assembled polymer-based amphiphiles are capable of forming nanoparticles in the range from a few tens to a few hundreds of nanometer. This size range is well suited to promote passive diffusion of nanoparticles, as has been reported by several groups.[16,17] Nonetheless, stability of self-assembled nanoparticles under physiological conditions is often questionable due to the strong dilution upon administration and the presence of other amphiphilic components such as proteins, lipids et cetera.[18] Subsequent micelle dissociation leads to uncontrollable biodistribution properties. Therefore it is critical to obtain a more comprehensive understanding of the *in vivo* fate of both amphiphilic polymers and self-assembled polymeric nanoparticles.[19] In this respect, a simple and straightforward approach to avoid premature disintegration of micellar nanomedicines is to stabilize them via crosslinking. [20,21] On the other hand, engineering hydrophilic compounds with hydrophobic lipid tails has recently been shown to be a very efficient strategy to deliver

immunologically active compounds to the draining lymph nodes through albumin hitchhiking.[22] In this regard, an exciting avenue for transiently thermoresponsive polymers would be to conjugate these to hydrophilic peptide or protein antigens, or non-small molecule molecular adjuvants (i.e. PAMPS such as TLR agonists, **Chapter 1**) to alter their solubility state from fully hydrophilic unimers to self-assembled micelles or generally albumin-binding amphiphiles. This has not been endeavored during this thesis due to the slow degradation of the DMDOMAm system, but will be addressed in future work of our research group using a new generation of ketal- and carbonate-based monomers that exhibit more favorable degradation behavior in a physiologically relevant window.

Initially intended as a side-project in this thesis, we evaluated the *in vitro* and *in vivo* immuno-biological behavior of hydrogel nanoparticles produced by the lab of Prof. Dr. Frank Caruso (University of Melbourne, Australia) (**Chapter 6**). These nanocapsules were fabricated through sequential adsorption of thiol- and pyridyldisulfide-modified poly(methacrylic acid) (PMA) onto sacrificial 200 nm sized mesoporous silica spheres, that are afterwards decomposed by HF treatment.[23-25] A major focus was to investigate the effect of PEGylation on the lymphatic transportation behavior of these hydrogel nanoparticles. PEGylation has proven its use for extending the half-life of therapeutic proteins and improving the plasma stability of nanoparticles.[26] We found that PEGylation had no influence on nanoparticle uptake by DCs *in vitro*, but strongly improved lymphatic transportation. In the course of these research endeavors, we also devoted attention to super resolution microscopy imaging of nanoparticle uptake by DCs. For this purpose, we collaborated with the group of Dr. Lorenzo Albertazzi (Institute for Bioengineering of Catalonia, Spain and Eindhoven University of Technology, Netherlands). Amongst the different kinds of super resolution microscopy, stochastical optical reconstruction microscopy (STORM) is applicable to the use of common organic dyes, in particular cyanines, and offers a resolution down to a few tens of nanometers. By contrast, the slow acquisition time makes it less applicable to live cell imaging, unless more sophisticated set-ups are deployed or other super resolution techniques including stimulated emission depletion (STED) microscopy are used. For our specific case, STORM allowed us to image nanoparticle uptake at a single nanoparticle and single endosome level, which is amongst the first reports on super resolution microscopy imaging of nanomedicines. In a parallel study, using poly(styrene) nanoparticles as model

nanomedicines, we also contributed to comparing the potential of STORM versus conventional confocal microscopy and TEM for intracellular imaging.

Based on the promising lymphatic transportation behavior of hydrogen nanoparticles, we have explored the ability of degradable core-crosslinked nanoparticles for lymph node focused vaccine delivery (**Chapter 7**). This approach has been pioneered by amongst others the Hubbell[16], Irvine[22] and Stayton[27] groups; mostly focusing on non-covalent entrapment and/or the use of non-degradable systems. Inspired by the work of Nuhn *et al.*[28], we exploited a nanogel system based on amphiphilic block copolymers that contain a hydrophilic PEG-like block and a solvophobic poly(pentafluorophenyl methacrylate) block containing activated ester repeating units. The latter affords self-assembly in polar aprotic solvents such as DMSO, which avoids hydrolysis of the activated esters that would occur in aqueous medium. This approach offers the possibility to dial in bisamine crosslinkers, amine-containing dyes and bioactive molecules; as well as handles for subsequent bio-conjugation. By introducing the crosslinks into the particle core, the surface and stealth properties of the PEG-like shell remain intact. To obtain nanogels that could degrade in response to the acidic pH in intracellular vesicles, a bisamine containing a linear ketal was used. To obtain fully hydrated nanogels, the remaining activated esters were converted to hydrophilic repeating units by addition of an excess of a hydrophilic monoamine. Based on the chain length of the block copolymers, nanogels ranging from 20 - 100 nm could be obtained. Contrary to the cyclic ketals used earlier in this thesis, the incorporation of a linear ketal rendered the nanogels degradable at pH 5 in a timeframe of a few hours.

This system was used to covalently attach a relatively hydrophobic small molecule imidazoquinoline TRL7/8 agonist via amide bond formation. This imidazoquinoline compound has been developed in the lab of Prof. Dr. Sunil David (University of Minnesota, U.S.) with whom our research group has an active collaboration. TLR7/8 agonists are currently in clinical trials but are prone to systemic inflammation.[29,30] Recently, the Seder group has shown that polymer conjugation allows for a better spatio-temporal control of the immune activation.[31] An important drawback of conjugating a small molecule imidazoquinoline TRL7/8 agonist to a hydrophilic polymer however, was uncontrolled aggregation due to hydrophobic interaction.[32] These phenomena could be avoided by accommodating the imidazoquinoline TRL7/8 agonist into the nanogels core, while still

allowing DC activation *in vitro*. More importantly, *in vivo* experiments in mice showed that, contrary to soluble imidazoquinoline TRL7/8 agonist which caused systemic inflammation, a lymph node focused immune activation was induced. Moreover, relative to soluble imidazoquinoline TRL7 agonist, more immune cells were attracted to the draining lymph node; and relative to blank nanogels, imidazoquinoline TRL7/8 agonist ligated nanogels were taken up to a higher extent by immune cells in the draining lymph nodes. This approach has huge potential for rational vaccine design and is currently under intensive further investigation in our research group.

In this regard, we aimed to engineer both the nanogel surface as well as the nanogel core with reactive handles for peptide- or protein-conjugation. This work was done during a 6 months research stay in the lab of Prof. Dr. Heather D. Maynard at the University of California in Los Angeles (U.S.). Based on our earlier experience with polymer-protein conjugation, we endeavored to devise a strategy that would survive the conditions used during the nanogels assembly. These include aqueous media, the presence of primary amines and basic pH. In this regard, activated esters for lysine-modification are immediately excluded and moreover, do not allow for site-specific conjugation. Maleimides are neither stable in presence of primary amines and are also prone to hydrolysis. Pyridyldisulfides would have been an option, but the ability of these compounds to undergo random disulfide exchange under physiological conditions limits their applicability. Therefore, we opted in first instance to exploit the presence of the thiocarbonyl RAFT end-group. The latter is cleaved in presence of primary amines into a free thiol. Earlier work by the Maynard group on soluble polymers has shown that these free thiols could be converted into cysteine-reactive vinyl sulfones by treatment with an excess of divinyl sulfone.[33] Therefore, block copolymers were synthesized with the thiocarbonyl RAFT group at the hydrophilic chain end. Self-assembly in DMSO, followed by core crosslinking and quenching of the remaining reactive esters with amines, induced aminolysis of the pending thiocarbonyl groups. By capping the resulting free thiol with 2,2'-dipyridyl disulfide before extensive purification, oxidation of the thiols was prevented and allowed for successful Michael-type reactions with divinyl sulfone upon treatment with a reducing agent. These vinyl sulfone-functionalized nanogels were found to efficiently conjugate to cysteine moieties in BSA as model protein. As a second approach, we also dialed cysteamine into the nanogel core which allowed in a next step to introduce vinyl sulfone moieties.

Both these approaches will be intensively used in future work by our research group for the ligation of peptide- and protein-based antigens. With respect to peptide-based antigens, nanogel ligation is expected to increase the efficiency by which the antigen is taken up by DCs, especially when co-delivered with a molecular adjuvant such as a imidazoquinoline TRL7 agonist. By consequence, we anticipate the magnitude of the T cell response - in particular cross-presentation to CD8 T cells - to strongly increase. One direction that holds high potential is anti-cancer vaccination where either minimal amino acid sequence epitopes or longer peptides that contain a proteasome cleavage site, are conjugated to the surface of the nanogels that were developed in this thesis. Also for HIV, antigenic peptide sequences have been identified that would be worth to explore in the context of co-delivery with TRL7/8 agonists.[34-36] With respect to protein-based antigens, we not only expect the T cell response to dramatically increase, but also expect the B cell response to benefit from antigen-nanogel conjugation. Indeed, presenting multiple copies of a same protein antigen to B cells, leads to B cell receptor clustering and more potent humoral antibody-based responses.

Besides protein antigens also protein-based targeting ligands can be conjugated to the nanogels-platform developed in this thesis. For example, the conjugation of nanobodies as targeting ligand is under investigation in our laboratory.[37-39] Nanobodies can be easily engineered via recombinant methods to contain a terminal cysteine, and due to their small size should fairly efficiently conjugate to the nanogels. In terms of payload, a TLR7/8 agonist could be envisioned for targeting the tumor stroma[40], or a cytostatic compound to target cancer cells or the tumor vasculature. Delivery of TRL7/8 agonist containing nanoparticles as such is also of interest for anti-tumor therapy, as peritumoral delivery of molecular adjuvants, especially those that provoke Th1 immunity, will lead to activation of DCs in the tumor stroma and in the tumor draining lymph nodes. In the latter case, DCs that have encountered tumor associated antigens can become activated towards enhanced CD8 T cell presentation and thus CTL induction.

Nonetheless, an eminent issue in the nanomedicine field is the outlook towards clinical translation. With only a few nanotechnological formulations on the market (e.g. Doxil and Abraxane), there is a growing consensus that the next generation of nanomedicines should preferably be highly defined and consist of benign compounds to comply with regulatory affairs. The general lack of protocols for characterization at physicochemical,

biological and physiological level might have been responsible for the failure of certain nanomedicines in late clinical stages.[41] In this respect, the European Medicines Agency (EMA) has undertaken initiatives to facilitate the development of nanomedicines, including the publication of several reflections papers on e.g. block copolymer micelles and liposomal products.[42] In any case, newly developed nanomedicines should allow for large scale production with excellent control over their properties in terms of size, dispersity and composition (i.e. critical quality attributes or CQAs).[21,43] A quick and successful translation of emerging nanotherapeutics could be facilitated by adapting the 'quality-by-design' approach (QbD).[44] In this respect, it is fundamental to identify and control the critical points during each manufacturing process (i.e. critical process parameters or CPPs). High throughput screening and Design of Experiment approaches can facilitate the assessment of justified variability in CQAs that still allows for reproducible preclinical characteristics (e.g. distribution profile, toxicity, efficacy).

With regard to the nanogel platform that was developed in this thesis, there is a need to rethink the chemical conjugation strategy to avoid the use of PFP-esters as the latter require tedious work-up and still hold the risk for trace amounts. Therefore a risk assessment should be performed to assess the chance of remaining impurities, and their impact on toxicity and CQAs.[43] A solution to this issue might be the use of poly(succinimide) which only releases water upon amide bond formation with primary amines.[45] Also other crosslinking chemistries could hold promise in this regard. The latter should exhibit a low toxicity profile and thorough *in vivo* pharmacokinetic studies will be required to assess whether the polymeric degradation products of our nanogel platform can indeed be secreted from the body as intended by their design with pH-sensitive crosslinks. Despite these challenges we still hope to have contributed to the emerging field of immuno-engineering, and further paved the road for the design of nanocarriers for vaccine delivery that can combine potent immune-stimulatory molecules with peptide or protein antigens to amplify both cellular and humoral immune responses.

## References


1 Broyer, R. M., Grover, G. N. & Maynard, H. D. Emerging synthetic approaches for protein-polymer conjugations. *Chem. Commun.* **47**, 2212-2226 (2011).

2 Cobo, I. *et al.* Smart hybrid materials by conjugation of responsive polymers to biomacromolecules. *Nat. Mater.* **14**, 143-159 (2015).

3 Boyer, C. *et al.* An overview of protein-polymer particles. *Soft Matter* **7**, 1599-1614 (2011).

4 Nicolas, J., Mantovani, G. & Haddleton, D. M. Living radical polymerization as a tool for the synthesis of polymer-protein/peptide bioconjugates. *Macromol. Rapid Commun.* **28**, 1083-1111 (2007).

5 Siegwart, D. J., Oh, J. K. & Matyjaszewski, K. ATRP in the design of functional materials for biomedical applications. *Prog. Polym. Sci.* **37**, 18-37 (2012).

6 Li, H. M. *et al.* Protein conjugation of thermoresponsive amine-reactive polymers prepared by RAFT. *Polym. Chem.* **2**, 323-327 (2011).

7 Scarano, W. *et al.* Folate Conjugation to Polymeric Micelles via Boronic Acid Ester to Deliver Platinum Drugs to Ovarian Cancer Cell Lines. *Biomacromolecules* **14**, 962-975 (2013).

8 Heredia, K. L. *et al.* Reversible siRNA-polymer conjugates by RAFT polymerization. *Chem. Commun.*, 3245-3247 (2008).

9 Mantovani, G. *et al.* Design and synthesis of N-maleimido-functionalized hydrophilic polymers via copper-mediated living radical polymerization: A suitable alternative to PEGylation chemistry. *J. Am. Chem. Soc.* **127**, 2966-2973 (2005).

10 Shen, B. Q. *et al.* Conjugation site modulates the in vivo stability and therapeutic activity of antibody-drug conjugates. *Nat. Biotechnol.* **30**, 184-189 (2012).

11 Sletten, E. M. & Bertozzi, C. R. Bioorthogonal Chemistry: Fishing for Selectivity in a Sea of Functionality. *Angew. Chem.-Int. Edit.* **48**, 6974-6998 (2009).

12 Ngo, J. T. & Tirrell, D. A. Noncanonical Amino Acids in the Interrogation of Cellular Protein Synthesis. *Accounts Chem. Res.* **44**, 677-685 (2011).

13 MacDonald, J. I. *et al.* One-step site-specific modification of native proteins with 2-pyridinecarboxyaldehydes. *Nature Chemical Biology* **11**, 326-U114 (2015).

14 Zhang, Q. *et al.* Well-Defined Protein/Peptide-Polymer Conjugates by Aqueous Cu-LRP: Synthesis and Controlled Self-Assembly. *J. Am. Chem. Soc.* **137**, 9344-9353 (2015).

15 Zou, Y. Q., Brooks, D. E. & Kizhakkedathu, J. N. A novel functional polymer with tunable LCST. *Macromolecules* **41**, 5393-5405 (2008).

16 Reddy, S. T. *et al.* Exploiting lymphatic transport and complement activation in nanoparticle vaccines. *Nat. Biotechnol.* **25**, 1159-1164 (2007).

17 Kaminskas, L. M. & Porter, C. J. H. Targeting the lymphatics using dendritic polymers (dendrimers). *Adv. Drug Deliv. Rev.* **63**, 890-900 (2011).

18 Talelli, M. *et al.* Polymeric micelles for cancer therapy: 3 C's to enhance efficacy. *Current Opinion in Solid State and Materials Science* **16**, 302-309 (2012).

19 Hafner, A. *et al.* Nanotherapeutics in the EU: an overview on current state and future directions. *Int. J. Nanomed.* **9**, 1005-1023 (2014).

20 Owen, S. C., Chan, D. P. Y. & Shoichet, M. S. Polymeric micelle stability. *Nano Today* **7**, 53-65 (2012).

21 Talelli, M. *et al.* Core-crosslinked polymeric micelles: Principles, preparation, biomedical applications and clinical translation. *Nano Today* **10**, 93-117 (2015).

22 Liu, H. P. *et al.* Structure-based programming of lymph-node targeting in molecular vaccines. *Nature* **507**, 519-522 (2014).

23 Cui, J. *et al.* Templated Assembly of pH-Labile Polymer-Drug Particles for Intracellular Drug Delivery. *Advanced Functional Materials* **22**, 4718-4723 (2012).

24 Cui, J. *et al.* Engineering Poly(ethylene glycol) Particles for Improved Biodistribution. *ACS Nano* **9**, 1571-1580 (2015).

25 Cui, J. *et al.* Mechanically Tunable, Self-Adjuvanting Nanoengineered Polypeptide Particles. *Advanced Materials* **25**, 3468-3472 (2013).

26 Harris, J. M. & Chess, R. B. Effect of pegylation on pharmaceuticals. *Nat. Rev. Drug Discov.* **2**, 214-221 (2003).

27 Wilson, J. T. *et al.* pH-Responsive Nanoparticle Vaccines for Dual-Delivery of Antigens and Immunostimulatory Oligonucleotides. *ACS Nano* **7**, 3912-3925 (2013).

28 Nuhn, L. *et al.* Cationic Nanohydrogel Particles as Potential siRNA Carriers for Cellular Delivery. *ACS Nano* **6**, 2198-2214 (2012).

29 Dudek, A. Z. *et al.* First in Human Phase I Trial of 852A, a Novel Systemic Toll-like Receptor 7 Agonist, to Activate Innate Immune Responses in Patients with Advanced Cancer. *Clin. Cancer Res.* **13**, 7119-7125 (2007).

30 Weigel, B. J. *et al.* Prolonged Subcutaneous Administration of 852A, a Novel Systemic Toll-like Receptor 7 Agonist, to Activate Innate Immune Responses in Patients with Advanced Hematologic Malignancies. *Am. J. Hematol.* **87**, 953-956 (2012).

31 Coffman, R. L., Sher, A. & Seder, R. A. Vaccine Adjuvants: Putting Innate Immunity to Work. *Immunity* **33**, 492-503 (2010).

32 Nuhn, L. *et al.* pH-degradable imidazoquinoline-ligated nanogels for lymph node focused immune activation. *Proceedings of the National Academy of Sciences* (2016).

33 Grover, G. N. *et al.* Trapping of Thiol-Terminated Acrylate Polymers with Divinyl Sulfone To Generate Well-Defined Semitelechelic Michael Acceptor Polymers. *Macromolecules* **42**, 7657-7663 (2009).

34 Zhou, T. *et al.* Structural definition of a conserved neutralization epitope on HIV-1 gp120. *Nature* **445**, 732-737 (2007).

35 Pantophlet, R. & Burton, D. R. GP120: Target for Neutralizing HIV-1 Antibodies. *Annual Review of Immunology* **24**, 739-769 (2006).

36 Kim, M. *et al.* Immunogenicity of Membrane-bound HIV-1 gp41 Membrane-proximal External Region (MPER) Segments Is Dominated by Residue Accessibility and Modulated by Stereochemistry. *J. Biol. Chem.* **288**, 31888-31901 (2013).

37 Talelli, M. *et al.* Nanobody - Shell functionalized thermosensitive core-crosslinked polymeric micelles for active drug targeting. *J. Control. Release* **151**, 183-192 (2011).

38 Talelli, M. *et al.* Intrinsically active nanobody-modified polymeric micelles for tumor-targeted combination therapy. *Biomaterials* **34**, 1255-1260 (2013).

39 Muyldermans, S. Nanobodies: Natural Single-Domain Antibodies. *Annu. Rev. Biochem.*. **82**, 775-797 (2013).

40 Ahmed, I. & Berth-Jones, J. Imiquimod: a novel treatment for lentigo maligna. *Br. J. Dermatol.* **143**, 843-845 (2000).

41 Sainz, V. *et al.* Regulatory aspects on nanomedicines. *Biochem. Biophys. Res. Commun.* **468**, 504-510 (2015).

42 Ehmann, F. *et al.* Next-generation nanomedicines and nanosimilars: EU regulators' initiatives relating to the development and evaluation of nanomedicines. *Nanomedicine* **8**, 849-856 (2013).

43 van Gaal, V. B. E. & Crommelin, J. A. D. in *Non-Biological Complex Drugs: The Science and the Regulatory Landscape* (eds J. A. Daan Crommelin & B. Jon S. de Vlieger) 11-76 (Springer International Publishing, 2015).

44 Duncan, R. & Gaspar, R. Nanomedicine(s) under the Microscope. *Molecular Pharmaceutics* **8**, 2101-2141 (2011).

45 Chen, M. S. *et al.* Synthesis of amphiphilic polysuccinimide star copolymers for responsive delivery in plants. *Chem. Commun.* **51**, 9694-9697 (2015).

# Chapter 9

# Summary and general conclusions

As explained in **Part I,** the focus of this thesis was the design of polymer-based nanoscale delivery systems that combine antigens and molecular adjuvants for efficient dendritic cell targeting. In **Chapter 1**, a short introduction to the workings of the immune system is presented, alongside the opportunities for nanotechnology to engineer the immune system. In **Chapter 2** an extensive overview is given on transiently thermoresponsive polymers. This class of polymers, described as polymers that lose their thermoresponsive properties through a chemical transformation in aqueous medium, is prominently present in the subsequent experimental chapters. Therefore, **Chapter 2** describes the state of the art in this field, discussing different types of chemical moieties and transformation reactions that lead to transiently thermoresponsive polymers. The applicability of these polymers is further discussed in a biomedical context.

In **Part II** of this thesis, the experimental work is described. In **Chapter 3**, the synthesis of protein-reactive polymers via RAFT polymerization is discussed. Four different types of protein-reactive moieties are explored, i.e. N-hydroxysuccinimidyl esters (NHS) respectively pentafluorophenyl esters (PFP) as lysine-reactive moieties; and pyridyldisulfides respectively maleimides as cysteine reactive moieties. NHS and PFP activated esters form an amide bond with lysine residues, whereas pyridyldisulfides and maleimides form a (reducible) disulfide respectively thioether bond with cysteine residues.

These RAFT CTAs were used for the polymerization of different types of monomers, including HEA as model hydrophilic monomer, HPMAm and HPMAm-$Lac_2$. The latter monomer was synthesized during a research stay in the lab of Prof. Dr. Wim Hennink (Utrecht University, The Netherlands) and yields transiently thermoresponsive polymers. Additionally, the group of Prof. Dr. Richard Hoogenboom (Ghent University) provided transiently thermoresponsive co-polymers based on HEA and DMDMA; and poly(2-ethyl-2-oxazolines) terminated with a cyclooctyn moiety. In **Chapter 4**, these polymers were used for protein conjugation using a ´grafting to´ approach. Generally, a large molar excess of polymer to protein was required to obtain full protein conjugation. Furthermore, conjugation efficiency strongly differed between different proteins and their pre-conditioning with reactive handles such as protected thiols or azides, that were substituted on lysine residues to respectively enhance maleimide/pyridyldisulfide conjugation efficiency or allow conjugation by SPAAC. Using the HEA/DMDMA copolymer system, transiently thermoresponsive polymer-protein conjugates were prepared that assemble into globules above the cloud point temperature of the HEA/DMDMA copolymer and hydrolyze into fully soluble (i.e. over a broad temperature range) conjugates in response to acid-triggered side chain hydrolysis of the ketal moieties in the DMDMA repeating units.

In **Chapter 5**, an alternative strategy for the synthesis of polymer-protein conjugates was elaborated on. Here, a protein-based macroCTA was synthesized by ligating a PFP-containing RAFT CTA onto BSA as model protein. As monomer DMDOMAm was used. This ketal-containing acrylamide yields transiently thermoresponsive polymers without the need for co-monomers (as was the case for the HEA/DMDMA system), with a cloud point around room temperature. RAFT polymerization of DMDOMAm in aqueous medium at ambient temperature was possible using VA-044 as low temperature water-soluble radical initiator. When a critical monomer conversion was reached, the polymer-protein conjugates precipitated from solution due to the thermoresponsive nature of p(DMDOMAm) that formed dehydrated globules. The advantage of this ´grafting from´ approach is that much polymer-protein conjugation efficiency is achieved without the presence of free polymer. This is beneficial as removal of free polymer requires tedious chromatographic purification. The BSA-p(DMDOMAm) conjugates were characterized by DLS for their temperature triggered self-assembly and acid-triggered disassembly behavior. Additionally, the hydrophobic pocket that was formed by the p(DMDOMAm) globules was used to

accommodate the hydrophobic dye Cy3 alkyne and the hydrophobic TLR7 agonist CL075. We found that the BSA-p(DMDOMAm) conjugates could efficiently solubilize these compounds and deliver them to DCs *in vitro*, evidenced by flow cytometry and confocal microscopy. Furthermore we showed that, whereas BSA-p(DMDOMAm) is inert to DCs, CL075 formulated in BSA-p(DMDOMAm) could potently activate DCs, as measured by the induction of surface maturation markers.

Whereas the previous chapters dealt with the design of non-covalently assembled structures composed of polymers, protein and TLR ligand; there are several good reasons to also explore covalently linked structures based on post-modification of preformed polymeric nanoparticles. Indeed, a 'grafting-from' RAFT conjugation approach as described in **Chapter 5**, requires a significant amount of protein to be technically feasible. Furthermore, it is unknown whether non-covalently assembled nanoparticles will remain intact *in vivo,* and the same holds true for the non-covalently loaded TLR agonist that was used. Therefore, in **Chapter 6**, we collaborated with the group of Prof. Frank Caruso (University of Melbourne, Australia) to investigate the effect of surface chemistry on the *in vitro* and *in vivo* immuno-biological behavior of 200 nm sized hydrogel nanoparticles. Here we found that engineering the surface with a low-fouling poly(ethylene glycol) coating dramatically enhanced lymphatic transportation *in vivo* in mice, whereas no effect was observed *in vitro* on DCs cultures. During these endeavors we also contributed to the development of a super resolution microscopy (i.e. STORM) method for imaging the intracellular fate of nanoparticles beyond the diffraction limit.

Based on the promising results obtained in **Chapter 6**, our research group developed a nanogel system with sub 100 nm dimensions that contained a poly(ethylene glycol)-like stealth coating to provide optimal tissue mobility; and a PFP activated ester core that contained acid-labile ketal crosslinks, hydrophilic moieties and the potent TLR7/8 agonist IMDQ (provided by the lab of Prof. Dr. Sunil David (University of Minnesota, U.S.)) ligated via amide bond formation. These nanogels could, albeit to a lesser extent than IMDQ in freely soluble form, activate DCs *in vitro*. More importantly, they provided a potent lymph node focused immune activation *in vivo* in mice, without causing the systemic inflammation found for soluble IMDQ. During a research stay in the group of Prof. Dr. Heather D. Maynard (University of California in Los Angeles, U.S.), this nanogel technology was further explored in **Chapter 7** for protein conjugation. Due to the limitations of activated ester-,

pyridyldisulfide- and maleimide-based conjugations encountered in the previous chapters, we explored here the use of vinyl sulfone (VS) as a cysteine-reactive moiety. The advantage of VS groups is that they can easily be introduced at the chain ends of RAFT polymers upon aminolysis of the thiocarbonyl CTA group by post-polymerization modification. We have demonstrated an efficient strategy to equip core-crosslinked polymer nanogels with cysteine-reactive VS moieties, that allow for the preparation of protein-ligated nanogels.

Overall, we have explored in this thesis several approaches for polymer-protein conjugation and were confronted with several pro´s and many cons of the different conjugation strategies that were used. Introducing azide-based reactive handles on lysine units followed by SPAAC-based polymer-protein conjugation was found to be highly efficient, but yielded non-site-specific conjugation that could be detrimental for the bioactivity of the resulting protein. The use of VS, introduced at the polymer chain end via post-polymerization modification, was found to be the most versatile cysteine-reactive conjugation strategy and was successfully used to obtain stable nanogel-protein conjugates in aqueous medium. The use of nanogels was also found to be highly promising for the delivery of immunologically active components to the lymph nodes. The findings in this thesis provide a rational basis for further vaccine development.

# Samenvatting en algemene conclusies

Zoals toegelicht in **Deel I**, lag de focus van deze thesis op de ontwikkeling van een polymeer-gebaseerd afgiftesysteem op nanoschaal, dat antigenen en moleculaire adjuvans combineerde voor de efficiënte *targeting* van dendritische cellen. In **Hoofdstuk 1** van deze thesis wordt een korte introductie gegeven over de werking van het immuunsysteem en de mogelijkheden binnen nanotechnologie om het immuun systeem te moduleren. In **Hoofdstuk 2** wordt een uitgebreid overzicht gegeven van transiënt thermoresponsieve polymeren. Deze klasse van polymeren, omschreven als polymeren die hun thermoresponsief gedrag verliezen na een chemische transformatie in waterig midden, komt uitvoerig aan bod in de volgende experimentele hoofdstukken. **Hoofdstuk 2** beschrijft daarom de nieuwste ontwikkeling binnen dit veld, inclusief de verschillende types van chemische structuren en modificaties die aanleiding geven tot transiënt thermoresponsieve polymeren. De toepasbaarheid van deze polymeren wordt besproken in een biomedische context.

In **Deel II** van deze thesis wordt het experimentele werk beschreven. In **Hoofdstuk 3** komt de synthese van proteïne-reactieve polymeren via RAFT polymerisatie aan bod. Vier verschillende types proteïne-reactieve groepen werden onderzocht, namelijk N-hydroxysuccinimidyl esters (NHS) respectievelijk pentafluorophenyl esters (PFP) als lysine-reactieve groepen; en pyridyldisulfides respectievelijk maleïmides als cysteïne-reactieve groepen. NHS en PFP geactiveerde esters vormen amide bindingen met lysine residu's, terwijl pyridyldisulfides en maleïmides (reduceerbare) disulfide respectievelijk thioether bindingen vormt met cysteïnes. Deze RAFT CTAs werden gebruikt voor de polymerisatie van verschillende types monomeren, zoals HEA als model hydrofiel monomeer, HPMAm en HPMAm-$Lac_2$. Dit laatste monomeer werd gesynthetiseerd tijdens een onderzoeksstage in het labo van Prof. Dr. Wim Hennink (Universiteit Utrecht, Nederland), en geeft aanleiding tot transiënt thermoresponsieve polymeren.

Bijkomend verschafte de groep van Prof. Dr. Richard Hoogenboom (Universiteit Gent) transiënt thermoresponsieve copolymeren gebaseerd op HEA en DMDMA, en poly(2-ethyl-2-oxazolines) getermineerd met een cyclooctyn groep. In **Hoofdstuk 4** werden deze polymeren gebruikt voor eiwitconjugatie via een 'grafting-to' strategie. In het algemeen was er een grote molaire overmaat aan polymeer vereist om complete eiwit conjugatie te verkrijgen. Bovendien varieerde de conjugatie efficiëntie sterk voor verschillende eiwitten en substituties met reactieve groepen zoals beschermde thiolen of azides, om respectievelijk de pyridyldisulfide/maleïmide conjugatie efficiëntie verhogen of conjugatie via SPAAC toe te laten. Met het HEA/DMDMA copolymeer systeem werden transiënt thermoresponsieve polymeer-eiwit conjugaten verkregen, die assembleerden in globulen boven de *cloud point* temperatuur ($T_{cp}$) van het copolymeer en degradeerden tot volledige oplosbare (d.w.z. over een brede temperatuursrange) conjugaten na zuur-gemedieerde hydrolyse van de ketal groepen in de zijketen van de DMDMA repeteereenheden.

In **Hoofdstuk 5** werd een alternatieve strategie uitgewerkt voor de synthese van polymeer-eiwit conjugaten. Hier werd een eiwit-gebaseerde macroCTA gesynthetiseerd door het ligeren van een PFP-bevattende RAFT CTA aan BSA als model eiwit. Als monomeer werd DMDOMAm gebruikt. Dit ketal-bevattende acrylamide geeft aanleiding tot transiënt thermoresponsieve polymeren zonder de behoefte aan comonomeren (zoals voor het HEA/DMDMA systeem), met een $T_{cp}$ rond kamertemperatuur. RAFT polymerisatie van DMDOMAm in waterig midden bij kamertemperatuur was mogelijk dankzij het gebruik van VA-044 als wateroplosbare lage temperatuur radicaalinitiator. Bij een kritische monomeer conversie precipiteerden de polymeer-eiwit conjugaten uit oplossing wegens het thermoresponsieve karakter van p(DMDOMAm), dat gedehydrateerde globulen vormde. Het voordeel van deze 'grafting-from' strategie is dat een hoge conjugatie efficiëntie kan worden bereikt zonder de aanwezigheid van vrij polymeer. Dit is voordelig aangezien het verwijderen van een overmaat aan vrij polymeer arbeidsintensieve chromatografische opzuivering vereist. De temperatuur-afhankelijke *assembly* en zuur-afhankelijke *disassemby* van de BSA-p(DMDOMAm) conjugaten werd gekarakteriseerd via DLS. Bijkomend werd de hydrofobe pocket van de p(DMDOMAm) globules gebruikt voor de encapsulatie van de hydrofobe kleurstof Cy3 en de hydrofobe TLR7 agonist. De BSA-p(DMDOMAm) conjugaten konden deze molecules efficiënt solubiliseren en afgeven aan DCs *in vitro,* zoals aangetoond met flow cytometrie en confocale microscopie. Bovendien werd aangetoond dat BSA-

p(DMDOMAm) conjugaten inert waren ten opzichte van DCs, terwijl CL075 geformuleerd in deze conjugaten DCs potent kon activeren zoals gemeten aan de hand van de inductie van maturatie merkers op hun oppervlak.

Terwijl de vorige hoofdstukken focusten op de ontwikkeling van niet-covalent gebonden structuren op basis van polymeren, eiwit en TLR ligand; is er ook gegronde interesse om covalent gebonden structuren te ontwikkelen via postmodificatie van eerder gevormde polymeer nanopartikels. Een 'grafting-from' RAFT strategie vergt inderdaad een substantiële hoeveelheid eiwit om technisch haalbaar te zijn. Bovendien blijft het onduidelijk of niet-covalent geassembleerde nanopartikels intact zullen blijven *in vivo*, wat ook geldt voor niet-covalent geladen TLR agonist. Daarom werkten we in **Hoofdstuk 6** samen met Prof. Dr. Frank Caruso (Universiteit Melbourne, Australië) om het effect van oppervlaktechemie te onderzoeken op het *in vitro* en *in vivo* immuno-biologisch gedrag van 200 nm hydrogel nanopartikels. We stelden vast dat het functionaliseren van het oppervlak met een *low-fouling* poly(ethylene glycol) coating het lymfatisch transport *in vivo* in muizen dramatisch verbeterde, terwijl er geen effect werd gezien *in vitro* in DCs culturen. Tijdens deze experimenten werkten we ook mee aan de ontwikkeling van een super resolutie microscopie methode (nl. STORM) voor het in beeld brengen van de intracellulaire lokalisatie van nanopartikels voorbij de diffractie limiet.

Gebaseerd op de veelbelovende resultaten in **Hoofdstuk 6**, werd er in onze onderzoeksgroep een nanogel systeem ontwikkeld met sub 100 nm dimensies. De nanogels waren samengesteld uit een poly(ethylene glycol)-*like stealth coating* voor optimale weefsel mobiliteit; en een PFP geactiveerde ester kern waarin zuur-gevoelige ketal crosslinks, hydrofiele ketens en de potente TLR7/8 agonist IMDQ (verschaft door Prof. Dr. Sunil David, Universiteit Minnesota, Verenigde Staten) geligeerd werden via amide bindingen. Deze IMDQ-bevattende nanogels konden DCs activeren *in vitro*, al was dit in mindere mate dan IMDQ in opgelost vorm. Bovendien zorgden zij voor een potente immuun activatie *in vivo* in muizen, gefocust in de lymfeknoop en zonder het veroorzaken van een systemische inflammatie zoals het geval voor vrij IMDQ. Tijdens een onderzoekstage in de groep van Prof. Dr. Heather D. Maynard (Universiteit Californië Los Angeles, Verenigde Staten) werd deze nanogel technologie verder ontwikkeld voor eiwit conjugatie (**Hoofdstuk 7**). Gezien de limitaties van conjugaties gebaseerd op geactiveerde esters, pyridyldisulfides en maleïmides zoals ondervonden in voorgaande hoofdstukken; onderzochten we het gebruik van vinyl

sulfone (VS) als cysteïne-reactieve groep. Het voordeel van VS is de gemakkelijke introductie op het keteneinde van RAFT-gebaseerde polymeren na aminolyse van de thiocarbonyl CTA groep via een postpolymerisatie modificatie. We hebben een efficiënte strategie aangetoond om gecrosslinkte polymeer nanogels te voorzien van cysteïne-reactieve VS groepen, die toelaat om eiwit-geconjugeerde nanogels te synthetiseren.

Samengevat hebben we in deze thesis verschillende strategieën onderzocht voor polymeer-eiwit conjugatie en werden we geconfronteerd met verscheidene pro's en vele contra's van de verschillende toegepaste benaderingen. Het gebruik van azide-bevattende reactieve groepen, die werden geïntroduceerd op lysine eenheden, gevolgd door SPAAC-gebaseerde polymeer-eiwit conjugatie was heel efficiënt; maar geeft aanleiding tot niet-site-specifieke conjugatie die schadelijk zou kunnen zijn voor de bio-activiteit van het gemodificeerde eiwit. Het gebruik van VS, die werd geïntroduceerd op het polymeer ketenuiteinde via postpolymerisatie modificatie, was de meest veelzijdige cysteïne-reactieve strategie en kon succesvol gebruikt worden voor de ontwikkeling van stabiele nanogel-eiwit conjugaten in water midden. Bovendien bleek het gebruik van dergelijke nanogels enorm veelbelovend voor de afgifte van immunologisch actieve molecules aan de lymfeknopen. De bevindingen in deze thesis verschaffen dan ook een rationele basis voor verdere vaccin ontwikkeling.

# Curriculum Vitae

## PERSONAL INFORMATION


| | |
|---|---|
| **Surname** | Vanparijs |
| **First names** | Nane Noëlle Josephine |
| **Nationality** | Belgian |
| **Date of birth** | March 2nd 1989 |
| **Home address** | Melkerijstraat 20, 900 Ghent, Belgium<br>Vanparijs.nane@gmail.com<br>+32 477 42 15 04 |
| **Work address** | Faculty of Pharmaceutical Sciences<br>Ottergemsesteenweg 460, 9000 Ghent, Belgium<br>Nane.vanparijs@ugent.be<br>+32 9 264 80 82 |


## EDUCATION

**2012 - present: PhD in Pharmaceutical Sciences**

Faculty of Pharmaceutical Sciences, Ghent University, Belgium

Title: Design of protein-reactive polymers and core-crosslinked nanoparticles in view of vaccine delivery

Promotor: Prof. Dr. B. G. De Geest

*Bijzonder Onderzoeksfonds* (BOF) fellowship of Ghent University

Nov 2012: Research stay at Utrecht University

Institute for Pharmaceutical Sciences, Utrecht University, the Netherlands

Principle Investigator of receiving research unit: Prof. Dr. W. E. Hennink

Oct 2015 - April 2016: Research stay at UCLA

Department of Chemistry and Biochemistry, University of California Los Angeles, U.S.

Principle Investigator of receiving research unit: Prof. Dr. H. Maynard

Research Foundation – Flanders (FWO) travel grant

**2007 - 2012: Master in Drug Development**

Graduated magna cum laude

Faculty of Pharmaceutical Sciences, Ghent University, Belgium

Jan - May 2011**:** Erasmus Exchange Program

Institute for Pharmaceutical Sciences, Utrecht University, the Netherlands

Master thesis: "Characterization of anti-IFN-β antibodies produced by transgenic (immune tolerant) and non-transgenic animals."

Promotors: Prof. Dr. W. E. Hennink (Utrecht) and Prof. Dr. J. Demeester (Ghent)

Jul 2011 - Aug 2012**:** Pharmacy Internship

Apotheek T'jollyn, Waregem, Belgium

## EXTRACURRICULAR ACTIVITIES

**1997 - 2009: Chiro**

Active member and leader of the youth movement Chiro Waregem Centrum

**2013 - present: Farmalumni**

Member of the organizing committee for alumni of Pharmaceutical Sciences at Ghent University

**2014 - present: Make-a-wish Foundation**

Volunteer for the Make-a-wish foundation Belgium-Flanders

## HONORS AND AWARDS

PhD fellowship (2 x 2 years) funded by *Bijzonder Onderzoeksfonds* (BOF) of Ghent University

Travel grant for a long stay abroad by Research Foundation – Flanders (FWO)

## SPECIALIST COURSES

Training: BD ACCURI™ C6 operator course, BD Biosciences European training and education center, Erembodegem (Belgium), October 16-18, 2012

## LANGUAGE SKILLS

| | Competence |
|---|---|
| **Dutch** | Native language |
| **English** | Excellent |
| **French** | Good |

## PUBLICATIONS IN PEER REVIEWED JOURNALS

Zhang, Z; Vanparijs, N; Vandewalle, S; Du Prez, F. E.; Nuhn, L.; De Geest, B. G.
**Squaric ester amides as hydrolysis-resistant functional groups for protein-conjugation of RAFT polymers** (Submitted manuscript)

Louage, B.; Nuhn, L.; Risseeuw, M. D. P.; Vanparijs, N.; . . . . ; Van Calenbergh, S.; De Geest, B. G.
**Well-Defined Polymer–Paclitaxel Prodrugs by a Grafting-from-Drug Approach**
Angewandte Chemie International Edition 2016, in press
IF 2015: 11.709

Vanparijs, N.; Nuhn, L.; Paluck, S.; Maynard, H.D.; De Geest, B.G.
**Core and shell reactive nanogels for protein conjugation via a combination of RAFT polymerization and vinyl sulfone post-modification**
Nanomedicine 2016, in press
IF 2015: 4.889

De Coen, R.; Vanparijs, N.; Risseeuw, M.; . . . ; Ayres, N.; Van Calenbergh, S.; Nuhn, L.; De Geest, B.G.
**pH-degradable mannosylated nanogels for dendritic cell targeting**
Biomacromolecules 2016, 17(7), 2479–2488
IF 2015: 5.583

Nuhn, L.; Vanparijs, N.; . . . ; Lambrecht, N.B.; Grooten, J.; David, S.A.; De Koker, S., De Geest, B.G.
**pH-degradable imidazoquinoline-ligated nanogels for lymph node focused immune activation**
Proceedings of the National Academy of Sciences 2016, 113(29), 8098-8103
IF 2015: 9.423

van der Zwaag, D.*; Vanparijs, N.*; Wijnands, S.; De Rycke, R.; De Geest, B.G.; Albertazzi, L.
**Super resolution imaging of nanoparticles cellular uptake and trafficking**
ACS Applied Materials & Interfaces 2016, 8(10), 6391–6399
IF 2015: 7.145

Lybaert, L.; Vanparijs, N.; Fierens, K.; Schuijs, M.; Nuhn, L.; Lambrecht, B.N.; De Geest, B.G.
**A generic polymer-protein ligation strategy for vaccine delivery**
Biomacromolecules 2016, 17(3), 874–881
IF 2015: 5.583

Li, H.; Fierens, K.; Zhang, Z.; Vanparijs, N.; Schuijs, M. J.; Van Steendam, K.; . . . De Geest, B. G.
**Spontaneous Protein Adsorption on Graphene Oxide Nanosheets Allowing Efficient Intracellular Vaccine Protein Delivery.**
ACS Applied Materials & Interfaces 2016, 8(2), 1147–1155
IF 2015: 7.145

De Koker, S.;* Cui, J.;* Vanparijs, N.;* Albertazzi, L.; Grooten, J.; Caruso, F.; De Geest, B. G.
**Engineering Polymer Hydrogel Nanoparticles for Lymph Node-Targeted Delivery.**
Angewandte Chemie International Edition 2016, 55(4), 1334-1339
IF 2015: 11.709

Glassner, M.; Maji, S.; de la Rosa, V. R.; Vanparijs, N.; Ryskulova, K.; De Geest, B. G.; Hoogenboom, R.
**Solvent-free mechanochemical synthesis of a bicyclononyne tosylate: a fast route towards bioorthogonal clickable poly(2-oxazoline)s.**
Polymer Chemistry 2015, 6, 8354-8359
IF 2015: 5.687

Vanparijs, N.; De Coen, R.; Laplace, D.; Louage, B.; Maji, S.; . . . ; Hoogenboom, R.; De Geest, B.G.
**Transiently responsive protein-polymer conjugates via a grafting-from RAFT approach: for intracellular co-delivery of proteins and immune-modulators.**
Chemical Communications 2015, 51(73), 13972-13975
IF 2015: 6.567

Zhang, Q.; Hou, Z.; Louage, B.; Zhou, D.; Vanparijs, N.; De Geest, B.G.; Hoogenboom R.
**Acid-labile thermoresponsive copolymers that combine fast pH trigered hydrolysis and high stability at neutral condition.**
Angewandte Chemie International Edition 2015, 54(37), 10879-10883
IF 2015: 11.709

Louage, B.; Zhang, Q. L.; Vanparijs, N.; Voorhaar, L.; Vande Casteele, S.; Shi, Y.; . . . De Geest, B. G.
**Degradable Ketal-Based Block Copolymer Nanoparticles for Anticancer Drug Delivery: A Systematic Evaluation.**
Biomacromolecules 2015, 16(1), 336-350.
IF 2015: 5.583

Vanparijs, N.;* Maji, S.;* Louage, B.; Voorhaar, L.; Laplace, D.; Zhang, Q.; . . . De Geest, B. G.
**Polymer-protein conjugation via a 'grafting to' approach - a comparative study of the performance of protein-reactive RAFT chain transfer agents.**
Polymer Chemistry 2015, 6(31), 5602-5614.
IF 2015: 5.687

Lybaert, L.; De Vlieghere, E.; De Rycke, R.; Vanparijs, N.; De Wever, O.; De Koker, S.; De Geest, B. G.
**Bio-Hybrid Tumor Cell-Templated Capsules: A Generic Formulation Strategy for Tumor Associated Antigens in View of Immune Therapy.**
Advanced Functional Materials 2014, 24(45), 7139-7150.
IF 2014: 11.805

Zhang, Q. L.; Vanparijs, N.; Louage, B.; De Geest, B. G; Hoogenboom, R.
**Dual pH- and temperature-responsive RAFT-based block co-polymer micelles and polymer-protein conjugates with transient solubility.**
Polymer Chemistry 2014, 5(4), 1140-1144.
IF 2014: 5.520

## ORAL PRESENTATIONS AT CONFERENCES

Transiently responsive protein-polymer conjugates via a grafting-from RAFT approach: For intracellular co-delivery of proteins and immune-modulators
N. Vanparijs, B.G. De Geest
**251st American Chemical Society (ACS) National Meeting** - San Diego, California - March 13-17, 2016

Transiently Responsive Protein-polymer Conjugates via a Grafting from RAFT Approach: for Intracellular Co-delivery of Proteins and Immune-modulators
N. Vanparijs, B.G. De Geest
**Pacific Polymer Conference (PPC)**- Kauai, Hawaii – December 9-13, 2015

Multi-responsive polymer-protein conjugates as immune-modulating strategy
N. Vanparijs, R. De Coen, B.G. De Geest
**249th American Chemical Society (ACS) National Meeting** - Denver, Colorado - March 22-26, 2015

## POSTER PRESENTATIONS AT CONFERENCES

Polymer-protein conjugation via a 'grafting to' approach – a comparative study of the performance of protein-reactive raft chain transfer agents
N. Vanparijs, S. Maji, B. Louage, L. Voorhaar, . . ., W. E. Hennink, R. Hoogenboom, B. G. De Geest
**Meeting of the Belgian-Dutch Biopharmaceutical Society** - Vlaardingen, the Netherlands - December 12th, 2014

Protein-reactive RAFT agents for the design of polymer-protein conjugates
N. Vanparijs, B. Louage, S. Maji, L. Voorhaar, Q. Zhang, R. Hoogenboom, B.G. De Geest
**248th American Chemical Society (ACS) National Meeting** - San Francisco, California - August 10-14, 2014.

Towards efficient polymer-protein conjugation
N. Vanparijs, B. Louage, S. Maji, L. Voorhaar, Q. Zhang, R. Hoogenboom, B.G. De Geest
**Knowledge for Growth (KfG)** - Ghent, Belgium - May 8th, 2014

Protein-reactive raft agents for the design of polymer-protein conjugates
N. Vanparijs, B. Louage, S. Maji, L. Voorhaar, Q. Zhang, R. Hoogenboom, B.G. De Geest
**13th European Symposium on Controlled Drug Delivery (ESCDD)** - Egmond aan Zee, the Netherlands - April 16-18, 2014.

Protein-reactive raft agents for the design of polymer-protein conjugates
N. Vanparijs, B. Louage, S. Maji, L. Voorhaar, Q. Zhang, R. Hoogenboom, B.G. De Geest
**Meeting of the Belgian-Dutch Biopharmaceutical Society** - Ghent, Belgium - December 18th, 2013